Lecture Notes on Extended X-ray Absorption Fine Structure (EXAFS)

Paolo Fornasini

Revised:

March 16, 2023

Contents

Chapter 1

Introduction

X-rays were discovered by W. Röntgen in November 1895 [Röntgen, 1896]. Some peculiar properties of the new radiation, like the high penetrating power and its dependence on atomic number and density, were immediately evident, and led to the first medical applications of radiography within a few months.
Less that twenty years later, the first diffraction experiments were done (Friedrich, Knipping and Laue in 1912 [Friedrich et al., 1912], W.H. Bragg and W.H. Bragg in 1913 [Bragg and Bragg, 1913]). Again in 1913, H.G.J. Moseley [Moseley, 1913] began to investigate the relation existing between the X-ray wavelengths and the energies of the levels of the just proposed Bohr atom [Bohr, 1913]. Since then, X-rays have become an invaluable tool for investigating microscopic properties of matter (structural, electronic, dynamical).
The advent of Synchrotron Radiation sources has led to an impressive progress in all X-ray techniques. The fine structures of the X-ray absorption coefficient (XAFS) were known since 1920 [Fricke, 1920, Kievit and Lindsay, 1930]; however, only in the seventies, thanks to the availability of synchrotron sources and to the development of a suitable interpretation scheme [Sayers et al., 1971a, Sayers et al., 1971b, Stern, 1974], become it possible to exploit them to get quantitative information on both the local geometric and electronic structure of matter.
A detailed history of the first development of XAFS has been written by R. Stumm von Bordwehr [Stumm von Bordwehr, 1989].

1.1 Interaction of X-rays with matter

The flux Φ of an X-ray beam is the number of photons crossing a unit section of the beam in the unit time. Upon traversing a sample of thickness x and cross sectional area larger than that of the beam (Fig. 1.1, left) the flux is reduced according to the exponential law

$$\Phi_{\text{out}} \;=\; \Phi_{\text{in}}\; \exp[-\mu x]\,, \tag{1.1}$$

where μ is the *linear attenuation coefficient* of the sample. The linear attenuation coefficient μ depends on the energy of the X-rays and on the composition and density of the sample. The contributions of single atomic species are tabulated as mass absorption coefficients μ/ρ [Thomson et al., 2009, Hubbell and Seltzer, 1996]

$$\frac{\mu}{\rho} \;=\; \frac{\sigma_a\, N_a}{A}\,, \tag{1.2}$$

where ρ is the density, σ_a is the atomic attenuation cross section, N_a is the Avogadro number and A is the atomic mass.

Three different mechanisms contribute to the attenuation of an X-ray beam (Fig. 1.1, right):

1. The dominant interaction for relatively low photon energies is **photo-electric absorption**: one photon is absorbed from the beam because of its interaction with an atom; the photon

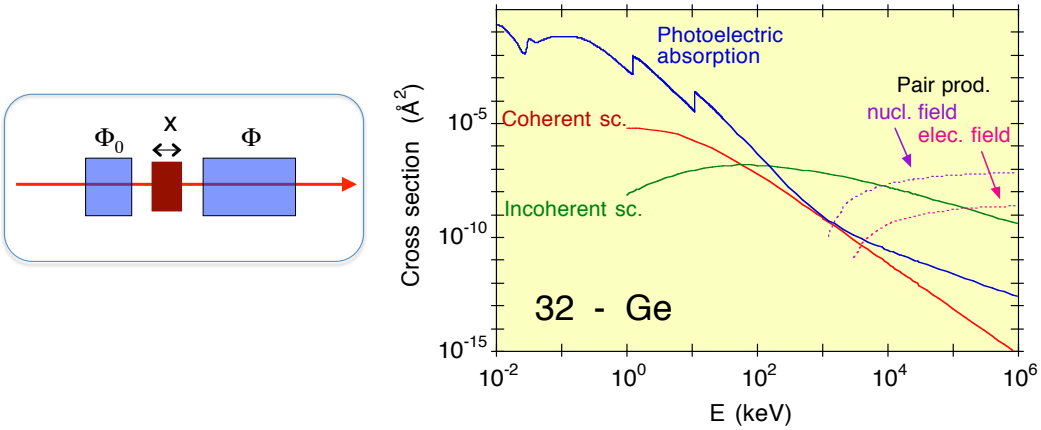

Figure 1.1: Left: an X-ray beam crossing a sample of thickness x. Right: atomic cross-sections for the different mechanisms of X-ray attenuation in Germanium: continuous line = photoelectric absorption, dashed line = unmodified scattering (Thomson), dotted line = modified scattering (Compton), dash-dotted lines = pair production.

energy is absorbed by the atom, which can be excited, with promotion of one or more electrons to higher bound energy levels, or ionized, with ejection of one or more electrons (this last phenomenon is called photo-ionization).

2. The second interaction, weaker than photo-absorption at low energies, is **scattering**: a photon is deflected from the original trajectory by the collision with an atom. The scattering of one photon from *one electron* can be

   - *modified* or *Compton* scattering, when the photon wavelength is modified by effect of the scattering process: the positive variation of the wavelength is $\Delta\lambda = \lambda_c(1-\cos\theta)$, where θ is the scattering angle and $\lambda_c = 0.002426$ Å is the Compton wavelength; according to quantum mechanics, the scattering from a completely free electron is always modified;

   - *unmodified* scattering, when the photon wavelength is unmodified by the scattering process, $\Delta\lambda = \lambda' - \lambda = 0$; as a consequence $E' = E$; the unmodified scattering corresponds to the classical Thomson theory of the scattering of X-rays from free electrons.

   For electrons bound in atoms, the statistical balance between modified and unmodified scattering depends on wether the energy lost by a photon undergoing Compton scattering, $\Delta E_{\rm com} \simeq \hbar\omega_{\rm in}\,\Delta\lambda/\lambda_{\rm in}$, is larger than the electron binding energy or not.

   When considering the scattering of X-rays from *an aggregate of atoms*, one speaks of

   - *elastic scattering* if the photon energy is conserved, $\hbar\omega_{\rm out} = \hbar\omega_{\rm in}$;
   - *inelastic scattering* if the photon energy is not conserved: inelastic scattering can be due not only to the Compton effect at the single electron level, but also to the interaction of the photon with collective excitations, of both electronic and vibrational nature.

3. The dominant interaction at high energies is **pair production**: the photon annihilates, giving rise to a pair e^+e^-. This process requires a photon energy larger than about 1 MeV (twice the electron rest mass), and cannot take place in vacuum. To guarantee the conservation of linear momentum, the photon must interact with an external field (nuclear or electronic).

The two interactions possible below 1 MeV, photoelectric absorption and scattering, give origin to three basic groups of experimental techniques [Als-Nielsen and McMorrow, 2011]:

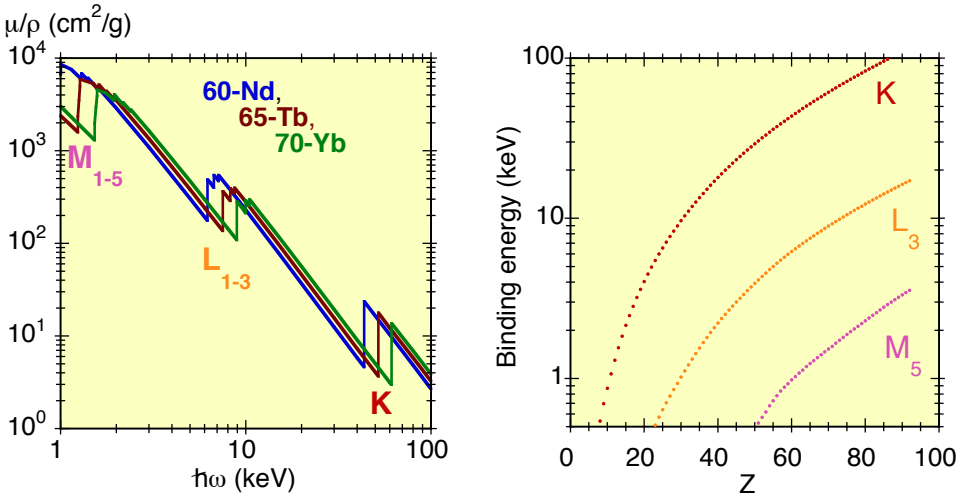

Figure 1.2: Left: X-ray mass absorption coefficients of Nd, Tb, Yb in the energy range fro 1 to 100 keV. Right: Binding energy of electrons in core levels K, L_3 e M_5 as a function of the atomic number Z.

1. **Spectroscopy** is due to the absorption mechanism, and gives mainly information on the electronic structure of matter. One speaks of X-ray *absorption* or *emission* spectrosopy, according to whether the absorption or the emission of X-rays is studied as a function of energy. In *photoelectron* spectroscopy, the electrons emitted from the sample upon absorption of X-ray photons are collected and analyzed.

2. **Elastic scattering** gives information on the atomic-scale geometrical structure of condensed systems (crystalline and non-crystalline solids, as well as liquids); elastic scattering from crystalline solids is often conventionaly referred to as *diffraction*. **Inelastic scattering** gives information on the distribution of electron momenta in atoms (via Compton scattering) as well as on atomic collective excitations.

3. **Imaging** gives macroscopic pictures of a sample, based on the different degree of attenuation of X-rays by different parts of the sample; it includes medical and industrial radiography and X-ray microscopy. Both absorption and scattering contribute to the attenuation responsible for imaging.

1.2 X-ray Absorption spectroscopy

We focus now our attention on X-ray energies ranging from about 1 keV to about 100 keV, corresponding to wavelengths from about 0.12 to about 12 Å, respectively. (The relation between energy $\hbar\omega$, in keV, and wavelength λ, in Ångström, is $\hbar\omega = 12.398/\lambda$).
In this energy range, the dominant attenuation mechanism is photoelectric absorption. We will then identify the linear absorption coefficient with the linear attenuation coefficient $\mu(\omega)$.
Besides, in this energy range, the behaviour of the photo-electric absorption coefficient is very simple and qualitatively very similar for different atomic species; these properties are at best evidenced by log-log plots, such as in Fig. 1.1, right, and in Fig. 1.2, left. When the energy of the absorbed X-ray photons increases, the absorption coefficient $\mu(\omega)$ progressively decreases (harder X-rays are more penetrating); the absorption depends on the atomic species too (heavier atoms are more absorbing). The smooth energy dependence of the photo-electric absorption coefficient is interrupted by sharp discontinuities, the *absorption edges*.

Table 1.1: High-energy absorption edges (in order of increasing photo-electron energy) and configurations of the electronic shells involved.

Edge:	M_5	M_4	M_3	M_2	M_1	L_3	L_2	L_1	K
Initial configuration:	$3d^{10}$	$3d^{10}$	$3p^6$	$3p^6$	$3s^2$	$2p^6$	$2p^6$	$2s^2$	$1s^2$
Final configuration:	$3d^9$	$3d^9$	$3p^5$	$3p^5$	$3s^1$	$2p^5$	$2p^5$	$2s^1$	$1s^1$
Final term:	$^2D_{5/2}$	$^2D_{3/2}$	$^2P_{3/2}$	$^2P_{1/2}$	$^2S_{1/2}$	$^2P_{3/2}$	$^2P_{1/2}$	$^2S_{1/2}$	$^2S_{1/2}$

1.2.1 Absorption edges

The absorption edges (Fig. 1.1, right, and Fig. 1.2, left) originate when the photon energy becomes high enough to extract an electron from a deeper level.
For historical reasons, the X-ray absorption edges are labelled by the consecutive alphabetical letters K, L, M ..., which correspond to the principal quantum numbers 1, 2, 3, ..., repectively (Fig. 1.2. The highest-energy absorption edge, the K edge, corresponds to the extraction of an electron from the deepest level, the 1s level.
The next higher-energy edges are the three L edges: L_1 corresponds to the extraction of an electron from a 2s level, the L_2 and L_3 edges correspond to the extraction of an electron from a 2p level. The distinction between the L_2 and L_3 edges is due to the different alignment of the atomic orbital and spin momenta, which gives rise to different spin-orbit contributions to the energy, as will be explained in § 2.2 and is summarized in Table 1.1 (which includes also the M edges for atoms with initial complete d shell).
The energy of each family of absorption edges increases monotonically with the atomic number Z, as depicted in Fig. 1.2, right panel. For example, the K-edge energy increases from 13.6 eV for Hydrogen (well below the X-rays region) to 115.606 keV for Uranium.
In the X-ray energy region (between 1 and 100 keV), the absorption coefficient between two consecutive edges depends on the photon energy and on the atomic number approximately as

$$\mu(\omega) \propto Z^4/(\hbar\omega)^3 \,. \tag{1.3}$$

Note: For historical reasons, the absorption edges should be labelled by Roman numerals, e.g. $L_{|}$, $L_{||}$ and $L_{|||}$ [Stumm von Bordwehr, 1989], since the Arabic numerals had been used at the beginnings of X-ray spectroscopy with a reverse meaning, the highest and lowest-energy L edges being named L_3 and L_1, respectively. In the present work we adhere to the modern literature and use Arabic numerals as substitutes of roman numbers.

1.2.2 Threshold energy and binding energy

The edge energy is generally defined as the threshold for ionisation of a given core level, and thus corresponds to the binding energy of the core level. Since the binding energies increase monotonically with the atomic number Z (Fig. 1.2, right), every edge energy corresponds to a well defined atomic species. This behaviour is at the origin of the selectivity of atomic species of X-ray spectroscopy techniques.

Isolated atoms

Let us first consider an isolated atom. After the absorption of an X-ray photon, an isolated atom can be, depending on the X-ray energy,

a) *excited*, if the photon energy is lower than the binding energy and corresponds to the energy difference between a core level and an upper unoccupied bound level; the electron of the core level is transferred to the bound unoccupied level;

b) *ionized*, if the photon energy is larger than the binding energy, so that the electron (hence called *photo-electron*) is ejected from the atom.

The binding energy of an electron level is the minimum energy necessary to extract the electron from the atom (ionisation energy).
The simplicity of the behaviour of the X-ray absorption coefficient and the similarity for different atomic species, as compared with the absorption coefficients in the optical region, is due to the fact that the binding energies of core levels are much higher than the differences in energy between the bound unoccupied atomic levels (Rydberg levels). The absorption spectra for X-rays are dominated by the core level excitation, with very little influence of the outer level structure. We see below, however, that the distribution of the outer levels can give rise to a fine structure of the absorption coefficient, localised near the edge, so that the accurate evaluation of the threshold energy can be far from trivial.

Molecules and condensed systems

For molecules and condensed systems, the photo-ionisation process is more complicated than for isolated atoms. For *molecules*, the photoelectron can suffer complex interactions with the surrounding atoms before escaping and the evaluation of the threshold energy can be more complicated than for atoms. In *condensed systems*, the photo-electron does not escape at all (with the exception of the events of photo-ionisation near the surface, which give rise to photo-emission spectroscopy). The binding energy is defined as the energy difference between the core level and the Fermi level for metals, the core level and the top of valence band for semiconductors.

Tables of binding energies

The currently available tables give the electron binding energies relative to the vacuum level (ionisation energies) for gases, relative to the Fermi level for metals and relative to the top of the valence band for semiconductors.
The binding energies of the L and K levels are listed in Table 1.2 for selected elements. The spacing between the L edges increases when the atomic number Z increases. In particular, the difference between the energies of the L_2 and L_3 edges id due to the spin orbit effect (see Chapter 2 for more details); the difference increases when the atomic number Z increases (Fig. 1.3).

Table 1.2: Binding energies (in eV) for the K and L edges of selected elements.

Z		L_3	L_2	L_1	K
20	Ca	346.2	349.7	438.4	4 038.5
30	Zn	1 021.8	1 044.9	1 196.2	9 659.0
40	Zr	2 223.	2 307.	2 532.	17 998.0
50	Sn	3 929.	4 156.	4 465.	29 200.
60	Nd	6 208.	6 722.	7 126.	43 569.
70	Yb	8 944.	9 978.	10 486.	61 332.

1.2.3 Fine structure

The smooth behaviour of the absorption coefficient depicted in Fig. 1.2 (left) is only an approximate behaviour. In correspondence of an edge, the absorption coefficient actually exhibits fine structure, the so-called **X-ray Absorption Fine Structure** (XAFS).

Isolated atoms

For isolated atoms (noble gases, metallic vapors) the XAFS is limited to a few eV around the edge, and reflects the transitions of the core electron to unoccupied bound levels (Rydberg levels).

The left panel of Fig. 1.4 refers to a very restricted energy region around the K edge of Argon. The transitions to Rydberg levels give rise to lorentzian-shaped structures (dotted peaks in the figure), whose width is due to the energy uncertainty of the excited core state, and is of the order of the eV,

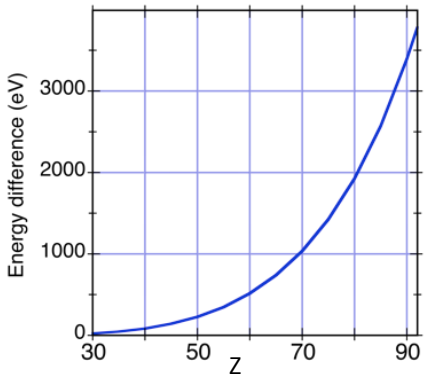

Figure 1.3: Spin-orbit splitting of the L_2 and L_3 edges as a function of the atomic number Z.

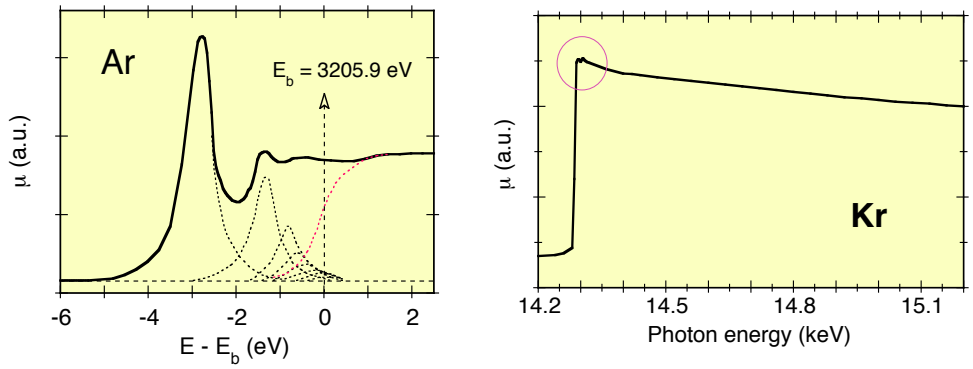

Figure 1.4: Fine structures at the K edges of Argon (left, continuous line) from ref. [Parrat, 1939] and Krypton (right).

much larger than the typical width for optical transitions. The ionisation threshold corresponds to the upper limit of the Rydberg series; the step-like behaviour of the threshold is transformed into an arctangent curve by effect of the excited core state width. The value $E_b = 3205.9$ eV was determined by best fitting the theoretical calculations to the experimental spectrum.

The right panel of Fig. 1.4 refers to an extended energy region around above the K edge of Krypton. The fine structure due to the transition to Rydberg levels reduces to the small peaks at the edge (within the circle), as effect of the excited core state width, which increases with the atomic number, and is thus larger than for Argon. The behaviour of the absorption coefficient above the edge is perfectly smooth, as expected for isolated atoms.

Molecules and condensed systems

In molecular gases and condensed systems, the XAFS, strongly influenced by the presence of the atoms surrounding the absorber one, can extend up to and beyond one thousand eV above the edge.

The left panel of Fig. 1.5 refers to the K edge edge of molecolar N_2. In addition to the transitions to atomic Rydberg levels in the region between 405 and 410 eV (whose amplitude has been enlarged 10 times), which converge to the ionisation threshold, other phenomena contribute to the XAFS, such as transitions to vibrationally excited states (pre-edge structures between 400 and 402 eV), double excitations (around 415 eV) and the so-called shape resonances (bump at about 420 eV).

The right panel of Fig. 1.5 refers to the K edge of crystalline germanium. Here the fine structure can be observed up to at least 1000 eV above the edge

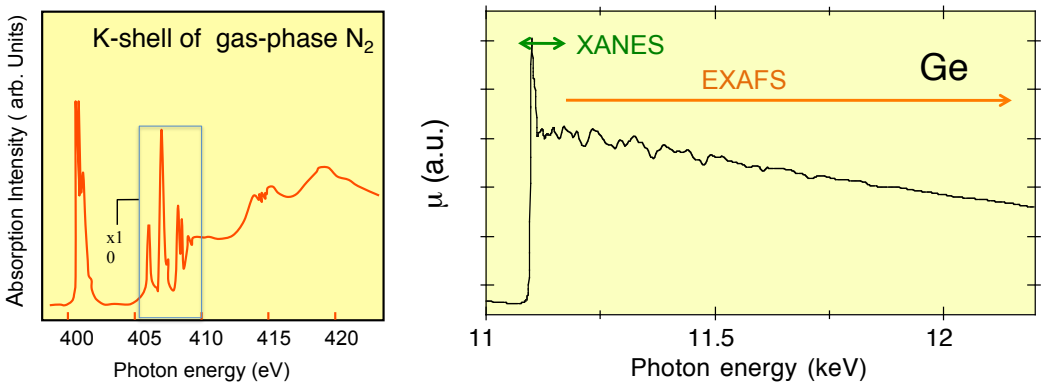

Figure 1.5: Fine structures at the K edges of molecular N_2 (left) from ref. [Chen et al., 1989] and crystalline Germanium (right).

Nomenclature

XAFS is customarily divided into two regions.

1. The structure within 30÷50 eV above the edge is called **XANES** (X-ray Absorption Near Edge Structure) or **NEXAFS** (Near Edge X-ray Absorption Fine Structure). From the XANES, information can be obtained on the local electronic as well as geometric structure. Sometimes, the features within a few eV around the edge are distinguished as *pre-edge structure* and *edge structure*.

2. The fine structure extending from the XANES region up to typically one thousand eV is called **EXAFS** (Extended X-ray Absorption Fine Structure). EXAFS carries information on the local geometric structure surrounding a given atomic species. The interpretation of EXAFS is nowadays quite well established, and easier than the interpretation of XANES.

Although the fine structures at the X-ray absorption edges had been detected since 1918-1919, and their first interpretation dates back to the thirties, it is only with the availability of high intensity synchrotron radiation beams at the end of the sixties and the development of a simple interpretation procedure for EXAFS at the beginning of the seventies that XAFS has become a widespread technique.

1.3 Interpretation of XAFS: XANES and EXAFS

An experimental X-ray absorption coefficient contains the contributions due to the excitation of different electronic shells. Let us consider, for example, the left panel of Fig. 1.2. For photon energies of 20 keV, electrons belonging to the 2s, 2p, 3s, 3p, 3d... levels can be excited, but not 1s electrons. For photon energies of 80 eV, the 1s electrons can be excited too.
For an effective interpretation of XAFS, it is convenient to consider the contribution to the absorption coefficient of only one core level, for example the 1s level (Fig. 1.4). The contribution from the 1s electron is zero below the K edge energy. The procedure for singling out the contribution of a given core electronic level from an experimental spectrum is depicted in the following chapters.
The basic behaviour of the absorption coefficient and of its fine structure at a given absorption edge can generally be interpreted in terms of a one electron process; non-negligible contributions can, however, come also from many-electron excitations.

The photoelectric absorption of X-rays can be satisfactorily accounted for by a mixed approach, where the atom is described in quantum mechanical terms, and the electromagnetic field is described within the classical approximation. The interaction between an atom and the electromagnetic field is treated within the framework of the time-dependent perturbation theory, which to first order leads to the so-called “golden rule”.

1.3.1 Final one-electron states and local structure

According to the golden rule, the absorption coefficient is proportional to the square of the matrix element of the interaction Hamiltonian connecting the atomic stationary state before the interaction (initial state) and the atomic stationary state after the interaction (final state). Since the initial state is the atomic ground state, independent of the photon energy, the fine structure of the absorption coefficient can be attributed only to the final state. Let us here qualitatively consider the final states as a function of the photon energy. For simplicity, only one-electron transitions are considered.

Isolated atoms

For an isolated atom, when the photon energy is lower than the photo-ionisation energy, the final one-electron states are the discrete Rydberg levels. The absorption coefficient is different from zero only when the photon energy corresponds to an allowed transition from core to Rydberg levels. For an isolated atom, when the photon energy is higher than the photo-ionisation energy, the final states are a continuum of free-electon states, and the absorption coefficient has no fine structure. For isolated atoms, the study of the X-ray absorption coefficient has little practical use.

Molecules and condensed systems

By far more important is the study of XAFS when the absorbing atom is embedded in a molecule or in a condensed system.
The discrete spectrum below the absorption edge can be now enriched by new final-state possibilities, due for example to vibrational properties of molecules, exciton levels in semiconductors, and so on.
Also for photon energies higher than the photo-ionisatione energy is the final state influenced by the environment of the absorbing atom. As a consequence, the XAFS reflects the modifications of the electronic structure induced by the local environment, which is in turn connected to the local geometric structure. Calculating the final state for the photo-electron within some 20 to 30 eV above the absorption edge is generally far from trivial. Two main approaches, in principle equivalent, are possible, one based on the molecular orbital theory, the other based on the theory of electron multiple scattering. Both approaches allow us to establish a connection between XAFS and local structure.
The most relevant advantage of the scattering approach is that, for photo-electron energies higher than say 20 to 30 eV, single scattering events are predominant in determining the final state, and multiple scattering events are generally negligible. The treatment of single scattering is relatively simple, and leads to the possibility of interpreting the XAFS in terms of an analytical expression depending on a few structural parameters.
The distinction of the two regions, XANES and EXAFS, in the absorption spectra can thus be explained in terms of the different possible approaches. In the EXAFS region the XAFS can be interpreted in terms of single scattering by a relatively easy formalism, which is considered in the following chapters; a phenomenological introduction to EXAFS is given immediately below. In the XANES region the interpretation of XAFS requires taking into account multiple scattering effects, or sometimes, alternatively, a molecular orbital approach.

Introductions to XAFS spectroscopy at different levels of difficulty and with different balance between theoretical and experimental issues are available in a number of excellent papers and books [Als-Nielsen and McMorrow, 2011, Brown and Doniach, 1980, Lee et al., 1981, Hayes and Boyce, 1982, Borovskii et al., 1986, Teo, 1986, Koningsberger and Prins, 1988, Stöhr, 1996, Rehr and Albers, 2000, Bunker, 2010].

1.3.2 A phenomenological introduction to EXAFS

A simple phenomenological picture is often used to explain the origin of EXAFS (Fig. 1.6) within the framework of the single scattering approach. When an X-ray photon of high enough energy is

absorbed by an atom, a core electron is ejected from the atom (ionization process). The kinetic energy of the photo-electron is the difference between the photon energy and the core binding energy. The outgoing photo-electron is described by a wave-function, approximated by a spherical wave in Fig. 1.6, whose wavelength decreases when the photon energy increases. If the absorber atom is not isolated, the photo-electron can be back-scattered by neighboring atoms, giving rise to an incoming spherical wave. The phase relationship between outgoing and incoming waves depends on the photo-electron wavelength and on the inter-atomic distance. The final photo-electron stationary state is thus the superposition of the outgoing spherical wave and the incoming back-scattered wave.
The variation of phase relationship as a function of photon energy influences the final state amplitude at the core site, giving rise to an interference phenomenon which modulates the absorption coefficient. The *frequency* of EXAFS oscillations depends on the *distance* between absorber and back-scatterer atoms. Their *amplitude* is proportional to the number of back-scatterer atoms.

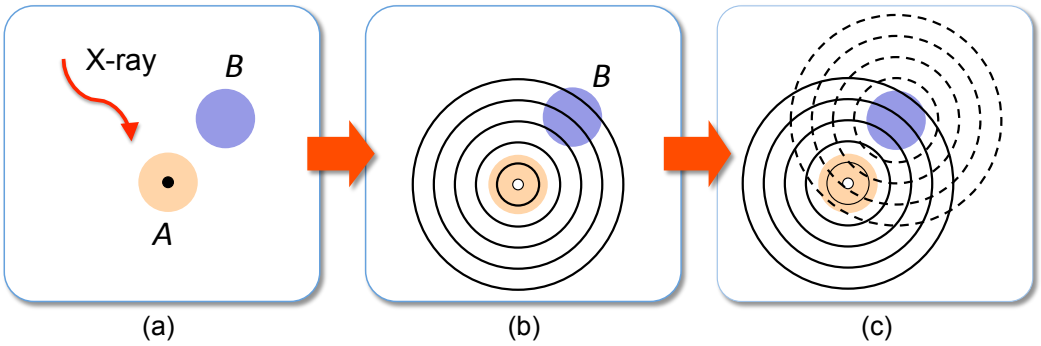

Figure 1.6: Schematic explanation of the EXAFS phenomenon: absorption of an X-ray photon by atom A (left), emission of the photo-electron wave (center), back-scattering of the photo-electron by atom B (right).

1.4 More on EXAFS

Two main peculiarities characterize EXAFS as a structural probe:

1. the *selectivity of atomic species*, which is achieved by tuning the X-ray energy to the corresponding absorption edge;
2. the *insensitivity to long-range order*, due to both the spherical nature of the photoelectron wave and the short mean free path of the photo-electron, typically limited to about 10 Å.

1.4.1 The EXAFS function

The EXAFS oscillations are generally expressed by the normalised adimensional function

$$\chi(k) \;=\; \frac{\mu - \mu_0}{\mu_0}\,. \tag{1.4}$$

An example of EXAFS function is given in Fig. 1.7 (right). In (1.4),

a) k is the wavenumber of the photoelectron, defined as

$$k \;=\; \sqrt{(2m/\hbar^2)\;(\hbar\omega - E_b)}\,, \tag{1.5}$$

where $\hbar\omega$ is the photon energy andE_b is the core electron binding energy;
b) μ is the measured absorption coefficient (red line in Fig. 1.7, left),
c) μ_0 is the absorption coefficient of an isolated atom (blue line in Fig. 1.7, left).

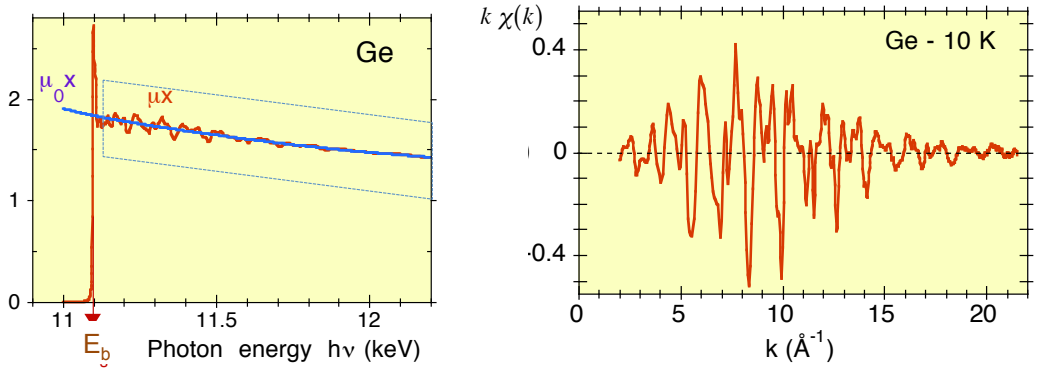

Figure 1.7: Left: experimental absorption coefficient μx at the K edge of Germanium, measured at $T = 10\,\mathrm{K}$ and plotted in arbitrary units as a function of the photon energy $h\nu = \hbar\omega$. Right: corresponding k-weighted EXAFS function $k\,\chi(k)$ plotted as a function of the photo-electron wavenumber k.

1.4.2 Basic information from EXAFS

The basic information that can be obtained from the analysis of EXAFS spectra concerns a few coordination shells surrounding the absorbing atom (typically within about 10 Å). The EXAFS function shown in Fig. 1.7 (right) is the superposition of the contributions of several coordination shells.

The contribution of each coordination shell is a sinusoidal-like function, such as those depicted in Fig. 1.8. For each coordination shells one can in principle obtain at least three important parameters:

1. The average inter-atomic distance $\langle r \rangle$, which is proportional to the frequency of the EXAFS oscillations (Fig. 1.8, left).
2. The coordination number N, which is proportional to the amplitude of the EXAFS signal (Fig. 1.8, centre).
3. The degree of local disorder, of both thermal and structural origin, measured by a Debye-Waller factor $\exp(-2k\sigma^2)$, which is responsible of the damping of the EXAFS signal (Fig. 1.8, right).

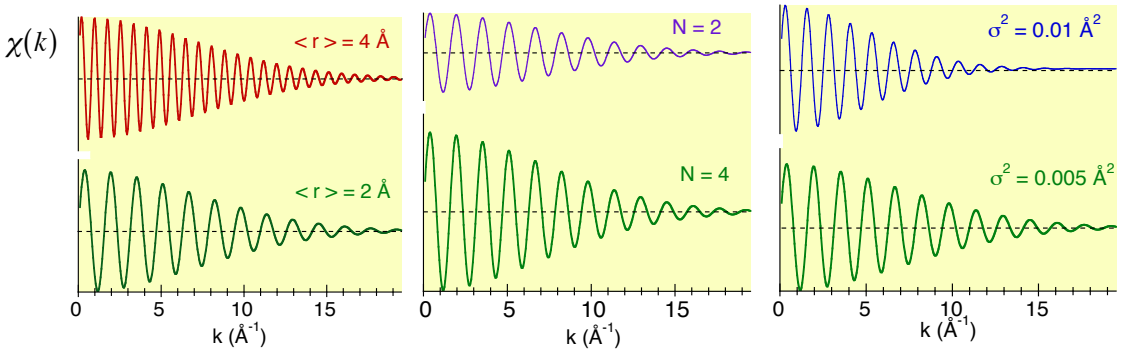

Figure 1.8: Basic information from EXAFS of a given coordination shell: the frequency is proportional to the inter-atomic distance (left), the amplitude is proportional to the coordination number (centre), the damping depends on the degree of thermal and structural disorder (right).

To get the values of the above parameters, $\langle r \rangle$, N and σ^2, from experimental spectra is far from immediate. The interaction of the photo-electron with both the emitting and the back-scattering atoms, as well as the non-negligible many-body effects have to be properly taken into account.

This task is nowadays accomplished with a good degree of accuracy by easily available theoretical computer codes, often supported by friendly data analysis codes.

The quantity and quality of information that can be obtained from an EXAFS spectrum depends on the quality of experimental data and on the number of available oscillations, say on the length of the signal. To allow an accurate quantitative analysis, the signal should extend to at least $k \simeq 15\,\text{Å}^{-1}$, corresponding to photon energies extending at least 900 eV above the edge.
This is in principle always possible for EXAFS measured at the K edges, unless the available spectrum is upper limited by the edge of another element present in the sample. The situation is different for L edges. EXAFS at the $L_{|||}$ edge can be severely limited by the presence of the $L_{||}$ edge; EXAFS at the $L_{|}$ edge can be contaminated by the residual EXAFS at the $L_{||}$ edge. These limitations are particularly strong for light elements, where the L edges are quite close in energy, and progressively relax for heavier elements (see Table 1.2).

1.4.3 Typical EXAFS applications

EXAFS is a very appealing local structural probe in some particular cases.

Local structure in non-crystalline materials. EXAFS gives complementary information with respect to elastic scattering of X-rays or neutrons. EXAFS is particularly useful for many-atomic materials, like semiconductor amorphous alloys or oxide glasses, thanks to the possibility of selecting the atomic species. (The interpretation of elastic scattering patterns for many-atomic non-crystalline materials is instead quite complicated). A peculiar advantage of EXAFS is the possibility of directly comparing the spectra of one given material in both crystalline and amorphous states, due to the insensitivity of EXAFS to long range order.

Local environment of atoms in eterogeneous matrices. This is the typical case of heterogeneous catalysts, active sites in biomolecules, impurities in semiconductors, luminescent rare-earth atoms in crystals and glasses. The active site is here represented by atoms or small clusters randomly dispersed in a matrix of different atomic species, also often disordered.

Systems with local properties different from average properties. In some crystalline systems such as solid ternary random solutions $A_xB_{1-x}C$, the distances between nearest-neighbours atoms are different according to the different species constituting the pair: AB, BC, AC. When the concentration x is varied, Bragg diffraction, sensitive only to long range order, measures the variation of the average interatomic distance, while EXAFS, selective of atomic species and sensitive to short range order, is able to discriminate the different behaviour of each atomic pair.

Local dynamics in crystalline solids. By performing temperature dependent EXAFS measurements, one can get original information on the local vibrational dynamics. In the case of crystalline solids, the sensitivity to the correlation of vibrational motion makes EXAFS a complementary technique to diffraction. EXAFS measures the *true* bond expansion of interatomic bonds and the mean square *relative* displacements of atomic pairs, while diffraction measures the *apparent* bond thermal expansions and the *absolute* mean square displacements of atoms. The joint use of EXAFS and diffraction has been recently exploited for the study of the local origin of negative thermal expansion in some crystalline solids.

Chapter 2

Photoelectric absorption of X-rays

This Chapter is dedicated to a study of the process of photo-absorption of X-rays by isolated atoms. The aim is to find a convenient expression of the absorption coefficient experimentally measured as a function of X-ray photons energy in terms of the initial and final states of the system atom-radiation, through a series of reasonable approximations. The effect of the atomic environment surrounding the absorbing atom, which gives rise to XAFS, is considered in the subsequent Chapter 3.
For photon energies between 1 and 30 keV, the leading interaction with matter is photo-electric absorption (Fig. 1.1); the total absorption coefficient μ introduced in Eq. (1.1) corresponds thus with a good approximation to the photo-electric absorption coefficient. From now on, we refer to μ as "absorption coefficient".
In Section 2.1 some useful phenomenological definitions are presented.
In Section 2.2 we seek for a general expression connecting the experimentally measured absorption coefficient $\mu(\omega)$, or equivalently the absorption cross section $\sigma_a(\omega)$, to the initial stationary quantum state of an atom (typically the ground state) and its possible final stationary states after the absorption of radiation (excited or ionised states).
In Section 2.3 a first important approximation is introduced, the time-dependent perturbation theory, which leads to the famous "Golden rule".
In Section 2.4, various further approximations are introduced in order to simplify the calculation of the absorption coefficient in most of the cases of real interest.
Section 2.5 is dedicated to an introduction to the processes of de-excitation of an atom, which follow the excitation due to the absorption of electromagnetic radiation.

2.1 Phenomenological considerations

Before going into the mathematical details of the interaction of X-rays with atoms, it is convenient to carefully introduce the physical quantities which enter in the phenomenological definition of the experimentally measured absorption coefficient.

2.1.1 Energy flux and photon flux

To measure the absorption coefficient, the intensity of the X-ray beam impinging on the matter sample and outgoing from it has to be conveniently measured. We compare here the two alternative possibilities, based on the complementary wave and particle approaches, respectively.
In spectroscopy experiments, one typically deals with monochromatic beams; actually, real beams are never perfectly monochromatic, the frequency being confined within a narrow interval $\Delta\nu$ around a nominal value ν_0. In the following, we will generally consider the behaviour of single-frequency plane electromagnetic waves; this shouldn't be considered a limitation, since real beams can be considered as a convenient superposition of different plane waves.

Furthermore, in the following we will substitute the frequency ν (measured in s^{-1}) by the angular frequency $\omega = 2\pi\nu$ (measured in $rad\,s^{-1}$). For short, the angular frequency ω will be simply referred to as frequency.
Electromagnetic waves consist in coupled electric and magnetic fields $\vec{E}$ and $\vec{B}$ perpendicular to the direction of propagation, with $\vec{E} \perp \vec{B}$ and $B = E/c$ (SI units). For monochromatic plane waves,

$$E = E_0 \cos(\vec{k}\cdot\vec{r} - \omega t)\,, \qquad k = \omega/c\,. \tag{2.1}$$

The wave point of view

The intensity of the X-ray beam can be expressed in terms of its energy density u (energy per unit volume, $J\,m^{-3}$). The energy density stored at a given time in a given point of an electromagnetic wave can be expressed as a function of the electric and magnetic fields as [Feynman et al., 1977]

$$u = \epsilon_0 E^2/2 + \epsilon_0 c^2 B^2/2 = \epsilon_0\, E^2 \tag{2.2}$$

(since $B = E/c$). In (2.2), ϵ_0 is the vacuum permittivity.
For a sinusoidal electromagnetic wave (2.1), the average energy density $\langle u\rangle$ is

$$\langle u\rangle = \epsilon_0\langle E^2\rangle = \epsilon_0 E_0^2/2\,. \tag{2.3}$$

For a number of applications, it is convenient to express the electric and magnetic fields $\vec{E}$ and $\vec{B}$ in terms of the scalar and vector potentials U and $\vec{A}$ (see Appendix A and [Feynman et al., 1977]), according to the general relations:

$$\vec{E} = -\vec{\nabla}U - \partial\vec{A}/\partial t\,, \qquad \vec{B} = \vec{\nabla}\times\vec{A}\,. \tag{2.4}$$

Different choices of the potentials are possible which give the same electric and magnetic fields. We refer here to the choice corresponding to the *Coulomb gauge*, characterised by $\vec{\nabla}\cdot\vec{A} = 0$. In addition, for an electromagnetic wave in vacuum we can neglect the static effects of electric charges, so that $U = 0$ (*radiation gauge*). This choice is justified by the fact that, as we will see below, the quantum treatment of the interaction between radiation and matter is better done if the electromagnetic waves are described in terms of the vector potential $\vec{A}$ within the radiation gauge.
In the radiation gauge, the relation between the electric field and the vector potential is simply $\vec{E} = -\partial\vec{A}/\partial t$. Besides, for a sinusoidal plane wave 2.3, also the vector potential has a sinusoidal behaviour,

$$A = A_0 \sin(\vec{k}\cdot\vec{r} - \omega t)\,, \quad A_0 = -E_0/\omega\,. \tag{2.5}$$

The average energy density 2.3 of a monochromatic electromagnetic plane wave of angular frequency ω can thus be expressed in terms of the amplitude of the vector potential as

$$\langle u\rangle = \epsilon_0\omega^2 A_0^2/2\,. \tag{2.6}$$

In the wave picture, the flux Φ of an X-ray beam is measured by the energy crossing the unit section of the beam in the unit time (SI units $J\,m^{-2}\,s^{-1}$):

$$\Phi = \langle u\rangle\, c\,, \tag{2.7}$$

where c is the speed of light.
The absorption coefficient μ measures the progressive reduction of the average energy density $\langle u\rangle$ due to the photoelectric absorption by matter:

$$\mu(\omega) = -\frac{1}{\langle u\rangle}\,\frac{d\langle u\rangle}{dx}\,. \tag{2.8}$$

By separating the variables in (2.8) and integrating over the sample thickness x, one obtains

$$\ln\langle u\rangle_{\rm out} - \ln\langle u\rangle_{\rm in} = -\mu\, x \tag{2.9}$$

and, taking into account (2.7),

$$\mu(\omega) \;=\; \frac{1}{x}\,\ln\frac{\Phi_{\rm in}}{\Phi_{\rm out}} \qquad \text{say} \qquad \Phi_{\rm out} = \Phi_{\rm in}\,\exp[-\mu x]\,. \tag{2.10}$$

Experimentally, μ is obtained by measuring the beam intensities $\Phi_{\rm in}$ and $\Phi_{\rm out}$ immediately before and after the matter sample of thickness x.
The absorption coefficient $\mu(\omega)$ depends on the frequency ω of the X-rays, as well as on the atomic species and the density of the sample. Its dimension is an inverse length.

The particle point of view

In the absorption and emission of electromagnetic radiation by matter, energy is exchanged by quanta, say photons of energy $\hbar\omega$. When studying X-ray absorption processes, it is generally more convenient to express the flux of the X-ray beam in terms of the number of photons of a given energy crossing the unit area in the unit time. Inserting (2.6) into (2.7), and taking into account that the photon energy is $\hbar\omega$, the flux measured in terms of photons is

$$\Phi \;=\; \frac{\epsilon_0\omega^2 A_0^2 c/2}{\hbar\omega} \;=\; \frac{\epsilon_0\omega A_0^2 c}{2\hbar} \tag{2.11}$$

and the absorption coefficient is again expressed by (2.10).

Note 1: The fluxes Φ in (2.7) and (2.11) correspond to the same physical phenomenon but are measured in different units, $\mathrm{J\,m^{-2}s^{-1}}$ the first one, $\mathrm{m^{-2}s^{-1}}$ the second one.

Note 2: In principle, the quantisation in terms of photons only describes the exchange of energy between radiation and matter. Considering the X-ray beam as a particle beam requires some clarification. Actually, a perfectly monochromatic plane wave has no spatial localisation, and is incompatible with a particle picture. However, as already observed, X-ray beams are never perfectly monochromatic. Relative frequency spreads $\Delta\omega/\omega$, mainly determined by the band-pass of crystal monochromators (Chapter 5), are typically of the order of 10^{-4}. The energy uncertainty corresponds to a momentum uncertainty, which reduces the position uncertainty and allows the description of the beam in terms of a superposition of localised wave-packets, say of photons.
For example, for E=30 keV, an energy uncertainty ΔE=3 eV corresponds to a position uncertainty along the beam direction $\Delta z \simeq 650$ Å.

2.1.2 The absorption coefficient

Atomic absorption cross section

For a monatomic sample, the macroscopic linear absorption coefficient $\mu(\omega)$ is connected to the atomic photo-absorption cross section $\sigma_a(\omega)$ through the relation

$$\mu(\omega) \;=\; \frac{N_a\,\rho}{A}\,\sigma_a(\omega) \;=\; n\,\sigma_a(\omega)\,, \tag{2.12}$$

where N_a is the Avogadro number, ρ is the mass density, A is here the atomic mass and n is the atomic number density (number of atoms per unit volume). The cross section σ_a has the dimension of an area.

The mass absorption coefficient

For each atomic species, one can find tabulated [Hubbell and Seltzer, 1996, Thomson et al., 2009, NIST, 2004] the mass absorption coefficient μ/ρ as a function of the X-rays energy $\hbar\omega$ or of the wavelength λ,

$$\frac{\mu}{\rho} \;=\; \frac{\sigma_a\;N_a}{A}\,. \tag{2.13}$$

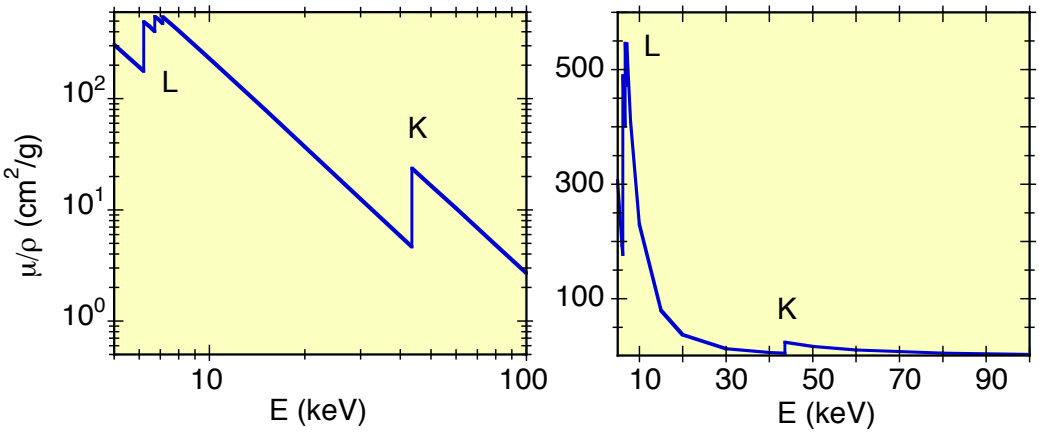

Figure 2.1: Mass absorption coefficient μ/ρ for 60-Nd plotted with logarithmic scales (left) and with linear scales (right).

Once the mass absorption coefficient (μ/ρ) is known, the flux attenuation law (1.1) for a given sample of density ρ can be evaluated by [Bertin, 1975]

$$\Phi_{\text{out}} = \Phi_{\text{in}} \exp\left[-\left(\frac{\mu}{\rho}\right) \rho\, x\right] . \tag{2.14}$$

Example: Let us consider an X-ray beam of wavelength $\lambda = 1\,\text{Å}$ (energy 12.4 keV) impinging on a sample of 32-Ge. From the absorption tables one can find that, for $\lambda = 1\,\text{Å}$, $\mu/\rho = 162.75\,\text{cm}^2/\text{g}$. Since $\rho = 5.46\,\text{g/cm}^3$ and $n = 4.41 \times 10^{22}\,\text{cm}^{-3}$, the atomic absorption cross section is $\sigma_a \simeq 2 \times 10^{-4}\,\text{Å}^2$.

The mass absorption coefficient for X-rays, (μ/ρ), is an atomic property of each element, largely independent of the state of aggregation [Bertin, 1975]. This is due to the fact that the photo-absorption of X-ray involves the electronic core levels, which are not affected by the state of aggregation.
This is generally not the case for lower energy electromagnetic radiation, whose absorption involves external energy levels, which in turn depend on the aggregation state.

Chemical compounds

For a chemical compound $P_x\,Q_y\ldots$ the total mass absorption coefficient can be decomposed into the weighted sum of the contributions of each atomic species,

$$\left(\frac{\mu}{\rho}\right)_{\text{tot}} = x \left(\frac{\mu}{\rho}\right)_P \frac{A_P}{M} + y \left(\frac{\mu}{\rho}\right)_Q \frac{A_Q}{M} + \ldots \tag{2.15}$$

where M is the molecular mass of the compound, A_i are the atomic masses of the components.
The additive rule (2.15), valid for X-rays, cannot be applied to the absorption of lower energy electromagnetic radiation (infrared, optical and ultraviolet).

Empirical behaviour of the mass absorption coefficient

In the energy interval between two contiguous absorption edges, the absorption coefficient decreases when the photon energy $\hbar\omega$ increases (Fig. 2.1).
The photoelectric behaviour is generally well described by the empirical *Victoreen law*:

$$\mu/\rho = C\,\lambda^3 - D\,\lambda^4 \tag{2.16}$$

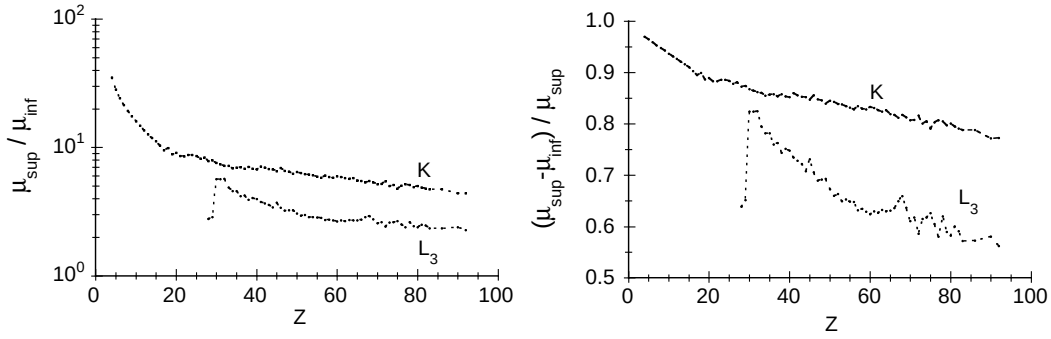

Figure 2.2: Jump ratio $r = \mu_{\rm sup}/\mu_{\rm inf}$ (left) and relative contribution to the absorption, $(\mu_{\rm sup} - \mu_{\rm inf})/\mu_{\rm sup} = 1 - 1/r$ (right).

where the parameters C and D depend on the atomic number Z and, for the same atomic species, can slightly differ for the intervals between different edges.
An alternative approximation for the photoelectric absorption is the Bragg-Pierce law

$$\mu/\rho = K' \, Z_m \, \lambda^n \,, \tag{2.17}$$

where K' is different for different elements and for intervals between different edges, $m \simeq 4$ and $n \simeq 3$.

The energy of the absorption edges increases when the atomic number Z increases (Fig. 1.2, right).

Jump ratios

At an absorption edge, the absorption coefficient abruptly jumps from a lower value $\mu_{\rm inf}$ to a higher value $\mu_{\rm sup}$. The difference $\delta\mu = \mu_{\rm sup} - \mu_{\rm inf}$ represents the *absolute* contribution to the absorption due to the excitation of an electron from a core level. The jump difference δ depends on Z and for a given element is larger for the L edges than for the K edge (Fig. 2.1, right).
The *relative* contribution to the absorption is expressed by $(\mu_{\rm sup} - \mu_{\rm inf})/\mu_{\rm sup} = 1 - 1/r$, where $r = \mu_{\rm sup}/\mu_{\rm inf}$ is the so-called *jump ratio*. The jump ratios r depend on the atomic number Z. The relative contribution to photoelectric absorption for a given element is larger for the K edge than for the L_3 edge (Fig. 2.2, right) [Bertin, 1975].

Half-thickness

A useful measure of the attenuation of an X-ray beam in a specific medium is the *half-value thickness* or *half-thickness*, say the sample thickness required to reduce by one-half the incident flux [Bertin, 1975], so that $\Phi_{\rm out} = \Phi_{\rm in}/2$.
From (2.14) one easily finds that the half-thickess is

$$x_{1/2} \;=\; \frac{\ln 2}{\mu} \;=\; \frac{0.693}{(\mu/\rho)\,\rho} \,. \tag{2.18}$$

The half-thicknesses of some substances at selected X-ray energies are listed in Table 2.1.

2.2 Interaction of an atom with the electromagnetic field

The photo-electric absorption of radiation by matter is a genuine quantum phenomenon and necessarily requires a quantum approach.

Table 2.1: Half-thickness (cm) for selected substances at selected X-ray wavelengths.

$\hbar\omega$ (keV)	Air	Mylar	Be	Al	Cu	Pb	
	0.0012	1.39	1.85	2.7	8.96	11.34	density (g/cm^3)
5	14.05	0.018	0.0085	0.001	0.0005	8.3e-5	
20	727.33	0.860	1.6641	0.075	0.0023	0.0007	
50	2719.8	2.468	2.4105	0.697	0.0296	0.0076	

2.2.1 The physical systems

For a general treatment of the interaction of electromagnetic radiation with matter, we should consider a quantum system composed of two subsystems: the atom and the electromagnetic field. The interaction process corresponds to a transition from an initial stationary state of the full system (matter + field) to a final stationary state of the full system (matter + field). During the transition, different events can take place, corresponding to the absorption, emission or scattering of electromagnetic radiation. In any case, the initial and final states of the full system have the same energy.

We are interested here in an absorption event, where a photon of the electromagnetic field disappears and its energy $\hbar\omega$ is employed to excite or ionise the atom. The absorption of X-rays typically concerns many-electron atoms, for which the binding energies of the innermost electrons are comparable with the energies of X-ray photons.

To describe the *photo-absorption* process, the quantum treatment of the electromagnetic field is not strictly necessary. One can rely on a semi-classical approach, were the atom is treated as a quantum system and the electromagnetic field is treated classically.

It is worth noting that a semi-classical approach cannot instead fully account for the reverse process, say the process of *photo-emission*: the semiclassical approach accounts only for the stimulated emission of electromagnetic radiation, the explanation of spontaneous emission requires a full quantum approach [Bransden and Joachain, 2003].

In the following, we shortly recall the description of the separate sub-systems: atom (§ 2.2.2) and electromagnetic field (§ 2.2.3); for the electromagnetic field, we consider both the classical and quantum descriptions. The interaction between atom and field is finally considered in § 2.2.4.

2.2.2 Quantum description of an isolated atom

For an N-electron isolated atom or ion, in the absence of the electromagnetic field, the time-independent hamiltonian is

$$H_0 = \sum_{j=1}^{N} \frac{P_j^2}{2m} + V \,, \tag{2.19}$$

where the sum is over all the N electrons; $\vec{P}_j$ is the generalised momentum of electron j, canonically conjugated to its position $\vec{r}_j$; for the isolated atom, the generalised momentum of each electron $\vec{P}_j$ is equal to the mechanical momentum $m\vec{v}_j$. The potential energy V is the sum of a number of terms of different importance (Coulomb interactions, spin-orbit interactions, spin-spin interactions and so on).

By solving the time-independent Schrödinger equation

$$H_0 \,|\Psi_s\rangle = E_s \,|\Psi_s\rangle \tag{2.20}$$

one obtains the stationary eigenstates $|\Psi_s\rangle$ of the many-electron atom and the corresponding energies E_s. The stationary state of the lowest energy is the ground state.

Note: By E_s and $|\Psi_s\rangle$ we refer here synthetically to both discrete atomic states, where all electrons

are bound, and continuum atomic states, where at least one electron is free.

The apparent simplicity of the Dirac notation of (2.20), where the atomic state is synthetically represented by a state vector $|\Psi\rangle$ defined in an abstract Hilbert space, should not mislead.

Independent electrons approximation

Actually, the solution of (2.20) is possible only at the expenses of a number of approximations. Its meaning is better grasped in the coordinate representation, where the state of the atom is represented by a wavefunction.
If only Coulomb interactions are considered, the Hamiltonian of eq. 2.19 can be written explicitly as

$$H_0 = \sum_j \frac{P_j^2}{2m} \; - \; \sum_{i=1}^{N} \frac{Ze^2}{4\pi\epsilon_0\, r_j} \; + \; \sum_{j=1}^{N} \sum_{i=1}^{j-1} \frac{e^2}{4\pi\epsilon_0\, r_{ji}}\,, \tag{2.21}$$

where $N = Z$ for a neutral atom.
The second sum in (2.21) is the central potential energy due to the attractive interaction of the electrons with the nucleus. The third sum is the non-central potential energy due to the repulsion between each pair of electrons.
The solution of (2.20) is generally performed within the independent electrons approximation, where each electron moves within an effective central potential which takes into account the attraction of the nucleus and the average effect of the mutual interactions between the electrons.
Within this approximation, the total wavefunction Ψ of the atom can be factorised as the product of the independent spin-orbitals of the single electrons. This leads to the well known shell and subshell electrons configurations: $1s^2$, $2s^2$, $2p^6$, $3s^2$, and so on.
To take into account the Pauli exclusion principle, each N-electron atomic eigenfunction Ψ_s is represented, in the coordinate representation, as a Slater determinant, say an antisymmetric sum of $N!$ products of N individual spin-orbitals. The effective potential energy and the single electron spin-orbitals can be determined by variational methods, such as the Hartree-Fock-Slater one.
For more details, see Chapter 8 of [Leighton, 1959], Chapter 4 of [Alonso and Finn, 1969] or Chapter 8 of [Bransden and Joachain, 2003].

Transitions between stationary states

The most general quantum state of the isolated atom is a linear combination of stationary eigenstates,

$$|\mathbf{\Phi}(t)\rangle \;=\; \sum_s b_s\, e^{-iE_s t/\hbar}\, |\Psi_s\rangle \tag{2.22}$$

where the time-dependence of each stationary state $|\Psi_s\rangle$ is the trivial one $\exp(-iE_s t/\hbar)$.

In the following we will be mainly concerned with initial and final states corresponding to simple stationary states,

$$|\mathbf{\Phi}_i(t)\rangle \;=\; e^{-iE_i/\hbar}|\Psi_i\rangle\,; \qquad |\mathbf{\Phi}_f(t)\rangle \;=\; e^{-iE_f/\hbar}\,|\Psi_f\rangle\,. \tag{2.23}$$

The interaction with the electromagnetic field induces a transition from an initial stationary state to a final stationary state; as we will see, to describe the time dependence of $|\mathbf{\Phi}(t)\rangle$ one requires that also the coefficients b_s in (2.22) be time-dependent: $b_i(t)$ and $b_f(t)$.

Atomic energy levels and X-ray absorption edges

Within the effective central potential approximation considered above, the electrons belonging to the same subshell (same principal and orbital quantum numbers, n and ℓ, respectively) share the same energy.
The central potential approximation cannot however completely account for the effect of electrons repulsion. If the residual repulsive interaction, as well as other minor contributions to the potential

energy, such as the spin-orbit interaction, are taken into account, the energy levels of the electrons are shifted with respect to the values of the central potential approximation.

If the non-central contribution to the reciprocal electrostatic repulsion is considered, only the atomic angular momentum $\vec{L} = \sum \vec{\ell}_j$ and atomic spin momentum $\vec{S} = \sum \vec{s}_j$ are conserved, not the momenta of single electrons. In addition, different reciprocal orientations of $\vec{L}$ and $\vec{S}$ give rise to different values of the total atomic angular momentum $\vec{J} = \vec{L} + \vec{S}$ and different contribution to the total atomic energy due to spin-orbit effects. That's why the the spectroscopic terms that label the atomic energy levels depend on the values of L, S and J.

For a completely filled subshell, one has $L = 0, S = 0, J = 0$, and the spectroscopic term is ${}^1S_0$, where the letter S corresponds to $L = 0$, the apex 1 indicates the singlet for $S = 0$ and the index 0 stays for $J = 0$.

An incompletely filled subshell (such as $2p^4$ or $3d^6$) can contribute in different ways to the total atomic energy, according to the different possible values of L, S and J. These differences are reflected in the corresponding spectroscopic terms.

These considerations are here relevant for understanding some peculiarities of the X-ray absorption edges, such as the energy difference between the L_2 and L_3 edges. Let us consider the photoionisation of different deep core electrons of a many-electron atom, induced by X-ray absorption. In the initial atomic state the deep subshells ($1s^2$, $2s^2$, $2p^6$, ...) are completely filled; to each subshell it thus corresponds a term ${}^1S_0$. In the final state one of the deep subshells is laking one electron ($1s^1$ or $2s^1$ or $2p^5$ ...) and the assignment of the corresponding term requires some attention.

Let us focus on the most common situations, say the K and L edges (see also Chapter 4 of [Alonso and Finn, 1969]).

a) **K and L_1 edges.** For both edges, an electron is extracted from a completely filled ns^2 shell (where n=1 and n=2 for the K and L_1 edges, respectively) corresponding to L=0, S=0, J=0, say to a term ${}^1S_0$.
After the X-ray absorption, the final state of the ionised shell, ns^1, corresponds to L=0, S=1/2, J=1/2, say to a term ${}^2S_{1/2}$.

b) **L_2 and L_3 edges.** For both edges, the initial state of the completely filled shell $2p^6$ corresponds to L=0, S=0, J=0, say to a term ${}^1S_0$.
After the X-ray absorption, the final state of the ionised subshell $2p^5$ corresponds to two possible alternatives, say L=1, S=1/2, J=1/2 (term ${}^2P_{1/2}$) or L=1, S=1/2, J=3/2 (term ${}^2P_{3/2}$). The two alternatives differ by the different value of the total momentum $J = L + S$, which in turn depends on the different relative orientations of L and S.
One can show that the configuration $2s^5$ corresponding to the term ${}^2P_{1/2}$ has a lower energy with respect to the same configuration corresponding to the term ${}^2P_{3/2}$. As a consequence, in the first case the photoelectron has an higher energy (L_2 edge) than in the second case (L_3 edge). Besides, since for J=1/2 one has two possible projections M_J=±1/2, while for J=3/2 one has four possible projections M_J=±3/2,±1/2, the intensity of the L_2 edge is half the intensity of the L_3 edge.

2.2.3 The electromagnetic field

Radiation gauge

As already noticed and as will be clearer below, the most convenient quantum approach to the interaction of radiation and matter requires that the electromagnetic field is described in terms of the vector potential $\vec{A}$ within the framework of the radiation gauge ($\vec{\nabla} \cdot \vec{A} = 0$ and $U = 0$), so that

$$\vec{E} = -(\partial \vec{A}/\partial t)\,, \quad \vec{B} = \vec{\nabla} \times \vec{A}\,. \tag{2.24}$$

For details, see Appendix A and [Bransden and Joachain, 2003, Cohen-Tannoudji et al., 2004, Chen and Kotlarchyk, 2007].

Classical description of the electromagnetic field

Let us consider here the classical description of the electromagnetic field, which is sufficient for the semi-classical approach to the matter-radiation interaction.
For the simplest case of a monochromatic plane wave, the vector potential at position $\vec{r}$ and time t is given by

$$\vec{A}(\vec{r},t) = A_0\,\hat{\epsilon}\,\cos(\vec{k}\cdot\vec{r}-\omega t) \tag{2.25}$$

$$= (A_0/2)\,\hat{\epsilon}\left[e^{i(\vec{k}\cdot\vec{r}-\omega t)} + e^{-i(\vec{k}\cdot\vec{r}-\omega t)}\right], \tag{2.26}$$

where $\vec{k}$ is the wavevector, $\omega = kc$ is the (angular) frequency and $\hat{\epsilon}$ is the polarisation unit vector, perpendicular to $\vec{k}$. A_0 is the amplitude of the oscillating wave (measured in Ns/C), whose square is proportional to the energy flux (Sec. 2.1).

Note 1: The vector potential $\vec{A}(\vec{r},t)$ can be expressed in an alternative form, which facilitates the transition to the quantum description considered below (see § A.4):

$$\vec{A}(\vec{r},t) = \mathcal{A}_\omega\,\hat{\epsilon}\left[\alpha\,e^{i\vec{k}\cdot\vec{r}} + \alpha^*\,e^{-i\vec{k}\cdot\vec{r}}\right] \tag{2.27}$$

where $\mathcal{A}_\omega$ only depends on the frequency ω

$$\mathcal{A}_\omega = \sqrt{\frac{\hbar}{2\epsilon_0(2\pi)^3\omega}} \tag{2.28}$$

(the quantity $\hbar$ is inserted to facilitate the transition to the quantum approach), and the amplitude of oscillations is now taken into account by the normal coordinates

$$\alpha = \alpha_0 e^{-i\omega t}, \quad \alpha^* = \alpha_0^* e^{-i\omega t} \tag{2.29}$$

which incorporate the time dependence.

Note 2: The most general expression of the vector potential at position $\vec{r}$ and time t is given, according to the Fourier analysis, as a superposition of plane waves (2.26) of different wavevectors $\vec{k}$ and polarisations $\hat{\epsilon}$. For more details, see Appendix A.

Quantum description of the electromagnetic field

A full quantum approach to the interaction of radiation with matter requires a quantum description also for the the electromagnetic field.

The transition from the classical to the quantum description of the electromagnetic field can be obtained according to the standard treatment of the harmonic oscillator in terms of annihilation and creation operators [Cohen-Tannoudji et al., 1973].

For a monochromatic wave (2.26), the transition from the classical to the quantum approach is obtained by substituting the classical normal variables α and α^* (2.29) of (2.27) with the annihilation and creation operators a and $a^\dagger$ (see § A.5) [Cohen-Tannoudji et al., 2004]
Accordingly, the vector potential operator becomes a linear combination of creation and annihilation operators. For a monochromatic plane wave,

$$\vec{A}(\vec{r},t) = \hat{\epsilon}\sqrt{\frac{\hbar}{2\epsilon_0(2\pi)^3\omega}}\left[a\,e^{i(\vec{k}\cdot\vec{r})} + a^\dagger\,e^{-i(\vec{k}\cdot\vec{r})}\right] \tag{2.30}$$

From the creation and annihilation operators one obtains the number operator [Cohen-Tannoudji et al., 1973]

$$\hat{n} = a^\dagger a\,. \tag{2.31}$$

The Hamiltonian operator for the electromagnetic wave can be expressed in terms of the number operator, according to the well known expression for the harmonic oscillator

$$H_{\text{wave}} \;=\; \hbar\omega \left[a^\dagger a + \frac{1}{2}\right] \;=\; \hbar\omega \left[\hat{n} + \frac{1}{2}\right] \tag{2.32}$$

whose eigenvalues are

$$E_n \;=\; \hbar\omega \left[n + \frac{1}{2}\right] . \tag{2.33}$$

The stationary eigenstates of the Hamiltonian H_{wave} are

$$|\, n \,\rangle \tag{2.34}$$

corresponding to a well defined number n of photons within the plane wave. A general quantum state of the electromagnetic wave is a linear superposition of stationary eigenstates.

A stationary eigenstate of the system atom+wave is the product of the atomic state and the field state:

$$|\Psi_{\text{at}}\rangle \,|\, n \,\rangle \tag{2.35}$$

The vector potential operator acts on the eigenstates of the monochromatic electromagnetic wave according to the effects of the creation, annihilation and number operators, which are

$$a^\dagger \,|n\rangle \;=\; \sqrt{n+1}\;|n+1\rangle \tag{2.36}$$

$$a \,|n\rangle \;=\; \sqrt{n}\;|n-1\rangle \tag{2.37}$$

$$\hat{n} \,|n\rangle \;=\; n\;|n\rangle \tag{2.38}$$

Note 3: Also in the quantum approach, as in the classical one, the most general expression of the electromagnetic field is given, according to the Fourier analysis, by a superposition of plane waves. For more details, see Appendix A.

2.2.4 The radiation-matter interaction

Let us now consider the effect of the interaction between the atom and the electromagnetic field, which leads to the photo-absorption process.

Let us suppose that the atom is initially in its stationary ground state $|\Psi_i\rangle$ of energy E_i. When interacting with the electromagnetic field, the atom can absorb an X-ray photon of energy $\hbar\omega$ and undergo a transition to one of the possible final stationary states $|\Psi_f\rangle$ of energy $E_f = E_i + \hbar\omega$.

The photon energy $\hbar\omega$ is used to promote one or more atomic electrons to unoccupied discrete levels (*excitation*) or to the continuum of free states (*ionization*).

For the interpretation of EXAFS oscillations, we are interested in the process by which a single core electron (typically belonging to the K or to an L shell) is ejected from the atom, so that the final stationary state $|\Psi_f\rangle$ is represented by the atom with a core hole (absence of an electron in a core level) and a free photo-electron. Other possible processes leading to different final stationary states $|\Psi_f\rangle$ with the same energy E_f (e.g. when two or more electrons are excited by the same photon) contribute to the damping of the EXAFS oscillations and have to be conveniently taken into account (see Chapter 3).

In the semiclassical approach the quantum treatment is limited to the atom, and the process of photo-absorption can be schematised as

$$|\Psi_i\rangle \qquad \xrightarrow{\hbar\omega} \qquad |\Psi_f\rangle \,. \tag{2.39}$$

In the full quantum treatment, also the electromagnetic field is quantised, and the process of absorption of a single photon can be schematised as

$$|\Psi_i\rangle \,|n\rangle \qquad \longrightarrow \qquad |\Psi_f\rangle \,|n-1\rangle \,. \tag{2.40}$$

Time evolution of quantum states

A quantum system evolves in time according to the time-dependent Schrödinger equation

$$i\hbar\frac{\partial}{\partial t}|\mathbf{\Phi}(t)\rangle \;=\; H\,|\mathbf{\Phi}(t)\rangle\,, \tag{2.41}$$

where H is the Hamiltonian operator and $|\mathbf{\Phi}(t)\rangle$ is the quantum state (2.22) of the atom in the semiclassical approximation or of the system atom+field in the full quantum approach.
Our next step is to introduce a convenient Hamiltonian operator H, suitable to describe the interaction between the atom and the electromagnetic field.

The full Hamiltonian operator

When the atom is embedded in the electromagnetic field, the Hamiltonian operator of the isolated atom (2.19) has to be modified. If the radiation gauge is used ($\vec{\nabla}\cdot\vec{A}=0, U=0$) and the relativistic interaction of the electron spin with the magnetic field is neglected, the Hamiltonian becomes (see Appendix A and [Cohen-Tannoudji et al., 2004])

$$H=\sum_j\left\{\frac{1}{2m}\,\left[\vec{P}_j+e\vec{A}(\vec{r}_j,t)\right]^2\right\}\;+\;V(\vec{r}_1\ldots\vec{r}_N)\,, \tag{2.42}$$

where $\vec{P}_j$ is the generalised momentum of the j-th electron (which in the coordinate representation becomes $-i\hbar\vec{\nabla}_j$), $-e=q$ is the negative electric charge of the electron and $\vec{A}$ is the vector potential. It is worth remembering that the generalised momentum $\vec{P}_j$ depends on the gauge choice of the electromagnetic potentials and doesn't correspond to the mechanical momentum; actually, the mechanical momentum corresponds to the quantity in square brackets in (2.42), say $m\vec{v}_j=\vec{P}_j+e\vec{A}$.

If the electron spin $\vec{S}$ is considered too, the total Hamiltonian becomes

$$\hat{H}=\sum_j\left\{\frac{1}{2m}\,\left[\vec{P}_j+e\vec{A}(\vec{r}_j,t)\right]^2+\frac{e}{m}\,\vec{S}_j\cdot\vec{B}(\vec{r}_j)\right\}\;+\;V(\vec{r}_1\ldots\vec{r}_N)\,, \tag{2.43}$$

where $\vec{B}$ is the magnetic induction field. In the following, we neglect the interaction of the electron spin with magnetic fields and the terms $\vec{S}\cdot\vec{B}$ are no more considered.

Note: In principle, a full Hamiltonian should contain also a term describing solely the electromagnetic field [Zangwill, 2012]. However, this term has no relevance for the interaction of radiation with matter here considered and has been thus omitted.

Interaction hamiltonian

Once the square of the binomial term $[\vec{P}_j+e\vec{A}(\vec{r}_j)]^2$ in (2.42) has been expanded, the Hamiltonian can be decomposed into the sum of two terms, the unperturbed hamiltonian H_0, which has the same expression as (2.19) for the isolated atom, and the interaction hamiltonian H_I:

$$H=H_0+H_I. \tag{2.44}$$

The second term H_I of (2.44) describes the interaction between the electromagnetic field and the electrons and is the sum of two terms:

$$H_I \;=\; H_{I1}+H_{I2} \;=\; \frac{e}{m}\sum_j\vec{A}(\vec{r}_j,t)\cdot\vec{P}_j \;+\; \frac{e^2}{2m}\sum_j A^2(\vec{r}_j,t)\,. \tag{2.45}$$

The radiation gauge guarantees that, since $\vec{P}$ commutes with $\vec{A}$, the commutativity of the classical product $\vec{P}\cdot\vec{A}$ is preserved: in radiation gauge, $\vec{P}\cdot\vec{A}=\vec{A}\cdot\vec{P}$ (for details, see Appendix A).

The two terms in (2.45) have different magnitudes and describe different phenomena:

1. The first term H_{I1} is linear in $\vec{A}$. It describes phenomena where one photon is annihilated (absorption) or created (emission). One says that this term is 'first-order in the interaction", since it involves the first power of the vector potential.
2. The second term H_{I2} is quadratic in $\vec{A}$. It describes phenomena where two photons are involved, e.g. scattering phenomena or two-photons absorption or emission. It is generally weaker than the first term, and is said to be "second-order in the interaction", since it involves the second power of the vector potential. As a matter of fact, one experimentally finds that for X-ray energies below 100 keV the cross section for scattering (two-photons process) is much smaller than the cross section for absorption (see Fig. 1.1, right).

In the following, we consider only the first term H_{I1} of (2.45).

Semiclassical and full quantum approaches

The vector potential operator $\vec{A}$ appearing in the interaction Hamiltonian H_I of (2.45) is expressed by (2.26) in the semiclassical approach and by (2.30) in the full quantum approach, respectively.

In the semiclassical approach, the $\vec{A}$ operator (2.26) only acts on the atomic state vector $|\mathbf{\Phi}\rangle$.

In the full quantum approach, the $\vec{A}$ operator (2.30) acts on the product state $|\mathbf{\Phi}\rangle\,|n\rangle$. The vector potential $\vec{A}$ acts on the field state $|n\rangle$ through the creation and destruction operators, a and $a^\dagger$, respectively. For the absorption processes here considered, only the term containing the destruction operator $a^\dagger$ has to be retained, which leads to the transition $|n\rangle \rightarrow |n-1\rangle$.

In the following, we only consider the semiclassical approach of the atom-radiation interaction.

2.2.5 Transition rates

In principle, the time-dependent Schrödinger equation (2.41) can describe the time evolution of a quantum system. However, its solution is in general a prohibitive task, and this is particularly true in the present case of interaction of an atom with the electromagnetic radiation. In the semiclassical approach, the many-electron atomic state $|\mathbf{\Phi}(t)\rangle$ is a time-dependent linear combination of stationary states $|\Psi_s\rangle$ and the electromagnetic field can in principle affect the state of each electron.

Actually, in order to interpret the atomic absorption cross section $\sigma_a(\hbar\omega)$ introduced in (2.12), we don't need to know the very details of the time evolution of the atomic state $\mathbf{\Phi}(t)\rangle$. It is sufficient to evaluate the probabilites that, as effect of the interaction with the electromagnetic field, the atom evolves from the initial stationary ground state $|\Psi_i\rangle$ to well defined final stationary states $|\Psi_f\rangle$.

The probability of the transition $i \rightarrow f$ *per unit time* is called transition rate w_{fi}.

The atomic absorption cross section $\sigma_a(\hbar\omega)$ is equal to the sum of the transition rates w_{fi} from the initial stationary ground state $|\Psi_i\rangle$ to each one of the possible final stationary states $|\Psi_f\rangle$, divided by the beam flux (2.11):

$$\sigma_a(\omega) \;=\; \frac{2\hbar}{\epsilon_0 \omega A_0^2 c} \sum\nolimits_f w_{fi}\,. \tag{2.46}$$

Even the evaluation of the transition rates w_{fi} is however far from trivial, and has to be performed through a sequence of suitable approximations, which form the subject of the two subsequent sections.

2.3 Time-dependent perturbation theory

The first approximation for the calculation of the transition rates w_{fi} is based on the time-dependent perturbation theory.

It is assumed that the interaction of a given photon with the atom is limited to a finite time interval, so that the interaction is switched on at a time t_i and switched off at a time t_f. The

Hamiltonian $H(t)$ is thus time-dependent. A further time dependence of the Hamiltonian is due to the oscillatory behaviour of the electromagnetic field, described by the vector potential $\vec{A}(t)$ according to (2.26).

Excellent introductions to the time-dependent perturbation theory and to its applications to different topics (scattering from a constant potential, matter-radiation interaction, etc.) can be found in a number of Quantum Mechanics textbooks, e.g. [Cohen-Tannoudji et al., 1973, Merzbacher, 1970]. A review can be found also in Appendix B of the present book. In the following, we give a synthetic account, focused on the semiclassical approach.

Transition probabilities

Basically, in order to account for the interaction of the atom with the electromagnetic field during the time interval $t_i \to t_f$, the constant coefficients b_s, which appear in the expression (2.22) of the atomic state $|\mathbf{\Phi}(t)\rangle$ as a linear combination of stationary states $|\psi_s\rangle$, have to be substituted by time-dependent coefficients $b_s(t)$:

$$|\mathbf{\Phi}(t)\rangle \;=\; \sum_s b_s(t)\, e^{-iE_s t/\hbar}\, |\Psi_s\rangle\,. \tag{2.47}$$

The probability of finding the atom in a given stationary state $|\Psi_s\rangle$ at time t is thus $|b_s(t)\, \exp(-iE_s t/\hbar)|^2 = |b_s(t)|^2$. The time dependence of the probability $|b_s(t)|^2$ guarantees the possibility of modifying the linear combination of stationary states (2.47) and in particular the possibility of a transition from an initial stationary state $|\Psi_i\rangle$ to a final stationary state $|\Psi_f\rangle$.
When the atom is in the initial stationary state $|\Psi_i\rangle$, the coefficients b are $b_i(t_i) = 1$ and $b_f(t_i) = 0$.
When the atom is in the final stationary state $|\Psi_f\rangle$, the coefficients b are $b_i(t_f) = 0$ and $b_f(t_f) = 1$.

In order to evaluate a transition rate w_{fi} we should first be able to evaluate the time-dependent probability $\mathcal{P}_{fi}(t) = |c_{fi}(t)|^2$ of transition from an initial stationary state $|\Psi_i\rangle$ to a final stationary state $|\Psi_f\rangle$; the quantity $c_{fi}(t)$ is the transition amplitude.
In the perturbative approach, the probability of transition $\mathcal{P}_{fi}(t)$ is expressed as a sum of contributions of increasing degree of approximation and of decreasing importance.

For the X-ray absorption processes here considered, the interaction is sufficiently weak that the perturbative expansion can be limited to the first order term. One finds (see Appendix B for details) that the general expression of the transition probability $\mathcal{P}_{fi}(t)$ limited to the first-order term is

$$\begin{aligned} \mathcal{P}^{(1)}_{fi}(t) \;=\; |c^{(1)}_{fi}(t)|^2 \quad &= \quad \frac{1}{\hbar^2}\left| \int_{t_i}^{t_f} dt\; e^{iE_f t/\hbar}\, \langle \Psi_f \,|\, H_{\rm int} \,|\, \Psi_i \rangle\, e^{-iE_i t/\hbar} \right|^2 \\ &= \quad \frac{1}{\hbar^2}\left| \int_{t_i}^{t_f} dt\; \langle \Psi_f \,|\, H_{\rm int} \,|\, \Psi_i \rangle\; e^{i\omega_{fi} t} \right|^2 \end{aligned} \tag{2.48}$$

where the interaction Hamiltonian $H_{\rm int}$ has to be here identified with the time-dependent first term $H_{I1}(\vec{r}, t)$ of (2.45), $\omega_{fi} = (E_f - E_i)/\hbar$ is the Bohr frequency connecting the two atomic energy levels, and the integral is evaluated between the initial and final times of the interaction. For an absorption process, where $E_f > E_i$, the Bohr frequency is positive, $\omega_{fi} = (E_f - E_i)/\hbar > 0$.

Let us now insert the explicit expression of the vector potential

$$\vec{A}(\vec{r}, t) \;=\; A_0 \hat{\epsilon}\, \sin(\omega t - \vec{k}\cdot\vec{r}) \;=\; \frac{1}{2i}\, A_0\, \hat{\epsilon}\left[e^{i\omega t} e^{-i\vec{k}\cdot\vec{r}} + e^{-i\omega t} e^{i\vec{k}\cdot\vec{r}} \right], \tag{2.49}$$

in the interaction Hamiltonian H_{I1} of (2.45). One can show (see Appendix B for details) that, for the absorption process, the transition probability to first order in the perturbative expansion is

$$\mathcal{P}_{fi}(T, \omega) \;=\; \frac{|W_{fi}|^2}{4\hbar^2} \left| \frac{1 - e^{i(\omega_{fi} - \omega)T}}{\omega_{fi} - \omega} \right|^2 \;=\; \frac{|W_{fi}|^2}{4\hbar^2} \left\{ \frac{\sin[(\omega_{fi} - \omega)T]/2}{(\omega_{fi} - \omega)/2} \right\}^2, \tag{2.50}$$

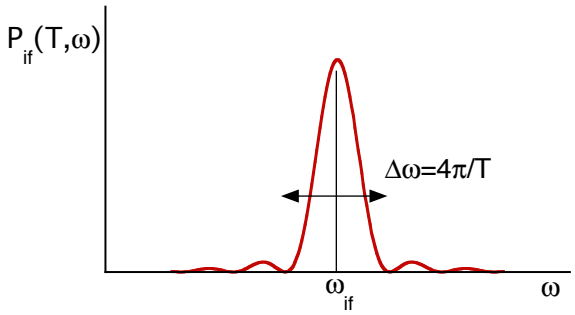

Figure 2.3: Plot of the absorption probability $\mathcal{P}_{if}(T,\omega)$ as a function of the electromagnetic field frequency ω for a given interaction time T. $\omega_{fi} = (E_f - E_i)/\hbar$ is the Bohr frequency connecting the final and initial atomic energy levels.

where $T = t_f - t_i$ is the time duration of the interaction, ω is the radiation frequency and

$$W_{fi} = \frac{eA_0}{m} \left\langle \Psi_f \left| \sum_j e^{i\vec{k}\cdot\vec{r}} \hat{\epsilon} \cdot \vec{P}_j \right| \Psi_i \right\rangle . \tag{2.51}$$

The first-order probability $\mathcal{P}_{fi}(T,\omega)$ of (2.50) thus depends on two factors:

a) the time-independent matrix element W_{fi} which only depends on the spatial dependence of the vector potential $\vec{A}$,
b) a time-dependent factor (in curly brackets in 2.50), which depends on the frequency ω of the perturbation, on the Bohr frequency ω_{fi} and on the duration T of the interaction.

Resonance condition

The time-dependent factor in curly brackets in (2.50) is a typical *diffraction function*.
The behavior of the transition probability (2.50) is represented in Fig. 2.3 as a function of the electromagnetic field frequency ω for a given value of the interaction time T.
The main properties of the transition probability $\mathcal{P}_{fi}(t,\omega)$ represented in Fig. 2.3 are:

a) The function has a peak centred on $\omega = \omega_{fi}$ (resonance condition), say for $\hbar\omega = E_f - E_i$ (energy conservation), and progressively weaker oscillations when the difference between ω and ω_{fi} increases.
b) The peak width is inversely proportional to the interaction time, $\Delta\omega = 2\pi/T$; the violation of the energy conservation, leading to finite probability for $\omega \neq \omega_{fi}$, is possible for short times, according to the time-energy uncertainty principle, $\Delta E\,\Delta T \geq \hbar$. For $T \to \infty$, the peak width tends to zero: energy is conserved.
c) The peak height is proportional to the square of the time T. The transition probability $\mathcal{P}_{fi}(T,\omega) = (|W_{fi}|^2/2\hbar^2)T^2$ increases indefinitely with the square of the interaction time, so that the transition probability per unit time $w_{fi} = d\mathcal{P}_{fi}/dt$ linearly increases with the interaction time.

To summarise, when the interaction time T increases, the peak of the absorption probability progressively narrows around the value $\omega = \omega_{fi}$, and its value $P_{fi}(T,\omega_{fi}) = (|W_{fi}|^2/2\hbar^2)T^2$ increases with the square of time T.
This means that, for sharply defined discrete initial and final atomic states and for a purely monochromatic radiation, the transition rate $w_{fi} = d\mathcal{P}_{fi}/dT$ is proprtional to T, say it increases indefinitely with time. This un-physical result depends on the inadequacy of the first-order approximation when long interaction times are considered. Taking into account higher order perturbation terms, or using other kinds of approximation, one can show that the system oscillates in time between the initial and final states [Cohen-Tannoudji et al., 1973].

Actually, in the realistic cases here considered, we are concerned nor with sharply defined final states nor with perfectly monochromatic radiation, so that the expression (2.50) for the transition probability has to be conveniently modified, as we see in the following.

The Golden Rule

In EXAFS spectroscopy, we are concerned with the transition from an initial atomic discrete stationary state $|\Psi_i\rangle$ to a final stationary state $|\Psi_f\rangle$ belonging to a continuous distribution of energy values, since the energy of the free photo-electron is not quantised. The discrete value ω_{fi} of Eq. (2.50) and Fig. 2.3 becomes now a continuous distribution of values.
Since the final state of energy $E_f = \hbar\omega_f$ belongs to a continuum, we can only evaluate the probability that after the interaction time T the system is in a final state whose energy belongs to an interval ΔE_f centered on E_f, so that (2.50) becomes

$$\delta\mathcal{P}_{fi}(T, E_f) \;=\; \frac{1}{4\hbar^2}\int_{\Delta E_f} |\tilde{W}_{fi}(E)|^2\,\rho(E)\left\{\frac{\sin[(\tilde{\omega}-\omega)T]/2}{(\tilde{\omega}-\omega)/2}\right\}^2 dE\,, \tag{2.52}$$

where $\rho(E)$ is the density of final states, $\tilde{\omega} = (E - E_i)/\hbar$ and

$$\tilde{W}_{fi}(E) = \frac{eA_0}{m}\left\langle \Psi_f(E)\left|\sum\nolimits_j e^{i\vec{k}\cdot\vec{r}}\hat{\epsilon}\cdot\vec{P}_j\right|\Psi_i\right\rangle . \tag{2.53}$$

Exploiting the properties of the delta function, the resonant factor in curly brackets can be transformed

$$\left\{\frac{\sin[(\tilde{\omega}-\omega)T]/2}{(\tilde{\omega}-\omega)/2}\right\}^2 \quad\xrightarrow[T\to\infty]{}\quad 2\pi T\;\delta(\tilde{\omega}-\omega) \;=\; 2\pi T\,\delta(E - E_i - \hbar\omega)\,, \tag{2.54}$$

so that, after calculating the integral, one finds finally

$$\delta\mathcal{P}_{fi}(T, E_f) \;=\; \frac{\pi}{2\hbar}\,T\,|W_{fi}|^2\,\rho(E_f)\,, \tag{2.55}$$

where $E_f = E_i + \hbar\omega$. The probability (2.55) increases proportionally to the time T.
The transition rate is now independent of time

$$w_{fi} \;=\; \frac{d}{dT}\delta\mathcal{P}_{fi} \;=\; \frac{\pi}{2\hbar}\,|W_{fi}|^2\,\rho(E_f) \tag{2.56}$$

where $\rho(E_f)$ is the density of final states in correspondence with the energy value $E = E_f$.
Equation (2.56) was called *Golden rule* by Enrico Fermi, in view of its widespread applications.
In the case of interest here, say of the photo-electric absorption, the Golden rule (2.56) becomes

$$w_{fi} \;=\; \frac{\pi e^2 A_0^2}{2\hbar m^2}\;\left|\,\langle\,\Psi_f|\sum\nolimits_j e^{i\vec{k}\cdot\vec{r}_j}\,\hat{\epsilon}\cdot\vec{P}_j\,|\Psi_i\,\rangle\,\right|^2 \;\;\rho(E_f)\,. \tag{2.57}$$

The Golden Rule allows one to reduce a complicated process of time-dependent dynamical interaction to the calculation of a matrix element between the two initial and final stationary states of the atom. One can notice that, in the expression of the interaction Hamiltonian in (2.57), the time dependence of the vector potential has disappeared.

Note 1: As already noted, the initial and final stationary states $|\Psi_i\rangle$ and $|\Psi_f\rangle$ of the atom are generally approximated by Slater determinants of one-electron spin-orbitals, calculated with different one-electron self-consistent potentials.

Note 2: The Golden rule is an approximate expression, valid for relatively weak interaction. Actually, the linear dependence on time of the probability (2.55) implies that, for sufficiently long time, the probability becomes un-realistically larger than one. The weaker the interaction, the longer the time necessary to attain large probability values. For a strong interaction, it would be necessary to add higher-order terms to the perturbation expansion.

Note 3: The derivation of the Golden rule presented above is based on the consideration of transitions to electronic continuum states. Actually, even the excited discrete states are not sharply

defined in energy; nor is the incoming radiation strictly monochromatic. In all cases thus a density of states $\rho(E)$ should be considered, leading to a large validity of the Golden rule.

In spite of the strong simplification of the perturbative approach, the calculation of the matrix element in (2.57) is still very complicated, since the absorption process involves in principle all the electrons within the atom (many-body problem). Further approximations are considered in the next Section 2.4.

In addition, as it was anticipated in Chapter 1, for a non-isolated atom the final states $|\Psi_f\rangle$ are influenced by the atomic environment; understanding and quantitatively expressing this influence is necessary in order to get structural information from EXAFS. This problem is considered in detail in Chapter 3.

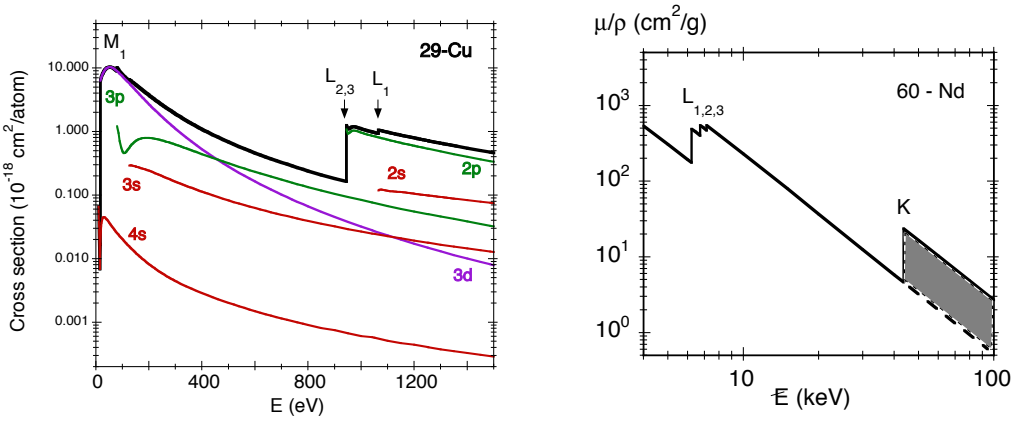

Figure 2.4: Left: Photo-ionisation cross sections for Cu calculated by Yeh [Yeh, 1993]; the black line is the total cross section; the contributions of the different initial levels are in colour (the calculations don't include the 1s level, K edge at 8979 eV). Right: Mass absorption coefficient of Nd; the dashed area represents the contribution due to the absorption of photons of energy sufficient to extract the 1s electrons. Notice the logarithmic scales in both plots.

2.4 Further approximations

The total absorption cross section σ_a (2.46), which is obtained from experimental measurements, is the sum of the contributions of transitions from the atomic ground state $|\Psi_i\rangle$ to all possible stationary final states $|\Psi_f\rangle$ compatible with the conservation of energy.
The final goal of this book is the interpretation of the fine structure at a given absorption edge, for example the K edge, which corresponds to the extraction of an electron from the $1s^2$ shell (see Fig. 1.4, right, or Fig. 1.5).
We can thus perform a first sorting of the final states $|\Psi_f\rangle$ by considering only the final states presenting a core hole in the electronic shell from which the photoelectron is extracted, say the final states pertaining to the corresponding absorption edge (§ 1.2, table 1.1).
A comparison of the contributions of the final states corresponding to different absorption edges to the total absorption cross section of copper, calculated for photon energies in the range from 0 to 1500 eV, is shown in Fig. 2.4, left.

Experimentally, one measures the *total* absorption coefficient, say the total absorption cross section. The contribution of a given absorption edge, e.g. the K edge, to the total absorption coefficient (dashed area in Fig. 2.4, right) can be singled out through a relatively simple procedure which will be explained in § 6.1 as the first step of the analysis of EXAFS signals.

Even if we confine ourselves to the contribution of a given absorption edge, say to the emission of the photo-electron from a given atomic level, different final states $|\Psi_f\rangle$ are still possible. Actually, the energy $\hbar\omega$ of the absorbed photon can be all transferred to one electron, e.g. a 1s electron, giving rise to the final state of interest for the EXAFS interpretation, but it can also be partly employed for the excitation or ionisation of the other electrons, giving rise to other final states.

Let us now introduce some further approximations, which facilitate the interpretation of the EXAFS signal.

2.4.1 One electron approximation

As it was anticipated in Chapter 1, the EXAFS oscillations are due to the coherent superposition of the outgoing and incoming spherical waves of one photo-electron.
The experimental absorption coefficient corresponding to a given absorption edge contains the contributions of the transitions to different final states, say the contributions of different excitation channels. For a given photon energy $\hbar\omega$, the different excitation channels are characterised by the emission of photoelectrons with different energies.
We need thus distinguish the excitation channel that gives rise to the intense coherent EXAFS signal experimentally observable from all the other channels, whose contributions to EXAFS are incoherent (Fig. 2.5).

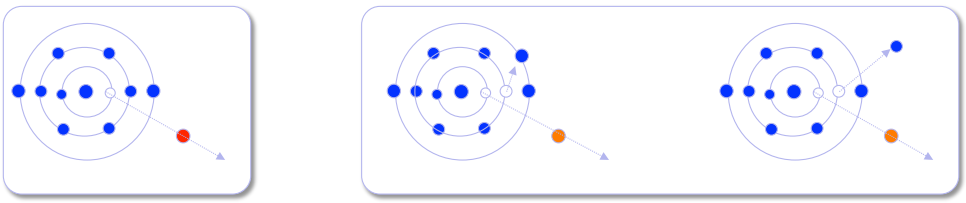

Figure 2.5: Schematic representation of an elastic transition (left panel) and of two possible inelastic transitions (right panel).

Elastic and inelastic transitions

The excitation channel giving rise to an intense coherent EXAFS signal corresponds to the so called *elastic* (or fully relaxed) transitions [Brown and Doniach, 1980], where

a) one core electron is ejected from the atom as a photo-electron; as a consequence, a hole is left in the corresponding core shell (the so called core hole); for example an electron is ejected from the $1s^2$ shell, leaving an incomplete shell $1s^1$;
b) the remaining $N-1$ passive electrons of the atom simply relax their orbitals around the core hole, say in the potential energy modified by the absence of a 1s electron.

In the other excitation channels, called *inelastic* channels, the relaxation of the $N-1$ passive electrons is accompanied by their excitation (in competition with the core electron excitation); one distinguishes two kind of excitation processes of the passive electrons:

- shake-up processes in the case of bound excited states,
- shake-off processes in the case of continuum excited states.

In the inelastic channels, the X-ray photon energy is distributed over all the excited electrons in different possible ways, so that the photoelectron has a distribution of different energies. The possible EXAFS signals of photo-electrons of different energies sum up incoherently and give rise to a damping of the experimentally observed oscillations. We will consider in Chapter 3 how to cope with this problem in the interpretation of the EXAFS signal.

By taking into account the distinction between elastic and inelastic channels, the total atomic absorption cross section corresponding to a given edge can be decomposed as

$$\sigma_{\rm a}(\omega) \;=\; \sigma_{\rm el}(\omega) \;+\; \sigma_{\rm inel}(\omega)\,, \tag{2.58}$$

or, in terms of transition rates,

$$\sum\nolimits_f w_{fi} \;=\; w_{\rm el} \;+\; \sum w_{\rm inel}\,, \tag{2.59}$$

Elastic cross section

Let us focus our attention on the elastic channel, which gives rise to coherent EXAFS oscillations. The atomic cross section for elastic absorption can be expressed, from (2.46) and (2.57), as

$$\sigma_{\rm el}(\omega) \;=\; \frac{2\hbar}{\epsilon_0\omega A_0^2 c}\; w_{\rm el} \;=\; \frac{\pi e^2}{\epsilon_0\omega c m^2}\; \left|\, \langle\, \Psi_{f,r}^{N-1}\psi_f|\; e^{i\vec{k}\cdot\vec{r}}\hat{\epsilon}\cdot\vec{P}\;|\Psi_i^{N-1}\psi_i\,\rangle\,\right|^2\; \rho(\epsilon_f)\,. \tag{2.60}$$

In is important to stress the following points regarding the interpretation of (2.60):

a) the interaction Hamiltonian H_{I1} of (2.45) is considered to operate now only on the core electron *(one-electron approximation)*, of which $\vec{r}$ and $\vec{P}$ are the vector position and the generalised momentum, respectively;
b) in the expression $|\Psi_i^{N-1}\psi_i\,\rangle$ of the initial stationary atomic state, the contribution ψ_i of the core electron, on which the interaction Hamiltonian acts, has been formally separated from the contribution Ψ_i^{N-1} of the other (passive) electrons;
c) in the expression $|\Psi_{f,r}^{N-1}\psi_f\rangle$ of the final state, the contribution ψ_f of the photo-electron has been formally separated from the contribution $\Psi_{f,r}^{N-1}$ of the passive electrons relaxed around the core hole;
d) the photo-electron energy ϵ_f belongs to a continuum of values; according to the Golden rule, $\rho(\epsilon_f)$ represents the density of final states in correspondence of the value ϵ_f;
e) the *conservation of energy* requires that

$$E_i^N + \hbar\omega \;=\; E_{f,r}^{N-1} + \epsilon_f\,, \tag{2.61}$$

where E_i^N is the total energy of the atom in the initial stationary state, $\hbar\omega$ is the photon energy, $E_{f,r}^{N-1}$ is the total energy of the system of $N-1$ passive electrons relaxed around the core hole in the final stationary state and ϵ_f is the photo-electron energy.

Note: In principle, both atomic states $|\Psi_i^{N-1}\psi_i\,\rangle$ and $|\Psi_{f,r}^{N-1}\psi_f|$ have to be globally considered, say they cannot be factorised as the product of the core electron state and the passive electron state. This is due to the fact that the photo-electron can interact with the passive electrons. In the coordinate representation, this amounts to say that the initial and final wave functions cannot be factorised as the product of the core electron wave-functions and the passive electrons wave-functions.
This factorisation is made possible by a further approximation, the sudden approximation, that is considered below.

2.4.2 Sudden approximation

When the photo-electron energy is relatively high, its interaction with the passive electrons of the absorbing atoms can be neglected (*sudden approximation*). Within the sudden approximation, the atomic wave-functions can be factorised in the contributions ψ_i and ψ_f of the active electron and Ψ_i^{N-1} and $\Psi_{f,r}^{N-1}$ of the passive electrons [Stern, 1988], so that the elastic cross section can be written as:

$$\sigma_{el}(\omega) \;=\; \frac{\pi e^2}{\epsilon_0\omega c m^2}\; \left|\, \langle\, \psi_f|\; e^{i\vec{k}\cdot\vec{r}}\hat{\epsilon}\cdot\vec{P}\;|\psi_i\,\rangle\,\right|^2\; S_0^2\;\rho(\epsilon_f) \tag{2.62}$$

where the factor

$$S_0^2 \;=\; \left| \langle\, \Psi_{f,r}^{N-1} | \Psi_i^{N-1} \,\rangle \right|^2 \tag{2.63}$$

is the square of the superposition integral of the passive electrons wavefunctions. The value of S_0^2 is generally included between 0.7 and 0.9.

The sudden approximation is generally good already a few eV above the edge, typically in the EXAFS region. It is then possible to calculate EXAFS by considering only the final state of the photo-electron.
It is the one-electron final state $|\psi_f\rangle$ that contains the information on the local structure around the absorbing atom.

In virtue of a sum rule for the photo-electric absorption, the total absorption cross section $\sigma_a(\omega)$ of Eq. (2.58) corresponds to the one-electron elastic absorption cross section of Eq. (2.62) in the hypothesis that passive electrons undergo no relaxation, i.e. $S_0^2 = 1$. The actual value of the superposition integral $S_0^2 < 1$ measures then the fraction of total absorption due to the elastic transitions.

Note: $|\psi_i\rangle$ and $|\psi_f\rangle$ are eigenstates of the effective one-electron initial and final state Hamiltonians, respectively; they are thus calculated with different self-consistent potentials [Rehr & Albers].

2.4.3 Electric dipole approximation

Let us now focus the attention on the interaction Hamiltonian of (2.62). The exponential $\exp(i\vec{k}\cdot\vec{r})$, which describes the spatial sinusoidal behaviour of the electromagnetic wave, can be expanded in a power series of $i\vec{k}\cdot\vec{r}$

$$e^{i\vec{k}\cdot\vec{r}} \;=\; 1 \;+\; i\vec{k}\cdot\vec{r} \;-\; (\vec{k}\cdot\vec{r})^2/2 \;... \tag{2.64}$$

The calculation of $\sigma_{\rm el}(\omega)$ is greatly simplified when the expansion (2.64) can be reasonably truncated at the first term:

$$e^{i\vec{k}\cdot\vec{r}} \;\simeq\; 1\,. \tag{2.65}$$

The substitution (2.65) represents the electric dipole approximation, which amounts to neglect the spatial dependence of the vector potential. (The reason of the name "electric dipole" is made clear below).
The electric dipole approximation is reasonable when $|\vec{k}\cdot\vec{r}_j|^2 \ll 1$ [Stern, 1988], say when the wavelength of the electromagnetic field $\lambda = 2\pi/k$ is much larger than the size of the interacting material system, so that the system sees a substantially uniform field.
Actually, the X-ray wavelengths are typically comparable with the atomic dimensions. However, in the one-electron approximation, the electromagnetic field interacts only with a core electron, whose orbital extension can be significantly smaller than the X-ray wavelength.
To give some quantitative hints, the radii of the $1s, 2s, 2p$ orbitals are shown in Fig. 2.66, left, while in the right panel the products kr and $(kr)^2$ are shown for the K edge X-rays.

In the electric dipole approximation, the expression of the elastic cross section (2.62) is simplified into

$$\sigma_{el}(\omega) \;=\; \frac{\pi e^2}{\epsilon_0 \omega c m^2} \left| \langle\, \psi_f |\; \hat{\epsilon}\cdot\vec{P}\; |\psi_i\,\rangle \right|^2 \; S_0^2 \; \rho(\epsilon_f) \tag{2.66}$$

In (2.66), the dipole operator appears in the so-called dipole-velocity form (or momentum form) $\hat{\epsilon}\cdot\vec{P}$. In the coordinate representation, (2.66) becomes

$$\sigma_{el}(\omega) \;=\; \frac{\pi e^2 \hbar^2}{\epsilon_0 \omega c m^2} \left| \int d^3r \; \psi_f^*(\vec{r}) \; \hat{\epsilon}\cdot\vec{\nabla}\psi_i(\vec{r}) \right|^2 \; S_0^2 \; \rho(\epsilon_f) \tag{2.67}$$

Alternative expressions of the dipole operator

It is convenient to express the dipole operator in an alternative form with respect to (2.66). In the alternative form the dipole operator is expressed in terms of the position operator of the electron $\vec{r}$ instead of the momentum operator $\vec{P}$.
Starting point is the commutator relation

$$[\vec{r}, H_0] \;=\; \frac{i\hbar}{m}\,\vec{P}\,, \tag{2.68}$$

where H_0 is the unperturbed Hamiltonian of the atom. A demonstration of this relation can be found in Section B.5 of Appendix B.
Exploiting the commutation relation, one can perform the following substitutions:

$$\begin{aligned} \langle\psi_f|\,\vec{P}\,|\psi_i\rangle &= \frac{m}{i\hbar}\,\langle\psi_f|\,\vec{r}H_0 - H_0\vec{r}\,|\psi_i\rangle \\ &= im\,\frac{E_f - E_i}{\hbar}\,\langle\psi_f|\,\vec{r}\,|\psi_i\rangle \\ &= im\,\omega\,\langle\psi_f|\,\vec{r}\,|\psi_i\rangle\,, \end{aligned} \tag{2.69}$$

where ω is the Bohr angular frequency connecting the initial and final electron states, corresponding to the angular frequency of the absorbed photon. In (2.69), the dipole operator appears in the so-called dipole-length form (or position form).
Substituting the matrix element of (2.69) in (2.66), one obtains the alternative expression of the absorption cross section

$$\sigma_{el}(\omega) \;=\; \frac{\pi e^2\omega}{\epsilon_0 c}\;|\,\langle\,\psi_f|\;\hat{\epsilon}\cdot\vec{r}\;|\psi_i\,\rangle\,|^2\;\;S_0^2\;\rho(\epsilon_f)\,. \tag{2.70}$$

In the coordinate representation, (B.87) becomes

$$\sigma_{el}(\omega) \;=\; \frac{\pi e^2\omega}{\epsilon_0 c}\;\left|\int d^3r\;\psi_f^*(\vec{r})\;\hat{\epsilon}\cdot\vec{r}\,\psi_i(\vec{r})\right|^2\;\;S_0^2\;\rho(\epsilon_f) \tag{2.71}$$

The presence of the product $e\,\vec{r}$ is at the origin of the name "electric dipole" for the approximation.

Validity of the dipole approximation

The electric dipole approximation is reasonable when $\vec{k}\cdot\vec{r} \ll 1$, say when $kr \ll 1$ or $\lambda \gg 2\pi r$. [But according to Stern $(\vec{k}\cdot\vec{r})^2 \ll 1$ [Stern, 1988]. Verify !!]
The size of the $1s$ orbitals depends on the atomic number Z; the dependence calculated by the Hartree-Fock approximation is shown in Fig. 2.6 (left) for the $1s, 2s, 2p$ orbitals. For the $1s$ orbitals, $r \simeq a_0/Z$, where $a_0 = 0.53$ Å (Bohr radius).
The K-edge X-ray energy (in keV) depends on Z approximately as $E \simeq 1.98 - 0.219Z + 0.015Z^2$, and $kr \simeq 0.5Er$.
The approximate dependence of kr and $(kr)^2$ on$Z$ shown in Fig. 2.6 (right).
Quadrupole corrections are of the order $(Z\alpha)^2$, where $\alpha \simeq 1/137$ [Rehr & Albers].

Selection rules

Within the dipole approximation, the angular momentum *selection rules* hold:

$$\Delta\ell \;=\; \pm 1, \qquad \Delta s \;=\; 0, \qquad \Delta j \;=\; \pm 1, 0, \qquad \Delta m \;=\; 0. \tag{2.72}$$

For one-electron transitions, the selection rule $\Delta l = \pm 1$ implies that:

a) if the initial core state has s symmetry (ℓ=0, edges K and L_1), the final state has p symmetry (ℓ=1);
b) if the initial core state has p symmetry, (ℓ=1, edges L_2 and L_3), the final state can be of both s or d symmetry (ℓ=0 or ℓ=2, respectively).

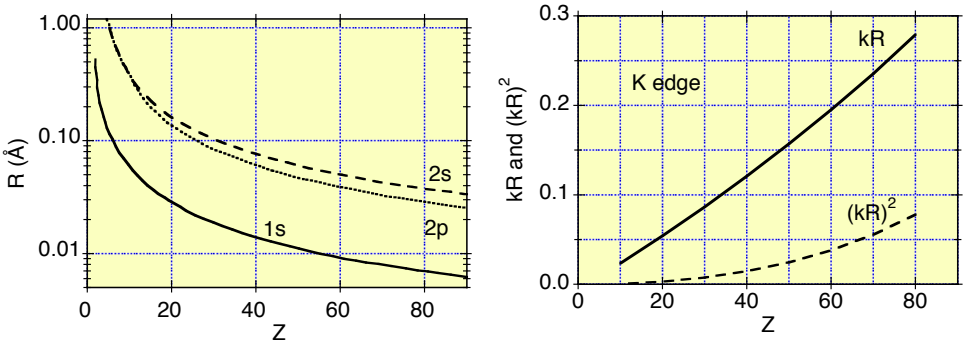

Figure 2.6: Left: radii of the maximum charge density for the $1s, 2s, 2p$ orbitals calculated by the Hartree-Fock approximation as a function of Z. Right: dependence of $kR = \lambda R/2\pi$ and $(kR)^2$ on Z for X-rays corresponding to K edges.

2.4.4 EXAFS and density of final states

In most SRO theories of EXAFS, the density of final states $\rho(\epsilon_f)$ is assumed to be that of a free electron of energy $\hbar^2 k^2/2m = \epsilon_f - \epsilon_0$. The value ϵ_0 is the effective average potential energy felt by an excited electron, and is also called "inner potential".
The justification for assuming a free electron density of states is that above in the EXAFS region (above about 30 eV) the band effects on the density of states are negligible (Stern 1974 [Stern, 1974]).

2.4.5 Direction of emission of photoelectrons

A give photoelectron energy ϵ_f corresponds to a continuum of possible directions of the linear momentum. The emission of the photoelectron is however not isotropic; there is a well defined correlation between the direction of photoelectron emission and the direction of the electric field polarisation $\hat{\epsilon}$.
Let θ be the angle between the direction of emission and the polarisation $\hat{\epsilon}$ of the electric field. The emission is connected to the angle θ by the relation

$$N(\theta) \;\propto\; 1 + \frac{\beta}{2}\left(3\cos^2\theta - 1\right), \tag{2.73}$$

where β is an asymmetry parameter that depends on the orbital from which the electron is emitted (Fig. 2.7). The asymmetry parameter β is determined by the relative amplitudes of the up ($\ell \to \ell + 1$) and down ($\ell \to \ell - 1$) channels in the matrix element.
For the emission from $1s$ levels (K edges) the asymmetry parameter is constant, $\beta = 2$.

2.5 De-excitation of an atom

An atom, excited or ionized by absorption of an X-ray photon, contains a core hole. This configuration, in spite of corresponding to a stationary state of the unperturbed Hamiltonian, is unstable, and the atom spontaneously tends to relax, filling the core hole with an electron from an upper level and thereby reducing its energy.

2.5.1 De-ecxitation mechanisms

Two types of de-excitation mechanisms are possible (Fig. 2.8):

1. radiative de-excitation (with emission of *fluorescence* radiation),
2. non-radiative de-excitation (with emission of *Auger effect* electrons).

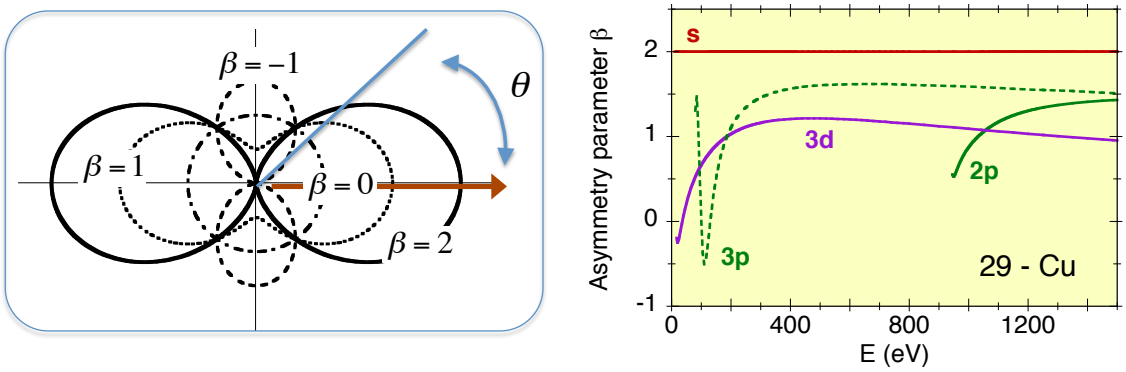

Figure 2.7: Left: Distributions of angular emission for different values of the asymmetry parameter β; the horizontal arrow represents the direction of electric field polarisation; the value $\beta = 2$ corresponds to emission from $1s$ core orbitals. Right: values of the asymmetry parameter as a function of photon energy for different orbitals, calculated by Yeh [Yeh, 1993]; the value $\beta = 2$ for $1s$ orbitals has been estrapolated below the edge energy (8979 eV).

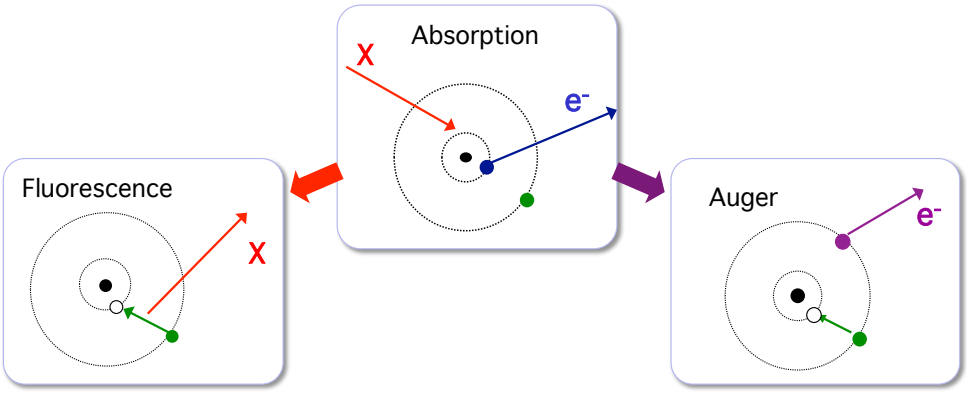

Figure 2.8: An atom excited by absorption of an X-ray (central panel) can be de-excited by two mechanisms: fluorescence (left panel) or Auger (right panel).

Radiative de-excitation: characteristic lines

The core-hole is filled by an electron coming from an upper level. In the radiative de-excitation, the energy made available by this process is emitted as an X-ray photon (*fluorescence photon*). The energy of a fluorescence photon is the difference of the energies of the two levels involved in the electronic transition. Since the energy levels are characteristic of each atomic species, fluorescence X-rays are emitted at well defined energies, which univocally identify the atomic species. They are called *characteristic emission lines*.

Non-radiative de-excitation: Auger electrons

The core-hole is again filled by an electron coming from an upper level. In non-radiative de-excitation, the energy made available by this process is used to expel an electron from an upper level of the atom. It is a *two electrons* process. The emitted electron is called *Auger electron*. Also Auger electrons have well defined energies, which univocally identify the atomic species.

Non radiative de-excitation transitions arise from the electrostatic interaction between two electrons in an atom initially singly ionised in a core shell.

One can further distinguish the non-radiative effects:

- if the filling electron comes from an upper shell (as is always the case for a core hole of the K shell) one properly speaks of Auger effect
- if the filling electron comes from an upper sub-shell of the same shell of the core hole, one speaks of Coster-Kronig effect

Fluorescence yield

The two de-excitation mechanisms (radiative and non-radiative) are in competition. Their relative influence is measured by the *fluorescence yield*

$$\eta_s \;=\; X_s/(X_s + A_s) \tag{2.74}$$

where s labels a given absorption edge (K, L_1, ...), X_s and A_s are the emission probabilities of a fluorescence photon and an Auger electron, respectively. The fluorescence yield depends on the atomic number (Fig. 2.9, left). The probability of Auger electron production increases when the difference between the energy of the levels decreases, say when Z decreases [de Groot and Kotani, 2008], according to the approximate law (§8.3 of [Chen and Kotlarchyk, 1997])

$$\eta_s \;=\; \frac{1}{1 + \alpha Z^{-4}}\,, \tag{2.75}$$

where
$\alpha \simeq 1.12 \times 10^6$ for the K-shell fluorescent yield
$\alpha \simeq 6.4 \times 10^7$ for the averageL-shells fluorescent yield.
A review of calculations and measurements can be found in [Bambynek et al., 1972].

2.5.2 Core-hole lifetime

The total de-excitation probability per unit time determines the *core-hole lifetime*. The deeper the core hole and the larger the atomic number Z, the larger is the number of upper levels from which an electron can drop to fill the core hole and consequently the shorter is the core-hole lifetime τ_h. Typical values of τ_h for X-ray excitations are $10^{-15} \div 10^{-16}$ seconds.
The core-hole lifetime τ_h represents an upper limit to the time allowed to the photo-electron for probing the local structure surrounding the absorber atom.
Because of the time-energy uncertainty relation, the core-hole lifetime is associated with an *energy width of the excited state* $\Gamma_h \simeq \hbar/\tau_h$. The width Γ_h contributes to the resolution of x-ray absorption experimental spectra. For a given edge, the larger the atomic number Z, the lower is the lifetime τ_h and the larger the energy width Γ_h (Fig. 2.9, right).

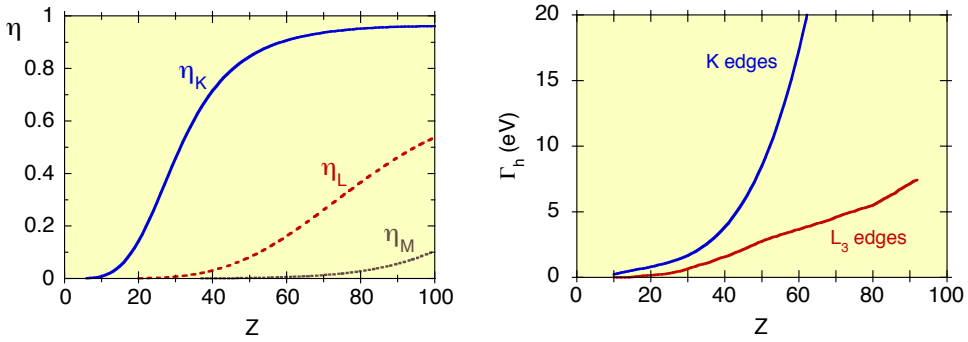

Figure 2.9: Average fluorescence yield η (Eq. 2.74) for the K, L and M edges *(left)* and width Γ_h of the K and L_3 excited states *(right)* as a function of the atomic number Z.

2.5.3 Photo-absorption measurement

The intensity of the fluorescence and of the Auger emission are strictly connected (even if generally not proportional) to the absorption coefficient: the stronger the absorption, the stronger the fluorescence and Auger emissions.
The measurement of the fluorescence or Auger intensities as a function of the energy of the X-ray beam impinging on the sample can be used to evaluate the absorption coefficient, alternatively to the direct measurement of the attenuated beam past the sample.

Chapter 3

Origin of EXAFS

In Section 2.4 of Chapter 2, we have seen that, within a set of reasonable approximation (one-electron, electric dipole, sudden), the absorption cross section in the EXAFS energy region can be expressed as

$$\sigma_{el}(\omega) \;=\; \frac{\pi e^2 \omega}{\epsilon_0 c} \; |\, \langle\, \psi_f |\; \hat{\eta} \cdot \vec{r}\; |\psi_i\,\rangle\, |^2 \;\; S_0^2 \;\rho(\epsilon_f)\,. \tag{3.1}$$

In the EXAFS region, the density of final states $\rho(\epsilon_f)$ varies slowly and monotonously. EXAFS oscillations are thus described by the matrix element $|\langle\psi_f|\hat{\eta}\cdot\vec{r}|\psi_i\rangle|^2$. The structural information is contained in the one-electron final state $|\,\psi_f\rangle$.
In the following, we want to find the relation between local structure and EXAFS oscillations. For concreteness, we consider the contribution of a K edge to the absorption coefficient.
We start by supposing that $S_0^2 = 1$, say that intrinsic inelastic transitions are negligible; their contribution will be taken into account later on.

3.1 The atomic absorption coefficient

For an isolated atom, the final state $|\,\psi_f^0\rangle$ is represented by a photoelectron which moves away from the atom as an outgoing wave, and eq. (3.1) becomes

$$\sigma_0(\omega) \;\propto\; \left|\, \langle\, \psi_f^0 |\; \hat{\eta} \cdot \vec{r}\; |\psi_i\,\rangle\, \right|^2 . \tag{3.2}$$

The correspnding atomic absorption coefficient is

$$\mu_0 \;=\; n\,\sigma_0 \;\propto\; \left|\, \langle\, \psi_f^0 |\; \hat{\eta} \cdot \vec{r}\; |\psi_i\,\rangle\, \right|^2 , \tag{3.3}$$

where n is the atomic number density (number of atoms per unit volume).
In the energy region between two consecutive absorption edges, the atomic absorption coefficient decreases monotonically as a function of the photon energy $\hbar\omega$ (Fig. 3.1); this trend is generally expressed as a function of the photon wavelength λ by the Victoreen empirical law

$$\mu_0/\rho \;=\; C\,\lambda^3 \;-\; D\,\lambda^4\,, \tag{3.4}$$

where C and D are two constants.
Values of the mass attenuation coefficients μ_0/ρ for elements and selected compounds are available in the web site of NIST [NIST, 2004]. Efforts to improve the experimental accuracy of mass attenuation coefficients are made by several researchers [Chantler et al., 2001, Padežnik Gomilšek et al., 2011, Chantler et al., 2012]. A tutorial calculation of the attenuation coefficient of hydrogen can be found in Section 7.1 of [Als-Nielsen and McMorrow, 2011].

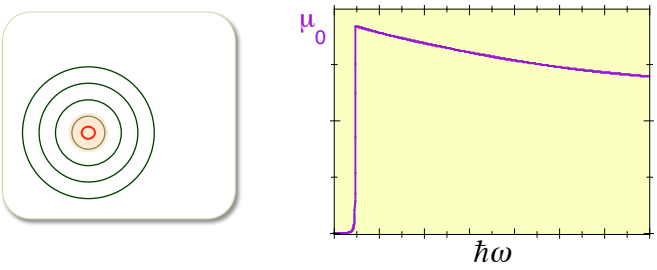

Figure 3.1: The outgoing photo-electron (left) and the atomic absorption coefficient of an isolated atom (right).

3.1.1 The photo-electron wave-number

The dynamical properties of the photo-electron are characterised the wavelength λ or by the wave-number $k = 2\pi/\lambda$ (don't confuse with the analogous quantities of X-ray photons). The photoelectron wave-number k is connected to the photo-electron energy ϵ_f and to the photon energy $\hbar\omega$ by

$$k = \sqrt{(2m/\hbar^2)\,\epsilon_f} = \sqrt{(2m/\hbar^2)\,(\hbar\omega - E_b)} \tag{3.5}$$

where E_b is the core electron binding energy.
Numerically, if k is measured in Å^{-1} and ϵ in eV,

$$k = 0.51233\,\sqrt{\epsilon}\,.$$

The energy $\epsilon_f = \hbar\omega - E_b$ and the corresponding wave-number k refer to a photo-electron that is completely free, say at a relatively large distance from the initial core orbital.
Photo-electron wave-number k (left) and wavelength λ (right) are shown in Fig. 3.2 as a function of the photo-electron energy ϵ_f. Note the little variation of λ for energies ϵ_f larger than 200-300 eV.

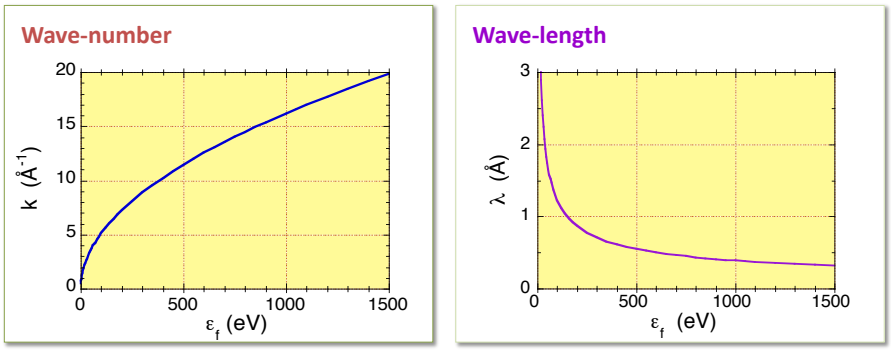

Figure 3.2: Photo-electron wave-number k (left) and wavelength λ (right) as a function of the photo-electron energy $\epsilon_f = \hbar\omega - E_b$.

3.1.2 The free electron propagator

The photo-electron state is characterized by its angular momentum. It is convenient to consider the photo-electron as a free electron, and taking into account the interaction with the emitting atom by a suitable k-dependent phaseshift.
In polar coordinates, the Schrödinger equation for the free electron leads to (§6 of Appendix B of [Messiah, 1970])

$$\left[\frac{1}{\rho}\,\frac{d^2}{d\rho^2} + 1 - \frac{\ell(\ell+1)}{\rho^2}\right] f_\ell = 0,$$

where $\rho = kr$. The spherical Bessel functions j_ℓ are special solutions of this equation.
The free electron propagators are the Hankel functions of the first kind $h_\ell^{(+)}$, linear combinations of the outgoing spherical Bessel functions. Explicit general form:

$$h_\ell^{(+)} = \frac{e^{i\rho}}{\rho} \sum_{s=0}^{\ell} \frac{i^{s-\ell}}{2^s s!} \frac{(\ell+s)!}{\ell-s)!} \rho^{-s}$$

In particular:

$$h_0^{(+)} = \frac{e^{i\rho}}{\rho}, \qquad h_1^{(+)} = \frac{e^{i\rho}}{\rho}\left[\frac{1}{\rho} + \frac{1}{\rho^2}\right] = \frac{e^{i\rho}}{\rho^2}\left[1 + \frac{1}{\rho}\right].$$

For a photoelectron ejected from a K shell, $\ell = 1$ and the free photoelectron wavefunction is $h_1^{(+)}$ [Stern, 1974, Müller and Schaich, 1983].
For $\rho = kr \gg \ell$ (typically in the EXAFS region), the propagator $h_1^{(+)}$ reduces to [Müller and Schaich, 1983]

$$h_1^{(+)} = \frac{e^{i\rho}}{\rho^2}. \tag{3.6}$$

3.2 Non-isolated atom: origin of EXAFS

If the absorber atom is non-isolated (molecular gases, condensed systems) the photo-electron can interact with the surrounding atoms and undergo scattering (Fig. 3.3). In the EXAFS region, the photo-electron energy is much larger than the electron–atom interaction energy (of the order of some eV), so that the interaction causes a weak perturbation to the the final state:

$$|\psi_f\rangle = |\psi_f^0 + \delta\psi_f\rangle. \tag{3.7}$$

and the absorption coefficient becomes

$$\mu(\omega) \propto \left|\langle \psi_f^0 + \delta\psi_f | \hat{\eta}\cdot\vec{r}\,|\psi_i\rangle\right|^2. \tag{3.8}$$

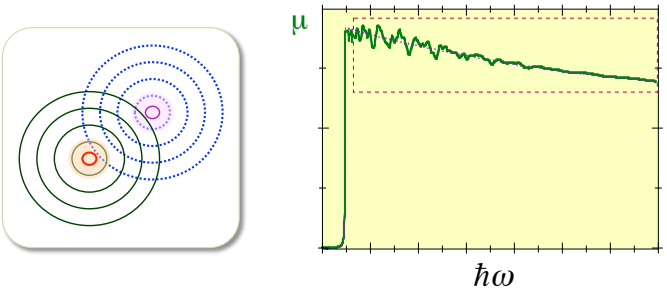

Figure 3.3: The outgoing and back-scattered photo-electron (left) and the absorption coefficient of a non-isolated atom (right).

3.2.1 Basic interference effect

The perturbation $|\delta\psi_f\rangle$ corresponds phenomenologically to the incoming wave of the backscattered electron. The final state is modified so that

$$|\psi_f|^2 = |\psi_f^0|^2 + 2\mathrm{Re}\left\{\psi_f^0\ \delta\psi_f\right\} + |\delta\psi_f|^2. \tag{3.9}$$

The presence of the perturbation $|\delta\psi_f\rangle$ modifies the superposition integral of the final state with the initial core state $|\psi_i\rangle$ in the matrix element with respect to (3.3), so that

$$\mu(\omega) \propto \left|\langle \psi_f^0 | \hat{\eta}\cdot\vec{r}|\psi_i\rangle\right|^2 + 2\mathrm{Re}\left\{\langle\psi_f^0|\hat{\eta}\cdot\vec{r}|\psi_i\rangle\ \langle\delta\psi_f|\hat{\eta}\cdot\vec{r}|\psi_i\rangle\right\} + \left|\langle\delta\psi_f|\hat{\eta}\cdot\vec{r}|\psi_i\rangle\right|^2. \tag{3.10}$$

Our problem is now to find an expression for the perturbation $|\delta\psi_f\rangle$.

3.2.2 The perturbation $\delta\psi_f$ for a two-atomic system

A number of different but equivalent derivations of the EXAFS function (3.19) have been proposed [**?**, Hayes and Boyce, 1982, Stern, 1974, Borovskii et al., 1986]. None of them is however sufficiently simple for an introductory account.
In the following, we will highlight the basic concepts from a phenomenological point of view, following the approach of [Brown and Doniach, 1980]. Only ideal systems composed of atoms frozen at their equilibrium positions are at first considered; thermal disorder is introduced later on.

The simpler system consists of two atoms, an absorber A and a back-scatterer B; let R be the distance between the two nuclei (Fig. 3.4). For a given value $\hbar\omega$ of the energy of the absorbed photon, the quantum state of the emitted photoelectron is characterised by the wavenumber k, defined in (3.5). The photo-electron is subjected to the potentials of the emitting atom A and of the scattering atom B, which are generally approximated by dividing the space into three regions (Fig. 3.4), corresponding respectively to:

I - a spherically symmetric attractive potential centred on atom A;
II - a constant *inner potential*, connected to the potentials of regions I and III;
III - a spherically symmetric attractive potential centred on atom B.

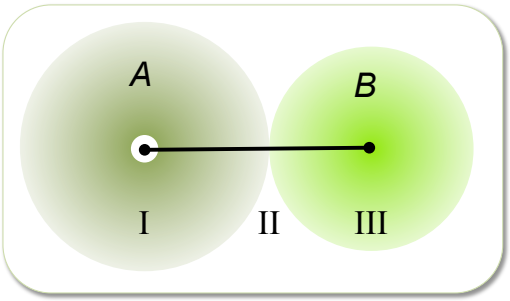

Figure 3.4: Absorber atom A and back-scatterer atom B at a distance R. The coloured regions I and II schematically represent the spherically symmetric potentials created by the two atoms, the remaining region II represents the inner potential (muffin-tin approximation). The small white circle at the centre of region I schematically represents the $1s$ core orbital.

The wavefunction ψ_i of the initial $1s$ core state of angular momentum $\ell = 0$ is confined within the core volume schematically represented by the white circle at the centre of region I in Fig. 3.4. Also the final state wavefunction ψ_f^0 for the isolated atom, of angular momentum $\ell = 1$, has to be known only within the core volume at the centre of region I, in order to evaluate the superposition integrals of Eq. (3.19).
Actually, the explicit knowledge of ψ_i and ψ_f^0 is not necessary to calculate the EXAFS function (3.19). It is sufficient to understand how the perturbation $\delta\psi_f$ develops along the photo-electron path $A \to B \to A$ and to evaluate its superposition integral with the initial core state ψ_i.

The photo-electron emission is more probable in the direction of polarisation of the photon beam; the angular part of the outgoing wavefunction depends on the dipole term $\hat{\eta} \cdot \vec{r}$. Let us focus our attention on the radial part of the wavefunction.

At the centre of region I, corresponding to the core orbital, the outgoing photo-electron wavefunction is $\psi_f(0) = \psi_f^0(0)$, the same as for an isolated atom. At the border of region I, the radial part of the photo-electron wavefunction can be approximated, for high enough energies ($kr \gg 1$), as

$$\psi_f^0(0)\ \frac{e^{ikr}}{2kr}\ e^{i\delta_1}\,, \tag{3.11}$$

where k is the wavenumber defined in (3.5) and the phase-shift δ_1 takes into account the effect of the potential of region I.

Let us now consider the interaction between the photo-electron and the atom B in region III. If the photo-electron has high enough energy, the interaction is important only with the nucleus and the inner electrons of atom B. We can then restrict the scattering to a spatial region very small with respect to the interatomic distance R (*small atom approximation*) and neglect the curvature of the wave impinging on atom B (*plane wave approximation*).
Within these approximations, the scattering process is described in terms of a complex amplitude of back-scattering from atom B in the direction of atom A, $t(k,\pi)$, which can be expressed as a function of the partial-wave phase-shifts δ_ℓ [Joachain, 1975] as

$$t(k,\pi) \;=\; \sum\nolimits_{\ell=0}^{\infty} (-1)^\ell \,(2\ell+1)\, e^{i\delta_\ell} \,\sin\delta_\ell \tag{3.12}$$

At the border of region III, the radial part of the backscattered wave is approximated as

$$\underbrace{\left[\psi_f^0(0)\;\frac{e^{ikR}}{2kR}\;e^{i\delta_1}\right]}_{\text{wave impinging on B}} \quad t(k,\pi) \quad \underbrace{\left[\frac{e^{ikr'}}{kr'}\right]}_{\text{scattered by B}} \tag{3.13}$$

where r' is the distance from atom B.

At the absorber core site (centre of region I), the final backscattered wave function is obtained by substituting $r' = R$ in (3.13) and adding a further phase-shift δ_1 to account for the potential of region I.

The final wavefunction at the core site can be conveniently expressed as

$$\delta_f(0) \;=\; \psi_f^0(0)\;\;\frac{1}{2}\;e^{i\delta_1}\;\frac{e^{ikR}}{kR}\;\;t(k,\pi)\;\;\frac{e^{ikR}}{kR}\;\;e^{i\delta_1}\,, \tag{3.14}$$

In Eq. (3.14) both outgoing and scattered wave-functions contain k at the denominator, according to [Stern, 1988], corresponding to a total factor $1/k^2$.
In most treatments, however, a factor $1/k$ is present in the EXAFS formula, the other $1/k$ factor being included into the scattering amplitude $f_B(k,\pi) = (1/k)\,t(k,\pi)$. Such a convention is used in the following, so that

$$\delta_f(0) \;=\; \psi_f^0(0)\;\;\frac{1}{2k}\;\underbrace{e^{i\delta_1}}_{\text{inter.}}\;\underbrace{\frac{e^{ikR}}{R}}_{\text{propag.}}\;\;\underbrace{f_B(k,\pi)}_{\text{inter.}}\;\;\underbrace{\frac{e^{ikR}}{R}}_{\text{propag.}}\;\;\underbrace{e^{i\delta_1}}_{\text{inter.}}, \tag{3.15}$$

Eq. (3.15) contains two types of factors:

a) factors describing the interaction of the photoelectron with atoms A and B, such as $e^{i\delta_1}$ and $f_B(k,\pi)$;
b) factors describing the propagation of the photoelectron from atom A to atom B and from atom B to atom A, such as e^{ikR}/R.

Such a basic structure is shared by more sophisticated approaches, which can take into account also multiple scattering (MS) events.

3.2.3 The absorption coefficient

Revriting (3.15)

$$\delta_f(0) \;=\; \psi_f^0(0)\;\;\frac{1}{2k}\;e^{i2\delta_1}\;\frac{e^{i2kR}}{R^2}\;f_B(k,\pi) \tag{3.16}$$

and inserting in (3.10), one can better understand the meaning of the different terms.

1. The first term of (3.10) corresponds to the atomic absorption coefficient of an isolated atom (3.3).

2. The second term of (3.10) side accounts for the interference between the outgoing and incoming waves and is responsible for the EXAFS oscillations.
3. The third term of (3.10) has a smooth k-dependence and doesn't contribute to EXAFS oscillations; being second-order in the perturbation $\delta\psi_f$, it gives a small contribution to the atomic absorption coefficient μ_0.

The third term of (3.10) represents a small correction to μ_0, which is taken into account when the EXAFS function is determined from experimental data (see below).

3.3 The EXAFS function

The EXAFS function is defined as the difference between the actual absorption coefficient μ and the atomic absorption coefficient μ_0, normalized to μ_0 (Fig. 3.5):

$$\chi(k) = \frac{\mu - \mu_0}{\mu_0} \tag{3.17}$$

and is generally expressed as a function of the wave-number k (3.5) rather than of the energy. The amplitude of the EXAFS oscillations ranges typically between 1 and 10 % of the absorption coefficient.

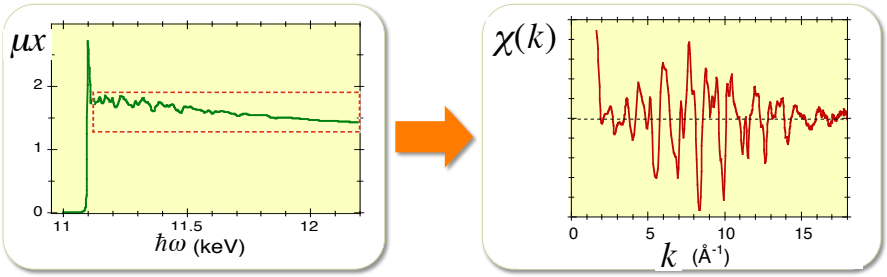

Figure 3.5: Left: experimental absorption coefficient μx as a function of photon energy. Right: corresponding normalised EXAFS function (3.17).

Note 1: What one actually measures is the product μx, where x is the sample thickness, and the corresponding product $\mu_0 x$. The (generally unknown) sample thickness x is anyway cancelled in (3.17).

Note 2: In the derivation of (3.17) from experimental data, μ_0 contains the small contribution of the third term of (3.10). The coefficient μ_0 is estimated from experimental data by evaluating the average behaviour of the actual absorption coefficient μ (see Chapter on data analysis). It doesn't thus correspond to the true atomic coefficient and contains also the smooth contribution of the third term in (3.10).

3.3.1 EXAFS for a two-atomic system

Inserting the absorption coefficients (3.3) and (3.10) in the EXAFS function (3.17) and considering the third term of (3.10) embedded in ν_0, one obtains

$$\chi(k) = \frac{2\mathrm{Re}\left\{\langle\psi_f^0|\,\hat{\eta}\cdot\vec{r}\,|\psi_i\rangle\ \langle\delta\psi_f^0|\,\hat{\eta}\cdot\vec{r}\,|\psi_i\rangle\right\}}{\left|\,\langle\,\psi_f^0|\ \hat{\eta}\cdot\vec{r}\ |\psi_i\,\rangle\,\right|^2} \tag{3.18}$$

In the coordinate representation, the EXAFS function can be expressed in terms of wave-function integrals as

$$\chi(k) \;=\; \frac{2\mathrm{Re}\int d\vec{r}\;\left[\psi_f^{0*}(\vec{r})\;\hat{\eta}\cdot\vec{r}\;\psi_i(\vec{r})\right]\;\left[\delta\psi_f^{*}(\vec{r})\;\hat{\eta}\cdot\vec{r}\;\psi_i(\vec{r})\right]}{\int d\vec{r}\;\left|\psi_f^{0*}(\vec{r})\;\hat{\eta}\cdot\vec{r}\;\psi_i(\vec{r})\right|^2} \tag{3.19}$$

The integral in the numerator of Eq. (3.19) is responsible for the interference between the outgoing and incoming wave-functions.

The leading contribution to all integrals of Eq. (3.19) comes from the limited spatial region of the core orbital, which represents both the *source* and *detector* for the photo-electron probing the surrounding structure. Only in this limited spatial region is it in principle necessary to know both ψ_f^0 and $\delta\psi_f$.
The central problem is now to evaluate the perturbation $\delta\psi_f$ at the core region in terms of the interatomic distance, in order to connect the EXAFS function to the structural parameters.

If the result expressed by eq. (3.14) is properly inserted into eq. (3.19), one gets

$$\chi(k) \;=\; 3(\hat{\boldsymbol{\eta}}\cdot\hat{\mathbf{R}})^2\,\frac{1}{kR^2}\;\mathrm{Im}\left\{f_B(k,\pi)\;e^{2i\delta_1}\;e^{2ikR}\right\}. \tag{3.20}$$

By separating modulus and phase of the complex backscattering amplitude and grouping the phase terms,

$$f_B(k,\pi)\;e^{2i\delta_1} \;=\; |f_B(k,\pi)|\;e^{i\phi(k)}, \tag{3.21}$$

we can write Eq. (3.20) in real form:

$$\chi(k) \;=\; 3(\hat{\boldsymbol{\eta}}\cdot\hat{\mathbf{R}})^2\,\frac{1}{kR^2}\;|f_B(k,\pi)|\;\sin\left[2kR+\phi(k)\right]. \tag{3.22}$$

Basically, the EXAFS signal has a sinusoidal behaviour, with frequency $2R$ proportional to the inter-atomic distance. The phase of the sine function is perturbed by the phase-shift $\phi(k)$, while the amplitude is modulated by $|f_B(k,\pi)|$.

3.3.2 Backscattering amplitude and phaseshifts

The k dependence of backscattering amplitudes and phaseshifts is different for different atomic species.
The central atom phaseshift δ always decreases monotonously when the wavevector k increases (Fig. 3.6, right). The modulus of the backscattering amplitude $|f(k,\pi)|$ decreases monotonously for low-Z atomic species; it becomes higher at high k values and progressively more structured when Z increases (Fig. 3.6, centre). Correspondingly, the backscattering phaseshift exhibits a more structured behaviour when Z increases (Fig. 3.6, right).
The different behaviour of the backscattering amplitude and phase-shift for different Z values is currently exploited for distinguishing the atomic species of the scattering atom with reasonable approximation.
For realistic spherical waves (say if the plane wave approximation is released), phase-shifts and amplitudes weakly depend also on the interatomic distance: $\phi(k,r)$, $|f(k,\pi,r)|$ [Rehr and Albers, 2000].

3.3.3 Many-atomic systems

Let us now consider a system composed of more than two atoms. The generalization of (3.20) is immediate, so long as multiple scattering events can be neglected: the EXAFS function can be built up as a sum of two-atomic contributions (3.20), with different interatomic distances R_j from the absorber atom.

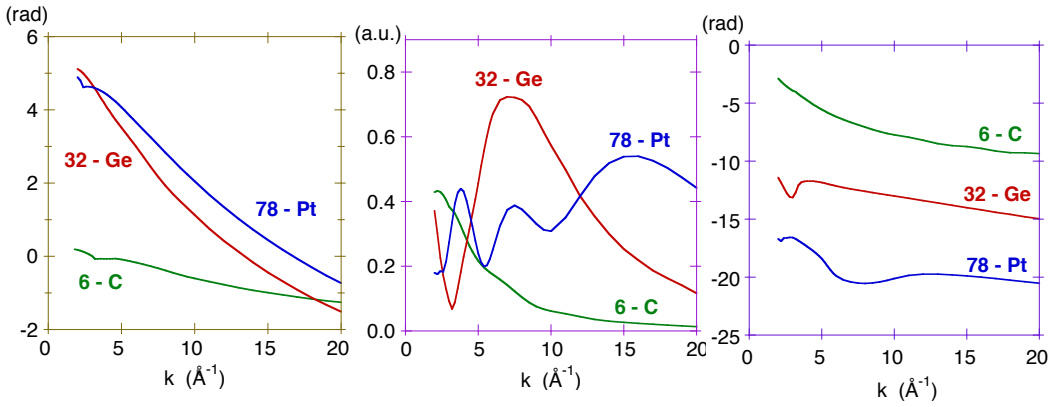

Figure 3.6: Central atom phaseshifts (left), backscattering amplitudes (centre) and backscattering phaseshifts (right) calculated for selected atomic species by FEFFIT 6.1 within the plane wave approximation. The total phaseshift $\phi(k)$ of (3.21) and (3.22) is the sum of the phaseshifts of the left and right panels.

Isotropic samples

Very often, EXAFS measurements are performed on isotropic samples, such as polycrystalline powders, amorphous materials, liquids or gases. In the following, we consider only isotropic samples, for which the polarization term can be averaged, $\langle \hat{\boldsymbol{\eta}} \cdot \hat{\mathbf{R}} \rangle = 1/3$, leading to a simplified treatment which neglects the angular part of the wavefunctions.
For an isotropic sample, the EXAFS function is

$$\chi(k) \;=\; \frac{1}{k} \sum\nolimits_j \frac{1}{R_j^2} \;\mathrm{Im}\; \left\{ f_j(k,\pi)\; e^{2i\delta_1}\; e^{2ikR_j} \right\} , \tag{3.23}$$

where R_j is the distance of the j-th atom from the absorber atom.

Coordination shells

In many cases, atoms can be grouped into coordination shells , each one containing N_s atoms of the same species at the same distance R_s from the absorber atom.
Coordination shells are well defined for perfect crystals when thermal motion is neglected (Fig. 3.7, left). Thermal motion introduces a spread of interatomic distances within each shell (see below). In non-crystalline systems generally only a few coordination shells can be distinguished, which are anyway less sharply defined than in crystals, due to structural disorder (Fig. 3.7, right).

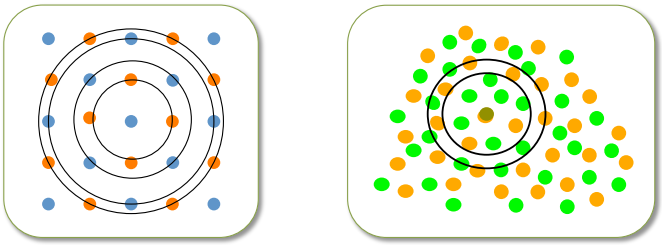

Figure 3.7: For crystals (left) the coordination shells of a given atom are in principle perfectly defined at any distance. For non-crystalline systems (right) the coordination shells are quite well defined only at short distances.

EXAFS for one coordination shell

Let us consider a coordination shell of a perfect crystal, neglecting any thermal disorder. All N atoms of the shell share the same distance R from the absorbing atom. The final state (3.7) is transformed into

$$|\psi_f\rangle \;=\; |\psi_f^0 \;+\; N\,\delta\psi_f\rangle. \tag{3.24}$$

The absorption coefficient (3.10) becomes

$$\mu(\omega) \;\propto\; \left|\langle\psi_f^0|\,\hat\eta\cdot\vec r\,|\psi_i\rangle\right|^2 \;+\; 2\,N\,\mathrm{Re}\left\{\langle\psi_f^0|\,\hat\eta\cdot\vec r\,|\psi_i\rangle\;\langle\delta\psi_f|\,\hat\eta\cdot\vec r\,|\psi_i\rangle\right\} \;+\; N^2\,\left|\langle\delta\psi_f|\,\hat\eta\cdot\vec r\,|\psi_i\rangle\right|^2. \tag{3.25}$$

1. The first term again corresponds to the atomic absorption coefficient of an isolated atom (3.3).
2. The second term, accounting for the interference between the outgoing and incoming waves and responsible for the EXAFS oscillations, is N times the term for a single backscatterer atom.
3. The third term, proportional to N^2, doesn't contribute to EXAFS oscillations and gives a small contribution to the atomic absorption coefficient μ_0.

EXAFS and coordination shells

In general, it is convenient to rewrite (3.20) separating the contributions of the different coordination shell:

$$\chi(k) = \frac{1}{k}\;\sum_s\;\frac{N_s}{R_s^2}\;\mathrm{Im}\left\{f_s(k,\pi)\;e^{2i\delta_1}\;e^{2ikR_s}\right\}. \tag{3.26}$$

The sum in (3.26) is on the index s, which labels the coordination shells. The parameter N_s is the *coordination number* of shell s.
The effects of thermal and structural disorder are considered below.

3.4 Inelastic effects

As it was shown in Chapter 2, the total absorption cross section is the sum of two terms,

$$\sigma_a(\omega) \;=\; \sigma_{\mathrm{el}}(\omega) \;+\; \sigma_{\mathrm{inel}}(\omega)\,. \tag{3.27}$$

The treatment that leads to (3.26) is based on elastic (fully relaxed) transitions and corresponds to the first term on the right of (3.27). Let us now study how inelastic phenomena affect the EXAFS signal. Two types of inelastic effects have to be distinguished:

a) intrinsic effects, which are many-body interactions within the absorber atom and correspond to σ_{inel} in (3.27);
b) extrinsic effects, which are many-body interactions of the photoelectron with electrons not belonging to the emitting atom.

3.4.1 Intrinsic inelastic effects

In the inelastic excitation channels of the X-ray absorption process, the relaxation of the $N-1$ passive electrons is accompanied by their excitation (shake-up and shake-off processes). The X-ray photon energy is distributed over all the excited electrons, and the photoelectron has a distribution of possible energies, so that the corresponding EXAFS signals sum up incoherently and give rise to a damping of the experimentally observed oscillations.

The net effect is a reduction of the coherent EXAFS signal with respect to that calculated for purely elastic excitations in (3.26). One can show that the fraction of the total cross section (3.27)

that corresponds to the elastic channel $\sigma_{\rm el}$ is measured by the superposition integral of the passive electrons wavefunctions

$$S_0^2 \;=\; \left| \langle\, \Psi_{f,r}^{N-1} | \Psi_i^{N-1} \,\rangle \right|^2 . \tag{3.28}$$

In order to reproduce an experimental signal, the EXAFS function (3.26), based on the elastic cross section, has to multiplied by the factor S_0^2, which typically amounts to $0.7 \div 0.9$.

3.4.2 Extrinsic inelastic effects

Extrinsic inelastic effects are losses during the photo-electron propagation, due to excitations (plasmons, core-hole) and inelastic scattering.

From a phenomenological point of view, the extrinsic inelastic losses are taken into account by a k-dependent mean free path $\lambda_e(k)$ (don't confuse λ with the photo-electron wavelength).

From a theoretical point of view, the extrinsic inelastic losses are connected to a complex-valued and energy-dependent *self-energy operator* $\Sigma(E)$.
The complex-valued self-energy operator plays, for an excited state, the same role that the real-valued exchange-correlation potential plays for the ground state.
The real part of $\Sigma(E)$ gives rise to a shift of the EXAFS oscillations with respect to ground-state calculations.
The imaginary part of $\Sigma(E)$ gives rise to the mean free path, $\lambda_e \simeq k/|{\rm Im}\Sigma(E)|$.

3.4.3 Extrinsic inelastic effects: mean free path

Extrinsic inelastic effects are losses of the energy of the photoelectron during its propagation, due to excitations (core-hole and plasmons) and inelastic scattering by other single electrons.
From a phenomenological point of view, the extrinsic inelastic losses are measured by a k-dependent mean free path $\lambda(k)$ (don't confuse λ with the photo-electron wavelength).

From a theoretical point of view, the extrinsic inelastic losses are connected to a complex-valued and energy-dependent *self-energy operator* $\Sigma(E)$.
The complex-valued self-energy operator plays, for an excited state, the same role that the real-valued exchange-correlation potential plays for the ground state.
The real part of $\Sigma(E)$ gives rise to a shift of the EXAFS oscillations with respect to ground-state calculations.
The imaginary part of $\Sigma(E)$ gives rise to the mean free path, $\lambda_e \simeq k/|{\rm Im}\Sigma(E)|$.

Two distinct phenomena contribute to the total mean free path λ:

a) the core-hole lifetime τ_h, which depends on the atomic number Z (the higher Z, the shorter τ_h) and establishes the distance $\lambda_h = v\tau_h$ the photo-electron can travel before the de-excitation of the absorber atom;
b) the energy-dependent photo-electron mean-free path λ_e, determined by the inelastic interactions with single electrons and collective excitations (plasmons).

The smaller of the two contributions determines the actual value of λ, according to:

$$\frac{1}{\lambda} \;=\; \frac{1}{\lambda_h} \;+\; \frac{1}{\lambda_e}. \tag{3.29}$$

At low energies, in the XANES region, the mean free path is determined by λ_h, while in the EXAFS region the contribution of λ_e is predominant (Fig. 3.8).
The mean free path measures the average distance an excited electron can travel before losing coherence with its initial state.

The extrinsic inelastic effects are generally taken into account in the EXAFS formula by a phenomenological factor $\exp[-2R_j\lambda(k)]$, where $\lambda \simeq 5 - 15$ Å. The mean free path factor progressively reduces the amplitude of EXAFS oscillations when R_j increases, contributing to making EXAFS insensitive to long range order.

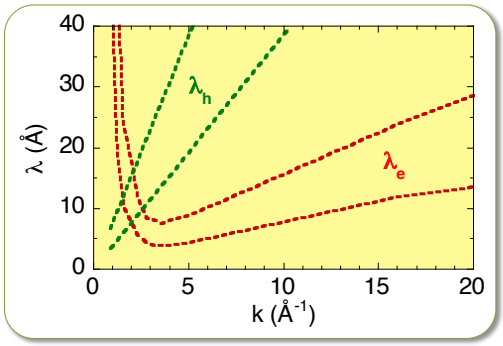

Figure 3.8: Mean free path as a function of the wavevector k. The values λ_e measured for different elements are included between the two continuos lines. The dashed lines include the λ_h values for the K edges of atoms with Z between 30 and 50.

3.4.4 EXAFS formula including inelastic effects

To summarize, the EXAFS equation taking into account inelastic effects is:

$$\chi(k) \;=\; \frac{S_0^2}{k} \sum\nolimits_j \frac{e^{-2R_j/\lambda}}{R_j^2} \;\mathrm{Im}\; \left\{ f_j(k,\pi)\; e^{2i\delta_1}\; e^{2ikR_j} \right\}. \tag{3.30}$$

If atoms can be grouped into coordination shells, one can rewrite Eq. (3.30) separating the contributions of different coordination shell, as in (3.26):

$$\chi(k) = \frac{S_o^2}{k} \sum_s N_s \;\mathrm{Im}\left\{ f_s(k,\pi)\; e^{2i\delta_1}\; \frac{e^{-2R_s/\lambda}}{R_s^2}\; e^{2ikR_s} \right\}. \tag{3.31}$$

3.5 Multiple scattering

Up to now, we have considered only single scattering (SS) paths of the photo-electron, consisting in two "legs", the first one from the the emitting atom A to the scattering atoms B, the second one from the scattering atom B back to the emitting atom A (two examples are shown in the rigth panel of Fig. 3.9).

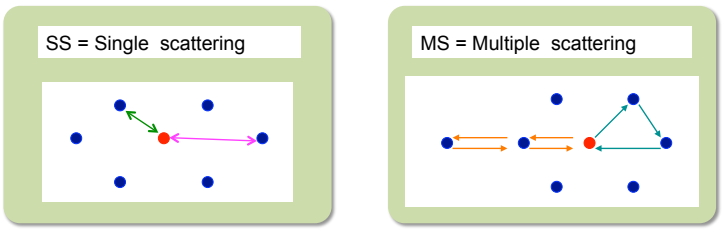

Figure 3.9: Left: possible single scattering paths originating from and terminating at a given central atom (red). Right: possible multiple scattering paths originating from and terminating at a given central atom (red).

Actually, multiple scattering (MS) paths are possible too, where the photoelectron is scattered by two or more atoms before coming back to the emitting atom A. Two significant examples are shown in the right panel of Fig. 3.9): *a)* a triangular path $A \to B \to C \to A$ and *b)* a collinear path $A \to B \to C \to B \to A$, where the photoelectron is forward scattered by atom B.
Multiple scattering events are very important in the XANES region, due to the relatively low energy of the photoelectron. They are generally quite weak in the EXAFS region, but not at all

negligible; particularly strong is the contribution of collinear MS paths, due to the high amplitude for scattering at 180° (forward scattering).

To take into account MS effects, the absorption coefficient is conveniently written as

$$\mu(k) \;=\; \mu_0(k)\,[1+\chi_2(k)+\chi_3(k)+\chi_4(k)+\cdots]\,, \tag{3.32}$$

where the terms χ_p of the sum are distinguished by the number p of legs of the scattering paths. The term $\chi_2(k) \equiv \chi(k)$ corresponds to the single scattering contributions up to now considered. In the EXAFS region, the series (3.32) is fast convergent. The convergence becomes progressively slower when the wavevector k decreases, say approaching the XANES region.
It has been demontrated [Rehr and Albers, 2000] that the contribution of MS paths to the EXAFS signal can be expressed, similar to the SS contribution, as the product of an amplitude factor and an oscillating factor; for a given path p,

$$\chi_p(k) \;=\; A_p(k,\{\mathbf{r}\}_p)\,\sin\left[kR_p+\phi_p(k,\{\mathbf{r}\}_p)\right]\,, \tag{3.33}$$

where $\{\mathbf{r}\}_p$ represents the set of all vector distances inside the path, R_p is the total path length, and A_p and ϕ_p are effective amplitude and phaseshift functions which depend on the potential acting on the photo-electron.

3.6 Disorder effects on EXAFS

Equation (3.31) refers to the unphysical situation of a system where the atoms are frozen at their equilibrium positions.

Thermal disorder

In real systems, atoms are affected by thermal vibrations, whose amplitude increases with temperature but, for quantum reasons, is not negligible even near zero kelvin. The instantaneous positions of atoms are spread around the equilibrium positions according to statistical distributions (thermal ellipsoids, left panel of Fig. 3.10).
The period of atomic vibrations ($\simeq 10^{-12}$ s) is much larger than the photo-electron time of flight ($10^{-16} \div 10^{-15}$ s). A single photo-electron samples an instantaneous distance between emitting and backscattering atom (Fig. 3.10, left). An EXAFS spectrum, resulting from the contributions of a large number of photo-electrons, samples a *distribution* of instantaneous interatomic distances r for each coordination shell (Fig. 3.10, right).

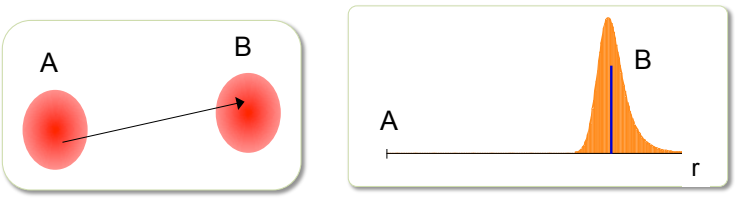

Figure 3.10: Left: a single photoelectron samples an instantaneous relative distance r between the thermal ellipsoids of the emitting and the backscattering atoms. Right: and EXAFS spectrum samples a one-dimensional distribution of instantamneous distances.

The distributions $\rho(r)$ of distances for germanium at different temperatures are shown in Fig. 3.11. The distribution $\rho(r)$ corresponds to a radial distribution function (RDF). The smooth dashed line corresponds to $4\pi r^2\,\rho_0$, where $\rho_0 = 4.42$ atoms/Å is the number density of germanium.

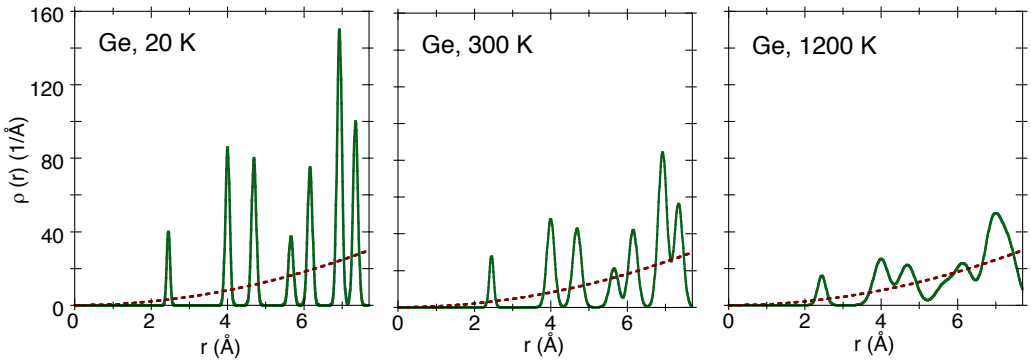

Figure 3.11: Real distributions of distances for germanium at different temperatures. The distributions of the different coordination shells have been considered as gaussian. The widths have been estimated from the experimental Debye-Waller factors [Purans et al., 2008, Purans et al., 2009] for the first three coordination shells at 20 and 300 K and extrapolated for the outer coordination shells and at 1200 K.

Structural disorder

The distribution of interatomic distances can be further enlarged and modified by the presence of structural disorder. Some examples of structural disorder are schematically depicted in Fig. 3.12.

a) Distorted coordination shells in crystals are characterised by the presence of two or more slightly different interatomic distance, which cannot be experimentally discriminated as different coordination shells.
b) In some crystalline systems, the absorber atom can be found in two or more structurally different sites, which again cannot be discriminated as different coordination shells (*sites disorder*).
c) In non-crystalline systems, the nearest-neighbour coordination is very similar to that in the corresponding crystals, the inter-atomic pair distances are however not exactly equal.
d) In nano-crystals, the distances between nearest-neighbour atoms are different according to whether the atomic pair is near the surface or at the centre of the cluster; one thus expects a static distribution of distances, to be convoluted with the distribution due to thermal motion.

A peculiar kind of disorder is **compositional disorder**, consisting in the presence of atoms of different species in the same coordination shell.

3.6.1 EXAFS formula for disordered systems

Let us consider here only coordination shells containing *one atomic species* (say without compositional disorder).
Due to disorder, the contribution to the EXAFS function of a given coordination shell (or more generally of a given scattering paths) can be expressed in terms a configurational average of the distance-dependent factors [Freund et al., 1989]:

$$\chi_s(k) = \frac{S_o^2}{k}\, N_s\, \mathrm{Im}\left\{ f_s(k,\pi)\, e^{2i\delta_1} \left\langle \frac{e^{-2r/\lambda}}{r^2}\, e^{2ikr} \right\rangle dr \right\}. \tag{3.34}$$

In the case of purely thermal disorder, with no structural contributions, the brackets $\langle\ \rangle$ in Eq. (3.34) indicate a canonical average.

Equivalently, the distance between absorber and back-scatterer atoms of a given coordination shell, instead of having a single value R_s, like in (3.31), varies according to a probability distribution $\rho(r)$,

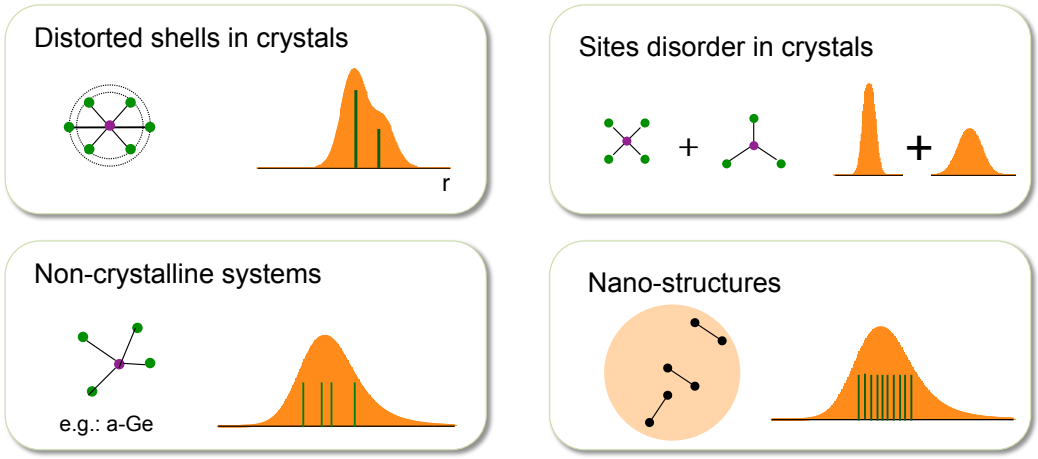

Figure 3.12: Some examples of structural disorder that can contribute to enlarge the distribution of distances due to thermal disorder.

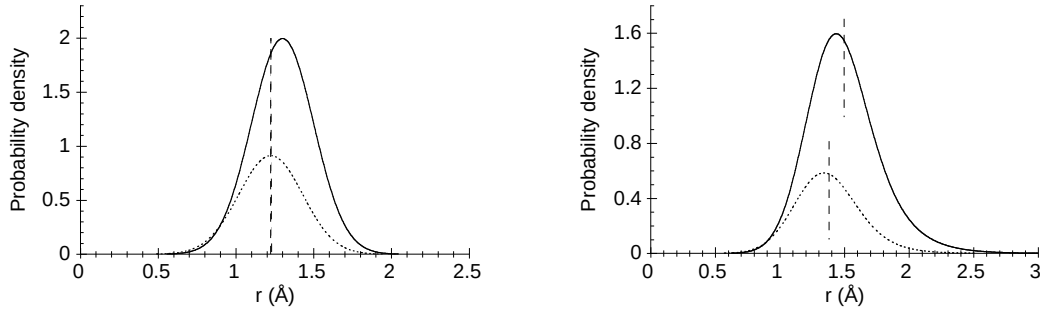

Figure 3.13: Comparison between real (continuous lines) and effective (dotted lines) distributions, Eq. (3.36), for a realistic mean free path $\lambda = 8$ Å. (The low-order corresponding cumulants are listed in Table 3.1). *Left.* Real gaussian distribution $(1/\sigma\sqrt{2\pi})\exp[(r-R)^2/2\sigma^2]$, with $R = 1.3$ Å and $\sigma = 0.2$ Å; the vertical dashed line indicates the average value of the effective distribution. *Right.* Real skewed distribution $B\,\exp[-B(r-R)]$, with $R = 1.3$ Å and $B = 5$ Å^{-1}, convoluted with a gaussian of standard deviation $\sigma = 0.2$ Å; the vertical dashed lines indicate the average values of the two distributions.

normalized to unity, and the EXAFS signal is generated from an average over this distribution. The EXAFS equation for one coordination shell becomes [Stern et al., 1975]

$$\chi_s(k) = \frac{S_o^2}{k}\, N_s\, \mathrm{Im}\left\{ f_s(k,\pi)\, e^{2i\delta_1} \int_0^\infty \rho(r)\, \frac{e^{-2r/\lambda}}{r^2}\, e^{2ikr}\, dr \right\}. \tag{3.35}$$

Real and effective distributions

The distribution $\rho(r)$ in Eq. (3.35) is commonly referred to as *real distribution* and corresponds to the partial radial distribution function (RDF) around the absorbing atomic species.
It is convenient to group all r-dependent factors into an *effective distribution*

$$P(r,\lambda) = \rho(r)\, \frac{e^{-2r/\lambda}}{r^2}, \tag{3.36}$$

so that the EXAFS equation can be rewritten as

$$\chi_s(k) = \frac{S_o^2}{k}\, N_s\, \mathrm{Im}\left\{ f_s(k,\pi)\, e^{2i\delta_1} \int_0^\infty P(r,\lambda)\, e^{2ikr}\, dr \right\}. \tag{3.37}$$

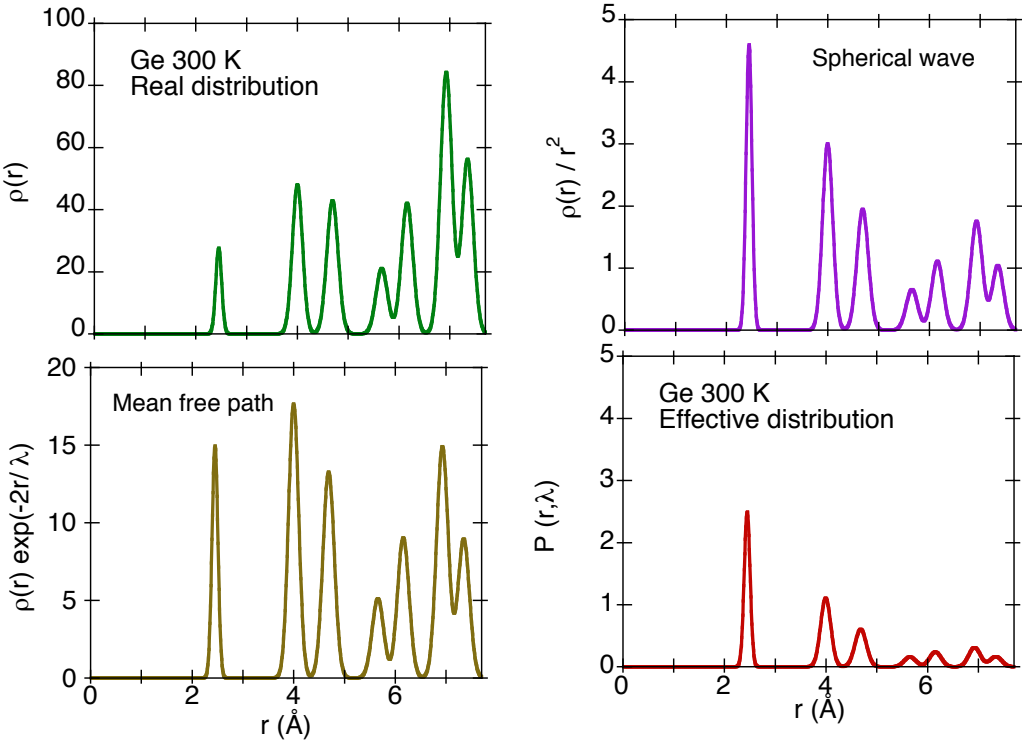

Figure 3.14: Top left: real distribution $\rho(r)$ for germanium at 300 K (left). Top right: the effect of spherical wave attenuation $1/r^2$. Bottom left: the effect of photoelectron mean free path $\exp(-2r/\lambda)$ (here $\lambda = 8$ Å). Bottom right: effective distribution $P(r,\lambda) = \rho(r)\exp(-2r/\lambda)/r^2$. Notice the different vertical scales in the different panels.

The effective distribution, contrary to the real distribution, is not normalised to one; besides, its shape is different and its average value lower (two tutorial examples are given in Fig. 3.13). The difference between real and effective distributions is physically due to the progressive attenuation of the photoelectron spherical wave with distance: the low-r part of the real distribution has a higher weight than the high-r part.
A realistic example is given in (Fig. 3.14), referred to germanium at 300 K. One can here separately evaluate the spherical wave effect $1/r^2$ and the photoelectron mean free path effect $\exp(-2r/\lambda)$ in generating the effective distribution from the real distribution. Both the reduction of the global amplitude and the damping of outer shells with respect to the inner shells are stronger for the spherical wave effect than for the mean free path effect.
Notice that in the example of Fig. 3.13 the distance 1.3 Å is much shorter than the first shell distance in Ge (Fig. 3.14), and much weaker is the spherical wave attenuation effect.

The inversion problem

The integral in Eq. (3.37) is the Fourier transform of the effective distribution $P(r,\lambda)$, or, in the probability language, its *characteristic function*. The conjugate variable is $2k$ in the case of EXAFS. The characteristic function is a complex function of a complex variable; its full knowledge is equivalent to the knowledge of the distribution $P(r,\lambda)$.
The fundamental problem of EXAFS analysis is to recover the distribution $P(r,\lambda)$, and hence $\rho(r)$, from the experimental spectrum $\chi(k)$. No exact solution can be given to this problem, because an experimental spectrum never corresponds to the full characteristic function, as expressed by Eq. (3.37), but has a finite extension, within the values $k_{\min}$ and $k_{\max}$. In particular, for $k_{\min} \leq 2 \div 3$

Å^{-1} the EXAFS signal generally cannot be utilized, due to: *a)* difficulty in determining the atomic absorption coefficient μ_0 in the vicinity of the edge, *b)* effects of the core-hole lifetime on the low-energy electrons, *c)* influence of multiple scattering processes.

The problem of recovering $\rho(r)$ from $\chi(k)$ is generally solved by hypothesising physically sound structural models and optimising the parameters of their distributions $\rho(r)$ by best fit of eq. (3.35) to the experimental EXAFS spectrum [Filipponi, 2001].

For weak disorder, the distributions of distances (both real and effective) can be parameterised in terms of a few statistical parameters, called cumulants, which are linear combinations of the more familiar moments. Correspondingly, the EXAFS signal can be expressed in terms of a few leading cumulants, as is shown below.

3.6.2 Distributions and cumulants

If all the initial moments $\alpha_n = \langle x^n \rangle$ of a probability distribution $\Phi(r)$ exist, the characteristic function can be expanded in Mac Laurin series around $k = 0$:

$$\int_{-\infty}^{\infty} \Phi(r)\, e^{2ikr}\, dr \;=\; \alpha_0 \,\langle e^{2ikr} \rangle \;=\; \alpha_0 \left[1 \,+\, \sum_{n=1}^{\infty} (2ik)^n \, \alpha_n / n! \right] \tag{3.38}$$

where α_0 is the normalisation integral: $\alpha_0 = 1$ for the real distribution $\rho(r)$, while $\alpha_0 \neq 1$ for the effective distribution $P(r, \lambda)$.
Alternatively, the characteristic function can be expanded as the *exponent* of a Mac Laurin series around $k = 0$. In this case:

$$\int_{-\infty}^{\infty} \Phi(r)\, e^{2ikr}\, dr \;=\; \exp \left[\sum_{n=0}^{\infty} (2ik)^n \, C_n / n! \right] \tag{3.39}$$

The expansion coefficient C_n are called *cumulants*. The convergence interval of the series in Eq. (3.39) depends on the peculiarities of the distribution $\Phi(r)$.
The lowest-order cumulants can easily be connected to the initial moments $\alpha_n = \langle r^n \rangle$ and to the central moments $\mu_n = \langle (r - \langle r \rangle)^n \rangle$, and have simple interpretations.

a) $C_0 = \ln \alpha_0$ depends on the normalization of the distribution;

b) $C_1 = \alpha_1 = \langle r \rangle$ is the mean value of the distribution;

c) $C_2 = \mu_2 = \langle (r - \langle r \rangle)^2 \rangle$ is the variance;

d) $C_3 = \mu_3 = \langle (r - \langle r \rangle)^3 \rangle$ measures the distribution asymmetry;

e) $C_4 = \mu_4 - 3\mu_2^2$ measures the flatness of the distribution.

For a gaussian distribution, the cumulants C_n are zero for $n > 2$. The cumulants C_3, C_4 ... then measure the deviation of a distribution from the gaussian shape.

3.6.3 Cumulant expansion of EXAFS

Let us now consider the cumulant expansion of the characteristic function of the effective distribution $P(r, \lambda)$:

$$\int_{-\infty}^{\infty} P(r, \lambda)\, e^{2ikr}\, dr \;=\; \exp \left[\sum_{n=0}^{\infty} (2ik)^n \, C_n / n! \right] \tag{3.40}$$

By inserting Eq. (3.40) into Eq. (3.37) and making use of Eq. (3.21), one obtains the EXAFS formula as a function of cumulants [Bunker, 1983, Crozier et al., 1988]:

$$\begin{aligned} \chi_s(k) \;=\; & (S_o^2/k)\; N_s\; |f_s(k,\pi)|\; \exp\left(C_o - 2k^2 C_2 + 2k^4 C_4/3 - 4k^6 C_6/45 \ldots\right) \\ & \times\; \sin\left[2kC_1 - 4k^3 C_3/3 + 4k^5 C_5/15 \ldots + \phi(k)\right]. \end{aligned} \tag{3.41}$$

Table 3.1: Lowest-order cumulants of the real distributions depicted in Fig. 3.13 and of the corresponding effective distributions. Notice that in going from the real to the effective distributions the 1st and 3rd cumulants decrease, while the 2nd cumulant increases.

	Gaussian		Skewed	
	real	effect.	real	effect.
1st cumulant (Å)	1.30	1.22	1.50	1.38
2nd cumulant (10^{-2}Å^2)	4.00	4.25	7.99	6.78
3rd cumulant (10^{-2}Å^3)	0	-0.21	15.9	8.19

Odd and even cumulants determine phase and amplitude of the EXAFS signal, respectively.
Equation (3.43) contains the cumulants C_i of the *effective* distribution $P(r,\lambda)$, while one is interested in the cumulants C_i^* of the *real* distribution $\rho(r)$. The effective distribution is not normalized to one; the normalization factor can be approximated as

$$\exp(C_o) \;=\; \exp(-2C_1/\lambda)/C_1^2. \tag{3.42}$$

3.7 Parametrization of EXAFS formula

For many applications, the extent of disorder is sufficiently small to allow the expression of the EXAFS formula in terms of a leading cumulants. In such cases, the EXAFS function for a given coordination shell (or for a given scattering path) can be expressed as

$$\chi_s(k) = \frac{S_o^2}{k}\; N_s\; |f_s(k,\pi)|\; \frac{e^{-2C_1/\lambda}}{C_1^2}\; e^{-2k^2C_2+2k^4C_4/3\cdots}\; \sin\left[2kC_1 - \frac{4k^3C_3}{3} ... + \phi(k)\right], \tag{3.43}$$

where the parameters C_i are the cumulants of the *effective* distribution $P(r,\lambda)$ [Bunker, 1983, Fornasini et al., 2001].
According to the probability theory, the cumulants characterise the position, width and shape of a distribution; in particular, C_1 is the mean value, C_2 is the variance and C_3 is a measure of the asymmetry of the distribution.
It is worth noting that even and odd cumulants determine the amplitude and the phase of the EXAFS signal, respectively.

Parameters of the real distribution

Actually, one is interested in the cumulants C_i^* of the *real* distribution $\rho(r)$. The first cumulant C_1^* of the real distribution $\rho(r)$ is significantly larger than the first cumulant C_1 of the effective distribution, as a consequence of the spherical nature of the photo-electron wave and its limited mean free path [Freund et al., 1989]:

$$C_1^* \;\simeq\; C_1 + \frac{2C_2}{C_1}\left(1 + \frac{C_1}{\lambda}\right). \tag{3.44}$$

The difference, of the order of some 10^{-3} Å, is automatically taken into account by most data analysis packages. The difference between higher-order cumulants of the two distributions is generally negligible [Fornasini et al., 2001]..

The lowest-order cumulants of the real distribution have simple interpretations:

1. The first cumulant $C_1^* = \langle r\rangle$ is the mean value of the distribution, say the average inter-atomic distance.

2. The second cumulant $C_2^* = \sigma^2 = \langle (r - \langle r\rangle)^2\rangle$ is the variance of the distribution or mean square relative displacement (MSRD); the exponential $\exp(-2k^2\sigma^2)$ of (3.43) is referred to as EXAFS Debye-Waller factor.

3. The third cumulant $C_3^* = \mu_3 = \langle (r - \langle r \rangle)^3 \rangle$ is the mean cubic relative displacement and measures the distribution asymmetry.
4. The fourth cumulant C_4^* measures the flatness of the distribution, say the symmetric deviation with respect to a gaussian shape.

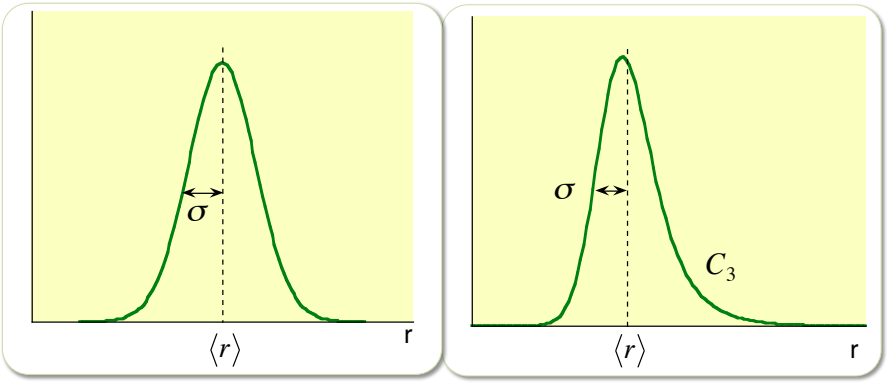

Figure 3.15: Symmetric distribution (left) and asymmetric distribution (right).

In some cases, the cumulant expansion can be truncated at the second order term, and eq. (3.43) reduces to the so called standard EXAFS formula

$$\chi_s(k) = \frac{S_o^2}{k} N_s \, |f_s(k,\pi)| \frac{e^{-2C_1/\lambda}}{C_1^2} e^{-2k^2 C_2} \sin\left[2kC_1 + \phi(k)\right] , \tag{3.45}$$

which amounts to consider a gaussian effective distribution $P(r, \lambda)$, which corresponds with good approximation to a gaussian real distribution $\rho(r)$ (Fig. 3.15, left):

$$\rho(r) = (1/\sigma\sqrt{2\pi}) \exp\left[-(r - \langle r \rangle)^2 / 2\sigma^2\right] , \tag{3.46}$$

where $C_1^* = \langle r \rangle$ is the average distance and $C_2^* = \sigma^2 = \langle (r - \langle r \rangle)^2 \rangle$ is the variance. The gaussian approximation, generally reliable for the second and outer coordination shells, is unfit for the first coordination shell, where the asymmetry of the pair interaction potential is more influent.

For the first coordination shell it is higly recommended to add the third cumulant $C_3^* = \langle (r - \langle r \rangle)^3 \rangle$ (mean cubic relative displacement) to account for the distribution asymmetry (Fig. 3.15, right):

$$\chi_s(k) = \frac{S_o^2}{k} N_s \, |f_s(k,\pi)| \frac{e^{-2C_1/\lambda}}{C_1^2} e^{-2k^2 C_2} \sin\left[2kC_1 - \frac{4k^3 C_3}{3} + \phi(k)\right] . \tag{3.47}$$

3.8 Summary

Using (3.43), or the more approximate expressions (3.46) or (3.47)), one can get original information on the local structure from the analysis of EXAFS, provided some "physical" quantities are known: phaseshifts, backscattering amplitude, inelastic terms.

3.8.1 Structural parameters

An EXAFS experiment samples a one-dimensional distribution of interatomic distances, which contains the contributions of all single and multiple scattering paths originating and terminating at the absorbing atom, within the reduced range determined by the spherical nature of the photoelectron wave and by its mean free path.

The following structural parameters can in principle be obtained for each coordination shell of the absorbing atom, considering only single scattering contributions to the EXAFS signal.

a) *Coordination number.* The amplitude of the EXAFS signal is directly proportional to the number N_s of atoms within the shell.
b) *Average inter-atomic distance.* The frequency of the EXAFS signal depends on the first cumulant C_1 of the effective distribution, which is connected by (3.44) to the average inter-atomic distance $\langle r \rangle$.
The argument of the sine function in (3.43) depends also on the third cumulant (and possibly on higher order odd cumulants); neglecting the third cumulant in the analysis can severely affect the accuracy of the value $\langle r \rangle$ for the first coordination shell.
c) *Debye-Waller factor.* The second cumulant $C_2 = \sigma^2$ (Debye-Waller exponent) corresponds to the *mean square relative displacement* (MSRD) of absorber and back-scatterer atoms.
The Debye-Waller factor $\exp[-2k^2\sigma^2]$ causes a damping of the EXAFS signal. The value of σ^2 increases with increasing temperature. Its temperature dependence gives original information on the local vibrational dynamics.
d) *Third cumulant.* The third cumulant measures the asymmetry of the distribution of distances. It is significant for the first coordination shell, but seems to be negligible for the outer coordination shells.

3.8.2 Phase-shifts, back-scattering amplitudes and inelastic terms

Two different procedures can be used to insert into Eq. (3.43) the "physical quantities" $|f(k,\pi)|$, ϕ, S_0^2 and λ for each coordination shell.

1. The "physical quantities" are experimentally obtained from the EXAFS of a reference sample of known structure. The local structure of the reference sample should be as much as possible similar to that of the unknown sample, in order to guarantee the *amplitude and phase-shift transferability.*
2. The "physical quantities" are calculated ab-initio [Rehr and Albers, 2000] by a number of easily available software packages [XAFS software, , GNXAS, 2015, FEFF, 2012], with a degree of accuracy sufficient for most applications.

3.8.3 Approximations

Let us recall here the main approximations on which Eq. (3.43) is based.

1. *Single scattering* - Only events are considered in which the photo-electron undergoes a single scattering (SS). Actually, the photo-electron can undergo also *multiple scattering* (MS) processes. The influence of MS is very important in the XANES region (see below, Sec. 6). In the EXAFS region MS events are less important, although sometimes not negligible. Anyway, the 1st-shell signal can be safely analysed within the SS approximation, since MS paths correspond to longer effective distances.
2. *Plane wave* - The curvature of the spherical wave impinging on the scattering atom is neglected. The larger are the photo-electron velocity and the inter-atomic distance, the better is the approximation. The curvature effects are consequently stronger in the lower-k region of the spectrum and for lighter scattering atoms. Anyway, backscattering amplitude and phase-shift values calculated within the spherical wave formalism are also available; they contain a slight dependence on the interatomic distance: $|f(k,\pi,r)|$, $\phi(k,r)$.
3. *Small disorder* - Eq. (3.43) can be used only if the cumulant series is fastly enough convergent within the k range of the EXAFS signal. If this is not the case, one should use Eq. (3.35) and try to build up physically sound models for $\rho(r)$.

Chapter 4

Interpretation of EXAFS

In this Chapter, we will thoroughly study the influence of the vibrational properties of molecules and solids on the EXAFS signal. The importance of this topic is twofold: on the one hand, it allows one to better understand the meaning of EXAFS parameters and to increase the accuracy of structural studies, on the other hand, it shows how to obtain from EXAFS original information on vibrational dynamics and thermal properties.

When only one coordination shell is considered, and the Single-Scattering approximation is valid, the EXAFS signal can be represented as $\chi(k) = A(k)\sin\Phi(k)$, and the main problem is to recover the real distribution $\rho(r)$ of interatomic distances from the $\chi(k)$ function. In case of moderate disorder, the distribution $\rho(r)$ can be parametrised in terms of its leading cumulants C_i^* [Bunker, 1983, Crozier et al., 1988]. The knowledge of the cumulants C_i^* as a function of temperature represents a useful source of information.

If the interpretation of thermal effects over an entire EXAFS spectrum is sought, including Multiple-Scattering (MS) effects, the most general solution is based on the generation of a large enough number of configurations of the system under study [Benfatto et al., 1989], so as to allow an accurate simulation of the EXAFS signal. If however a path-by-path procedure can be applied for treating Multiple Scattering, then one can again express the EXAFS signal for each scattering path (single or multiple) in the form $\chi(k) = A(k)\sin\Phi(k)$ [Rehr and Albers, 2000]. To each scattering path one can associate a distribution of lengths $\rho(r)$ and, for moderate disorder, use again the cumulant expansion method.

Some basic concepts of statistical thermodynamics are given in Appendix D.

4.1 Unidimensional model

An EXAFS experiment samples a unidimensional distribution of distances $\rho(r)$ for each scattering path. The first step for the phenomenological interpretation of EXAFS results is thus based on a unidimensional model. The unidimensional model is physically sound only for diatomic molecules; for more complex systems, the unidimensional model of EXAFS has to be further interpreted.

4.1.1 Diatomic molecules

Let us start by considering a system with only one internal degree of freedom, like a two-atomic molecule, characterized by a reduced mass $\mu = m_1 m_2/(m_1 + m_2)$. The motion of the two-atomic system can be decomposed into center of mass (CM) motion, rotation around an axis through the CM and oscillation around the CM. For the analysis of EXAFS spectra only the oscillatory motion is relevant and will be here considered (although the rotational motion in principle affects the interatomic potential and the frequency of oscillations).
Let r be the instantaneous inter-atomic distance. The interaction between the two atoms is described by a potential energy $V(r)$, with the minimum at $r = R_0$. An exact determination of the

potential energy $V(r)$ can be very difficult, and one often relies on phenomenological models, such as

a) the Morse potential energy

$$V(r) = D\,\left[1 - e^{-\beta(r-R_0)}\right]^2 = D\,\left[1 + e^{-2\beta(r-R_0)} - e^{-\beta(r-R_0)^2}\right] \tag{4.1}$$

where D is the depth of the potential well and β is a positive constant that controls the width of the potential well;

b) the Lennard-Jones potential energy

$$V(r) = 4\epsilon\left[-\left(\frac{\sigma}{r}\right)^6 + \left(\frac{\sigma}{r}\right)^{12}\right] \tag{4.2}$$

where ϵ measures the strength of the attraction, σ measures the radius of the repulsive core: for $r = \sigma$ one finds $\phi = 0$. At the position R_0 of the minimum of the potential energy one has $R_0 = \sqrt[6]{2}\,\sigma = 1.122\,\sigma$ and $V(R_0) = -\epsilon$.

It is convenient to introduce the instantaneous displacement $x = r - R_0$ and express the potential energy as a function of the displacement, $V(x)$. The potential energy can be expanded as a power series with respect to x,

$$V(x) \;=\; k_0\,x^2\,/\,2 \;+\; k_3\,x^3 \;+\; k_4\,x^4\ldots \tag{4.3}$$

where k_0 is the second order or harmonic force constant, while $k_3, k_4, ...$ are higher order or anharmonic force constants. The truncation of the expansion (4.3) at the second order term represents the *harmonic approximation*:

$$V(x) \;=\; k_0\,x^2\,/\,2 \tag{4.4}$$

The harmonic system oscillates with frequency

$$\omega = 2\pi\nu \;=\; \sqrt{k_0/\mu} \tag{4.5}$$

4.1.2 EXAFS cumulants

A typical EXAFS experiment samples, for a relatively long time, a large number of two-atomic systems in thermal equilibrium with a reservoir at temperature T. The EXAFS signal is proportional to the configurational average (provided the scattering amplitude can be considered independent of r) [Tranquada and Ingalls, 1983, Benfatto et al., 1989]:

$$\chi(k) \propto \left\langle \frac{\exp[-2r/\lambda(k)]}{r^2}\,\exp(2ikr)\right\rangle\,, \tag{4.6}$$

Equivalently, the configurational average of the previous equation can be expressed, within the plane-wave approximation, as the integral [Crozier et al., 1988, Vaccari and Fornasini, 2005]

$$\int_0^\infty \rho(r)\,\frac{\exp[-2r/\lambda(k)]}{r^2}\,\exp(2ikr)\,dr \;=\; \int_0^\infty P(r,\lambda)\,\exp(2ikr)\,dr \tag{4.7}$$

where $\rho(r)$ is the real distribution of distances and $P(r,\lambda) = \rho(r)\,\exp(-2r/\lambda)/r^2$ is an effective distribution.
The configurational average can be expanded in a power series of k, the coefficients C_n being the cumulants of the effective dirtsibution $P(r,\lambda)$:

$$\left\langle \frac{\exp[-2r/\lambda(k)]}{r^2}\,\exp(2ikr)\right\rangle \;=\; \int_0^\infty P(r,\lambda)\,\exp(2ikr)\,dr \;=\; \exp\left[\sum_{n=0}^{\infty}\frac{(2ik)^n}{n!}\,C_n\right] \tag{4.8}$$

The EXAFS signal for a coordination shell in the single scattering approximation can be parametrised in terms of the cumulants of the effective distribution [Bunker, 1983, Crozier et al., 1988]:

$$\begin{aligned}\chi_s(k) &= (S_o^2/k)\; N_s\; |f_s(k,\pi)|\; \exp\left(C_o - 2k^2C_2 + 2k^4C_4/3 - 4k^6C_6/45 \ldots\right) \\ &\quad \times\; \sin\left[2kC_1 - 4k^3C_3/3 + 4k^5C_5/15 \ldots + \phi(k)\right]. \end{aligned} \tag{4.9}$$

Odd and even cumulants determine phase and amplitude of the EXAFS signal, respectively. The first and second cumulants, $C_1 = \langle r\rangle$ and $C_2 = \sigma^2 = \langle (r - \langle r\rangle)^2\rangle$ are the average value and the variance of the effective distribution, respectively. Higher order cumulants quantify the deviation of the distribution from the gaussian shape; the third cumulant $C_3 = \langle (r - \langle r\rangle)^3\rangle$ is a measure of the distribution asymmetry.

We have intriduced above the cumulants C_i of the *effective* distribution $P(r, \lambda)$, while one is interested in the cumulants C_i^* of the *real* distribution $\rho(r)$.

The effective distribution is not normalized to one; the normalization factor can be approximated as

$$\exp(C_o) \;=\; \exp(-2C_1/\lambda)/C_1^2. \tag{4.10}$$

Different procedures for connecting the cumulants of the real and of the effective distributions (C_n^* and C_n, respectively) have been proposed, limited to the first cumulant [Freund et al., 1989, Bunker, 1983] or extended to higher order cumulants [Fornasini et al., 2001]. A relatively good approximation is obtained by the recursion formula [Vaccari, 2006, Vaccari et al., 2007]

$$C_n^* \;\sim\; C_n + 2C_{n+1}\big(1/C_1 + 1/\lambda\big) \quad \text{for} \quad n = 1, 2, 3, \ldots \tag{4.11}$$

The difference between the first cumulants ($n = 1$) of the real and effective distributions is significant and Eq. (4.11) is included in most data analysis packages. For higher order cumulants ($n \geq 2$), the difference is smaller and is frequently neglected.

Example: Let us give quantitative evaluations for CdTe and Cu. The difference of first cumulants is 7.2×10^{-3} Å for CdTe at 300 K and 1.2×10^{-3} Å for Cu at 500 K. The relative difference of second cumulants, evaluated through eq. (4.11) and checked by reconstructing the distributions and evaluating their cumulants, is 1.6 % for CdTe at 300 K and 3.5 % for Cu at 500 K.

The lowest-order EXAFS cumulants C_n^* are related to the initial and central moments of the real distribution by

$$C_1^* \;=\; \langle r\rangle \tag{4.12}$$

$$C_2^* \;=\; \mu_2 \;=\; \big\langle (r - \langle r\rangle)^2\big\rangle \tag{4.13}$$

$$C_3^* \;=\; \mu_3 \;=\; \big\langle (r - \langle r\rangle)^3\big\rangle \tag{4.14}$$

$$C_4^* \;=\; \mu_4 - 3\mu_2^2 \;=\; \big\langle (r - \langle r\rangle)^4\big\rangle - 3\mu_2^2 \tag{4.15}$$

can thus be evaluated as averages over a canonical ensemble.

Different definitions of cumulants

1. In the present approach, the cumulants characterise the shape of the distribution of distances; in particular, the first EXAFS cumulant is the average value of the distribution $\rho(r)$, $C_1^* = \langle r\rangle$. For nearest-neighbours, C_1^* is the bond-length.
   In many cases, one measures the relative values of the first cumulant with respect to a reference spectrum, for example in temperature-dependent measurements $\delta C_1^* = C_1^*(T) - C_1^*(T_0)$.
2. The first cumulant has been alternatively defined as the average difference between the instantaneous distance r and the average distance of a reference spectrum, for example in [Stern et al., 1992].

3. Yokoyama, in [Yokoyama et al., 1996], defines the cumulant expansion through

$$\langle \exp(2ikr) \rangle \;=\; \exp\left[2ikR_0 + \sum_n \frac{(2ik)^n}{n!}\, C_n \right] \tag{4.16}$$

where R_0 is the position of the minimum of the potential ("rest position"), assumed to be temperature independent. Accordingly, the first cumulant is $C_1 = \langle (r - R_0) \rangle = \langle x^0 \rangle$.
With respect to our approach, the distribution is only shifted, the second and higher order cumulants are unchanged [verify!!]. In [Yokoyama et al., 1996] the difference between cumulants of the effective and real distributions is considered negligible even for the first cumulant.

4. In [Fujikawa and Miyanaga, 1993], the cumulants M_n are directly defined in eq. (2.10) in terms of the relative atomic displacements with respect to the rest positions:

$$\langle \exp(2ik\Delta_\alpha) \rangle = \exp\left[\sum_n \frac{(2ik)^n}{n!}\, M_n \right] \tag{4.17}$$

where (rewritten in our notation)

$$\Delta_\alpha = \hat{R}_0 \cdot (\vec{u}_b^{\,0} - \vec{u}_a^{\,0}) = \Delta u_\parallel^0 \,, \tag{4.18}$$

$\vec{u}^{\,0}$ are the instantaneous atomic displacements with respect to the rest positions and $\vec{R}_0$ is the rest distance. The relations between cumulants and Δ_α are given in eq. (2.11):

$$M_1 = \langle \Delta_\alpha \rangle \,, \quad M_2 = \langle \Delta_\alpha^2 \rangle - \langle \Delta_\alpha \rangle^2 \,, \quad M_3 = \langle \Delta_\alpha^3 \rangle - 3\langle \Delta_\alpha^2 \rangle \langle \Delta_\alpha \rangle + 2\langle \Delta_\alpha \rangle^3 \tag{4.19}$$

Only the atomic displacements parallel to the bond direction are considered.

Relevance of the one-dimensional model

The study of the simple two-atomic system, besides its possible direct interest (dynamics of two-atomic molecules) is important also for understanding the behaviour of larger systems (like crystals), since in any case EXAFS samples a unidimensional distribution of distances.
In the following, we will first consider the harmonic approximation and then introduce the effects of anharmonicity. In both cases, we will separate the classical approach from the quantum approach.

4.1.3 Classical harmonic oscillator

For an harmonic oscillator, the equilibrium position R_0 corresponds to the minimum of the potential energy. The displacement of r with respect to R_0 depends on time according to

$$x(t) \;=\; r(t) - R_0 \;=\; A\, \cos(\omega t) \,. \tag{4.20}$$

The total energy of the classical harmonic oscillator is $E_{\rm cl} = k_0 A^2/2$.
The time-averaged displacement is $\langle x \rangle = 0$, and the time-averaged value of x^2 is

$$\langle x^2 \rangle \;=\; A^2\, \frac{1}{2\pi} \int_0^{2\pi} \cos^2(\omega t)\, d(\omega t) \;=\; \frac{A^2}{2} \;=\; \frac{E_{\rm cl}}{k_0} \,. \tag{4.21}$$

Let us now consider a classical harmonic oscillator in thermal equilibrium with a reservoir at temperature $T = 1/k_B\beta$ (or equivalently a statistical canonical ensemble of classical harmonic oscillators at the temperature T).
In the classical approximation, the canonical average of a quantity A is given by

$$\langle A \rangle \;=\; \frac{\int dx\, A e^{-\beta V(x)}}{\int dx\, e^{-\beta V(x)}} . \tag{4.22}$$

The average energy of the harmonic oscillator is, according to the theorem of equipartition:

$$\langle E_{\rm cl}\rangle = k_B T \tag{4.23}$$

where k_B is the Boltzmann constant. The average energy linearly depends on temperature (continuous line in Fig. 4.1, left) and is independent of force constant and reduced mass.
The average of the squared amplitude of vibration is thus

$$\langle A^2\rangle = \frac{2\langle E_{\rm cl}\rangle}{k_0} \tag{4.24}$$

and the variance of the canonical distribution of x is

$$\sigma^2 \;=\; \langle x^2\rangle \;=\; \frac{\langle A^2\rangle}{2} \;=\; \frac{\langle E_{\rm cl}\rangle}{k_0} \;=\; \frac{k_B T}{k_0}\,. \tag{4.25}$$

The variance of x, corresponding to the second cumulant C_2^* or Debye-Waller exponent,

- depends linearly on temperature, like the average energy;
- contrary to the energy, it depends also on the force constant, and then, via Eq. (4.5), on reduced mass and frequency.

4.1.4 Quantum harmonic oscillator - Cumulants

In harmonic approximation, the full hamiltonian operator is

$$\hat{H}_0 \;=\; T + V(x) \;=\; p^2/2\mu + k_0\, x^2/2. \tag{4.26}$$

A more detailed quantum treatment of the harmonic oscillator is given in Appendix D.5. The results there obtained can be used here, provided the mass m is substituted by the reduced mass μ. One can show that, when the harmonic oscillator is in thermal equilibrium with a reservoir at temperature $T = 1/k_B\beta$, the average energy is given by

$$\langle E\rangle \;=\; \hbar\omega\left[\frac{1}{2} + \frac{1}{e^{\beta\hbar\omega}-1}\right]\,, \tag{4.27}$$

where $\omega = \sqrt{k_0/\mu}$.
The temperature dependence of the average energy is shown in the left panel of Fig. 4.1; its main properties are:

- When $T \to \infty$ ($\beta \to 0$), then $\langle E\rangle \to k_B T$, independent of k_0 and μ, say independent of ω (classical approximation).
- When $T \to 0$ ($\beta \to \infty$), then $\langle E\rangle \to \hbar\omega/2 = (\hbar/2)\sqrt{k_0\mu}$ (zero point energy). The zero point energy is proportional to the angular frequency ω; for a given force constant k_0, the zero point energy depends on the reduced mass μ (isotopic effect).

A characteristic temperature θ can be associated to the angular frequency: $\theta = \hbar\omega/k_B = h\nu/k_B$. Numerically, θ [K] = 47.99 ν [THz].

Distribution and cumulants

Making use again of the treatment of Appendix D.5, one can show that the distribution of distances for a quantum harmonic oscillator has a gaussian shape

$$\rho(r) \;=\; (1/\sigma\sqrt{2\pi})\, e^{-(r-R_0)^2/2\sigma^2}; \qquad \rho(x) \;=\; (1/\sigma\sqrt{2\pi})\, e^{-x^2/2\sigma^2} \tag{4.28}$$

The **first cumulant** C_1^* of the real distribution $\rho(r)$, taking into account Eq. (D.70), is

$$C_1^* \;=\; \langle r\rangle \;=\; \langle R_0 + x\rangle \;=\; R_0 + \langle x\rangle \;=\; R_0. \tag{4.29}$$

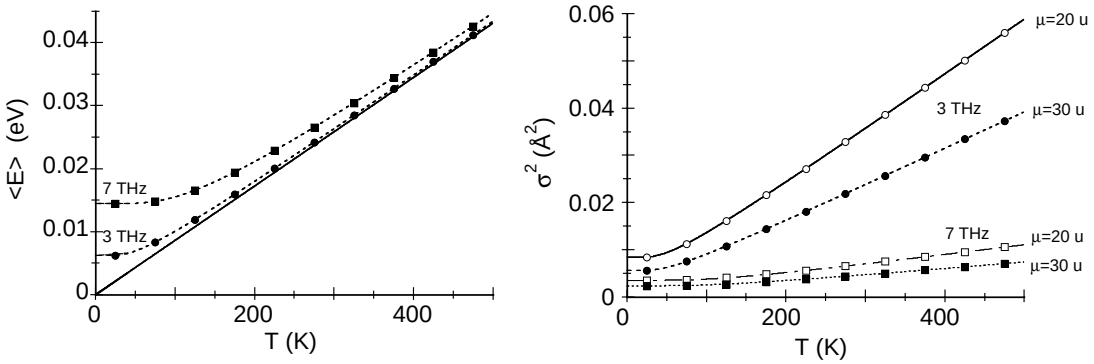

Figure 4.1: Average energy (left) and variance (right) σ^2 of an harmonic oscillator for different values of frequency $\nu = \omega/2\pi$ (3 THz, circles; 7 THz, squares) and reduced mass (20 amu, open symbols; 30 amu, full symbols).

It then corresponds to the position of the minimum of the potential energy R_0; there is no thermal expansion.

The **second cumulant** C_2^* is the variance σ^2 of the gaussian distribution $\rho(r)$, say the mean square relative displacement (MSRD) of absorber and backscatterer atoms.

$$C_2^* \;=\; \sigma^2 \;=\; \big\langle (r - \langle r \rangle)^2 \big\rangle \;=\; \langle x^2 \rangle. \tag{4.30}$$

Defining $z = \exp(-\beta\hbar\omega)$ and remembering that $\sigma_0^2 = \hbar/2\mu\omega$, it is easy to calculate σ^2, which can be expressed in different equivalent ways:

$$\sigma^2 \;=\; \sigma_0^2 \, \frac{1+z}{1-z} \;=\; \sigma_0^2 \coth\left(\frac{\beta\hbar\omega}{2}\right) \;=\; \frac{\hbar}{\mu\omega}\left[\frac{1}{2} + \frac{1}{e^{\beta\hbar\omega}-1}\right]. \tag{4.31}$$

Numerically,

$$\sigma^2 \;=\; \frac{0.505379}{\nu\,\mu} \coth(23.9962\,\nu/T)\,,$$

where σ^2 is measured in Å^2, the frequency $\nu = \omega/2\pi$ in THz and the reduced mass μ in atomic mass units.

Comparing Eqs. (4.27) and (4.31) one can see that

$$\sigma^2 = \langle E \rangle / k_0 = \langle E \rangle / \mu\omega^2\,. \tag{4.32}$$

The temperature dependence of σ^2 is shown in the right panel of Fig. 4.1, and is characterized by the following behaviour.

a) When $T \to 0$, then $\sigma^2 \to \sigma_0^2 = \hbar/2\sqrt{k_0\mu} = \hbar/2\mu\omega$. The zero point amplitude of vibrations, for a given force constant k_0, depends on the reduced mass μ (isotopic effect). Numerically (σ_0^2 in Å^2, ν in THz, μ in amu):

$$\sigma_0^2 = \frac{\hbar}{2\mu\omega} = \frac{0.505379}{\nu\mu}$$

The isotopic effect on the EXAFS Debye-Waller factor has been experimentally detected for germanium [Purans et al., 2008].

b) When $T \to \infty$, then $\sigma^2 \to \sigma_\infty^2 = k_B T/k_0 = k_B T/\mu\omega^2$. The slope of $\sigma_\infty^2(T)$ is inversely proportional to the force constant k_0, and thus depends on ω. Numerically (σ_0^2 in Å^2, ν in THz, μ in amu):

$$\sigma(\infty) = \frac{0.0210593}{\nu^2\mu}\,T$$

At last, the **3rd cumulant**, corresponding to the third central moment, is zero, $C_3^* = \langle x^3 \rangle = 0$. Also *higher order cumulants* are zero for the gaussian real distribution.

The cumulants C_n of the *effective distribution* are different from those of the real distribution (see § 3.6). The difference is generally significant only for the first cumulant.

4.1.5 Anharmonicity, classical approximation

Let us now consider an anharmonic potential energy, expressed through the series expansion (4.3)

$$V(x) \;=\; k_0\, x^2 \,/\, 2 \;+\; k_3\, x^3 \;+\; k_4\, x^4 \ldots \tag{4.33}$$

where again $x = r - R_0$ and R_0 is the position of the minimum of the potential energy (conventionally referred to as "rest position"). Note, however, that for the classic anharmonic oscillator R_0 corresponds to the equilibrium position only for $T = 0$.
The 3rd-order force constant is generally negative, $k_3 < 0$.
In the classical approximation, the EXAFS cumulants (E.30-E.33) can be expressed as a function of the lowest order force constants of the potential $V(x)$ by calculating the average values through the classical formula

$$\langle A \rangle \;=\; \frac{\int dx\, A e^{-\beta V(x)}}{\int dx\, e^{-\beta V(x)}}. \tag{4.34}$$

where

$$A_1 \;=\; \delta C_1^* = \langle x \rangle = \langle x \rangle - r_0 \tag{4.35}$$
$$A_2 \;=\; C_2^* = (x - \langle x \rangle)^2 = (r - \langle r \rangle)^2 \tag{4.36}$$
$$A_3 \;=\; C_3^* = (x - \langle x \rangle)^3 = (r - \langle r \rangle)^3 \tag{4.37}$$

and so on. One obtains [Stern et al., 1991]:

$$\delta C_1^*(T) \;=\; -\frac{3k_3}{k_0^2}\, k_B T \;-\; \frac{3k_3}{k_0^4}\left(\frac{45k_3^2}{k_0} - 32k_4\right)(k_B T)^2 \;+\; \ldots \tag{4.38}$$

$$C_2^*(T) \;=\; \frac{k_B T}{k_0} \;+\; \frac{3}{k_0^3}\left(\frac{12k_3^2}{k_0} - 4k_4\right)(k_B T)^2 \;+ \ldots \tag{4.39}$$

$$C_3^*(T) \;=\; -\frac{6k_3}{k_0^3}\,(k_B T)^2 \;-\; \frac{36sk_3}{k_0^5}\left(\frac{24k_3^2}{k_0} - 14k_4\right)(k_B T)^3 \;+\; \ldots \tag{4.40}$$

$$C_4^*(T) \;=\; \frac{12}{k_0^4}\left(\frac{9k_3^2}{k_0} - 2k_4\right)(k_B T)^3 \;+\; \ldots \tag{4.41}$$

A calculation extended to the 5th-order force constant is reported in the PhD Thesis of Tranquada [Tranquada, 1983]; the results up to the 4th-order force constant coincide with the results of Stern. Eq. (4.38) corresponds to Eq. (5.13) of Brüesch [Brüesch, 1982].
From Eqs. (4.38–4.41) one can draw the following conclusions for the classical approximation:

1. The thermal expansion δC_1^* is, to first order, proportional to the temperature T and to the 3rd-order force constant k_3. For $T = 0$, $\delta C_1^* = 0$.
2. The second cumulant C_2^* is, to first order, proportional to temperature: $C_2^* = \sigma_\infty^2 = k_B T / k_0$. The first order term is purely harmonic; anharmonicity is taken into account by higher order terms.
3. The third cumulant C_3^* is, to first order, proportional to the square of temperature.
4. The fourth cumulant C_4^* is, to first order, proportional to the cube of temperature.
5. By comparing the first-order expressions of the first two cumulants, one can see that (always to first order)

$$\delta C_1^* = -\frac{3k_3}{k_0}\, C_2^* \tag{4.42}$$

The same formal expression is found from the quantum treatment (see below).

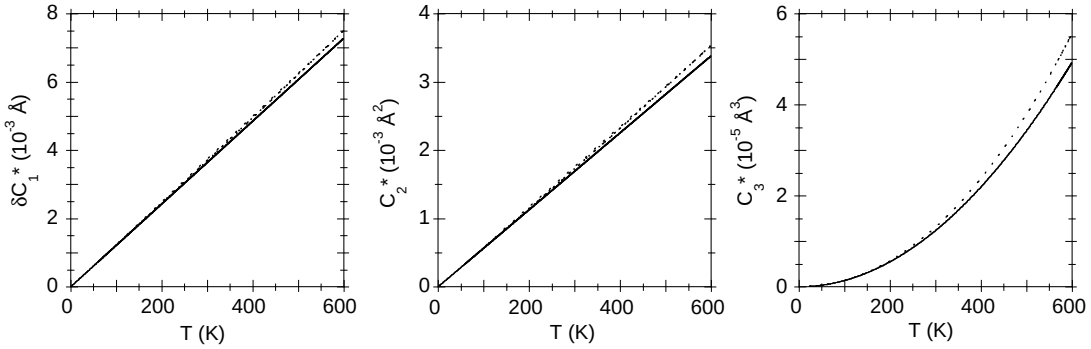

Figure 4.2: First three cumulants for the Bromine molecule Br_2, calculated in the classical approximation through Eqs. (4.38–4.41), using the force constants $k_0 = 15.28$ eV/Å^2, k_3 = -10.96 eV/Å^3, $k_4 = 6.6$ eV/Å^4 from [Huber and Herzberg, 1979]. Continuous and dashed lines are 1st and 2nd order approximations, respectively.

6. By comparing the first-order expressions of the first three cumulants, one can see that (always to first order)
$$\delta C_1^* = C_3^*/2C_2^* \tag{4.43}$$
This relation has sometimes been used to evaluate the thermal expansion in crystals directly from the third cumulant [Tröger et al., 1994].

A realistic example of the temperature dependence of the first three cumulants in the classical approximation (4.38)–(4.40) , including the second order terms, is given in Fig. 4.2 for the bromine molecule Br_2. The force constants k_0, k_3, k_4 from vibrational spectra [Huber and Herzberg, 1979] quoted by [Yokoyama, 1999] have been used; the force constant k_0 and k_3 are in good agreement with the experimental values from [Yokoyama et al., 1996].

4.1.6 Anharmonicity, quantum treatment

Quantum perturbative treatment

A quantitative relation between EXAFS cumulants and force constants for a system with one degree of freedom has been proposed by Frenkel and Rehr up to the third cumulant [Frenkel and Rehr, 1993] and extended by Yokoyama up to the fourth cumulant and to higher approximation orders for the second cumulant [Yokoyama et al., 1996, Yokoyama, 1999]. It is based on the perturbative approach of Ref. [Feynman, 1972], shortly treated in Appendix D.4.

Basically, the unperturbed Hamiltonian contains the potential energy of the harmonic oscillator and one defines again

$$\omega \;=\; \sqrt{k_0/\mu}, \qquad \sigma_0^2 \;=\; \hbar/2\mu\omega, \qquad z \;= e^{-\beta\hbar\omega}, \tag{4.44}$$

Numerically, if the frequencies $\nu = \omega/2\pi$ are measured in THz and the reduced masses μ in a.m.u.

$$k_0 \;=\; 4.093\times10^{-3}\,\mu\nu^2\,, \quad \sigma_0^2 \;=\; 0.505\frac{1}{\mu\nu}\,, \quad z \;=\; \exp\left[-48\,\frac{\nu}{T}\right]\,.$$

The following approximate expressions for the leading cumulants have been found.

1. The variation of the **1st cumulant** $\delta C_1^* = \langle r\rangle - R_0 = \langle x\rangle$ is, to first order,
$$\delta C_1^* \;=\; -\,\frac{3k_3\sigma_0^2}{k_0}\;\frac{1+z}{1-z} \;+\; \ldots \tag{4.45}$$
Note that, for the quantum oscillator, δC_1^* is not zero event for $T = 0$, owing to zero point energy.

Equation (4.45) corresponds to (15) of [Frenkel and Rehr, 1993], where $a = \delta C_1^*$, to (19) of [Yokoyama et al., 1996] and to (8) of [Yokoyama, 1999].

2. The **2nd cumulant** can be expressed as a sum $C_2^* \simeq C_2^{(0)} + C_2^{(1)} + C_2^{(2)}$, where the zero-order term (harmonic) is

$$C_2^{(0)} \;=\; \sigma_0^2 \, \frac{1+z}{1-z}, \tag{4.46}$$

the 1st-order term (negative if $k_4 > 0$) is

$$C_2^{(1)} \;=\; -\,\frac{12\,k_4\sigma_0^6}{\hbar\omega}\,\frac{(1+z)^2}{(1-z)^2} \;-\; \frac{24\,k_4\sigma_0^6}{k_BT}\,\frac{z(1+z)}{(1-z)^3} \tag{4.47}$$

and the 2nd-order term (positive) is

$$C_2^{(2)} \;=\; \frac{4\,k_3^2\sigma_0^8}{(\hbar\omega)^2}\,\frac{13z^2+58z+13}{(1-z)^2} \;+\; \frac{120\,k_3^2\sigma_0^8}{\hbar\omega k_BT}\,\frac{z(1+z)}{(1-z)^3}. \tag{4.48}$$

Equation (4.46) corresponds to (11) of [Frenkel and Rehr, 1993].

Equations (4.46) and (4.47) correspond to (20) of [Yokoyama et al., 1996] and to (10) and (11) of [Yokoyama, 1999].

The second order term (4.48) corresponds to (12) of [Yokoyama, 1999] (where however a factor 24 appears instead of 120 in the second term).

3. The **3rd cumulant** is, to first order,

$$C_3^* \;=\; -\,\frac{2k_3\sigma_0^4}{k_0}\,\frac{z^2+10z+1}{(1-z)^2} \;+\; \ldots \tag{4.49}$$

Equation (4.49) corresponds to (18) of [Frenkel and Rehr, 1993], to (21) of [Yokoyama et al., 1996] and to (13) of [Yokoyama, 1999].

4. The **4th cumulant** can be expressed as a sum $C_4^* \simeq C_4^{(1)} + C_4^{(2)}$, where the 1st-order term (negative if $k_4 > 0$) is

$$C_4^{(1)} \;=\; -\,\frac{12\,k_4\sigma_0^8}{\hbar\omega}\,\frac{z^3+9z^2+9z+1}{(1-z)^3} \;-\; \frac{144\,k_4\sigma_0^8}{k_BT}\,\frac{z^2}{(1-z)^4} \tag{4.50}$$

and the 2nd-order term (positive) is

$$C_4^{(2)} \;=\; \frac{12\,k_3^2\sigma_0^{10}}{(\hbar\omega)^2}\,\frac{5z^3+109z^2+109z+5}{(1-z)^3} \;+\; \frac{720\,k_3^2\sigma_0^{10}}{\hbar\omega k_BT}\,\frac{z^2}{(1-z)^4}. \tag{4.51}$$

Equation (4.50) corresponds to (22) of [Yokoyama et al., 1996] and to (15) of [Yokoyama, 1999] (where however $(\hbar\omega)^2$ appears instead of $\hbar\omega$ as a denominator in the first term).

The second order term (4.51) corresponds to (16) of [Yokoyama, 1999].

A comparison between the quantum treatment and the classical approximation at the lowest order terms is given in Fig. 4.3 for the case of the Br_2 molecule, again using the force constants from vibrational spectra [Huber and Herzberg, 1979] quoted by [Yokoyama, 1999].
The coefficients of thermal expansion for the Bromine molecule, calculated from the first-order quantum approximation to the first cumulant (4.45) and from the first-order classical approximation (4.38) are compared in Fig. 4.4.

In a recent anharmonic analysis of temperature-dependent EXAFS data for CdTe , the harmonic contribution C_2^0 to the second cumulant has been found to correspond to 91% of the total at 300 K;

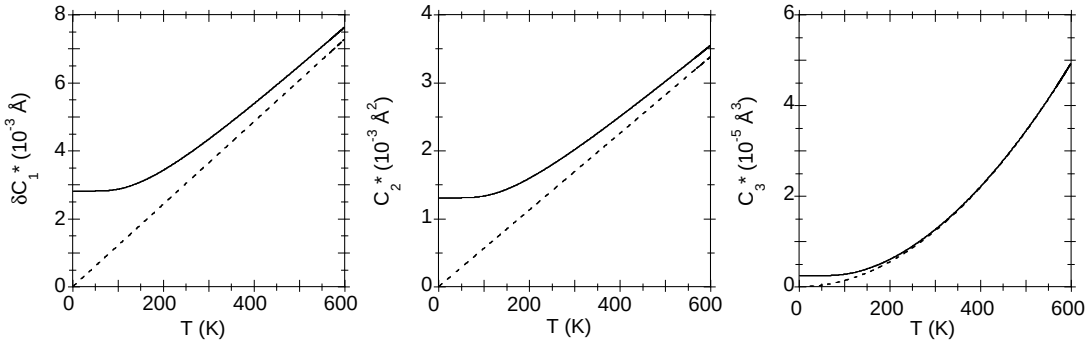

Figure 4.3: First three cumulants for Br_2 molecule, lowest order quantum calculations (continuous lines) and classical approximation (dashed lines). The same force constants as in Fig. 4.2 have been used.

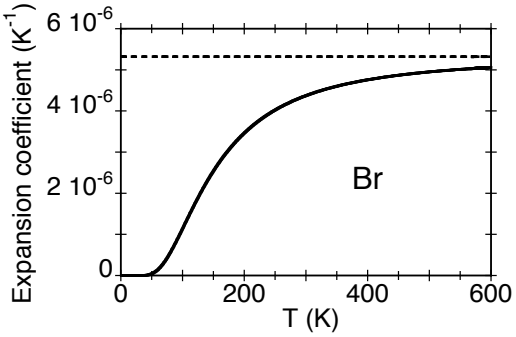

Figure 4.4: Thermal expansion coefficient of the Br_2 molecule: first order quantum approximation (continuous line) and first-order classical approximation (dashed line).

the anharmonic contribution is mainly due to the terms $C_2^{(2)}$ which depend on k_3; the terms $C_2^{(1)}$, which depend on k_4, are quite unimportant. As for the 4th cumulant, the two terms $C_4^{(2)}$ which depend on k_3, have been found to account for most of the fourth cumulant; the two terms $C_4^{(1)}$, which depend on k_4, give a very small contribution [Fornasini and Grisenti, 2015].

The quantum perturbative calculations have been further extended to the third order for the first, second and fourth cumulants and to the fourth order for the third cumulant by [Haug et al., 2008] in order to account for the high temperature anharmonicity effects.

Thermal expansion

By comparing Eq. (4.45) with Eq. (4.46) one can see that the thermal expansion of a system with one degree of freedom can be expressed, to first order, as

$$\delta C_1^* \;=\; -\,\frac{3k_3}{k_0}\,C_2^{(0)}. \tag{4.52}$$

To our knowledge, this relation has been for the first time proposed by [Frenkel and Rehr, 1993]. It can however be obtained even in the classical approximation. It is accurate, to first order, for unidimensional systems (two-atomic molecules), but is unsuitable for many-dimensional systems (see below).

4.1.7 Comparison of classical and quantum approximations

Harmonic oscillator

Let us compare the quantum behaviour

$$\sigma^2 \;=\; \frac{0.523788}{\nu\,\mu}\coth(24.008\,\nu/T)\,,$$

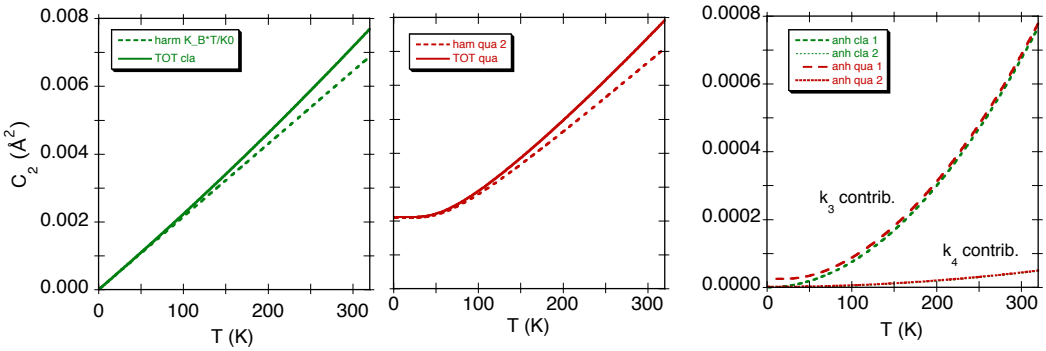

Figure 4.5: Second cumulant of CdTe. Left: classical approximation (4.39), total (continuous line) and harmonic part (dashed line). Centre: quantum approximation (4.46)+(4.47)+(4.48), total (continuous line) and harmonic part (dashed line). Right: comparison of the first anharmonic contributions depending on k_3 and on k_4: the classical and quantum expressions give very similar results.

with its classical approximation

$$\sigma(\infty) = \frac{0.0218278}{\nu^2 \mu} T$$

at 300 K in Table 4.1 for some systems. The case of Bromine is represented in Fig. 4.3. As one can see, the difference can be non negligible for accurate interpretations.

Table 4.1: Comparison between the quantum and classical approximations for the evaluation of cumulants.

	Harmonic		
	ν_0 [THz]	μ [amu]	$\sigma^2_{\text{qua}} - \sigma^2_{\text{cla}}$ [%]
Ge	7.7	35.0	11.1
Br	6.83	79.9	9.1
Cu	4.96	31.8	4.9
CdTe	3.86	59.76	3.35

Anharmonic contributions

The anharmonic analysis of the second cumulant of CdTe[Fornasini and Grisenti, 2015] has led to determine the force constants $k_0 = 4.01$ eV/Å^2, $k_3 = -2.69$ eV/Å^3 and $k_4 = -0.36$ eV/Å^4.

By means of (4.39) one can reconstruct the different contribution to the second cumulant in the classical approximation (Fig. 4.5, left).

By means of (4.46)+(4.47)+(4.48) one can reconstruct the different contribution to the second cumulant in the quantum approximation (Fig. 4.5, centre).

The classical and quantum approximation are in good agreement at high temperatures, the discrepancy at low temperatures being mainly due to the harmonic term. The anharmonic corrections are very similar for the classical and the quantum approximations (Fig. 4.5, right); for both approximations, the contributions of the terms depending on K_3 are much larger than the contributions of the terms depending on k_4.

4.1.8 Atomic displacements in two-atomic systems

We consider now the relation between the interatomic potential and the atomic displacements for a two-atomic molecule, as a particular case of the general Born-von Karman expansion of a crystal potential (from [Leibfried and Ludwig, 1961], page 282, linear chain, particular case of two atoms). This approach is preliminary for a better understanding of the interpretation of cumulants in many-atomic systems of next § 4.2 and 4.3 (see also [Fujikawa and Miyanaga, 1993]).

Let us consider two different expansions of the potential energy $V(r)$ in powers of the relative atomic displacements, one with respect to the rest distance, the other with respect to the mean distance.

To this purpose, it is convenient to distinguish:

1. The rest positions r_a^0 and r_b^0 of the two atoms and the rest distance $R_0 = r_b^0 - r_a^0$.
2. The mean positions r_a and r_b of the two atoms and the mean distance $R = r_b - r_a$.

Power expansion with respect to the rest distance R_0

The rest distance R_0 is the position of the minimum of $V(r)$.
Let u_a^0 and u_b^0 be the instantaneous atomic displacements from the *rest positions* and let $\Delta u_0 = u_b^0 - u_a^0$. The instantaneous distance is

$$r \;=\; R_0 + x^0 \;=\; R_0 + \Delta u_0 \tag{4.53}$$

The potential energy is expanded as

$$\begin{aligned} V(r) &= V(R_0 + \Delta u_0) && (4.54)\\ &= V(R_0) + \left(\frac{dV}{d\Delta u_0}\right)_0 \Delta u_0 + \frac{1}{2}\left(\frac{d^2V}{d\Delta u_0^2}\right)_0 (\Delta u_0)^2 + \frac{1}{3!}\left(\frac{d^3V}{d\Delta u_0^3}\right)_0 (\Delta u_0)^3 + \ldots && (4.55)\\ &= V(R_0) + \frac{1}{2}\left(\frac{d^2V}{d\Delta u_0^2}\right)_0 (\Delta u_0)^2 + \frac{1}{3!}\left(\frac{d^3V}{d\Delta u_0^3}\right)_0 (\Delta u_0)^3 + \ldots \end{aligned}$$

The first derivative at the position of potential minimum is zero. We recover the expression (4.33) of the pair interaction potential.
The average distance, first EXAFS cumulant, is

$$C_1^* \;=\; \langle r \rangle \;=\; R_0 + \langle x^0 \rangle \;=\; R_0 + \langle \Delta u_0 \rangle \tag{4.56}$$

Power expansion with respect to the average distance R

Let u_a and u_b be the instantaneous atomic displacements from the *mean positions* and let $\Delta u = u_b - u_a$. The instantaneous distance is

$$r \;=\; R + x \;=\; R + \Delta u\,. \tag{4.57}$$

The expansion of the potential energy now corresponds to the Born-von Karman expansion

$$\begin{aligned} V(r) &= V(R + \Delta u) && (4.58)\\ &= V(R) + \left(\frac{dV}{d\Delta u}\right)_{av} \Delta u + \frac{1}{2}\left(\frac{d^2V}{d\Delta u^2}\right)_{av} (\Delta u)^2 + \frac{1}{3!}\left(\frac{d^3V}{d\Delta u^3}\right)_{av} (\Delta u)^3 + \ldots \end{aligned}$$

This expression doesn't correspond to the expression (4.33) of the pair interaction potential.
The average distance, first EXAFS cumulant, is

$$C_1^* \;=\; \langle r \rangle \;=\; R + \langle x \rangle \;=\; R + \langle \Delta u \rangle \tag{4.59}$$

Harmonic approximation

In the harmonic approximation, the mean positions and rest positions coincide and $R = R_0$.
As a consequence, $x = x^0$, $u_i = u_i^0$, $\Delta u = \Delta u_0$
The average values

$$\langle \Delta u_0 \rangle = \langle x_0 \rangle = 0\,, \qquad \langle \Delta u \rangle = \langle x \rangle = 0 \tag{4.60}$$

so that

$$C_1^* = R_0 = R \tag{4.61}$$

There is no thermal expansion:

$$\delta C_1^* = \langle \Delta u \rangle = 0\,. \tag{4.62}$$

Second cumulant: since $r = R + \Delta u$ and $\langle \Delta u \rangle = 0$,

$$C_2^* = \big\langle (r - \langle r \rangle)^2 \big\rangle = \big\langle (r - R)^2 \big\rangle = \langle \Delta u^2 \rangle = \langle \Delta u_0^2 \rangle \tag{4.63}$$

Third cumulant: due to the symmetry of the potential and of the distribution,

$$C_3^* = \big\langle (r - \langle r \rangle)^3 \big\rangle = \big\langle (r - R)^3 \big\rangle = \langle \Delta u^3 \rangle = \langle \Delta u_0^3 \rangle = 0 \tag{4.64}$$

Note: Shorthand notation: $\langle \Delta u^2 \rangle = \langle (\Delta u)^2 \rangle$.
Distributions:

a) The distributions of atomic positions around their rest positions r_a and r_b are gaussian.
b) The distribution $\rho(r)$ of the distance $r = r_b - r_a$ is gaussian.

Anharmonic potential

For the anharmonic molecule, the potential energy is not symmetric with respect to R_0. The distributions of atomic positions and of interatomic distance are not symmetric.
Average positions and rest positions of the two atoms are different, $R \neq R_0$ and different are the expressions of cumulants in terms of the relative atomic displacement.
As a consequence, $x \neq x^0$, $u_i \neq u_i^0$ and $\Delta u \neq \Delta u_0$.
The standard Born-von Karman expansion is relative to the average positions, not to the rest positions (in the present case, it would be relative to the average distance R, not to the rest distance R_0).

1. **Expansion with respect to the rest distance.**
   The oscillations of atoms are asymmetric, and since R_0 is not the mean position, $\langle \Delta u_0 \rangle \neq 0$; for two equal masses, $\langle u_b^0 \rangle = -\langle u_a^0 \rangle \neq 0$.
   The first cumulant is again

$$C_1^* = \langle r \rangle = R_0 + \langle \Delta u_0 \rangle\,. \tag{4.65}$$

   The thermal expansion is

$$\delta C_1^* = \delta \langle \Delta u_0 \rangle\,. \tag{4.66}$$

   The second cumulant, since $r = R_0 + \Delta u_0$ and $\langle \Delta u_0 \rangle \neq 0$, is

$$\begin{aligned} C_2^* &= \big\langle (r - \langle r \rangle)^2 \big\rangle \;=\; \langle r^2 \rangle - \langle r \rangle^2 \\ &= \big\langle (\Delta u_0 - \langle \Delta u_0 \rangle)^2 \big\rangle \;=\; \langle \Delta u_0^2 \rangle - \langle \Delta u_0 \rangle^2 \end{aligned} \tag{4.67}$$

   say it is the variance of the distribution of Δu_0 values with respect to its non-zero average.
   The third cumulant, again since $r = R_0 + \Delta u_0$ and $\langle \Delta u_0 \rangle \neq 0$, is

$$\begin{aligned} C_3^* &= \big\langle (r - \langle r \rangle)^3 \big\rangle \;=\; \langle r^3 \rangle - 3\langle r^2 \rangle \langle r \rangle + 2\langle r \rangle^3 \\ &= \big\langle (\Delta u_0 - \langle \Delta u_0 \rangle)^3 \big\rangle \;=\; \langle \Delta u_0^3 \rangle - 3\langle \Delta u_0^2 \rangle \langle \Delta u_0 \rangle + 2\langle \Delta u_0 \rangle^3 \end{aligned} \tag{4.68}$$

   The expressiond for C_2^* and C_3^* coincide with eq. (2.11) of [Fujikawa and Miyanaga, 1993], where the displacements are evaluated with respect to the rest positions.

2. **Expansion with respect to the average distance.**
The oscillations of atoms are asymmetric, but the average displacement with respect to the mean position is always zero, so that $\langle u_b \rangle = \langle u_a \rangle = 0$, and $\langle \Delta u \rangle = 0$.
The first cumulant is
$$C_1^* = \langle r \rangle = R\,. \tag{4.69}$$
The thermal expansion is
$$\delta C_1^* = \delta R\,. \tag{4.70}$$
The second cumulant, since $r = R + \Delta u$, $R = \langle r \rangle$ and $\langle \Delta u \rangle = 0$, is
$$C_2^* = \big\langle (r - \langle r \rangle)^2 \big\rangle = \big\langle (r - R)^2 \big\rangle = \langle \Delta u^2 \rangle\,; \tag{4.71}$$
it is the variance of the distribution of Δu values with respect to the zero average.
The third cumulant is
$$C_3^* = \big\langle (r - \langle r \rangle)^3 \big\rangle = \big\langle (r - R)^3 \big\rangle = \langle \Delta u^3 \rangle \tag{4.72}$$

4.2 Many-atomic systems

Let us now consider the interpretation of EXAFS cumulants in systems composed by more than two atoms, say with more than one degree of freedom.
It seems convenient to distinguish different types of atomic aggregation:

a) Molecules
b) Unidimensional linear chain
c) Three-dimensional real crystals.
d) Non-crystalline solids and liquids.

For each type of system, we explore

- the harmonic approximation and the anharmonicity effects,
- the relation between total potential, effective pair potential and single pair potential
- the third cumulants and its connection to normal vibrations

An EXAFS experiment gives unidimensional information, expressed in terms of a unidimensional distribution of distances; here we will refer to the *real* distribution $\rho(r)$.
For the two-atomic molecule, the unidimensional distribution and its cumulant can be directly connected to the single-pair interaction potential, both in the harmonic approximation and including anharmonicity, as it was seen in § 4.1.
For many-atomic systems, the problem arises of finding the relation between the three-dimensional structure of the N-atomic system and the unidimensional distribution sampled by EXAFS.

4.2.1 Molecules

Triatomic linear molecules

Non-linear molecules

4.2.2 The one-dimensional linear chain

We assume that atoms can move only along the direction of the chain, not in perpendicular directions.
The total potential energy can be expanded in terms of atomic displacements (Born-von Karman expansion)

$$\begin{aligned} V &= V_0 + \sum_n \left(\frac{\partial V}{\partial u_n}\right)_{\{R\}} u_n + \frac{1}{2}\sum_{nn'} \left(\frac{\partial^2 V}{\partial u_n \partial u_{n'}}\right)_{\{R\}} u_n u_{n'} \\ &+ \frac{1}{3!}\sum_{nn'n''} \left(\frac{\partial^3 V}{\partial u_n \partial u_{n'} \partial u_{n''}}\right)_{\{R\}} u_n u_{n'} u_{n''} + \ldots \end{aligned} \tag{4.73}$$

where

- the partial derivatives are evaluated at the configuration of mean atomic positions $\{R\}$
- the displacements u are with respect to the mean atomic positions $\{R\}$

We consider only nearest-neighbours interactions.
For the statistical treatment, see for example [Miyanaga and Fujikawa, 1994].

Harmonic approximation

The nearest neighbours interaction is modelled by harmonic springs. The single-bond potential energy is quadratic, the force linearly depends on the displacements.

- No thermal expansion when temperature is changed
- Gaussian distributions of atomic positions at a given T
- Gaussian distributions of inter-atomic distances at a given T

Anharmonicity effects

The nearest neighbours interaction is modelled by anharmonic springs ($k_3 < 0$).

- Positive expansion of the inter-atomic distance when temperature is changed
- Distributions of atomic positions around the mean values at a given T is gaussian for symmetry reasons
- Distributions $\rho(r)$ of inter-atomic distances at a given T: according to the quantum perturbative calculations of [Miyanaga and Fujikawa, 1994] based on a single-pair Morse potential, the distribution is asymmetric and the 3rd cumulant is different from zero.

4.2.3 3-dimensional Crystals

Let us summarise here the main problems encountered when interpreting EXAFS in crystals.

Inter-atomic distances and thermal expansion

For crystals, from the experimental point of view it is important to understand the relations between the three distances and the relative thermal expansions which can be measured by EXAFS and elastic scattering of X-rays (or neutrons)

1. Distance between average atomic positions in crystals and corresponding thermal expansion, which, for crystals without internal coordinates, are proportional to the lattice parameter and its thermal expansion, respectively, measured by elastic scattering experiments.
2. Bond distance and bond thermal expansion in crystals, measured by the 1st EXAFS cumulant C_1^* and corresponding to the average value of the distribution of instantaneous distances $\rho(r)$ and its expansion.
3. Thermal expansion evaluated from the 3rd cumulant in the unidimensional model according to (4.52): $a = -(3k_3/k_0)C_2$ [Frenkel and Rehr, 1993].

A comparison of the three different thermal expansions for different systems is shown in Fig. 4.6.

- The bond expansion measured by EXAFS is always larger than the expansion evaluated from the measurement of lattice expansion by elastic scattering; this difference can be accounted for by the effect of perpendicular vibrations (see below).
- Less trivial is to understand the relation between the meaning of the expansion evaluated from the asymmetry of the distribution and its relation with the other two expansions. The difference between the relative expansions δC_1^* and δa corresponds to a break-down of the model for one degree of freedom to interpretat three-dimenasional situations.
  Note also that the expression $a = -(3k_3/k_0)C_2$ [Frenkel and Rehr, 1993] gives the absolute expansion for a unidimensional system; in Fig. 4.6 only relative expansions are compared (vertical axis arranged to have a zero value for the three different expansions at $T = 0$).

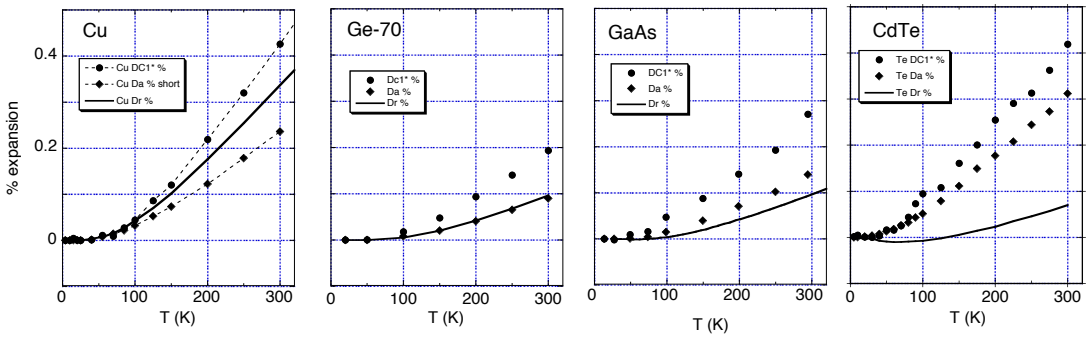

Figure 4.6: Thermal expansions measured for Cu [Fornasini et al., 2004], Ge [Purans et al., 2008], GaAs [Abd el All et al., 2012] and CdTe [Ahmed et al., 2013] : from first EXAFS cumulant δC_1^* (circles), from the asymmetry of the distance distribution δa, with $a = -(3k_3/k_0)C_2$ (diamonds) and from elastic scattering (continuous line) [Touloukian et al., 1977].

A comparison of the thermal expansion coefficients would be free from the problems related to the differences in absolute values of the different distances at $T = 0$.

Potential energies

A correlated problem is the relation between three types of potential energy:

1. The single-pair interaction potential energy
2. The effective pair potential energy, say the potential energy of interaction of a pair of atoms embedded into a crystalline (or non-crystalline) structure
3. The total potential energy, which for a crystal is generally expressed in terms of the Born-von Karman expansion in powers of the atomic displacements.

Examples? Lennard-Jones and Coulomb single-pair potentials?

Harmonic approximation and anharmonicity

The meaning of harmonic approximation is different for the different potential energies considered above. For example, an harmonic single-pair potential doesn't correspond to an harmonic crystal potential, and would give origin to a negative lattice thermal expansion [Barron, 1957].
The lattice thermal expansion is connected to the Born- von Karman anharmonicity of the crystal potential energy.

Crystals: information from Bragg diffraction

The difference and complementarity of diffraction and EXAFS can be traced back to the different nature of the scattering process and therefore to the different sensitivity to the correlation of atomic thermal motion.
Powder diffraction experiments allow measuring the mean cell parameters and their temperature dependence, derived from the probed ensemble of coherently diffracting crystalline domains. For systems with atoms only in special positions [??], the distances $R = |\langle \vec{r}_a \rangle - \langle \vec{r}_b \rangle|$ between the average positions in space of any two atoms can be obtained from the cell parameters by direct proportionality. It has recently been shown that it is possible to measure the anisotropic displacement parameters (ADP) U_{ij} from Rietveld refinement of good quality powder diffraction data, even if this kind of refinement is more common from neutron data [David et al., 1992, Kennedy, 1995] than from X-ray data [Dusek et al., 2001, Artioli, 2002]. From the ADPs, the MSDs along selected directions can be calculated, for example the MSDs parallel and perpendicular to a given bond direction, $U_{||}$ and $U_{\perp}$ respectively.

General properties of three-dimensional distributions of distances

See [Stern, 1997] and [Fornasini et al., 2001].

4.3 3D Atomic displacement expansion

4.3.1 Instantaneous inter-atomic distance in EXAFS

Let $\vec{R} = \langle\vec{r}_b\rangle - \langle\vec{r}_a\rangle$ be the average positions of atoms a and b and let $\vec{u}_a$ and $\vec{u}_b$ the instantaneous thermal displacements of the absorber and back-scatterer atoms, respectively, from their average positions. The instantaneous inter-atomic vector distance is then (Fig. 4.7)

$$\vec{r} = \vec{R} + \Delta\vec{u}, \tag{4.74}$$

where $\Delta\vec{u} = \vec{u}_b - \vec{u}_a$ is the *relative displacement* with respect to the average vector distance. The instantaneous scalar distance r is expressed as:

$$r \;=\; |\vec{R} + \Delta\vec{u}| \;=\; \left[\left(\vec{R} + \Delta\vec{u}\right)^2\right]^{1/2} \;=\; R\left[1 + 2\hat{R}\cdot\frac{\Delta\vec{u}}{R} + \frac{\Delta u^2}{R^2}\right]^{1/2}, \tag{4.75}$$

where $\hat{R} = \vec{R}/R$.
It is now convenient to introduce the projections of the instantaneous relative displacement $\Delta\vec{u}$ parallel and perpendicular to the inter-atomic bond:

$$\Delta u_\parallel \;=\; \hat{R}\cdot\Delta\vec{u}; \qquad (\Delta u_\perp)^2 \;=\; (\Delta u)^2 - (\Delta u_\parallel)^2\,, \tag{4.76}$$

so that $\hat{R}\cdot\Delta\vec{u} = \Delta u_\parallel$ in (4.75).
From now on, to simplify notation, we use the short-hand expressions

$$\Delta u^2\,, \qquad \Delta u_\parallel^2 \qquad \Delta u_\perp^2 \tag{4.77}$$

as substitute of the more precise expressions

$$(\Delta u)^2\,, \qquad (\Delta u_\parallel)^2 \qquad (\Delta u_\perp)^2\,. \tag{4.78}$$

We can now expand (4.75) making use of the general form of the binomial series

$$(1+x)^\alpha \;=\; \sum_{n=0}^{\infty}\binom{\alpha}{n}x^n\,,$$

where

$$\binom{\alpha}{n} \;=\; \frac{\alpha\,(\alpha-1)\cdots(\alpha-n+1)}{n!}\,, \qquad \binom{\alpha}{0} \;=\; 1$$

are the generalised binomial coefficients. For $\alpha = 1/2$,

$$(1+x)^{1/2} \;=\; \sum_{n=0}^{\infty}\binom{1/2}{n}x^n \;=\; 1 + \frac{x}{2} - \frac{x^2}{8} + \frac{x^3}{16} - \frac{5x^4}{128} + \cdots \tag{4.79}$$

For the present case of (4.75),

$$x \;=\; \frac{2\Delta u_\parallel}{R} + \frac{\Delta u^2}{R^2}\,.$$

Note: The values $2\Delta u_\parallel/R$ and $\Delta u^2/R^2$ in (4.75) can be estimated from the measured root-mean-square values of the parallel and perpendicular displacements. The values for some systems at 300 K are listed in Table 4.2.

Table 4.2: Experimental estimate of the values $2\Delta u_\parallel/R$ and $\Delta u^2/R^2$ from the measured parallel and perpendicular MSRDs at 300 K for some systems.

	Cu	Ge	GaAs	CdTe
$2(\langle\Delta u_\parallel^2\rangle)^{1/2}/R$	0.072	0.048	0.052	0.060
$\langle\Delta u^2\rangle/R^2$	0.0043	0.0036	0.0053	0.0092

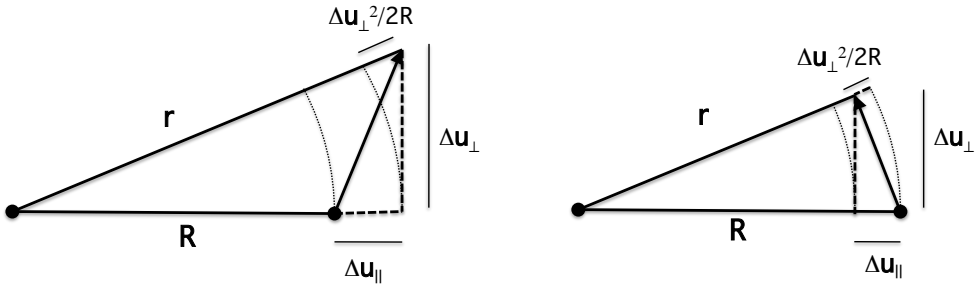

Figure 4.7: Schematic representation of the relation between the equilibrium distance $\vec{R}$ and the instantaneous distance $\vec{r} = \vec{R} + \Delta\vec{u}$. Two cases with $\Delta u_\parallel > 0$ and $\Delta U_\parallel < 0$ are considered on the left and on the right, respectively. The approximate geometrical extent of the term $\Delta u_\perp^2/2R$ is shown.

Truncating the expansion (4.79) at the fourth term one obtains

$$\begin{aligned} r \;\simeq\; & R + \Delta u_\parallel + \frac{\Delta u^2}{2R} - \frac{\Delta u_\parallel^2}{2R} - \frac{\Delta u_\parallel \Delta u^2}{2R^2} - \frac{\Delta u^4}{8R^3} \\ & + \frac{\Delta u_\parallel^3}{2R^2} + \frac{3\Delta u_\parallel^2 \Delta u^2}{4R^3} + \frac{3\Delta u_\parallel \Delta u^4}{8R^4} + \frac{\Delta u^6}{16R^6}\,. \end{aligned}$$

Substituting $\Delta u^2 = \Delta u_\parallel^2 + \Delta u_\perp^2$ and considering only terms of order up to $1/R^3$, the instantaneous scalar distance r is finally expressed as:

$$r \;\simeq\; R + \Delta u_\parallel + \frac{\Delta u_\perp^2}{2R} - \frac{\Delta u_\parallel \Delta u_\perp^2}{2R^2} + \frac{5\Delta u_\parallel^4}{8R^3} - \frac{\Delta u_\perp^4}{8R^3} + \frac{\Delta u_\parallel^2\, \Delta u_\perp^2}{2R^3}\,. \tag{4.80}$$

Multiple scattering paths

For multiple scattering paths (4.80) has been generalised as follows by Poiarkova and Rehr [Poiarkova and Rehr, 1999].
The equilibrium path is defined as

$$R_j \;=\; \frac{1}{2}\sum_{i=1}^{n_j} R_{ii+}\,, \tag{4.81}$$

where j is the path index, N_j is the number of legs, i is the site (atom) index, $i+ = i+1$ and R_{ii+} is the equilibrium distance between sites i and $i+1$.
The instantaneous distance is

$$r_j \;\simeq\; R_j + \frac{1}{2}\sum_{i=1}^{n_j} (\vec{u}_{i+} - \vec{u}_i)\cdot \hat{R}_{ii+}\,. \tag{4.82}$$

Note 1: The right-hand side of (4.82) corresponds to the first two terms of (4.80). Perpendicular vibrations are not taken into account.

Note 2: In (4.82) the sign of the difference $\vec{u}_{i+} - \vec{u}_i$ has been reverted with respect to eq. (6) of [Poiarkova and Rehr, 1999].

4.3.2 First cumulant. Mean interatomic distance

The first cumulant C_1^* of the real distribution of distances $\rho(r)$ is the average value $\langle r \rangle$ of the instantaneous distance expressed by (4.80). Let us now consider only the first four terms in the right-hand side of (4.80).

Since we are considering displacements with respect to the average atomic positions, one has

$$\langle \vec{u}_a \rangle = \langle \vec{u}_b \rangle = \langle \hat{R} \cdot \vec{u}_a \rangle = \langle \hat{R} \cdot \vec{u}_b \rangle \;=\; 0 \tag{4.83}$$

so that the average relative displacement is zero:

$$\langle \Delta u_{\parallel} \rangle \;=\; \langle \hat{R} \cdot (\vec{u}_b - \vec{u}_a) \rangle \;=\; \langle \hat{R} \cdot \vec{u}_b \rangle \,-\, \langle \hat{R} \cdot \vec{u}_a \rangle \;=\; 0\,. \tag{4.84}$$

In addition, even

$$\langle\, \Delta u_{\parallel}\, \Delta u_{\perp}^2 \,\rangle \;=\; 0\,; \tag{4.85}$$

as a matter of fact, for any pair of displacements $(\vec{u}_a, \vec{u}_b)$, the pair $(-\vec{u}_b, -\vec{u}_a)$ has the same probability [?? only in harmonic aproximation??]. To the two opposite pairs it correspond equal values $\Delta u_{\perp}^2$ but opposite values $\Delta u_{\parallel}$. For each value $(\Delta u_{\perp})^2$, $\Delta u_{\parallel}$ can assume with the same probability a positive value or its opposite.

In conclusion, one has

$$C_1^* \;=\; \langle r \rangle \;\simeq\; R \;+\; \langle\, \Delta u_{\perp}^2 \,\rangle / 2R \tag{4.86}$$

The last term in (4.86) depends on the Mean Square Relative Displacement in direction *normal* to the inter-atomic bond. It is always positive.

The first EXAFS cumulant C_1^* is always larger than the inter-atomic distance R; the difference grows with temperature (Fig. 4.8, left). The term $\langle \Delta u_{\perp}^2 \rangle$ cannot be directly obtained from experiment. It can however be calculated by inverting (4.86) if R is known from other techniques, like Bragg diffraction.

4.3.3 Second cumulant, Parallel MSRD

The second cumulant is the variance of the distribution of distances $\rho(r)$. For a given atomic pair,

$$C_2^* = \sigma^2 = \langle (r - \langle r \rangle)^2 \rangle \;=\; \langle r^2 \rangle - \langle r \rangle^2\,. \tag{4.87}$$

From the first three terms on the right-hand side of (4.80),

$$\langle r^2 \rangle \;\simeq\; R^2 + \langle \Delta u_{\parallel}^2 \rangle + \frac{\langle \Delta u_{\perp}^4 \rangle}{4R^2} + 2R \langle \Delta u_{\parallel} \rangle + \langle \Delta u_{\perp}^2 \rangle + \frac{\langle \Delta u_{\parallel}\, \Delta u_{\perp}^2 \rangle}{R} \tag{4.88}$$

and from (4.86)

$$\langle r \rangle^2 \;\simeq\; R^2 + \frac{[\langle \Delta u_{\perp}^2 \rangle]^2}{4R^2} + \langle\, \Delta u_{\perp}^2 \,\rangle\,. \tag{4.89}$$

Taking into account (4.84) and (4.85), the difference between (4.88) and (4.89) gives, for an atomic pair,

$$\begin{aligned} C_2^* \;&\simeq\; \langle \Delta u_{\parallel}^2 \rangle \;+\; \frac{\langle \Delta u_{\perp}^4 \rangle}{4R^2} - \frac{\left[\langle \Delta u_{\perp}^2 \rangle\right]^2}{4R^2} \\ &\simeq\; \langle \Delta u_{\parallel}^2 \rangle \;+\; \frac{1}{4R^2} \left\{ \langle \Delta u_{\perp}^4 \rangle - \left[\langle \Delta u_{\perp}^2 \rangle\right]^2 \right\} \end{aligned} \tag{4.90}$$

According to (4.90), the variance of the distribution of r distances, say the second cumulant C_2^*, contains two main contributions:

1. The leading contribution is the **parallel MSRD** (projection along the crystallographic bond direction)
$$\langle \Delta u_{\parallel}^2 \rangle = \left\langle \left[\hat{R} \cdot (\vec{u}_b - \vec{u}_a) \right]^2 \right\rangle \tag{4.91}$$
2. The second contribution is the variance of the distribution of $\Delta u_{\perp}^2$, divided by $4R^2$.
This term would be zero only if $\Delta u_{\perp}^2 = \langle \Delta u_{\perp}^2 \rangle$; this case would correspond to a conic pendulum with vertex on the absorbing atom, with $\langle \Delta u_{\parallel}^2 \rangle = 0$.

For a comparison with the relative extent of the two terms, see Fig. 1 of [Fornasini et al., 2001], where an additional term has been erroneously inserted in Eq. 4 with respect to the present (4.90); the term has however no influence on the main results shown in the figure.
For most real cases, it seems that the second term can be neglected.

MSRD for multiple scattering paths

For multiple scattering paths, the parallel MSRD (4.91) has been generalised as follows by Poiarkova and Rehr [Poiarkova and Rehr, 1999]

$$\sigma_j^2 = \frac{1}{4} \left\langle \left[\sum_{i=1}^{n_j} (\vec{u}_{i+} - \vec{u}_i) \cdot \hat{R}_{ii+} \right]^2 \right\rangle , \tag{4.92}$$

where the symbols have the same meaning as in (4.82).

4.3.4 Third cumulant, mean cubic relative displacement

The third cumulant is equal to the centred moment of order three of the distribution $\rho(r)$:

$$C_3^* = \langle (r - \langle r \rangle)^3 \rangle . \tag{4.93}$$

Let us first evaluate the instantaneous value $(r - \langle r \rangle)^3$, considering the first three terms of (4.80) for r and (4.86) for $\langle r \rangle$:

$$(r - \langle r \rangle)^3 = \left[\Delta u_{\parallel} + \frac{\Delta u_{\perp}^2}{2R} - \frac{\langle \Delta u_{\perp}^2 \rangle}{2R} \right]^3 \tag{4.94}$$

By substituting

$$a = \Delta u_{\parallel} , \quad b = \frac{\Delta u_{\perp}^2}{2R} \quad c = \frac{\langle \Delta u_{\perp}^2 \rangle}{2R} \tag{4.95}$$

one finds

$$(r - \langle r \rangle)^3 = a^3 + 3a^2(b-c) + 3a(b-c)^2 + (b-c)^3 . \tag{4.96}$$

Let us now consider the average value $\langle (r - \langle r \rangle)^3 \rangle$.
The first term

$$\langle a^3 \rangle = \langle \Delta u_{||}^3 \rangle = \langle [\hat{R} \cdot (\vec{u}_b - \vec{u}_a)]^3 \rangle \tag{4.97}$$

is not zero even if the vibrations are considered with respect to the average positions.
The second term

$$\langle 3a^2(b-c) \rangle = 3 \left[\left\langle \Delta u_{\parallel}^2 \frac{\Delta u_{\perp}^2}{2R} \right\rangle - \left\langle \Delta u_{\parallel}^2 \right\rangle \frac{\langle \Delta u_{\perp}^2 \rangle}{2R} \right] \tag{4.98}$$

is zero is the values of $\Delta u_{\parallel}^2$ and of $\Delta u_{\perp}^2$ are statistically independent, because in this case the average value of the product is equal to the product of average values [are they truly independent ??]
The third term

$$\langle 3a(b-c)^2 \rangle = 3 \left\langle \Delta u_{||} \left[\frac{\Delta u_{\perp}^2}{2R} - \frac{\langle \Delta u_{\perp}^2 \rangle}{2R} \right]^2 \right\rangle \tag{4.99}$$

is probably zero, since $(b-c)$ is an even function of the relative displacements. [verify...]

The fourth term

$$\left\langle (b-c)^3 \right\rangle = \frac{1}{8R^3} \left\langle \left[\Delta u_\perp^2 - \langle \Delta u_\perp^2 \rangle \right]^3 \right\rangle \tag{4.100}$$

is proportional to the mean cubic deviation of $\Delta u_\perp^2$ with respect to its average value; this term establishes a connection between the third cumulant and the perpendicular vibrations in harmonic approximation.

4.4 MSRD and vibrational dynamics

Let us consider the parallel MSRD (4.91) of a pair of atoms $a-b$ (Single Scattering case). The square can be expanded into the sum of three terms [Beni and Platzman, 1976]

$$\langle \Delta u_\parallel^2 \rangle \;=\; \langle (\hat{R}\cdot\vec{u}_b)^2 \rangle \;+\; \langle (\hat{R}\cdot\vec{u}_a)^2 \rangle \;-\; 2\,\langle (\hat{R}\cdot\vec{u}_b)(\hat{R}\cdot\vec{u}_a) \rangle. \tag{4.101}$$

The first two terms are the independent *Mean Square Displacements* (MSD) of absorber and back-scatterer atoms. The third term, the *Displacement Correlation Function* (DCF), depends on the correlation of atomic motions. The correlation term DCF decreases with increasing distance and vanishes for very large distances. The sensitivity to correlation is quite peculiar to EXAFS. In diffraction experiments, as a consequence of long-range averaging, the effect of short-range correlations is dispersed into thermal diffuse scattering, and the Debye-Waller factor obtained from the refinement of Bragg peaks measures only the uncorrelated MSD.

4.4.1 Parallel MSRD and dynamical matrix

In the **harmonic approximation**, the atomic displacements $\vec{u}$ of (4.101) can be expressed in terms of eigenvectors and eigenfrequencies of the dynamical matrix.

General expression

A general expression of the parallel MSRD of a pair of atoms $a-b$ is given by Eq. (11) of Crozier et al. [Crozier et al., 1988]:

$$\langle \Delta u_\parallel^2 \rangle \;=\; \frac{\hbar}{2\mu_{ab}} \sum_\lambda \left| \left(\sqrt{\frac{\mu_{ab}}{m_b}}\,\vec{\epsilon}_b(\lambda) - \sqrt{\frac{\mu_{ab}}{m_a}}\,\vec{\epsilon}_a(\lambda) \right) \cdot \hat{R} \right|^2 \;\; \frac{1}{\omega(\lambda)} \coth \frac{\hbar\omega(\lambda)}{2k_BT} \tag{4.102}$$

where the sum is over all normal modes of the real-space mass-adjusted dynamical matrix

$$D_{ab} \;=\; \frac{\partial^2 V / \partial\vec{u}_a \partial\vec{u}_b}{\sqrt{m_a m_b}}\,, \tag{4.103}$$

$\omega(\lambda)$ and $\vec{\epsilon}(\lambda)$ are eigenfrequencies and normalised eigenvectors, μ_{ab} is the reduced mass of the pair $a-b$ and

$$\frac{\hbar}{2\omega(\lambda)} \coth \frac{\hbar\omega(\lambda)}{2kT} \;=\; \langle |Q(\lambda)|^2 \rangle \;=\; \frac{\langle E(\lambda) \rangle}{\omega^2(\lambda)}\,. \tag{4.104}$$

The energy is distributed among normal modes according to the Maxwell-Boltzmann distribution (equivalent to the Bose-Einstei distribution for phonons):

$$\langle E(\lambda) \rangle \;=\; \left[\frac{1}{\exp[\hbar\omega(\lambda)/kT] - 1} + \frac{1}{2} \right] \hbar\omega(\lambda) \;=\; \frac{\hbar\omega(\lambda)}{2} \coth \left[\frac{\hbar\omega(\lambda)}{2kT} \right]. \tag{4.105}$$

Crystals

In crystals the translational symmetry allows one to decompose the solution of the real space dynamical matrix into the solution of **N** Fourier-transformed dynamical matrices, one for each value of phonon wave vector $\vec{q}$ (**N** is the number of primitive cells).

Eq. (4.102) transforms into

$$\langle \Delta u_{\parallel}^2 \rangle \;=\; \frac{1}{\mathbf{N}} \frac{\hbar}{2\mu_{ab}} \sum_{\vec{q},s} \; \frac{1}{\omega(\vec{q}s)} \; \coth \frac{\hbar\omega(\vec{q},s)}{2k_BT} \; \left| \left(\sqrt{\frac{\mu_{ab}}{m_b}}\, \vec{w}_b(\vec{q},s) e^{i\vec{q}\cdot\vec{R}} - \sqrt{\frac{\mu_{ab}}{m_a}}\, \vec{w}_a(\vec{q},s) \right) \cdot \hat{R} \right|^2 \tag{4.106}$$

where normal modes are now labelled by the wavevector $\vec{q}$ and the branch index s; the normalised eigenvectors $\vec{w}$ refer to a given value of $\vec{q}$. .
Alternatively, (4.106) can be written as

$$\boxed{\langle \Delta u_{\parallel}^2 \rangle \;=\; \frac{1}{\mathbf{N}} \sum_{\vec{q},s} \langle |Q(\vec{q},s,t)|^2 \rangle \; \left| \left(\frac{\vec{w}_b(\vec{q},s) e^{i\vec{q}\cdot\vec{R}}}{\sqrt{m_b}} - \frac{\vec{w}_a(\vec{q},s)}{\sqrt{m_a}} \right) \cdot \hat{R} \right|^2} \tag{4.107}$$

where again

$$\langle |Q(\vec{q},s,t)|^2 \rangle \;=\; \frac{\langle E(\vec{q},s) \rangle}{\omega^2(\vec{q},s)} \;=\; \frac{\hbar}{2\omega(\vec{q},s)} \coth \frac{\hbar\omega(\vec{q},s)}{2kT}. \tag{4.108}$$

and

$$\langle E(\vec{q},s) \rangle \;=\; \left[\frac{1}{\exp(\hbar\omega(\vec{q},s)/kT) - 1} + \frac{1}{2} \right] \hbar\omega(\vec{q},s) \;=\; \frac{\hbar\omega(\vec{q},s)}{2} \; \coth \left[\frac{\hbar\omega(\vec{q},s)}{2kT} \right]. \tag{4.109}$$

One can separate, in (4.107), the contribution due to the uncorrelated motion of atoms

$$\mathrm{MSD} \;=\; \frac{1}{\mathbf{N}} \sum_{\vec{q},s} \langle |Q(\vec{q},s,t)|^2 \rangle \; \left[\frac{|\vec{w}_b(\vec{q},s) \cdot \hat{R}|^2}{\sqrt{m_b}} - \frac{|\vec{w}_a(\vec{q},s) \cdot \hat{R}|^2}{\sqrt{m_a}} \right] \tag{4.110}$$

and the correlation term

$$\mathrm{DCF} \;=\; \frac{2}{\mathbf{N}\sqrt{m_b m_a}} \sum_{\vec{q},s} \langle |Q(\vec{q},s,t)|^2 \rangle \; \left[\vec{w}_b(\vec{q},s) \cdot \hat{R} \right] \left[\vec{w}_a(\vec{q},s) \cdot \hat{R} \right]^* \; e^{i\vec{q}\cdot\vec{R}}. \tag{4.111}$$

Coordination shells

The DW of a coordination shell is the average of the contributions from all the ab pairs, according to (4.102) or (4.107) :

$$\langle \Delta u_{\parallel}^2 \rangle_{\mathrm{shell}} \;=\; \frac{1}{N} \sum_{b=1}^{N} \langle \Delta u_{\parallel}^2 \rangle_b \,, \tag{4.112}$$

where the sum is over the N back-scattering atoms constituting the coordination shell.

Correlation effects

The contribution of a given pair of atoms ab to the total parallel MSRD depends:
a) on the phase relations between the two eigenvectors $\vec{\epsilon}_a$ and $\vec{\epsilon}_b$ (or $\vec{w}_a$ and $\vec{w}_b$) of each normal mode,
b) on the projections of the difference of the eigenvectors on the bond direction $\hat{R}_{ab}$.
c) In the case of crystals, it is convenient to disentangle, from the eigenvector phase difference, the intercell phase relation $e^{i\vec{q}\cdot\vec{R}}$ (as in eq. 4.107).

Projected VDOS

Let us consider again the general expression (4.102) for a pair of atoms. Following [Crozier et al., 1988], let us define

$$p_{ab}(\lambda) \;=\; \left| \left(\sqrt{\frac{\mu_{ab}}{m_b}}\, \vec{\epsilon}_b(\lambda) - \sqrt{\frac{\mu_{ab}}{m_a}}\, \vec{\epsilon}_a(\lambda) \right) \cdot \hat{R} \right|^2 \tag{4.113}$$

The quantity $p_{ab}(\lambda)$ measures the fractional contribution of mode λ to the parallel MSRD of the pair ab.
Crozier et al. define an initial "displacement state" where all atoms have zero velocity and

$$\vec{u}_b = \sqrt{\mu_{ab}/m_b}\,\hat{R}_{ab}\,, \quad \vec{u}_a = -\sqrt{\mu_{ab}/m_a}\,\hat{R}_{ab}\,, \quad \vec{u}_i = 0 \ (i \neq a, b) \tag{4.114}$$

The quantity $p_{ab}(\lambda)$ is the normalised probability that an initial displacement state is due to mode λ.
One can define a projected density of vibrational modes

$$\rho_{ab}(\omega) \ = \ \sum_{\lambda} p_{ab}(\lambda)\,\delta[\omega - \omega(\lambda)] \tag{4.115}$$

The parallel MSRD of a given atomic pair can then be expressed in terms of the vibrational density of states (VDOS) $\rho_{ab}(\omega)$ as [Crozier et al., 1988]:

$$\langle \Delta u_{\parallel}^2 \rangle \ = \ \frac{\hbar}{2\mu} \int_0^{\omega_{\max}} \frac{1}{\omega}\,\rho_{ab}(\omega)\,\coth\frac{\hbar\omega}{2kT}\,d\omega. \tag{4.116}$$

The dynamical information is contained in the projected density $\rho_{ab}(\omega)$.

MSRD for Bravais crystals

For crystals with one atom per primitive cell (Bravais crystals) the number $\mathbf{N}$ of cells coincides with the number of atoms: there is a unique mass m; there are three acoustic branches ($s = 1 \div 3$) and there is a unique eigenvector $\vec{w}(\vec{q}, s)$ of unit modulus for each normal mode.
Equation (4.107) becomes

$$\begin{aligned} \langle \Delta u_{\parallel}^2 \rangle \ &= \ \frac{1}{\mathbf{N}m} \sum_{\vec{q},s} \langle |Q(\vec{q}, s, t)|^2 \rangle \ \left[\vec{w}(\vec{q}, s) \cdot \hat{R}\right]^2 \ \left| e^{i\vec{q}\cdot\vec{R}} - 1 \right|^2 \\ &= \ \frac{1}{\mathbf{N}m} \sum_{\vec{q},s} \left\{ \frac{\hbar}{\omega(\vec{q}, s)} \coth\frac{\hbar\omega(\vec{q}, s)}{2kT} \left[\vec{w}(\vec{q}, s) \cdot \hat{R}\right]^2 \ \left[1 - \cos(\vec{q}\cdot\vec{R})\right] \right\} \end{aligned} \tag{4.117}$$

Equation (4.117) coincides with (18) of Beni and Platzman [Beni and Platzman, 1976] and (4) of Sevillano et al. [Sevillano et al., 1979] and corresponds to (4) of Böhmer and Rabe [Böhmer and Rabe, 1979].

4.4.2 Debye correlated model

For monatomic Bravais crystals, say crystals with one atom per primitive cell, the MSRD can be described by an approximate **correlated Debye Model**.
In this model only three acoustic branches are considered, with the same sound velocity v_s and the same linear dispersion relation. The first Brillouin Zone is substituted by a *Debye sphere* of radius q_D, containing $\mathbf{N}$ wavevectors. The volume of the Debye sphere is

$$V_D \ = \ \frac{4}{3}\pi q_D^3 \ = \ \frac{(2\pi)^3}{V_a}\,, \tag{4.118}$$

where V_a is the volume of the primitive cell in the real space. For monatomic Bravais crystals, V_a corresponds to the volume per atom.
The Debye wave vector is thus

$$q_D \ = \ \left(\frac{6\pi^2}{V_a}\right)^{1/3}. \tag{4.119}$$

The maximum frequency $\omega_D = q_D v_s$ is the *Debye frequency.*

The sum over $3\mathbf{N}$ normal modes of (4.117) is substituted by the integral over the Debye sphere, multiplied by 3:

$$\frac{1}{\mathbf{N}}\sum_{\vec{q},s} \;\rightarrow\; \frac{3}{V_D}\int_0^{q_D} dq \int_0^{\pi} d\theta \int_0^{2\pi} d\phi\, q^2\, \sin\theta = \frac{9}{2q_D^3}\int_0^{q_D} dq \int_0^{\pi} d\theta\, q^2\, \sin\theta\,. \tag{4.120}$$

The unit eigenvectors $\vec{w}$ are isotropically distributed in direction: the factor $[\vec{w}(\vec{q},s)\cdot\hat{R}]^2$ in (4.117) is substituted by the average of $\vec{w}\cdot\hat{R}$, where $\hat{R}$ is fixed and $\vec{w}$ spans a sphere of unit radius and surface $S=4\pi$:

$$\langle(\vec{w}\cdot R)^2\rangle = \frac{1}{4\pi}\int_0^{\pi} d\theta\;\cos^2\theta \int_0^{2\pi} d\phi\;\sin\theta \;=\; \frac{1}{3}\,. \tag{4.121}$$

As a consequence

$$\sigma_D^2 = \frac{3\hbar}{2q_D^3 m}\int_0^{q_D} dq\, q^2 \int_0^{\pi} d\theta\, \sin\theta\, \frac{1}{\omega}\,\coth\frac{\hbar\omega}{2kT}\;\left[1-\cos(\vec{q}\cdot\vec{R})\right]. \tag{4.122}$$

Since

$$\int_0^{\pi} d\theta\,\sin\theta\,\left[1-\cos(\vec{q}\cdot\vec{R})\right] = \int_0^{\pi} d\theta\,\sin\theta\,[1-\cos(qR\cos\theta)] = 2\left[1-\frac{\sin(qR)}{qR}\right] \tag{4.123}$$

one gets finally

$$\sigma_D^2(T) \;=\; \frac{3\hbar}{q_D^3 m}\int_0^{q_D} dq\; q^2\frac{1}{\omega}\coth\frac{\hbar\omega}{2kT}\;\left[1-\frac{\sin(qR)}{qR}\right]. \tag{4.124}$$

or equivalently

$$\sigma_D^2(T) \;=\; \frac{3\hbar}{\omega_D^3 m}\int_0^{\omega_D} d\omega\,\omega\coth\frac{\hbar\omega}{2kT}\;\left[1-\frac{\sin(qR)}{qR}\right]. \tag{4.125}$$

Equation (4.125) corresponds to equations (5)–(7) of Sevillano et al. [Sevillano et al., 1979]. The factor $1-\sin(qR)/qR$ is plotted in Fig. 4.8 (left panel).
Since $\omega = v_s q$ and $\omega_D = v_s q_D$, one can substitute $q = \omega q_D/\omega_D$ in (4.125), which becomes

$$\sigma_D^2(T) \;=\; \frac{3\hbar}{\omega_D^3 m}\int_0^{\omega_D} d\omega\,\omega\coth\frac{\hbar\omega}{2kT}\;\left[1-\frac{\omega_D\,\sin(\omega R q_D/\omega_D)}{\omega R q_D}\right]. \tag{4.126}$$

In general, q_D is a priori known from structural information; (4.126) thus depends on one parameter ω_D.

Projected VDOS for Debye model

The correlated Debye model (4.125) can be obtained from the general expression (4.116), provided 2μ is substituted by m and the projected VDOS is [Poiarkova and Rehr, 1999]

$$\rho_D(\omega) \;=\; \frac{3\omega^2}{\omega_D^3}\;\left[1\;-\;\frac{\sin(qR)}{qR}\right]. \tag{4.127}$$

Asymptotic limit

The asymptotic limit of (4.125) for $T\rightarrow\infty$ is given by the series

$$\sigma^2 \rightarrow \frac{6kT}{m\omega_D^2}\left[\frac{(q_D R)^2}{3\cdot 3!} - \frac{(q_D R)^4}{5\cdot 5!} + \frac{(q_D R)^6}{7\cdot 7!}...\right] \tag{4.128}$$

Alternative expression for the Debye model

An expression alternative to (4.125) is

$$\begin{aligned}\sigma_D^2(T) &= \frac{6\hbar}{m\omega_D}\left[\frac{1}{4}+\left(\frac{T}{\theta_D}\right)^2\int_o^{\theta_D/T}\frac{x}{e^x-1}\,dx\right] \\ &- \frac{6\hbar}{m\omega_D}\left[\frac{1-\cos(q_DR)}{2(q_DR)^2}+\left(\frac{T}{\theta_D}\right)^2\int_o^{\theta_D/T}\frac{(q_DRT/\theta_D)\,\sin(q_DRTx/\theta_D)}{e^x-1}\,dx\right] \quad (4.129)\end{aligned}$$

where the first term in square parentheses accounts for the uncorrelated motion of the two atoms, while the second term depends on the correlation.
Equation (4.129) corresponds to (6)–(7) of Böhmer and Rabe [Böhmer and Rabe, 1979] [verificare!] and, to within a factor of 2, to (19) of Beni and Platzman [Beni and Platzman, 1976].

It is worth noting that in the Debye correlated model the un-correlated term MSD depends on olny one parameter, ω_D or q_D. The correlation term DCF depends on both parameters ω_D and q_D.

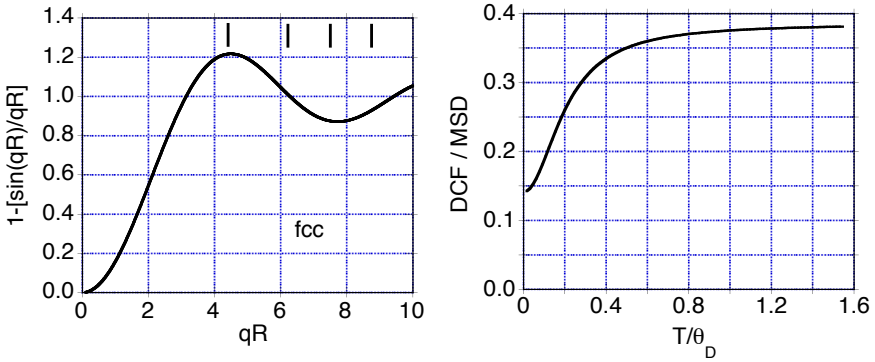

Figure 4.8: *Left.* Plot of $1-\sin(qR)/qR$ as a function of qR for fcc crystals; the vertical lines correspond to the q_DR_i values for the first four coordination shells. *Right.* Ratio DCF/MSD for the first shell of copper: $q_D = 2.548\,\text{Å}^{-1}$, $\theta_D = 323.37\,\text{K}$.

Ratio DCF/MSD. In the seminal paper of 1976 [Beni and Platzman, 1976], Beni and Platzman introduce the correlated Debye model and evaluate the ratio DCF/MSD for *bcc* and fcc monatomic crystals. The product q_DR depends on the structure (*bcc* or fcc), not on the values of the lattice parameter a.
The ratio DCF/MSD increases with temperature and stabilises, for $T \geq \theta_D$, at values near 0.4, slightly lower for fcc than for *bcc* (Fig. 4.8, right panel). The increase of the ratio DCF/MSD can be explained by considering the different temperature dependence of low-frequency modes and high-frequency modes (right panel of Fig. 4.1. At $T = 0\,\text{K}$, all modes contribute only with the zero-point vibrations. When temperature increases, the contribution to the DW exponent of low-frequency modes (highly correlated) increases faster than the contribution of high-frequency modes (less correlated). As a consequence, the ratio DCF/MSD increases up to the Debye temperature. In the classical regime the temperature dependence is linear for every frequency, and the ratio DCF/MSD becomes constant.

Debye model for non-monatomic crystals

The physical meaning of the correlated Debye model for non-monatomic non-Bravais crystals (such as Ge, GaAs, and so on), as well as for non-crystalline materials, is questionable.

The most reasonable choice is to use a value of Debye wavevector q_D calculated for V_a corresponding to the average volume per atom; for crystals, this choice corresponds the the extended BZ scheme (only three coincident acoustic branches).

4.4.3 Einstein model

A simpler alternative model, the **Einstein model**, is often used to parametrize the temperature dependence of the MSRD:

$$\boxed{\sigma_E^2 \;=\; \frac{\hbar}{\mu\omega_E}\left[\frac{1}{2}+\frac{1}{e^{\hbar\omega_E/kT}-1}\right] \;=\; \frac{\hbar}{2\mu\omega_E}\coth\left(\frac{\hbar\omega_E}{2kT}\right)} \tag{4.130}$$

where μ is the reduced mass of the absorber–backscatterer atomic pair. The Einstein model depends on one parameter, the frequency ω_E.
Numerically,

$$\sigma_E^2 \;=\; \frac{0.505379}{\nu_E\,\mu}\coth(23.9962\,\nu_E/T)\,,$$

where σ_E^2 is measured in Å^2, the frequency $\nu_E = \omega_E/2\pi$ in THz and the reduced mass μ in atomic mass units.

Equation (4.130) corresponds to (9) of Sevillano et al. [Sevillano et al., 1979] for monatomic crystals (where $M = 2\mu$).

The limiting values are:

a) For $T \to 0$, $\sigma_E^2 \to \hbar/2\mu\omega_E$; numerically

$$\sigma_0^2(0) = \frac{0.505379}{\nu_E\,\mu}$$

b) For $T \to \infty$, $\sigma_j^2 \to kT/\mu\omega_E^2$ (classical approximation); numerically,

$$\sigma_E^2(\infty) = \frac{0.0210539\,T}{\nu_E^2\mu}$$

where again σ_E^2 is measured in Å^2, the frequency $\nu_E = \omega_E/2\pi$ in THz and the reduced mass μ in atomic mass units.

To the Einstein frequency ν_E one can associate an Einstein temperature $\theta_E = \hbar\omega_E/k = h\nu_E/k$. Numerically, $\theta_E[K] = 47.99\ \nu_E[THz]$.

The Einstein frequency can be associated to an effective force constant of bond stretching, $k_\parallel = \mu(2\pi\nu_E)^2 = \mu\omega_E^2$. The effective force constant $k_\parallel$ can be significantly different from the bond-stretching force constants of lattice dynamical models. A comparison with the force constants k_r of a valence force field model for Ge, CdTe and CuCl is shown in [Abd el All et al., 2012].
Numerically: $k_\parallel[\mathrm{eV/Å^2}] = 4.091649 \times 10^{-3}\nu^2[\mathrm{THz}^2]\mu[\mathrm{amu}]$.

Einstein model and perpendicular MSRD

The Einstein model is used also to fit the temperature dependence of the perpendicular MSRD; taking into account that the perpendicular MSRD $\langle\Delta u_\perp^2\rangle$ has two perpendicular components, the Einstein model is [Vaccari and Fornasini, 2006]

$$\langle\Delta u_\perp^2\rangle \;=\; 2\,\sigma_\perp^2 \;=\; \frac{2\hbar}{\mu\omega_\perp}\left[\frac{1}{2}+\frac{1}{e^{\hbar\omega_\perp/kT}-1}\right] = \frac{\hbar}{\mu\omega_\perp}\coth\left(\frac{\hbar\omega_\perp}{2kT}\right) \tag{4.131}$$

The perpendicular Einstein frequency can be associated to an effective force constant of bond stretching, $k_\perp = \mu(2\pi\nu_\perp)^2 = \mu\omega_\perp^2$. The effective force constant $k_\perp$ is significantly different from the bond-bending force constants of lattice dynamical models. A comparison with the force constants k_θ of a valence force field model for Ge, CdTe and CuCl is shown in [Abd el All et al., 2012].

Einstein model and average energy

The Einstein model corresponds to considering the pair of absorber and back scatterer atoms as a single harmonic oscillator. The average energy stored in the harmonic oscillator is

$$< E > = \mu\omega^2\sigma^2 = \hbar\omega \left[\frac{1}{2} + \frac{1}{e^{\hbar\omega/kT} - 1}\right] . \tag{4.132}$$

For $T \to \infty$ (classical limit):

a) the energy stored in the relative parallel vibrations is $k_B T$, corresponding to one degree of freedom of oscillatory motion (two quadratic terms in the Hamiltonian)
b) the energy stored in the total relative vibrations (parallel + perpendicular) is $3k_B T$, corresponding to three degrees of freedom of oscillatory motion.

According to the classical equipartition of energy, the energy stored in the two atoms corresponds to 6 degrees of freedom: 3 of CM vibration, 3 of relative vibration.

Einstein model and dynamical matrix

According to [Poiarkova and Rehr, 1999], the square of the Einstein frequency ω_E^2 is the eigenvalue of the dynamical matrix corresponding to an eigenvector $|Q_{ab}(0)\rangle$ where all atomic displacements are zero but those of the the two atoms a and b, which are given by the initial displacements (4.114).
In synthetic form,

$$D\,|Q_{ab}(0)\rangle = \omega_E^2\,|Q_{ab}(0)\rangle\,, \quad \text{say} \quad \omega_E^2 = \langle Q_{ab}(0)|D\,|Q_{ab}(0)\rangle\,. \tag{4.133}$$

This expression has been generalised to the case of multiple scattering paths (see below).

4.4.4 Multiple scattering paths

Let us consider again the general expression of the parallel MSRD for a MS path j (4.82):

$$\sigma_j^2 = \frac{1}{4} \left\langle \left[\sum_{i=1}^{n_j} (\vec{u}_{i+} - \vec{u}_i) \cdot \hat{R}_{ii+}\right]^2 \right\rangle . \tag{4.134}$$

Following again Poiarkova and Rehr [Poiarkova and Rehr, 1999], the sum in (4.134) can be differently regrouped, focussing on the single atom displacements

$$\sigma_j^2 = \left\langle \left[\sum_{i=1}^{n_j} \vec{u}_i \cdot \left(\frac{\hat{R}_{ii-} + \hat{R}_{ii+}}{2}\right)\right]^2 \right\rangle . \tag{4.135}$$

Eq. (4.102) is adapted to the MS path j as

$$\sigma_j^2 = \frac{\hbar}{2\mu_j} \sum_{\lambda} \frac{1}{\omega(\lambda)} \coth\frac{\hbar\omega(\lambda)}{2k_B T} \sum_i \left| \sqrt{\frac{\mu_j}{m_i}} \left(\frac{\hat{R}_{ii-} - \hat{R}_{ii+}}{2}\right) \cdot \vec{\epsilon}_i(\lambda) \right|^2 \tag{4.136}$$

where the reduced mass μ_j of path j is defined as

$$\frac{1}{\mu_j} = \sum_{i=1}^{n_j} \frac{1}{m_i} \left(\frac{\hat{R}_{ii-} - \hat{R}_{ii+}}{2}\right)^2 . \tag{4.137}$$

MS projected VDOS

As a generalisation of (4.114) for the two-atom case, Poiarkova and Rehr define an initial normalised displacement state for the multiple scattering path, where all atoms have zero velocity, and only the atoms belonging to the scattering paths are displaced

$$|Q_j(0)\rangle \;=\; \left| \sqrt{\frac{\mu_j}{m_1}} \left(\frac{\hat{R}_{1n_j} - \hat{R}_{12}}{2} \right) , \dots , \sqrt{\frac{\mu_j}{m_i}} \left(\frac{\hat{R}_{ii-} - \hat{R}_{ii+}}{2} \right) , \dots \right\rangle \tag{4.138}$$

The term in square brackets in (4.136), in analogy with the two-atom case (4.113), measures the fractional contribution of mode λ to the parallel MSRD of the path j:

$$p_j(\lambda) \;=\; \left| \sqrt{\frac{\mu_j}{m_i}} \left(\frac{\hat{R}_{ii-} - \hat{R}_{ii+}}{2} \right) \cdot \vec{\epsilon}_i(\lambda) \right|^2 \;=\; |\langle \lambda \,|\, Q_j(0) \rangle|^2 \tag{4.139}$$

The projected density of vibrational modes for path j is defined as

$$\rho_j(\omega) \;=\; \sum_\lambda p_j(\lambda)\, \delta[\omega - \omega(\lambda)] \tag{4.140}$$

The parallel MSRD of a the MS scattering path j is then be expressed in terms of the vibrational density of states (VDOS) $\rho_j(\omega)$ as [Poiarkova and Rehr, 1999]:

$$\sigma_j^2 \;=\; \frac{\hbar}{2\mu} \int_0^{\omega_{\max}} \frac{1}{\omega}\, \rho_j(\omega)\, \coth \frac{\hbar\omega}{2kT}\, d\omega. \tag{4.141}$$

Einstein model

As a generalisation of (4.133), [Poiarkova and Rehr, 1999], define the square of the Einstein frequency ω_E^2 as the eigenvalue of the dynamical matrix corresponding to the eigenvector $|Q_j(0)\rangle$ of (4.138):

$$D\,|Q_j(0)\rangle \;=\; \omega_E^2\,|Q_j(0)\rangle\,, \quad \text{say} \quad \omega_E^2 \;=\; \langle Q_j(0)|D\,|Q_j(0)\rangle\,. \tag{4.142}$$

4.4.5 MSRD calculations

Diagonalisation of the dynamical matrix

Equation of motion method

The equation of motion (EM) method allows one to obtain spectra for linear harmonic problems without diagonalisinf the dynamical matrix [Beeman and Alben, 1977].
Let us consider a system of N atoms. Within the harmonic approximation the $3N$ coupled equation of motion are

$$m_i \frac{d^2 x_{i\alpha}}{dt^2} \;=\; \sum_{j\beta} \Phi_{i\alpha,j\beta}\; x_{j\beta}\,, \tag{4.143}$$

where Φ are the 2nd order coupling coefficients. Once a convenient set of initial conditions has been chosen

$$x_{i\alpha}(t=0) \;=\; x_{i\alpha}^0\,, \tag{4.144}$$

the equations of motion can be integrated to obtain the displacements up to a time T and the VDOS can be calculated according to [Beeman and Alben, 1977]

$$\rho(\omega) \;=\; \frac{2}{\pi} \int_0^T \sum_{i\alpha} A_{i\alpha}\; x_{i\alpha}(t)\, \cos(\omega t)\, \exp(-\lambda t^2)\, dt\,. \tag{4.145}$$

To calculate the VDOS, the quantities $A_{i\alpha}$ and $x_{i\alpha}^0$ are set equal to

$$A_{i\alpha} \;=\; \sqrt{2}\, \cos\theta_{i\alpha}\,, \quad x_{i\alpha}^0 \;=\; \sqrt{2}\, \cos\theta_{i\alpha}\,, \tag{4.146}$$

where $\theta_{i\alpha}$ are random angles uniformly distributed between 2 and 2π. An average over several $\rho(\omega)$ computed for different $\theta_{i\alpha}$ is necessary to obtain an accurate VDOS.
The cutoff parameters T and λ lead to a finite resolution in the density of states, which reduces to a delta function in the limit $T \to \infty, \lambda \to 0$.

Since matrix diagonalisation is not required, the EM method is quite efficient in dealing with very large structures. An application of the method to calculate the vibrational states of a model amorphous metal was made in 1977 by Rehr and Alben [Rehr and Alben, 1977].

Later on, in 1999, the method was applied by Poiarkova and Rehr [Poiarkova and Rehr, 1999] to calculate the projected VDOS and the Debye-Waller factor of multiple scattering paths in Cu, Ge and Zn tetraimidazole, starting from a few local parameters in a valence force field model.

Recursion methods

4.4.6 Anharmonicity effects

Chapter 5

Experimental techniques

The XAFS technique requires the measurement of the x-ray absorption coefficient as a function of photon energy. In principle, any source characterised by a continuous spectrum is suitable for XAFS measurements. Actually, Synchrotron radiation is the ideal source for XAFS, thanks to the continuous spectrum of high intensity and strong vertical collimation; besides, the high degree of polarisation is advantageous in several applications.
Section 5.1 is dedicated to a short review of the basic properties of x-ray sources.

A laboratory for x-ray spectroscopy with synchrotron radiation (Fig. 5.1) is generally composed by:

a) an *optical apparatus*, containing a monochromator and one or more x-ray mirrors;

b) a *measurement apparatus*, containing sample holders and detectors for measuring the absorption coefficient.

5.1 X-ray sources for XAFS

5.1.1 Laboratory sources

Sealed tubes

Rotating anode sources

5.1.2 Synchrotron Radiation: general properties

Let us first consider the general properties of the electromagnetic radiation emitted by a single electron moving at relativistic velocity and submitted to a centripetal acceleration.

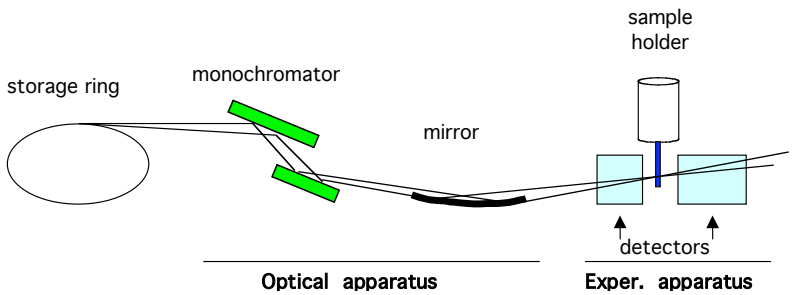

Figure 5.1: Schematic picture of a synchrotron radiation laboratory for XAFS experiments.

Angular collimation

Continuous spectrum

Polarisation

Time structure

The energy lost by the electron at every turn due to S.R. emission is restored by a radio-frequency (RF) cavity. Within the RF cavity the voltage is varied sinusoidally. In order to receive the right amount of energy, the electron has a well defined phase relationship with the RF voltage. As a consequence, the electrons circulating in the storage ring are organised in bunches of very short time duration, separated by longer time intervals.

Example: time structure of ESRF:

- Time duration of one bunch: 20 ps.
- The time interval between bunches depends on the number of stored bunches:
  - minimum 2.82 ns (992 bunches)
  - maximum 2.81 μs (1 bunch)

The time structure can be exploited in pump–probe XAFS experiments.

5.1.3 Synchrotron Radiation: bending magnets

5.1.4 Synchrotron Radiation: insertion devices

Insertion devices are arrays of magnets of alternating polarity inserted into straight sections of the storage ring lattice. Let λ_u be the spatial period of the magnetic structure and g the gap, say the vertical distance between the two arrays of magnetic lattices.
The vertical magnetic field depends on the magnetic period λ_u and on the gap g according to

$$B_z(s) \;=\; \frac{B_0}{\cosh(\pi g/\lambda_u)}\,\cos\frac{2\pi s}{\lambda_u}\,, \tag{5.1}$$

where s is the longitudinal coordinate along the average beam direction. The magnetic field depends on the gap value g.
The magnetic field induces an oscillating trajectory. The transverse position and the angular deviation with respect to the straight trajectory are given by

$$x(s) \;=\; x_0\,\cos(2\pi s/\lambda_u)\,, \qquad \alpha(s) \;=\; \alpha_0\,\cos(2\pi s/\lambda_u)\,, \tag{5.2}$$

The amplitudes x_0 and α_0 are

$$x_0 \;=\; \frac{K}{\gamma}\,\frac{\lambda_u}{2\pi}\,, \qquad \alpha_0 \;=\; \frac{K}{\gamma}\,, \tag{5.3}$$

where K is

$$K \;=\; \frac{eB\lambda_u}{2\pi cm_e} \;=\; 8.934\times B[T]\times\lambda_u[cm] \tag{5.4}$$

The properties of the emission from insertion devices depend on the product $K=\alpha_0\gamma$. Remember that the angle of emission of Synchrotron Radiation is about $1/\gamma$.

High-K devices: Wigglers

When $K>1$, the angular amplitude of the beam oscillations is larger than the angle of emission of the S.R. beam. The electromagnetic waves emitted by the different poles add incoeherently.
The spectrum is continuous, like for bending magnets. The advantages over bending magnets are:

- critical energy depending on the wiggler magnetic field, independent of the lattice requirements: typically, wigglers are used to increase the critical energy with respect to bending magnets
- flux proportional to the number of wiggles

Undulators

When $K < 1$, the angular amplitude of the beam oscillations is smaller than the angle of emission of the S.R. beam. There is interference between electromagnetic waves emitted by different poles, giving rise to monochromatic radiation of fundamental frequency ν_1 and its harmonics ν_n. One can show that, for one electron, the energy of the n-th harmonic is a function of the angle θ and of the K parameter:

$$E_n(\theta) \;=\; \frac{2hc\gamma^2 n/\lambda_u}{1 + K^2/2 + \gamma^2\theta^2}\,. \tag{5.5}$$

The flux of monochromatic radiation in the forward direction is proportional to the square N^2 of the number of wiggles. The bandwith for the harmonic of order n is

$$\frac{\Delta E_n}{E_n} \;\simeq\; \frac{1}{nN}\,. \tag{5.6}$$

In principle, due to their monochromatic emission, undulators appear unsuitable for XAFS experiments.
One can however obtain tunability over a continuous spectrum by exploiting various properties:

1. The energy depends on the angle θ of emission according to (5.5); the angle-integrated flux spreads over an energy range.
2. An actual electron beam is made by many-electron bunches; the source emittance is connected to the energy spread of the photon beam: high (horizontal) beta sections correspond to large (horizontal) electron beam sizes, which give rise to enlargement of the energy spread of photon beam.
3. The frequency of the different harmonics depends on the parameter K, according to (5.5). The parameter K in turn depends on the magnetic field B_z, which can be varied by varying the gap g.
   Two techinques can be utilized to vary the gap:
   a) mechanically varying the gap during the acquisition of a spectrum
   b) tapered undulators, where the gap varies along the device length, giving rise to a continuous spectrum

5.2 X-ray optical instrumentation

5.2.1 Monochromators

Basic tasks of a monochromator are:

- selecting a beam of energy $E = \hbar\omega$, defined within a width ΔE, from the continuous synchrotron radiation spectrum;
- executing scans over predefined energy ranges.

The monochromators for x-rays are perfect crystals, working according to the Bragg law:

$$2\,d_{hkl}\;\sin\theta_b \;=\; n\,\lambda, \tag{5.7}$$

where d_{hkl} is the distance between the (hkl) crystallographic planes, θ_b is the incidence angle, n is an integer and λ is the x-ray wavelength. The energy scan is obtained by rotating the crystal around an axis parallel to the Bragg planes and normal to the beam direction It is worth remembering some important properties:

a) Only crystallographic planes for which the structure factor $F(hkl) \neq 0$ give rise to diffraction; for example, Bragg reflection from (110) planes of silicon is forbidden.

b) The maximum wavelength selected for a given family of planes is $\lambda = 2d$, in correspondence with normal incidence.

Table 5.1: Distance $2d$ corresponding to selected planes of silicon and germanium crystals.

Planes:	Si(111)	Si(220)	Si(311)	Si(400)	Si(331)	Si(511)	Ge(111)	Ge(220)
$2d$ (Å):	6.2708	3.84	3.28	2.7154	2.5	2.08	6.5328	4.0004

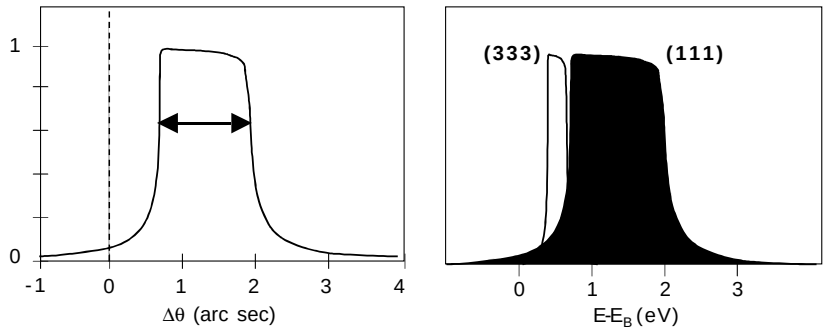

Figure 5.2: Left: typical rocking curve of a crystal monochromator, plotted against the shift with respect to the Bragg angle (the vertical dashed line). Right: comparison of the rocking curves of the (111) and (333) reflections of silicon.

- In addition to the wavelength $\lambda = 2d \sin\theta$ (fundamental), also the wavelengths $\lambda/2, \lambda/3, ...$ (harmonics) are selected. Harmonics are sources of noise in XAFS.

For x-ray energies higher than 2 keV, the crystals most frequently utilized are silicon and germanium. Table 5.1 shows the $2d$ values for some relevant families of planes.
The x-ray beam is diffracted by the monochromator within a finite angular interval, whose center is slightly shifted with respect to the Bragg angle θ_b. The profile of the diffracted intensity as a function of the angle is called *rocking curve* (Fig. 5.2, left). The width of the rocking curve (*Darwin width*) and its shift with respect to the Bragg angle amount to a few arc-seconds ($1'' = 4.8\times10^{-6}$ rad). The Darwin widths are always larger for fundamental reflections than for harmonics (Fig. 5.2, right).

In general, the x-ray monochromators for synchrotron radiation are based on consecutive Bragg reflections from two parallel crystals. In this way, the outgoing beam has fixed horizontal direction. Two main configurations are possible (Fig. 5.3).

a) *Channel-cut monochromators.* The two Bragg-reflecting faces belong to a single mono-crystal, suitably machined. This monochromator is simple to realise, mechanically stable, easy to use. On the other hand, the outgoing beam is contaminated by harmonics; besides, the crystal cannot focalize the beam.

b) *Independent crystals monochromators.* The main advantage of independent crystals is the possibility of slightly detuning their Bragg angles. In this way, by exploiting the smaller Darwin width of harmonics with respect to the fundamental wavelength (Fig. 5.2, right), it is possible to reduce the harmonic content of the outgoing beam. Besides, the single crystals can be thin enough to be curved, allowing the beam focalization in the horizontal plane.

The energy resolution ΔE of the monochromatic beam depends on two factors:

a) the Darwin width of the crystal;

b) the vertical angular divergence Ω of the beam; to a good approximation, $\Omega = (d + s)/\ell$, where s is the vertical dimension of the source, d the aperture of the collimating slits, ℓ the distance between source and monochromator.

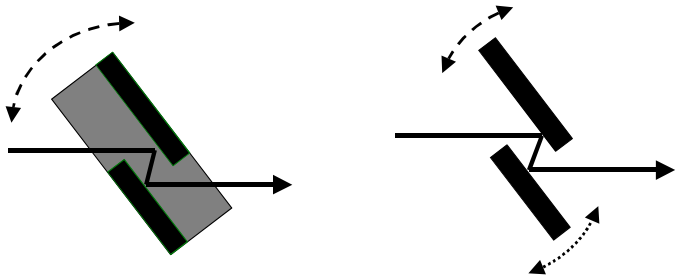

Figure 5.3: Channel cut monochromator (left) and independent-crystals monochromator (right)

The *relative resolution* can be easily obtained by deriving the Bragg law, Eq. (5.7):

$$\Delta E/E \;=\; \Delta\lambda/\lambda \;=\; \Delta\Theta \;\mathrm{cotg}\theta_b. \tag{5.8}$$

where Θ (in radians) is the convolution between Darwin width and beam divergence. Typically, $\Delta E/E \sim 10^{-4} \div 10^{-5}$.

5.2.2 Mirrors

Frequently, the monochromator is accompanied by one or more x-ray mirrors, whose aims are:

a) to contribute to the rejection of harmonics;

b) to collimate and focalize the beam.

The x-ray mirrors are based on the phenomenon of *total reflection*. Basically, the index of refraction can be expressed as

$$n \;=\; 1 - \delta - i\beta. \tag{5.9}$$

The imaginary part β is proportional to the absorption coefficient μ. The real part $1-\delta$ is negative for x-rays. The parameter δ, which is proportional to the density ρ of the material and to λ^2, is very small, of the order of $10^{-6} \div 10^{-5}$.
Total external reflexion occurs for incidence angles smaller than the critical angle θ_c, that depends on the x-ray wavelength and material density according to

$$\theta_c \;=\; \sqrt{2\delta} \;\propto\; \lambda\sqrt{\rho_e} \tag{5.10}$$

and is of the order of milliradians. By properly choosing the incidence angle of the beam on the mirror, it is possible to obtain the reflection of only the fundamental wavelength, and the rejection of the harmonics. Besides, by slightly bending the mirror surface, it is possible to focalize the beam (typically in the vertical plane). Because of the small values of the critical angle θ_c, the longitudinal dimensions and the bending radii of the x-ray mirrors are very large.

5.3 X-ray detectors

Several types of X-ray detectors are used in XAFS experiments. Their role is to convert the X-ray energy into an electrical signal.
One can distinguish two main modes of operation:

- Current integrating mode. Single photons are not distinguished; this mode is particularly suitable for the high fluxes of S.R.
- Pulse counting mode. Each single photon is separately counted, so that its energy can in principle be discriminated; the maximum count rate is however limited.

5.3.1 Ionisation chambers

An ionisation chamber is a vessel containing two parallel plane electrodes, filled with gas. X-ray photons ionise the gas, typically 20–40 eV are necessary to create an electron–ion pair. Charged particles are collected by the electrodes.
Ionisation chamber are current integrating detectors. The output current has to be proportional to the energy deposited by the absorbed X-rays and independent of the accelerating voltage of the electrodes.
The accelerating voltage has to be

- sufficiently high to prevent recombination of electrons and ions,
- sufficiently low to avoid further ionisation of the gas by the electrons, resulting in amplification (which voulkd lead to the proportional counter regime).

Ionisation chambers have to be operated in the voltage region corresponding to the plateau: current independent of voltage.
The response of ionisation chambers depend on the filling gas and its pressure.

5.3.2 Photodiodes

In photodiodes the energy of x-ray photons creates electron–hole pairs. The electric field at the junctions separate electrons from holes.
Photodiodes can be used in the current integrating mode, as ionisation chambers.
PIN = Positive–Intrinsic–Negative
PIPS = Passivated Implanted Planar Silicon

5.3.3 Scintillators

Scintillators transform x-ray pulses into visible light pulses.
Typical scintillator materials: doped NaI, plastic (anthracene), YAP (yttrium-aluminum perovskite).
Visible light pulses are counted by photomultipliers (photocathode + dynodes).

5.3.4 Solid-state detectors

Pulse-counting detectors.
Usually 13 or 19 or more Si or Ge elements.
Maximum count rate per element limited to a few hundred thousand counts per second.
Energy resolution no better that 130 eV.
They must be operated at LN temperature.
Silicon Drift Detectors (SDD) providing higher throughput are under development.

Problems with counting detectors: pile-up and dead time.

5.3.5 Diffractive analysers

When using pulse-counting detectors, in many cases a weak signal has to be discriminated from an intense background (e.g. for very diluted samples). To avoid saturation of the pulse counting detector by the background signal, it is advisable to reject the backgraound before it reaches the detector.
To this purpose, conventional crystal monochromators in Bragg geometry require very small focal spot size.
New types of diffractive analyzers have been developed: Pyrolitic Graphite, adaptive Bragg, MAAD (multilayer array analyzer detectors), BCLA (bent crystal Laue analysers).

5.4 Measurement of the absorption coefficient

According to (1.1), the absorption coefficient $\mu = \ln(\Phi_0/\Phi)/x$ is proportional to the ratio between the photon fluxes impinging on and outgoing from the sample. Different instrumental configurations can be used to measure μ, depending on the sample dimension and composition as well as on the kind of sought information.

a) Direct measurement of μ through transmission experiments.

b) Indirect measurements of decay products, whose yield is proportional to μ.

   - Detection of fluorescence photons (FLY, fluorescence yield).
   - Detection of emitted electrons (AEY, Auger electrons yield; PEY, partial electrons yield; TEY, total electrons yield).
   - Detection of optical luminescence (XEOL-PLY, x-ray excited optical photoluminescence).

c) Detection schemes for time-resolved EXAFS (quick-EXAFS, energy-dispersive detection).

In the following sections, the most frequently used detection schemes are described in some detail.

5.5 Transmission measurements

The photon fluxes Φ_0 e Φ can be directly measured by two detectors placed immediately in front and past the sample (Fig. 5.4, left). In general, to bear the high synchrotron radiation fluxes, *ionization chambers* with plane parallel electrodes, some tens of centimeters long, are used as detectors (Fig. 5.4, right).
The absorption of x-ray photons inside the ionization chambers creates ion-electron pairs. The electrodes, maintained at a potential difference of the order of about 100 eV, collect a low intensity current (typically $10^{-10} \div 10^{-8}$ A). The electrical signals I_0 and I generated by the two ionization chambers are proportional to the reduction of the photon flux within each chamber.
One can easily see that the connection between measured currents I_0, I and photon fluxes Φ_0, Φ is

$$I_0/I \;=\; C(\omega)\;(\Phi_0/\Phi)\,, \tag{5.11}$$

where $C(\omega)$ is a smoothly varying function of the photon energy, determined by the ionization chambers efficiency. The measured quantities I_0, I are connected to the absorption coefficient μ by the relation

$$\mu x \;=\; \ln(\Phi_0/\Phi) \;=\; \ln I_0/I - \ln C(\omega)\,, \tag{5.12}$$

where the additive term $\ln C(\omega)$ can be easily subtracted in the data analysis procedures (see Chapter 6).
The efficiency of ionization chambers can be fitted to different spectral regions by varying the atomic species of the filling gas and its pressure.

To optimize the signal to noise ratio, the sample has to be relatively thin, typically about 10 μm. When the sample is in powder form, compressed in a pellet or deposited on a thin film, one must be careful to avoid holes or inhomogeneities, which could cause spurious variations of the EXAFS amplitude. A rule of thumb is to verify the similarity of EXAFS spectra obtained from samples of different thicknesses.
Transmission measurements are preferred, when possible, in virtue of their easiness and accuracy. In some cases, however, they are not suitable, for example for diluted samples or for surface measurements.

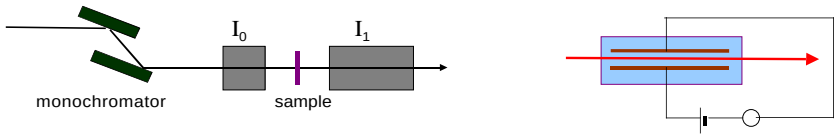

Figure 5.4: Left: layout of a direct transmission measurement apparatus (not to scale). Right: electrical connections of an ionization chamber.

5.6 Fluorescence detection

When the absorbing species A is a tiny fraction of the entire sample, its contribution μ_A to the total absorption coefficient $\mu_{\rm tot}$ can be exceedingly small. For concentrations typically lower than 1 % (diluted samples), the XAFS structures at the absorption edge of the absorbing species μ_A are comparable to the statistical noise of the total measured absorption coefficient $\mu_{\rm tot}$. In this case, transmission measurements are ineffective.
In general, for diluted samples one resorts to fluorescence measurements, in which the intensity I_f of the fluorescence emitted at frequency ω_f by the absorbing species A, as a result of radiative de-excitation (Sec. 2.3), is measured as a function of incident energy $\hbar\omega$ (Fig. 5.5, top left).

5.6.1 Fluorescence intensity

Let us first consider the fluorescence emitted by a thin slab at a depth z_n below the sample surface (Fig. 5.5, top right); the incident beam impinges at an angle θ_i and the fluorescent beam outgoing at an anlgle θ_f is collected within a solid angle Ω (in many experimental apparatuses, $\theta_i = \theta_f = 45°$). The total fluorescence intensity emitted by a slab of thickness dz_n is

$$I_f(\omega_f)\,dz \;=\; \Phi_0(\omega)\,\underbrace{\exp\left[-\frac{\mu_{\rm tot}(\omega)z_n}{\sin\theta_i}\right]}_{\text{input absorption}}\,\underbrace{\eta_f\,\mu_a(\omega)\,\frac{dz}{\sin\theta_i}}_{\text{fluor.}}\,\underbrace{\exp\left[-\frac{\mu_{\rm tot}(\omega_f)z_n}{\sin\theta_f}\right]}_{\text{fluor. absorption}}\,\frac{\Omega}{2\pi}\,. \tag{5.13}$$

According to (5.13), the fluorescence intensity

a) is proportional to the impinging photon flux Φ_0 (at frequency ω), attenuated by the absorption from all atoms (total) through the sample thickness z_n;
b) is proportional to the absorption coefficient $\mu_a(\omega)$ of the atomic species a at the frequency ω and to the fluorescence yield η_f;
c) is attenuated by the absorption from all atoms (total) through the sample thickness z_n;
d) is proportional to the solid angle $\Omega/4\pi$ determined by the detector acceptance.

Usually, the fluorescence detector is placed such as the incoming and outgoing beams form an angle of 90° in the horizontal plane, in order to minimise the influence of elastically scattered photons. The sample surface is usually placed at 45° with respect to both incoming and outgoing beams.
Let us now integrate (5.13) over the full sample thickness z, for the realistic case of $\theta_i = \theta_f = 45°$. The total fluorescence intensity is

$$I_f(\omega_f) \;=\; \Phi_0(\omega)\,\eta_f\,\frac{\Omega}{4\pi}\,\frac{\mu_a(\omega)}{\mu_{\rm tot}(\omega)+\mu_{\rm tot}(\omega)}\,[1-\exp A]\;, \tag{5.14}$$

where

$$A \;=\; \sqrt{2}\,z\,[\mu_{\rm tot}(\omega)+\mu_{\rm tot}(\omega_f)]\;. \tag{5.15}$$

5.6.2 Two limiting cases: thin and thick samples

One can now distinguish the two cases of thin and thick samples.

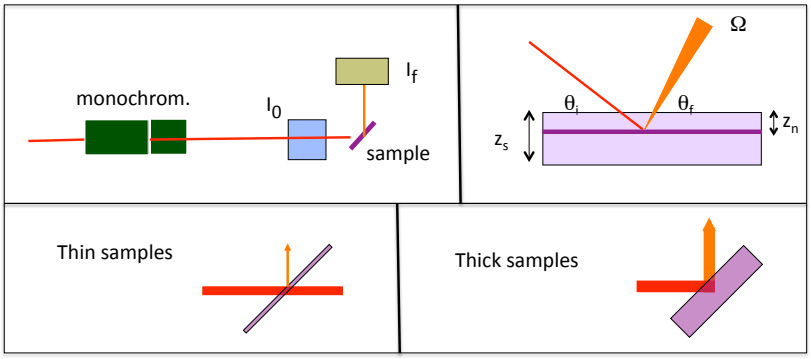

Figure 5.5: Top left: layout of an apparatus for fluorescence measurements (top view of the horizontal plane). Top right: fluorescence from a thin slab. Bottom left: thin sample. Bottom right: thick sample.

Thin samples

For *thin samples* (Fig. 5.5, bottom left), since z is small, one can truncate the expansion of $\exp A$ in (5.14) to the second term, so that $1 - \exp A \simeq 1 - 1 + A = A$, and finally on can simplify

$$I_f(\omega_f) \;\propto\; \mu_a(\omega)\,. \tag{5.16}$$

For thin samples, only a small fraction of the impinging beam intensity is absorbed, and the fluorescence signal is I_f is proportional to the absorption coefficient of the species a, independently of the degree of dilution.

Thick samples

For *thick samples* (Fig. 5.5, bottom right), since z_s is large, one has $1 - \exp A \simeq 1$, and (5.14) becomes

$$I_f(\omega) \;=\; \Phi_0(\omega)\,\frac{\Omega}{4\pi}\,\eta_f\,\frac{\mu_a(\omega)}{\mu_{\rm tot}(\omega) \,+\, \mu_{\rm tot}(\omega_f)}\,. \tag{5.17}$$

For a thick sample, all the beam intensity is absorbed.

a) If the atomic species a is concentrated, above its absorption edge one has $\mu_a(\omega) \simeq \mu_{\rm tot}(\omega)$; besides, $\mu_{\rm tot}(\omega) \gg \mu_{\rm tot}(\omega_f)$, so that the fraction in (5.17) is nearly constant $\simeq 1$. The variation of $\mu_a(\omega)$ only changes the penetration depth of the beam, but does not modulate the intensity of the fluorescence signal.
b) If the atomic species a is diluted (typically $< 1\%$), one has instead $\mu_a(\omega) \ll \mu_{\rm tot}(\omega)$, the fraction in (5.17) is not constant, and the fluorescence intensity $I_f(\omega_f)$ reflects the oscillations of the absorption coefficient $\mu_a(\omega)$.

5.6.3 Detection of fluorescence signals

In fluorescence measurements, one directly measures the fluorescence intensity $I_f(\omega)$ and the signal I_0 of a detector placed before the sample. I_0 is connected to the incoming flux by an efficiency factor, decreasing with energy, $I_0(\omega) = C(\omega)\,\Phi_0(\omega)$. This fact has to be properly accounted for in the analysis of the signal.

The possibility of revealing XAFS of elements approaching p.p.m. level dilution strongly depends on the quality of the detector system.
For a recent review, see [Heald, 2015].

Fluorescence detectors should fulfil the following requirements:

a) to measure only the fluorescence radiation, eliminating the background due to elastic and inelastic scattering and unwanted fluorescence lines;
b) to select a solid angle as large as possible.

Polarisation (90° detection) is used to minimise scattering, but is less effective for large solid angles.
Three main types of detectors can be distinguished (sometimes combined together):

a) Filter-slit systems
b) Multi-element solid state detectors
c) Crystal analysers

Filter-slit systems

The fluorescence is lower in energy than most of the scattering. An X-ray filter with an edge in between can be used to reduce the scattered background.
For K-edge filters the absorption coefficient for the scattered radiation can be six to seven times higher than for the fluorescence signals. Since the transmission depends exponentially on the absorption coefficient, dramatic background reductions can be achieved with a small loss in the fluorescence signal. Also, since the filter is providing the energy discrimination a large-area non-energy- resolving detector can be used that can collect a very large solid angle [copied from Heald].

Example: Let us consider a Cu diluted sample; the K edge is at 8979 eV, the Kα fluorescence is at 8037 eV.
A Ni filter will strongly absorb the scattered radiation with energy higher than its K edge (8333 eV); the absorption of the Cu Kα fluorescence will be much weaker.
The Ni filter will however emit its own Kα fluorescence at 7470 eV.

The filter fluorescence can be minimised by appropriate collimators (Soller slits).

Solid-state detectors

SSD (typically Si or Ge) are energy-dispersive detectors. They collect all of the photons and for each photon output a signal proportional to the photon energy.
The energy resolution is good enough to separate the fluorescence signal from most of the background. However, they need to handle the total count rate that is incident upon them. Their main limitation is a maximum count rate of the order of $10^5 - 10^6$.
Systems with multiple detectors, up to several hundred, have been developed to overcome the problem.
Currently the best detectors are the silicon drift detectors (SDDs): with proper dead-time correction they can handle about 106 counts/s with approximately 3% energy resolution.

Crystal analysers

Diffraction-based crystal analysers allow the ultimate energy resolution.
Perfect crystals have energy resolutions much better than needed; the line-width of the fluorescence lines are generally larger than the perfect crystal acceptance.
Different approaches have been developed to overcome the low efficiency of perfect crystals (mosaic crystals, strain in bent crystals).

5.7 Electrons detection

Because of the high penetration of x-rays, transmission measurements are sensitive to the bulk properties of a sample. To study surface properties, it is convenient to measure the flux of electrons emitted by the sample as a consequence of x-ray absorption (Fig. 5.6, top left): photoelectrons and Auger electrons. The intensity of the flux of both kind of electrons is proportionale to the absorption coefficient. However, the energy of photoelectrons varies when the photon energy varies,

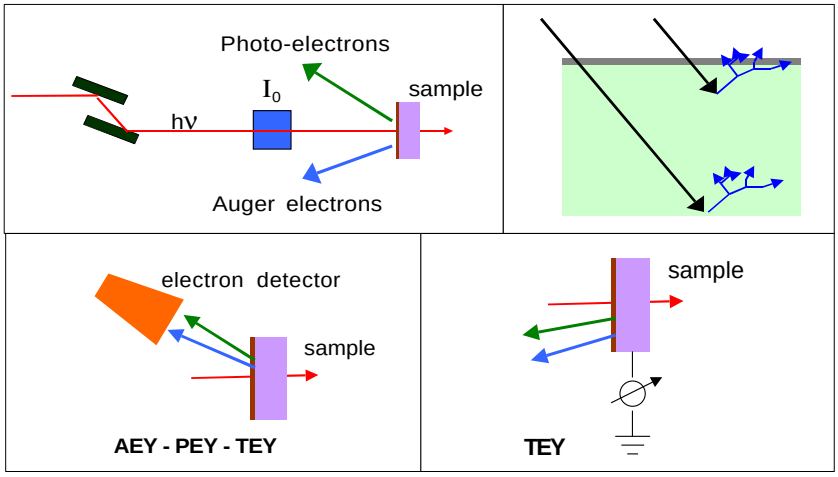

Figure 5.6: Top left: layout of an apparatus for electron yield measurements. Top right: X-rays (straight arrows) have a penetration depth of the order of 500 Å, while electrons have mean free parhs of the order of 5–10 Å (thin dark surface layer); secondary eletrons (scattered paths) have escape depths of the order of 50–100 Å. Bottom left: electron detector in vacuum. Bottom right: electric curcuit for the detection of the total electron yield.

while the energy of Auger electrons is constant and depends of the atomic species. The detection of Auger electrons is thus used to study the local environment of selected atomic species, like atoms adsorbed on a surface of different composition (*Surface EXAFS*, for short SEXAFS).
Since electrons have a short mean free path, of the order of 5–10 Å, only Auger and photoelectrons directly generated in the vicinity of the surface can be detected. The inelastic collisions of both Auger and photoelectrons give however rise to secondary electrons, with a large spread of possible energies, whose global escape depth can be of the order of 50–100 Å(Fig. 5.6, top right), and whose intensity is again proportional to the absorption coefficient.
According to the different requirements, one can utilize different detection procedures.

a) One can detect only the Auger electrons emitted by a given atomic species, by means of a detector with a narrow energy window(AEY, Auger electrons yield); this detection scheme is particularly suited to study the environment of adsorbed atoms: the intensity of the Auger beam reproduces the XAFS structures; however, when the photon energy is varied, unwanted contributions from photoelectrons of the substrate can enter the detector and seriously contanimane the signal.

b) One can detect a large fraction of the emitted electrons, both Auger and photoelectrons and their secondary, by means of a detector with a large energy window (PEY, partial electrons yield); in this way the contamination from the substrate is diluted, although the signal to background ratio is reduced.

c) One can detect all emitted electrons (TEY, total electron yield). For adsorbate studies, this method further dilutes the contamination from the substrate and reduces the signal to background ratio. The TEY detection is sometimes used to study the surface XAFS of bulk materials: in this case one can show that the full TEY signal is proportional to the absorption coefficient.

The detection of electrons emitted by a surface must be done in vacuum, by means of suitable detectors (Fig. 5.6, bottom left), simple electron multipliers for TEY or energy analyzers for AEY. For bulk TEY, the electrons can be collected by a very simple electric circuit (Fig. 5.6, bottom right).

5.8 Alternative layouts for XAFS measurement

Several different measurement schemes have been developed to meet different specific requirements: time-resolved, high-pressure, magnetic dichroism, and so on.

5.8.1 Quick XAFS (QEXAFS)

In standard XAFS measurements the energy scan is done by rotating the monochromator in discrete steps. At each step, the detectors signals are integrated for a time interval sufficiently long to reduce the statistical noise below a predetermined level. This methodology is unsuitable to study fast time-dependent phenomena. Even working with high flux sources, the acquisition speed is often limited by the requirements of mechanical stabilization of the monochromator. The acquisition time of an EXAFS spectrum by a standard method is generally longer than 10 to 20 minutes.
In *Quick XAFS*, the monochromator, typically a single channel-cut crystal, is mounted on an oscillating cradle, which is in turn mounted on a coarse goniometer. One EXAFS spectrum is scanned during a fast oscillation of the cradle, over an amplitude of the order of a few degrees and time duration that can be less than 50 ms.
Very quick data acquisition is required, based on ion chambers or solid-state detectors and fast analog to digital converters.
Typical applications of Quick-EXAFS are the real-time studies of catalytic reactions.
Recent implementations of Quick-EXAFS developed by R. Frahm have been made at SLS-SuperXAS (2008) and Soleil-SAMBA (2009).

5.8.2 Dispersive XAFS

In *Dispersive XAFS* (EDXAS), the selection of the beam energy is obtained by geometrical methods (Fig. 5.7). A large incoming white (say non-monochromatized) beam impinges on a curved crystal "poly-chromator"; the different parts of the beam impinge on different parts of the crystal at different Bragg angles, corresponding to different energies covering the entire EXAFS interval.
The curved crystal focalizes all the outgoing monochromatic beams on a single point, where the sample is placed. The sample is thus simultaneously crossed by beams of all the selected energies. Once the sampled has been crossed, the beam is again dispersed on a position sensitive detector, such as an array of photodiodes, on which the entire EXAFS spectrum is simultaneously detected. By this method, the beam is naturally focalised on a small region of the sample and the acquisition times can be reduced to a few milliseconds.
Advantages of dispersive XAFS:

- No mechanical movements are necessary; there is an intrinsic stability in the focal spot position and in the energy scale.
- Simultaneous acquisition of all data points
- Acquisition time determined by acceptable statistics

Disadvantages:

- Critical in terms of temporal and spatial beam stability and sample presentation
- Only trasmission mode
- X-ray beam not perfectly focussed through the sample
- No reference measurements during acquisition

In general, dispersive spectrometers are installed on bending magnet sources, which yield a sufficiently large horizontal divergence to obtain, with reasonable radii of curvature of the polychromator crystal, an energy dispersion covering a whole EXAFS spectrum.
The ESRF-ID24 dispersive spectrometer is instead connected to an undulator source through a non-conventional optical scheme. By exploiting the undulator high brilliance, a focal spot of about 5×5 μm^2 can be obtained on the sample.
Most common applications of dispersive XAFS (EDXAS):

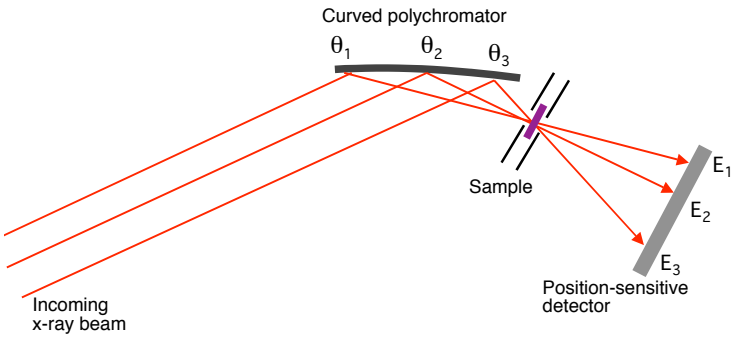

Figure 5.7: Schematic layout of an apparatus for dispersive XAFS measurements.

- Time resolved XAFS; typical application is the in situ study catalytic reactions.
- High-pressure studies (tens of GPa) using a diamond-anvil cell, where the small and stable focal spot is exploited.
- X-ray dichroism studies. The stability and speed of dispersion spectrometers can be exploited to increase the sensitivity to small differences in XAS spectra, for example generated by the rotation of a magnetic field.
- Micro-XAFS chemical mapping.

5.8.3 Time-resolved XAFS: time slicing

This method is useful to monitor the relaxation of a system after an external excitation.
The system is excited at a given time (by a laser pulse, a pressure jump, the insertion of a catalyser, etc). The absorption coefficient at a given value of energy in the XAFS region is measured as a function of time. After full relaxation, the excitation is reproduced in exactly the same way (on the same system or on an identical system) and the absorption coefficient is measured as a function of time at a different energy value. By a suitable number of excitations, one can measure the time evolution of the absorption coefficient at a suitable number of energy values, sufficient to reproduce the EXAFS signals as a function of time.

5.8.4 Pump-probe experiments

Ultra-fast measurements. Exploits the time structure of Synchrotron Radiation.

5.8.5 Grazing incidence, Reflexafs

5.9 Sample conditioning

By properly choosing the sample-holder, the physical and chemical environment of the sample can be controlled. One can use cryostats (liquid nitrogen down to 77 K or liquid helium down to 4 K) or ovens to vary the sample temperature. Low temperatures are currently used to reduce the thermal damping of EXAFS. Temperature scans are used to study phase transitions, local thermal expansion, lattice dynamics, etc. Diamond anvil cells are used to perform measurements under very high pressures (tens of GPa). Chemical reactions, like catalysis, can be studied in suitable cells.

Chapter 6

EXAFS analysis

Different methodologies can be chosen to analyze EXAFS spectra, depending on the sample nature and complexity, the type on information sought, the availability of computing power, and sometimes also personal taste.

6.1 Extraction of the EXAFS signal

The determination of the normalised EXAFS function $\chi(k)$ starting from the experimental signal is in principle different for different detection methods (transmission, fluorescence, electron yield, etc.) [Bunker, 2010].
Let us consider here the case of direct transmission measurements (§ 4.2) and focus on the absorption spectrum at the K edge of a given element within a compound. According to (5.11), the output of the measurement is

$$\ln(I_0/I) \;=\; \ln(\Phi_0/\Phi) + \ln\, C(\omega) \;=\; \mu_t(\omega)x + \ln\, C(\omega) \tag{6.1}$$

where I_0, I are the detector signals, Φ_0, Φ are the photon fluxes, $\mu_t(\omega)$ is the total absorption coefficient and x is the thickness of the sample. $C(\omega)$ is a smoothly varying function of the photon energy.

6.1.1 Singling out the contribution of the studied edge

The first step of the analysis consists in extracting the contribution $\mu(\omega)x$ of the K edge of the selected element from the experimental signal:

$$\mu(\omega)x \;=\; \ln(I_0/I) \;-\; \mu_n(\omega)x \tag{6.2}$$

where μ_n is the contribution of all the other excitations of the selected element plus the excitations of the other elements of the compound; $\mu_n x$ includes also the contribution of $C(\omega)$ of eq. (6.1).
In the pre-edge energy region, $\mu_n x = \ln(I_0/I)$. Above the edge energy, $\mu_n x$ is estimated by extrapolating the pre-edge behavior (fig. 6.1, left).
Fitting the relatively short pre-edge region with a realistic Victoreen-like behaviour generally can easily lead to non-negligible distortion when the Victoreen curve is extrapolated to the much longer post-edge energy interval.
As a consequence, one prefers to fit the pre-edge region by a straight line, which is then extrapolated above the edge. Also this procedure introduces a distortion of the calculated absorption coefficient $\mu(\omega)x$ above the edge. The distortion is compensated when the atomic absorption coefficient is calculated (see below).

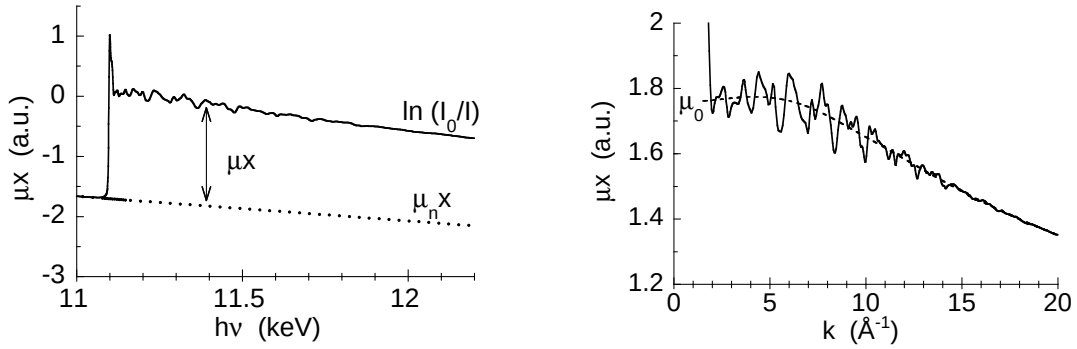

Figure 6.1: Left: Experimental absorption signal for crystalline germanium, measured at 10 K (continuous line). The dotted line is the extrapolation of the pre-edge behavior. The difference (continuous – dotted) is the product μx relative to the K edge. Right: Evaluation of the atomic absorption coefficient; the dashed line corresponds to two 4th-degree polynomials, joined at k=10 Å^{-1}.

6.1.2 The edge energy

The **photo-electron wavenumber** k is defined in Eq. (3.5). In general the core electron binding energy E_b is unknown, and k is experimentally determined as

$$k \;=\; \sqrt{(2m/\hbar^2)\;(\hbar\omega - E_s)} \;=\; 0.51233\;\sqrt{\hbar\omega - E_s}, \tag{6.3}$$

where E_s is a *threshold energy*, arbitrarily chosen in correspondence of some characteristic point of the *edge*, for example the first inflection point. The last equality in Eq. (6.3) holds for wavenumbers measured in Å^{-1} and energies in eV.
The discrepancy between E_b ed E_s, a priori unknown, is conventionally called E_0, so that $E_b = E_s + E_0$. If the subsequent quantitative analysis is made by comparison with a reference EXAFS, the same criterion must be used in determining E_s for both samples; the difference ΔE_0 is anyway treated as a free parameter to be optimized by best-fit. If the analysis is made by comparison with theoretical simulations, the E_0 value is a free parameter to be optimized by fit.

6.1.3 The atomic absorption coefficient

The **atomic absorption coefficient** μ_0 is now necessary to calculate the EXAFS function $\chi(k) = (\mu - \mu_0)/\mu_0$ (Eq. 3.17). To evaluate μ_0 one looks for a curve which averages the oscillations of the absorption coefficient. A frequently utilized approach is based on polynomial splines (Fig. 6.1, right). This step of the analysis is generally made by a trial and error procedure, and requires patience and skillfulness.
Since the absorption coefficient above the edge has been distorted by the procedure of linear fit of the pre-edge region, it can be preferable to obtain the normalised EXAFS signal as

$$\chi(k) \;=\; \frac{\mu(k) - \mu_0(k)}{\mu_1(k)} \tag{6.4}$$

where $\mu_1(k)$ is a smooth Victoreen-like function ($\propto \lambda^{2.8}$, where λ is here the photon wavelength) with absolute values normalized to the absorption jump of each spectrum.

6.1.4 Information from the EXAFS signal

The EXAFS signal can directly give qualitative information. For example (Fig. 6.2) the EXAFS of crystalline germanium at 77 K is much more structured than the one of amorphous germanium, since many coordination shells contribute to the former, only one to the latter. When temperature increases, the EXAFS of c-Ge becomes simpler, because thermal disorder more strongly damps the contributions of the outer shells.

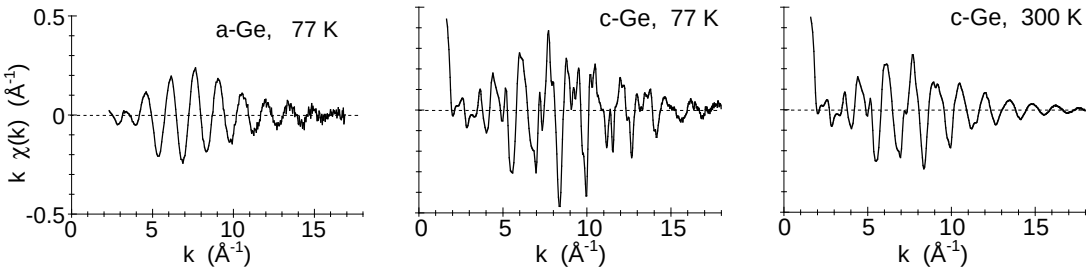

Figure 6.2: EXAFS of amorphous germanium at 77 K (left), and of crystalline germanium at 77 and 300 K (center and right, resp.)

6.2 Fourier filtering

The direct quantitative analysis of the entire EXAFS signal $\chi(k)$, in principle feasible, is seldom performed. In general, one prefers a different approach, which includes the Fourier transform and back-transform of the EXAFS signal.

6.2.1 Direct Fourier transform

The Fourier transform from the space of wavevectors k to the conjugate space of distances r is performed through the integral

$$F(r) \;=\; \int_{k_{\min}}^{k_{\max}} \chi(k)\; W(k)\; k^n\; \exp(2\mathrm{i}kr)\; dk \tag{6.5}$$

where $W(k)$ is a window function that reduces the spurious oscillations induced by the finite k range. The factor k^n is used to balance the low-k and high-k regions of the spectrum (typically $n = 1 - 3$). The limits $k_{\min}$ and $k_{\max}$ are chosen so as to exclude both the low-k signal, where the EXAFS formula is unreliable (typically $k_{\min} > 2 - 4$ Å^{-1}), and the high-k signal, where the signal to noise ratio is small.
The Fourier transform $F(r)$ of Eq. (6.5) is a *complex function*, in principle extending over the entire r axis, and made of a real and an imaginary part, Re$F(r)$ and Im$F(r)$, respectively. The modulus of $F(r)$

$$|F(r)| \;=\; \sqrt{[\mathrm{Re}F(r)]^2 \,+\, [\mathrm{Im}F(r)]^2} \tag{6.6}$$

is characterized by peaks in correspondence of the leading frequencies $2r$ of the $\chi(k)$ signal, say of the most important scattering paths in real space (Fig 6.3). In general, the most prominent peaks correspond to single scattering paths (coordination shells).
The $F(r)$ function is not a true radial distribution function: the positions of the peaks are at slightly shorter distances, by about $0.2 - 0.3$ Å, than the real distances, due to the phase-shifts $\phi_s(k)$ present in the total phases $\Phi = 2kR_s + \phi_s$ of each scattering path. Besides, the shape of the peaks is strongly influenced by the artefacts of the Fourier transform algorithm.

Important qualitative and sometimes also quantitative information is contained in the Fourier transforms $F(r)$. Let us consider some examples.

1. A non-zero $F(r)$ at shorter distances than the first-shell peak suggests a poor evaluation of the atomic absorption coefficient μ_0, which introduced unphysical low-frequency oscillations. The procedure for determining the atomic absorption coefficient μ_0 should be repeated ab-initio.
2. The height of the peaks depends on the coordination number and on the degree of thermal and structural disorder.
3. The differences between Fourier transforms reflect the effects induced on a given sample by variations of temperature, pressure, chemical environment, etc. (Fig. 6.4).

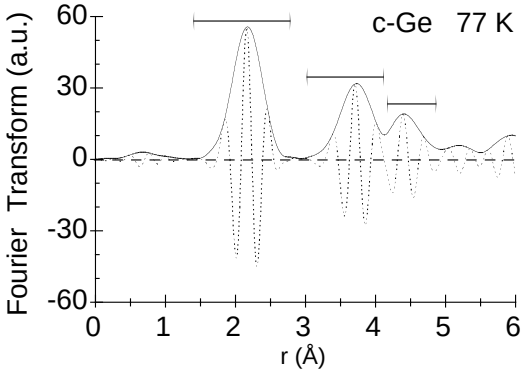

Figure 6.3: Fourier transform of EXAFS of crystalline germanium at 77 K: imaginary part (dashed line) and modulus (continuous line). The first three coordination shells are singled out.

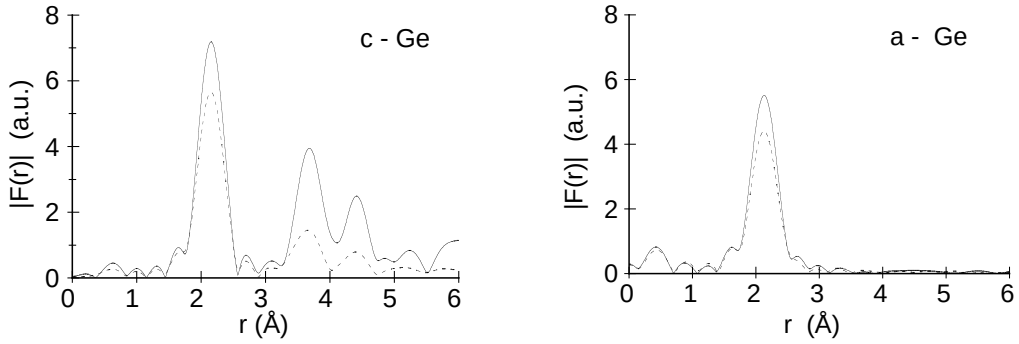

Figure 6.4: Moduli of Fourier transforms of crystalline and amorphous germanium at 77 K (continuous lines) and 300 K (dashed lines).

3. The comparison between Fourier transforms of different samples allows to evaluate differences in distances or disorder effects (Fig. 6.4).
4. Peaks not corresponding to possible inter-atomic distances can be due to non-negligible multiple scattering effects.

6.2.2 Inverse Fourier transform

The contribution of a given coordination shell (or of a given scattering path) can be singled out by an inverse Fourier transform limited to the corresponding interval $r_{\min} \div r_{\max}$, with window $\tilde{W}(r)$:

$$\tilde{\chi}(k) \;=\; (2/\pi) \int_{r_{\min}}^{r_{\max}} F(r)\; \tilde{W}(r)\; \exp(-2\mathrm{i}kr)\; dr. \tag{6.7}$$

The Fourier filtered signal $\tilde{\chi}(k)$ is in principle a complex quantity.
Where the direct and inverse transforms performed for r spanning the entire real axis from $-\infty$ to $+\infty$, one would obtain Im $\tilde{\chi}(k) = 0$ and Re $\tilde{\chi}(k)$ would correspond to the original signal, to within the artefact os the Fourier filtering procedure.
Actually, the inverse transform is done on an interval of only positive r values. As a consequence, both real and imaginary parts of $\tilde{\chi}(k)$ are different from zero. The real part corresponds to the filtered EXAFS signal:

$$\mathrm{Re}\;\tilde{\chi}(k) \;=\; \chi_s(k) \;=\; A_s(k)\; \sin\Phi_s(k) \tag{6.8}$$

where $A_s(k)$ and $\Phi_s(k)$ synthetically indicate the total amplitude and phase of the EXAFS of the s-th shell. The imaginary part Im $\tilde{\chi}(k)$ is used to separately calculate the amplitude and phase of

the filtered signal:

$$A_s(k) \;=\; \sqrt{[\mathrm{Re}\,\tilde{\chi}(k)]^2 \,+\, [\mathrm{Im}\,\tilde{\chi}(k)]^2}; \qquad \Phi_s(k) \;=\; \mathrm{arctg}\;[\mathrm{Re}\,\tilde{\chi}(k)/\mathrm{Im}\,\tilde{\chi}(k)]. \tag{6.9}$$

6.3 Quantitative determination of structural parameters

The final step of EXAFS analysis consists in the quantitative evaluation of the structural parameters: average inter-atomic distances $\langle r\rangle$, coordination numbers N, Debye-Waller exponents σ^2. If the first-shell contribution is well singled out in the Fourier transform $F(r)$, the corresponding back-transformed signal $\tilde{\chi}(k)$ can be safely analysed within the single scattering approximation. The outer shell contributions cannot generally be completely disentangled and are mixed with contributions from multiple scattering paths, which cannot be neglected in refined analyses. In any case, according to (3.43), to obtain the values of the structural parameters from an experimental EXAFS spectrum, one must know the scattering amplitudes $|f(k)|$, phase-shifts $\phi(k)$ and inelastic factors S_0^2 and $\lambda(k)$ of each relevant scattering path.
Most available software packages [XAFS software, , GNXAS, 2015, FEFF, 2012] allow a sorting of all the relevant single and multiple scattering paths for a given model structure, as well as the *ab-initio* calculation of scattering amplitudes and phasesihfts for the different scattering paths and an evaluation of the mean free path $\lambda(k)$. It is thus possible to simulate a theoretical EXAFS function $\chi_{\mathrm{sim}}(k)$ for the given model structure. The structural parameters of the studied system can be obtained by building up a suitable starting model structure, calculating $\chi_{\mathrm{sim}}(k)$ for the model structure, comparing with the experimental EXAFS $\chi_{\mathrm{exp}}(k)$ and refining, by a best-fitting procedure, the values of the parameters, including the edge shift $E_0 = E_b - E_s$.
In principle, the fit of theory to experiment could be done over the entire original EXAFS spectrum. More frequently, the fit is limited to a filtered portion of the signal, corresponding for example to the first shell, or to an interval of distances including a number of coordination shells. The comparison of theory with experiment can be done in the r space after Fourier transform or on the k space after back-transform. In any case, since Fourier transforms introduce distortions, it is strictly necessary that both calculated and experimental EXAFS spectra undergo exactly the same transform procedures before comparison.
The maximum number of independent parameters that can reasonably be obtained from an EXAFS spectrum depends on the quantity and quality of available information. According to a conservative rule of thumb based on information theory, the maximum number of independent parameters obtainable from a Fourier filtered EXAFS signal is

$$n_{\mathrm{ind}} \;\simeq\; (2\,\Delta k\,\Delta r)/\pi, \tag{6.10}$$

where $\Delta k = k_{\mathrm{max}} - k_{\mathrm{min}}$ and $\Delta r = r_{\mathrm{max}} - r_{\mathrm{min}}$ are the intervals of the direct and inverse Fourier transforms, respectively.

6.4 Separate analysis of amplitude and phase

If the Fourier filtered coordination shell is made by one atomic species and if a reference sample of known structure is available, then the EXAFS analysis can be completed in a rather simple and elegant way. The method, sometimes called *ratio method*, consists in the separate comparison of phases and amplitudes of the EXAFS signals of the sample under study with those of the reference. The procedure cancels the "physical" parameters $|f_s(k,\pi)|$, ϕ_s, S_0^2 and λ, supposed to be identical in both samples.
The ratio method was invented by Stern *et al* [Stern et al., 1975], extended by Bunker [Bunker, 1983] and Tranquada *et al* [Tranquada and Ingalls, 1983, Tranquada and Ingalls, 1986] to include cumulants. A presentation including the energy shift has been given by Freund *et al* [Freund et al., 1989].
Sample and reference will be here identified by the apices s and m, respectively.

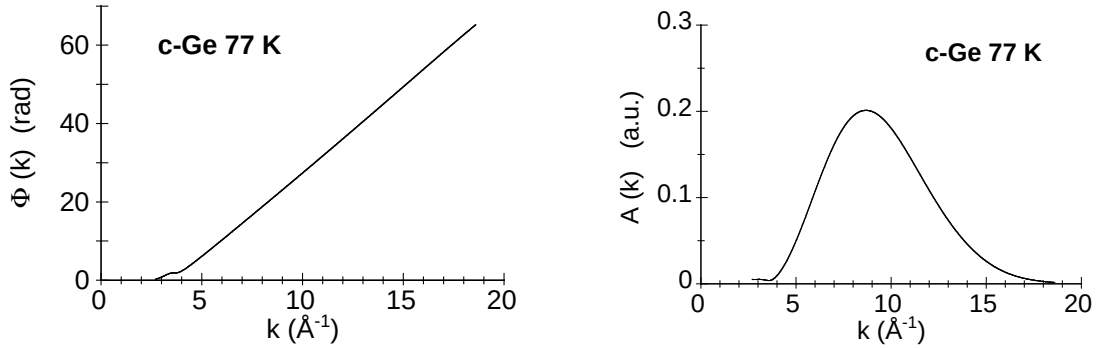

Figure 6.5: Total phase $\Phi(k)$ and amplitude $A(k)$ of the 1st-shell EXAFS of crystalline germanium. The Fourier filtering introduces artifacts, particularly strong at the extreme k values.

Amplitude and phase (Fig. 6.5) are obtained through Eqs. (6.9). They can be expressed as a function of cumulants as

$$A(k) = (S_o^2/k)\ N\ |f(k,\pi)|\ \exp\left(C_o - 2k^2C_2 + 2k^4C_4/3\ ...\right) \quad (6.11)$$

$$\Phi(k) = 2kC_1\ -\ 4\,k^3C_3/3\ ...\ +\ \phi(k). \quad (6.12)$$

Phase analysis

If the phaseshifts of both samples are identical, $\phi^s(k) = \phi^m(k)$, they can be eliminated by subtracting the total phase of the reference from the one of the sample:

$$\Phi^s(k) - \Phi^m(k) = 2k(C_1^s - C_1^m) - 4\ k^3(C_3^s - C_3^m)\,/3\ +\ ... \quad (6.13)$$

In this way it is also possible to eliminate the artifacts of the Fourier filtering and reduce possible multiple scattering and curved waves effects.
A polynomial fit allows to get the differences between the first odd cumulants: $\Delta C_1 = C_1^s - C_1^m$, $\Delta C_3 = C_3^s - C_3^m$, ... It is useful to plot $\Delta\Phi/2k$ against k^2 (Fig. 6.6, left): the intercept then gives ΔC_1, the slope is proportional to ΔC_3 and deviations from linearity imply a non negligible influence of ΔC_5.

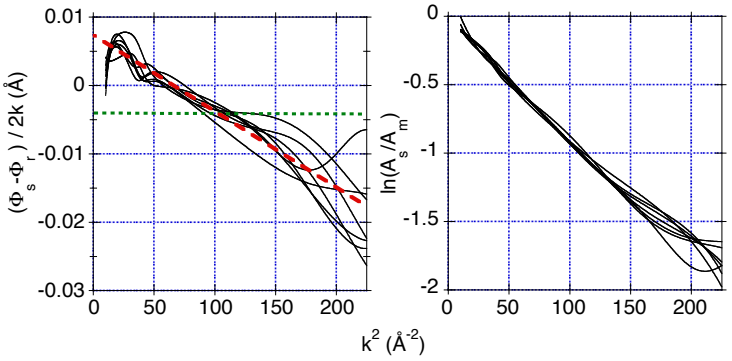

Figure 6.6: EXAFS at the Te K edge of CdTe: comparison of phases (left) and amplitudes (right) of seven files measured at 300 K with the average of six reference files measured at 20 K. Data from [Abd el All et al., 2013]

Amplitude analysis

If $|f(k,\pi)|$, S_0^2 and λ of both samples are identical, they can be eliminated by dividing the sample amplitude by the reference amplitude. In this way, it is also possible to eliminate the Fourier filtering artifacts and reduce possible multiple scattering and curved wave effects. The logarithm of the amplitude ratio is

$$\ln \frac{A^s(k)}{A^m(k)} \;=\; \ln \frac{N^s}{N^m} + (C_o^s - C_o^m) - 2k^2(C_2^s - C_2^m) + 2k^4(C_4^s - C_4^m)/3 - \;... \tag{6.14}$$

A polynomial fit to

$$\ln \frac{A^s(k)}{A^m(k)} - (C_o^s - C_o^m) \;=\; \ln \frac{N^s}{N^m} - 2k^2(C_2^s - C_2^m) + 2k^4(C_4^s - C_4^m)/3 - \;... \tag{6.15}$$

allows one to evaluate the ratio of coordination numbers N^s/N^m and the differences between the first even cumulants: $\Delta C_2 = C_2^s - C_2^m$, $\Delta C_4 = C_4^s - C_4^m$, ...
It is useful to plot $\ln[A^s(k)/A^m(k)] - (C_o^s - C_o^m)$ against k^2 (Fig. 6.6, right): the intercept gives the coordination number, the slope is proportional to ΔC_2 and deviations from linearity imply a non negligible influence of ΔC_4.
The term

$$C_o^s - C_o^m \;=\; -2\,(C_1^s - C_1^m)/\lambda - 2\;[\ln C_1^s - \ln C_1^m] \tag{6.16}$$

is often but not always negligible. It can be easily estimated from a rough knowledge of interatomic distances of sample and model and of the mean free path. The second term in (6.16) is larger than the first term.

6.5 Uncertainty evaluation

As for any experimental result, the values of structural parameters obtained from EXAFS analysis are meaningless if not accompanied by a reliable estimate of their uncertainties (error bars). A sound assessment of the uncertainty of EXAFS results requires a careful evaluation of random fluctuations and systematic errors in both experimental and data analysis procedures. The following tentative systematic analysis has taken from [Abd el All et al., 2013].

The influence of counting statistics is generally negligible in transmission measurements at third generation S.R. sources. A number of other factors should be however taken into account: temperature fluctuations of the sample; temperature fluctuations and mechanical instabilities of monochromator, mirrors and their supports; calibration and resolution of the monochromator angular encoder; electron beam fluctuations. All these factors can lead to non-negligible uncertainties of the photon energy and, on a non perfectly homogeneous sample, to variations of the amplitude of EXAFS. Not to speak of possible systematic errors, related for example to the sample temperature calibration, photon beam energy calibration, sample deterioration, and so on.
Not all these factors can reasonably be under complete control of the synchrotron radiation users or even of the beamline scientists. Suitable experimental strategies and data analysis procedures, joined to a critical discussion of results, can anyway lead to a sound *a posteriori* evaluation of uncertainties and of their most relevant causes.

As a general rule of experimental practice, EXAFS measurements in a given condition (e.g. on a given sample at a given temperature) should be repeated a convenient number of times, typically at least three times. When this happens, the different spectra are frequently summed, to obtain an average EXAFS function $\chi(k)$. We consider preferable to analyse separately each spectrum. The resulting cumulants represent a restricted sample of a parent population of values due to short-term fluctuations. It is reasonable to account for these fluctuations by evaluating the uncertainty as the standard deviation of the distribution of mean values; this contribution to uncertainty decreases when the number of spectra increases.
As a numerical example, let us consider the phase analysis of seven files measured at 300 K at the Te K edge and compared with the average reference file at 20 K (Fig. 6.6, left). For the

fitting interval $k = 4$ to 14 Å^{-1}, the values of the odd cumulants of the effective distribution were $\Delta C_1 = (0.73 \pm 0.04) \times 10^{-2}$ Å and $\Delta C_3 = (1.65 \pm 0.11) \times 10^{-4}$ Å^3.

A second source of uncertainty is connected to the data analysis procedure. Different windows and k weigths in Fourier transform and backtransform, as well as different fitting intervals in k space lead to different values of cumulants. In this respect, the ratio method, based on the separate analysis of phases and amplitudes, is by far less affected by statistical correlation effects than the non-linear fitting procedures. The different values of cumulants obtained by different choices of data analysis parameters cannot be considered as independent samples of a parent distribution: increasing the number of fitting intervals cannot decrease the final uncertainty. The different values can be considered as sampling a uniform distribution, and the corresponding uncertainty can be evaluated as the standard deviation of the distribution, $\sigma_n = \Delta(\delta C_n)/\sqrt{12}$. The point here is not the repetition of the fitting procedure over a large number of fitting intervals, but a sound choice of the width $\Delta(\delta C_n)$ of the uniform distribution, which in turn depends on the choice of the extrema $k_{\min}$ and $k_{\max}$ of the fitting intervals. In the ratio method, the largest fitting interval can be chosen as the interval where the phase differences (Fig. 6.6 left) or the logarithms of amplitudes ratios (Fig. 6.6 right) of different files measured in the same conditions show a reasonable agreement. The visual choice suffers from some arbitrariness, but leads generally to quite conservative estimates of uncertainty, in view of the large sensitivity of the phase and amplitude plots to tiny discrepancies of the spectra.
As a numerical example, let us consider again the phase analysis of the seven files measured at 300 K at the Te K edge (Fig. 6.6, left) and focus on the first cumulant. The three fitting intervals from $k_{\min} = 4$ to $k_{\max} = 13$, 14 or 15 Å^{-1} give different average values of the first cumulant, 0.678, 0.73 and $0.8{\times}10^{-2}$ Å; the contribution to the total uncertainty is $0.035{\times}10^{-2}$ Å.

An important contribution to the evaluation of uncertainty is represented by the comparison of independent measurements performed on the same system, for example in different laboratories or on samples of different thicknesses and possibly at two different absorption edges.

A last point for the evaluation of the quality of results is the comparison of the temperature dependence of the cumulants with a reasonably smooth behaviour. An interesting example is given in [Abd el All et al., 2013] by the sequence of cumulants obtained from the Te and Cd edges between 50 and 150 K. The quantities derived from the phase analysis of the Te K edge (odd cumulants and perpendicular MSRD) are characterised by a tiny deviation from the expected smooth temperature dependence; this effect is absent in the quantities derived from the Cd K edge. In this case, the discrepancies between the results from Te and Cd edges are consistent with the uncertainty bars: one can reasonably assume that, had a larger number of spectra been measured at each temperature, the Te data would have been in better agreement with a smooth temperature dependence. One cannot however exclude the possibility that the observed kinks are due to long-period fluctuations of the experimental apparatuses or to occasional systematic errors, which anyway escaped our direct detection; in such a case, they can be considered as a measure of the extent of long-term reproducibility of a routine experiment performed on a standard beamline.

External accuracy checks can rely on the comparison of experimental results with theoretical models.

Chapter 7

XANES

This last Section is dedicated to XANES. Starting point for treating XANES is the Golden Rule in dipole approximation, Eq. (**??**), like for EXAFS. The interpretation of XANES is however by far more complicated. We will give here only an introductory phenomenological account.
Two different approaches to XANES can be distinguished, which have been developed in different times and scientific environments. The first approach focusses on the electronic structure; it is particularly suited to study the XANES in the very proximity of the edge. The second approach focusses on geometric structure and on the multiple scattering of the photo-electron; it is particularly suited to give a unified picture of XANES and EXAFS. To the extent that electronic and geometric structure are interconnected, the two approaches, apparently rather different, are actually connected, and in many cases equivalent.

7.1 XANES and electronic structure

In the proximity of an edge, the x-ray absorption coefficient depends on the transitions of the photo-electron to low-lying un-occupied states. Let us summarize here some general properties.
a) The initial state is a well defined *core level*, almost insensitive to the chemical environment. The edge structures directly reflect the modulations of the *density of un-occupied electronic states* of lower energy.
b) The initial one-electron core state is a localized wavefunction. As a consequence, the edge structures sample the density of final states *projected on the absorber site*.
c) The initial core state has a well defined angular momentum symmetry. By virtue of the electric dipole selection rules, the edge structures sample the density of final states *projected on the angular momentum*. For example, K and L_1 edges, corresponding to s initial levels, sample the density of p final states. L_2 and L_3 edges, corresponding to p initial levels, sample the density of s and d final states.
d) The excited state corresponding to an x-ray core hole has typically an energy width Γ_h of the order of several eV (Fig. **??**). The edge structures reflect the density of final states *convoluted with the* Γ_h *width*, in addition to instrumental resolution.

Let us now consider some examples.
In **atomic systems**, the situation is relatively simple. Let us consider the K edge of Argon gas shown in Fig. **??**, left. The zero of the energy axis corresponds to the *ionization threshold* at 3205.9 eV, determined by XPS. The structures at lower energies correspond to transitions from the 1s core level to Rydberg states 4p (main peak at -3 eV), 5p, ..., np. The lifetime of the excited state produces the widening of Rydberg peaks and the arctangent shape of the edge.
In **molecular systems**, transitions to atomic Rydberg states still contribute to the edge structures. In general, however, the edge structures are dominated by transitions to valence orbitals and resonant states both below and above the ionization threshold. Their interpretation in terms of electronic states is quite complicated; the best results are generally obtained by a multiple scattering approach (one speaks of MSR, multiple scattering resonances).

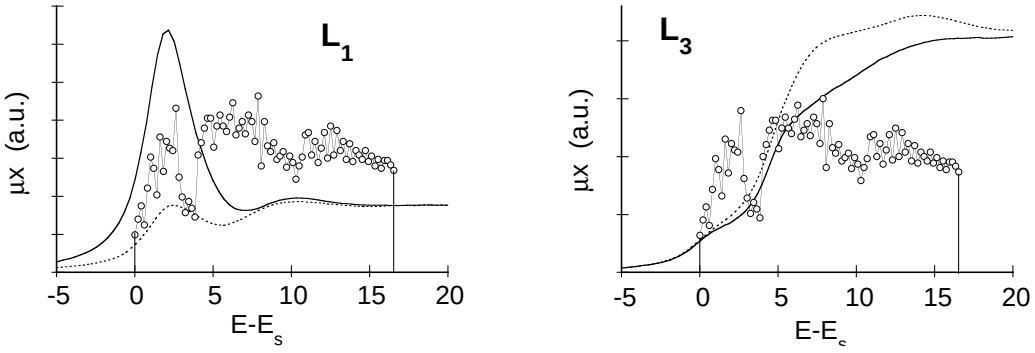

Figure 7.1: Fine structure at the L_1 and L_3 edges of antimony (continuous lines) and iodine (dashed lines) in SbSI. The sensitivity to atomic site and to angular momentum is evident. Circles show the calculated total density of states at the bottom of conduction band.

In **crystalline solids** the long-range order simplifies the description and calculation of electronic states. The edge structures are sensitive to the density of un-occupied states in the low-lying part of the conduction band, projected on the absorber site and angular momentum, and can be compared with band calculations (Fig. 7.1).

7.2 XANES and multiple scattering

EXAFS can be interpreted with good accuracy in terms of *single scattering* (SS) of the photo-electron. *Multiple scattering* (MS) phenomena are generally, although not always, negligible.
In the XANES region, on the contrary, MS phenomena become very important. This can be intuitively understood by two considerations: *a)* the photo-electron kinetic energy is small with respect to the interaction potential, making more probable the scattering; *b)* the photo-electron mean free path is larger.

7.2.1 Multiple scattering paths

According to Eq. (**??**), the absorption coefficient in the EXAFS region can be expressed, in SS approximation, as

$$\mu(k) \;=\; \mu_0(k)\;[1+\chi_2(k)]\,, \tag{7.1}$$

where μ_0 is the atomic absorption coefficient and χ_2 the EXAFS function. The label "2" has been added to remember that the photo-electron path is made of 2 *segments*, from absorber to back-scatterer atom and viceversa, respectively.
To take into account multiple scattering effects, Eq. (7.1) is modified as follows:

$$\mu(k) \;=\; \mu_0(k)\;[1+\chi_2(k)+\chi_3(k)+...+\chi_n(k)+...]\,. \tag{7.2}$$

In Eq. (7.2) the generic term χ_n represents the contribution due to all possible *paths of order* n, say composed of n segments (Fig.**??**). For example, χ_3 corresponds to all paths in which the photo-electron is backscattered twice.
In principle, Eq. (7.2) contains an unlimited number of terms χ_n. Each term χ_n in turn corresponds to different paths, whose number grows very fastly when n increases. The relative weight of the different terms in Eq. (7.2) depends on the photo-electron energy. Going down from high to low energy, it is useful to distinguish three regimes.
a) In the EXAFS region the terms χ_n of order $n > 2$ are negligible; we are in the *single scattering* (SS) regime.
b) In the IMS region (*intermediate multiple scattering*), only a limited number of terms χ_n ($n > 2$) is important; one can then calculate the absorption coefficient $\mu(k)$ to a good approximation by evaluating only the most significant terms χ_n.

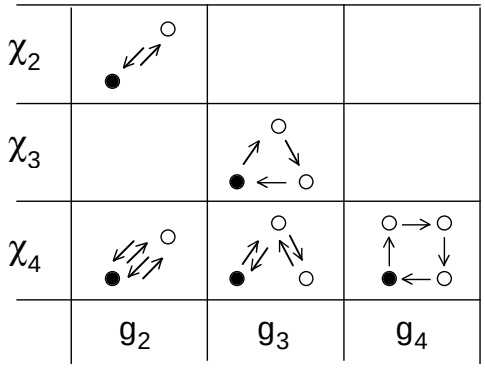

Figure 7.2: Examples of multiple scattering paths. Each row correspond to a given contribution χ_n. Each column corresponds to a given n-body correlation function g_n.

c) At low energies, in the FMS region (*full multiple scattering*), the series of Eq. (7.2) converges very slowly or does not converge at all; the absorption coefficient can be obtained only through a direct calculation of the full scattering operator.
Multiple scattering calculations of XANES are evidently much more complicated than single scattering calculations of EXAFS. In particular, it is impossible to interpret XANES by a simple parametrized equation.
If thermal disorder effects are neglected, for each multiple scattering path a contribution

$$\chi_n(k) \;=\; A\left(k, \{\vec{r}\}\right)\; \sin\left[kR_p + \Phi\left(k, \{\vec{r}\}\right)\right] \tag{7.3}$$

should be considered, formally similar to the standard EXAFS formula, but substantially much more complicated. In Eq. (7.3), R_p is half the total photo-electron path. $\{\vec{r}\}$ is the set of coordinates describing all interested atoms, A e Φ are functions depending on the potential acting on the photo-electron.
A multiple scattering calculation is based on the following steps: *a)* assumption of a geometrical structure; *b)* sorting of the paths relevant for the application of Eq. (7.2): *c)* calculations of the A and Φ functions of Eq. (7.3) for each path; *d)* optimization of structural parameters by best fit to the experimental spectrum.
The multiple scattering formalism requires the presence of a cluster of atoms surrounding the absorber atom, independently of any degree of long range order. It represents then a unifying framework for treating molecules and condensed systems, both crystalline and amorphous.

7.2.2 N-body correlations

The complexity of multiple scattering calculations is balanced by the possibility of obtaining from XANES three-dimensional structural information, e.g. on bonding angles and n-body correlation functions.
The scattering paths including only the absorber and one back-scatterer atom contain information only on the *two-body correlation function* $g_2(r)$. This is the case of EXAFS (χ_2), but also of some paths of order $n > 2$ (Fig.7.2). The $g_2(r)$ function is connected to the *real* distribution $\rho(r)$ by $\rho(r) = 4\pi r^2 g_2(r)$.
The scattering paths including the absorber and two different scatterer atoms contain information on the *three-body correlation function* $g_3(r_1, r_2, \phi)$, where r_1 and r_2 are inter-atomic distances, ϕ the bonding angle (Fig.7.2).

Appendix A

Basic electrodynamics

In this Appendix, some basic concepts of electrodynamics are reviewed, the main goal being to support the description of the interaction of electromagnetic radiation with material systems.

In Section A.1, the description of the electromagnetic field in terms of the $\vec{E}$ and $\vec{B}$ vectors and of the Maxwell equations is accounted for; the interaction of the radiation field with electrical charges is described, in the classical approximation, by the Coulomb-Lorentz force.
The interaction of radiation with atoms requires a quantum approach. The use of the Coulomb-Lorentz force is out of question in quantum mechanics. The right approach has to be sought within the hamiltonian formalism. The first step in this direction (Section A.2) is the introduction of the scalar and vector potentials, which play a key role in both classical and quantum hamiltonian approaches. Thanks to the gauge invariance, the potentials represent a flexible mathematical instrument which facilitates field calculations in different physical situations.
Sections A.3 and A.5 are dedicated to the expression of the electromagnetic fields in the reciprocal space and to their quantisation in terms of photons.
At last, the Lagrange and Hamilton formalisms for the interaction of radiation with matter are introduced in Section A.6. The expression of the interaction Hamiltonian which concludes this section is a necessary input for the subsequent Appendix B, where the radiation-matter interaction is approached within the time-dependent perturbation formalism.

The International System of units (SI) is used for electromagnetic quantities.
Basic references: [Feynman et al., 1977, Cohen-Tannoudji et al., 2004, Zangwill, 2012].

A.1 Maxwell equations and Lorentz force

The Maxwell equations connect the electric and magnetic fields to their sources, the electric charges and currents. The dynamic effect of the electric and magnetic fields on the electric charges is described by the Lorentz force.
Maxwell equations and Lorentz force represent the law of electromagnetism.

A.1.1 Maxwell equations

The electromagnetic field is described by the electric field $\vec{E}$ and the magnetic induction field $\vec{B}$.

Maxwell equations in integral form

The four Maxwell equations in integral form connect the electric and magnetic fields to the electric charge q and the electric current I.

Electrostatic Gauss law:

$$\int_S \vec{E} \cdot \vec{u}_n \, dS \; = \; \frac{q}{\epsilon_0} \tag{A.1}$$

Magnetostatic Gauss law:

$$\int_S \vec{B} \cdot \vec{u}_n \, dS \;=\; 0 \tag{A.2}$$

Faraday-Henry law:

$$\oint_L \vec{E} \cdot d\vec{\ell} \;=\; -\frac{d}{dt} \oint_S \vec{B} \cdot \vec{u}_n \, dS. \tag{A.3}$$

Ampère-Maxwell law:

$$\oint_L \vec{B} \cdot d\vec{\ell} \;=\; \mu_0 \, I \;+\; \epsilon_0 \mu_0 \frac{d}{dt} \oint_S \vec{E} \cdot \vec{u}_n \; dS. \tag{A.4}$$

Maxwell equations in differential form

Making use of the Gauss and Stokes theorems

$$\int_S \vec{C} \cdot \vec{u}_n \, dS \;=\; \int_V \vec{\nabla} \cdot \vec{C} \, dV \,, \qquad \oint_L \vec{C} \cdot \vec{\ell} \, dS \;=\; \int_S \vec{\nabla} \times \vec{C} \, dS \,, \tag{A.5}$$

where $\vec{C}$ is a generic vector, the integral Maxwell equations can be transformed into their differential form, where the electric and magnetic fields are connected to the charge density ρ and to the current density $\vec{J}$:

$$\vec{\nabla} \cdot \vec{E} \, (\vec{r}, t) \;=\; \frac{1}{\epsilon_0} \, \rho \, (\vec{r}, t) \tag{A.6}$$

$$\vec{\nabla} \cdot \vec{B} \, (\vec{r}, t) \;=\; 0 \tag{A.7}$$

$$\vec{\nabla} \times \vec{E} \, (\vec{r}, t) \;=\; -\frac{\partial}{\partial t} \vec{B} \, (\vec{r}, t) \tag{A.8}$$

$$\vec{\nabla} \times \vec{B} \, (\vec{r}, t) \;=\; \frac{1}{c^2} \frac{\partial}{\partial t} \vec{E}, (\vec{r}, t) \;+\; \frac{1}{\epsilon_0 c^2} \vec{J} (\vec{r}, t) \tag{A.9}$$

Continuity equation

From (A.6) and (A.9) one can derive the equation of continuity, which corresponds to the conservation of electric charge:

$$\frac{\partial}{\partial t} \rho \, (\vec{r}, t) \;+\; \vec{\nabla} \cdot \vec{J} \, (\vec{r}, t) \;=\; 0 \,. \tag{A.10}$$

S.I. Units

- the electric field E is measured in $\mathrm{V\,m^{-1}}$
- the magnetic induction B is measured in T
- the electric charge density ρ is measured in $\mathrm{C\,m^{-3}}$
- the current density J is measured in $\mathrm{A\,m^{-2}}$
- the vacuum permittivity ϵ_0 is 8.8544×10^{-12} $\mathrm{N^{-1} m^{-2} C^2}$.

A.1.2 Maxwell equations in vacuum, wave equations

In vacuum, where no electric charges are present ($\rho = 0$ and $\vec{J} = 0$), the differential Maxwell equations reduce to:

$$\vec{\nabla} \cdot \vec{E} \, (\vec{r}, t) \;=\; 0 \tag{A.11}$$

$$\vec{\nabla} \cdot \vec{B} \, (\vec{r}, t) \;=\; 0 \tag{A.12}$$

$$\vec{\nabla} \times \vec{E} \, (\vec{r}, t) \;=\; -\frac{\partial}{\partial t} \vec{B} \, (\vec{r}, t) \tag{A.13}$$

$$\vec{\nabla} \times \vec{B} \, (\vec{r}, t) \;=\; \frac{1}{c^2} \frac{\partial}{\partial t} \vec{E}, (\vec{r}, t) \tag{A.14}$$

Let us take the curl of (A.13) and (A.14); remembering that $\vec{\nabla} \times (\vec{\nabla} \times \vec{v}) = \vec{\nabla}(\vec{\nabla} \cdot \vec{v})$ and making use of (A.11) and (A.12) one finds the two wave equations for the electric and magnetic fields:

$$\frac{\partial^2}{\partial t^2} \vec{E}\,(\vec{r}, t) \;=\; c^2\, \nabla^2\, \vec{E}\,(\vec{r}, t) \tag{A.15}$$

$$\frac{\partial^2}{\partial t^2} \vec{B}\,(\vec{r}, t) \;=\; c^2\, \nabla^2\, \vec{B}\,(\vec{r}, t) \tag{A.16}$$

Wave equation

The two above equations (A.15) and (A.16) imply the same form for the six components of the two vectors $\vec{E}$ and $\vec{B}$,

$$\nabla^2 \psi \;-\; \frac{1}{c^2}\, \frac{\partial^2 \psi}{\partial t^2} \;=\; 0 \tag{A.17}$$

say

$$\frac{\partial^2 \psi}{\partial x^2} \;+ \frac{\partial^2 \psi}{\partial y^2} + \frac{\partial^2 \psi}{\partial z^2} - \;\frac{1}{c^2}\, \frac{\partial^2 \psi}{\partial t^2} \;=\; 0 \tag{A.18}$$

where ψ can be one of the different scalar quantities $E_x, E_y, E_z, B_x, B_y, B_z$.
Different functions $\psi(t, x, y, z)$ can satisfy the wave equation (A.17).
As a further consequence of the Maxwell equations, one can show that in an electromagnetic wave the electric and magnetic fields are always perpendicular, $\vec{B} \perp \vec{E}$, and that both $\vec{E}$ and $\vec{B}$ are perpendicular to the propagation direction. Besides, the the oscillating electric and magnetic fields are not independent, but are connected by the scalar relation $E = cB$.

Plane waves

One can easily verify that any functions

$$\psi(t, x) = f(t - x/c)\,, \qquad \psi(t, x) = f(t + x/c) \tag{A.19}$$

satisfie the differential wave equation (A.17). They represent plane waves propagating in the forward and in the backward x direction, respectively, with velocity c.
By considering three functions (A.19) satisfying the wave equation (A.18) for the three components E_x, E_y, E_z of the electric field, one can build up three-dimensional electromagnetic waves.
Any function representing a possible plane electromagnetic wave can be expressed a a Fourier integral of sinusoidal plane waves. That's why one give particular attention to sinusoidal waves

Spherical waves

By expressing the Laplacian operator ∇^2 as a function of the radial distance, one can rewrite the wave equation (A.17) as

$$\frac{\partial^2 (r\psi)}{\partial r^2} \;-\; \frac{1}{c^2}\, \frac{\partial^2 (r\psi)}{\partial t^2} \;=\; 0 \tag{A.20}$$

The solution is a spherical wave

$$r\,\psi(t, r) = f(t - x/c)\,, \qquad \psi(t, r) = \frac{f(t - x/c)}{r}\,. \tag{A.21}$$

The function ψ diverges for $r \to 0$. Actually, a spherical wave requires a source at the origin (or in the region around the origin). Taking into account the source s, the wave equation becomes

$$\frac{\partial^2 (r\psi)}{\partial r^2} \;-\; \frac{1}{c^2}\, \frac{\partial^2 (r\psi)}{\partial t^2} \;=\; -s\,, \tag{A.22}$$

or, in cartesian coordinates,

$$\nabla^2 \psi \;-\; \frac{1}{c^2}\, \frac{\partial^2 \psi}{\partial t^2} \;=\; -s\,. \tag{A.23}$$

It is important to realise that for $r \to 0$, say near the source,

$$\nabla^2\psi \; - \; \frac{1}{c^2}\,\frac{\partial^2\psi}{\partial t^2} \; \simeq \nabla^2\psi \tag{A.24}$$

(the time derivative is negligible with respect to the space derivatives) and

$$\frac{f(t-x/c)}{r} \; \simeq \; \frac{f(t)}{r}\,. \tag{A.25}$$

Near the source, the solution to the wave equation can be calculated as for the static case. The solution propagates radially with velocity c.

A.1.3 Coulomb-Lorentz force

Let us now consider the effects of the magnetic and electric fields on an electric charge. The force acting on a charge q which at time t is in position $\vec{r}$ and moves with velocity $\vec{v}$ (*Coulomb-Lorentz force*) is

$$\vec{F}\,(\vec{r},t) \; = \; q\,\left[\vec{E}\,(\vec{r},t) \; + \; \vec{v}\times\vec{B}\,(\vec{r},t)\right]\,. \tag{A.26}$$

For a non relativistic particle, the classical dynamic equation is

$$m\,\frac{d^2}{dt^2}\,\vec{r}\,(t) \; = \; q\,\left(\vec{E}\,(\vec{r},t) \; + \; \vec{v}\,(t)\times\vec{B}\,(\vec{r},t)\right) \tag{A.27}$$

For a relativistic particle, the dynamic equation is

$$\frac{d}{dt}\,(\gamma m\vec{v}) \; = \; q\,\left(\vec{E} \; + \; \vec{v}\,(t)\times\vec{B}\right) \tag{A.28}$$

where

$$\gamma \; = \; \left[1-\frac{v^2}{c^2}\right]^{-1/2} \tag{A.29}$$

Comments

- The four Maxwell equations are first-order, the Coulomb-Lorentz equation is second-order.
- The evolution of the fields depends on ρ and $\vec{J}$ through the Maxwell equations. The motion of the charged particles depends on the fields through the Coulomb-Lorentz equation.
- The dynamical state of the global system particles + fields is given, at each instant t_0, by the values of the fields at all points $\vec{r}$ and the positions $\vec{r}_i$ and velocities $\vec{v}_i$ of all the particles.

A.1.4 Energy and momentum

It is an experimentally confirmed fact that the electromagnetic field can store and transport energy. Energy is a conserved quantity. The theory of relativity requires that energy is locally conserved: no simultaneous transfer of energy between distant points can happen.
We want to inquire how the electromagnetic energy can be expressed as a function of the electric and magnetic fields [Ref. Feynman II, Ch. 27].

Poynting theorem

The local conservation of energy can be expressed by a continuity equation in integral form

$$-\,\frac{\partial}{\partial t}\int_V u\,dV \; = \; \sum_\Sigma \vec{S}\cdot d\vec{n} + \int_V \vec{E}\cdot\vec{J}\,dV\,, \tag{A.30}$$

where $u(\vec{r},t)$ is the local energy density, $\vec{S}$ is the energy flux through the surface Σ which encloses the volume V and the last term represent the exchange of energy between the field and matter.

The continuity equation (A.30) can be readjusted and expressed in differential form as

$$\vec{E} \cdot \vec{J} \;=\; -\frac{\partial}{\partial t} u - \vec{\nabla} \cdot \vec{S}\,. \tag{A.31}$$

Extracting the current density $\vec{J}$ from the last Maxwell equation (A.9),

$$\vec{J} \;=\; -\epsilon_0 \,\frac{\partial}{\partial t}\vec{E} + \epsilon_0 c^2\, \vec{\nabla} \times \vec{B}\,,$$

one can express the left side of (A.31) in terms of electric and magnetic fields:

$$\vec{E} \cdot \vec{J} \;=\; -\epsilon_0\, \vec{E} \cdot \frac{\partial}{\partial t}\vec{E} + \epsilon_0 c^2 \vec{E} \cdot (\vec{\nabla} \times \vec{B})\,; \tag{A.32}$$

transforming the last term of (A.32) according to

$$\vec{E} \cdot (\vec{\nabla} \times \vec{B}) \;=\; \vec{B} \cdot (\vec{\nabla} \times \vec{E}) + \vec{\nabla} \cdot (\vec{B} \times \vec{E})$$

and taking into account that $\vec{\nabla} \times \vec{E} = -\partial \vec{B}/\partial t$, one finds the final form of (A.32):

$$\vec{E} \cdot \vec{J} \;=\; -\frac{\partial}{\partial t}\left[\frac{\epsilon_0}{2}\; E^2 + \frac{\epsilon_0 c^2}{2} B^2\right] - \epsilon_0 c^2 \vec{\nabla} \cdot (\vec{E} \times \vec{B})\,. \tag{A.33}$$

Energy

Let us now compare the two expressions (A.31) and (A.33) for the local conservation of energy. By equating the first terms of the right-hand sides of the two equations, one can express the energy density u of the electromagnetic field as

$$u(\vec{r}, t) \;=\; \frac{1}{2}\epsilon_0 \,\left[E^2(\vec{r}, t) + c^2 B(\vec{r}, t)\right]\,. \tag{A.34}$$

The total energy of a classical system particles + fields is

$$H \;=\; \sum\nolimits_i \frac{1}{2} m_i v_i^2(t) \;+\; \frac{\epsilon_0}{2} \int d^3 r\; \left[E^2(\vec{r}, t) + c^2\, B^2(\vec{r}, t)\right] \tag{A.35}$$

By equating the second terms of the right-hand sides of the two equations, one can express the energy flux density $\vec{S}$ as the *Poynting vector*

$$\vec{S}(\vec{r}, t) \;=\; \epsilon_0 c^2 \vec{\nabla} \cdot [\vec{E}(\vec{r}, t) \times \vec{B}(\vec{r}, t)]\,. \tag{A.36}$$

Note: The choice is not unique; the Poynting vector is defined to within a vector of zero divergence.

For an electromagnetic wave, where $E = cB$, the energy density and the modulus of the Poynting vector magnitude are, respectively,

$$u \;=\; \epsilon_0\, E^2\,, \qquad S \;=\; \epsilon_0 c E^2 \;=\; uc\,. \tag{A.37}$$

Linear momentum

The density $\vec{g}$ of linear momentum of the electromagnetic field is connected to the energy flux (Poynting vector) by

$$\vec{S} \;=\; c^2\, \vec{g}\,. \tag{A.38}$$

The total linear momentum of a classical system particles + fields is thus

$$\vec{P} \;=\; \sum\nolimits_i m_i \vec{v}_i(t) \;+\; \epsilon_0 \int d^3 r\; \left[\vec{E}\,(\vec{r}, t) \times \vec{B}\,(\vec{r}, t)\right] \tag{A.39}$$

The demonstration is cumbersome and ius here not given.
Let us consider some examples.

Example 1: Relativistic particles of rest mass $m \neq 0$.
Let n be the number of particles per unit volume. It is easy to see that

$$\vec{g} = n\,\gamma m\vec{v}\,, \qquad \vec{S} = n\,\gamma mc^2\,\vec{v}\,. \tag{A.40}$$

Example 2: Relativistic particles of rest mass $m = 0$ (photons).
Let n be the number of photons per unit volume. The photon energy and momentum are

$$\epsilon = h\nu = cp\,, \qquad \vec{p} = \hbar\vec{k} = \frac{h\nu}{c}\hat{u}\,. \tag{A.41}$$

The magnitudes of energy flux and momentum density are

$$S = n\epsilon c\,, \qquad g = np = n\epsilon/c\,. \tag{A.42}$$

Example 3: Plane wave impinging on a charge q and exerting the force $\vec{F} = q(\vec{E} + \vec{v} \times \vec{B})$.
The electric field induces a motion of the charge with velocity $\vec{v} \perp \vec{B}$. As a consequence, the magnetic field induces a force in the direction of propagation (radiation pressure) of magnitude $F_B = qvB = qvE/c = vF_e/c$. The average power lost by the field is $dW/dt = \langle vF_E \rangle$. The radiation pressure is

$$\frac{\langle F_B \rangle}{A} \;=\; \frac{1}{A}\frac{dp}{dt} \;=\; \frac{1}{A}\frac{1}{c}\frac{dW}{dt}\,, \tag{A.43}$$

whence

$$gc \;=\; S/c\,. \tag{A.44}$$

A.1.5 Angular momentum

The total angular momentum of a classical system particles + fields is

$$\vec{J} \;=\; \sum\nolimits_i [m_i\,\vec{r}_i(t) \times \vec{v}_i(t)] \;+\; \epsilon_0 \int d^3r\, \left\{\vec{r} \times \left[\vec{E}\,(\vec{r},t) \times \vec{B}\,(\vec{r},t)\right]\right\} \tag{A.45}$$

A.2 Scalar and vector potentials

[Reference: [Feynman et al., 1977] II, Section 18-6].

The properties of an electromagnetic field are completely specified by the knowledge of the electric and magnetic fields $\vec{E}(\vec{r},t)$ and $\vec{B}(\vec{r},t)$, say by their six components.

In many instances it is however more convenient to describe the electromagnetic field by two alternative quantities, the vector potential $\vec{A}(\vec{r},t)$ and the scalar potential $U(\vec{r},t)$. Let us first see how the two potentials are connected to the electric and magnetic fields.

A) The Maxwell equation (A.7), $\vec{\nabla}\cdot\vec{B} = 0$, implies that a vector field $\vec{A}$ exists, such that $\vec{B} = \vec{\nabla}\times\vec{A}$.
B) By substituting $\vec{B} = \vec{\nabla} \times \vec{A}$ in the Maxwell equation (A.8), one gets

$$\vec{\nabla} \times \left(\vec{E} + \frac{\partial\vec{A}}{\partial t}\right) = 0\,, \qquad \text{so that} \quad \vec{E} + \frac{\partial\vec{A}}{\partial t} = -\vec{\nabla}U\,,$$

since a vector whose curl is zero can be expresses as the gradient of a scalar function.

In conclusion, the two vectors $\vec{B}(\vec{r},t)$ and $\vec{E}(\vec{r},t)$ can be connected to a scalar field $U(\vec{r},t)$ and a vectorial field $\vec{A}(\vec{r},t)$ through the following relations:

$$\vec{B} = \vec{\nabla} \times \vec{A}\,, \qquad \vec{E} = -\,\vec{\nabla}U - \frac{\partial\vec{A}}{\partial t} \tag{A.46}$$

Note 1: $\vec{A}$ and $\vec{E}$ are polar vectors, $\vec{B}$ is an axial vector.

Note 2: The potentials $\vec{A}$ and U are not observable quantities, as the electric and magnetic fields are (see below). Actually, they are useful mathematical entities, which simplify the treatment of a number of problems. One first advantage is that they characterise the electromagnetic field in terms of only four scalar quantities (U, A_x, A_y, A_z) instead of the six components of $\vec{E}$ and $\vec{B}$.
We will see later on that the potentials $\vec{A}$ and U facilitate the Lagrangian and Hamiltonian formulations of the interaction of radiation with matter.

Maxwell equations with potentials

Maxwell equations (A.7) and (A.8) have been used to define the scalar and vector potentials.
By substitution, the two remaining Maxwell equations (A.6) and (A.9) can be expressed in terms of the potentials as follows:

$$\nabla^2 U(\vec{r},t) = \frac{1}{\epsilon_0}\rho(\vec{r},t) - \vec{\nabla}\cdot\frac{\partial}{\partial t}\vec{A}(\vec{r},t) \tag{A.47}$$

$$\left[\frac{1}{c^2}\frac{\partial^2}{\partial t^2} - \nabla^2\right]\vec{A}(\vec{r},t) = \frac{1}{\epsilon_0 c^2}\vec{J}(\vec{r},t) - \vec{\nabla}\left[\vec{\nabla}\cdot\vec{A}(\vec{r},t) + \frac{1}{c^2}\frac{\partial}{\partial t}U(\vec{r},t)\right] \tag{A.48}$$

Only two equations are thus sufficient to connect the potentials to the charge and current densities.

A.2.1 Gauge transformations of potentials

The potentials $\vec{A}$ and U are not observable quantities; the Maxwell equations are unchanged if the following substitutions are made:

$$\vec{A} \rightarrow \vec{A} + \vec{\nabla} f(\vec{r},t) = \vec{A}', \qquad U \rightarrow U - \frac{\partial}{\partial t} f(\vec{r},t) = U', \tag{A.49}$$

where $f(\vec{r},t)$ is any differentiable function of $\vec{r}$ and t.
By substituting $\vec{A} \rightarrow \vec{A}'$ and $U \rightarrow U'$, the fields $\vec{E}$ and $\vec{B}$, say the observable quantities of the electromagnetic field, are unchanged:

$$\vec{B} = \vec{\nabla}\times\vec{A}', \qquad \vec{E} = -\vec{\nabla}U' - \frac{\partial\vec{A}'}{\partial t}. \tag{A.50}$$

The two vectors $\vec{A}$ and $\vec{A}'$ have the same curl $\vec{B}$, but, according to (A.49), a different divergence:

$$\vec{\nabla}\cdot\vec{A}' = \vec{\nabla}\cdot\vec{A} + \nabla^2 f(\vec{r},t). \tag{A.51}$$

The arbitrariness of the function $f(\vec{r},t)$ implies the arbitrariness in the choice of $\vec{\nabla}\cdot\vec{A}$ (*gauge choice*). This arbitrariness may be exploited to optimise the choice of the potentials according to the peculiarities of the phenomenon to be described.
One can show that the basic equations of both classical and quantum mechanics are not affected by different gauge choices.
The two most commonly used gauges are the Lorenz and the Coulomb gauge.

Note: The Lorenz gauge is due to the Danish physicist Ludwig Lorenz, not to be confused with the Dutch physicist Hendrick Lorentz.

A.2.2 Lorenz gauge

By imposing to the potentials the condition (Lorenz gauge)

$$\vec{\nabla}\cdot\vec{A} = -\frac{1}{c^2}\frac{\partial U}{\partial t}, \tag{A.52}$$

the Maxwell equations (Gauss and Ampère laws) for the potentials (A.47) and (A.48) become:

$$\nabla^2 U - \frac{1}{c^2}\frac{\partial^2 U}{\partial t^2} = -\frac{\rho}{\epsilon_0} \tag{A.53}$$

$$\nabla^2 \vec{A} - \frac{1}{c^2}\frac{\partial^2 \vec{A}}{\partial t^2} = -\frac{\vec{J}}{\epsilon_0 c^2} \tag{A.54}$$

The symmetry of (A.53) and (A.54) is appealing; the scalar and vector potentials are uncoupled, the scalar potential is connected to the charge density, the vector potential to the current density.

Fields in vacuum, electromagnetic waves and potentials

In vacuum, the Maxwell equations for the potentials in the Lorenz gauge (A.53) and (A.54) reduce to the wave equations

$$\nabla^2 U - \frac{1}{c^2}\frac{\partial^2 U}{\partial t^2} = 0 \tag{A.55}$$

$$\nabla^2 \vec{A} - \frac{1}{c^2}\frac{\partial^2 \vec{A}}{\partial t^2} = 0 \tag{A.56}$$

The electromagnetic waves can thus be described in terms of the four scalar quantities U, A_x, A_y, A_z.

A.2.3 Coulomb gauge (radiation gauge)

By imposing to the potentials the alternative condition

$$\vec{\nabla} \cdot \vec{A} = 0\,, \tag{A.57}$$

the Maxwell equations for the potentials become:

$$\nabla^2 U = -\frac{\rho}{\epsilon_0}\,, \tag{A.58}$$

$$\nabla^2 \vec{A} - \frac{1}{c^2}\frac{\partial^2 \vec{A}}{\partial t^2} = -\frac{\vec{J}}{\epsilon_0 c^2}\,. \tag{A.59}$$

The Coulomb gauge does not preserve the relativistic covariance, and is suited for static charge distributions (the term $\partial^2 U/\partial t^2$ is missing).
For *empty space* ($\rho = 0, \vec{J} = 0$), one can add the condition $U = 0$ and obtain the wave equation containing only the vector potential:

$$\nabla^2 \vec{A} - \frac{1}{c^2}\frac{\partial^2 \vec{A}}{\partial t^2} = 0\,. \tag{A.60}$$

The choice $U = 0, \vec{\nabla} \cdot \vec{A} = 0$ is also called *radiation gauge*. The radiation gauge is particularly useful to treat the interaction of radiation with matter (see below).

A.2.4 The potentials and their sources

In the **static case** (say when the distributions of charges and currents are independent of time), the Maxwell equations reduce to

$$\vec{\nabla} \cdot \vec{E} = \rho/\epsilon_0 \qquad \vec{\nabla} \times \vec{B} = \mu_0 \vec{J} \tag{A.61}$$

$$\vec{\nabla} \times \vec{E} = 0 \qquad \vec{\nabla} \cdot \vec{B} = 0 \tag{A.62}$$

Since now $\vec{E} = \vec{\nabla} U$ (no $\vec{A}$ contribution), the relation between scalar potential and electric charge is the Poisson equation

$$\nabla^2 U = -\rho/\epsilon_0\,. \tag{A.63}$$

For the magnetic field, since $\vec{B} = \vec{\nabla} \times \vec{A}$,

$$\vec{\nabla} \times \vec{B} = \vec{\nabla} \times (\vec{\nabla} \times \vec{A}) = \vec{\nabla}(\vec{\nabla} \cdot \vec{A}) - \nabla^2 \vec{A} = \mu_0 \vec{J}. \tag{A.64}$$

In the Coulomb gauge, $\vec{\nabla} \cdot \vec{A} = 0$, the relation between vector potential and current density becomes

$$\nabla^2 \vec{A} = -\mu_0 \vec{J}. \tag{A.65}$$

The potentials at point 1 depend on the distributions of charge ρ and current $\vec{J}$ at various points 2 according to the well known expressions:

$$U(1) = \frac{1}{4\pi\epsilon_0} \int \frac{\rho(2)}{r_{12}}\, dV_2\,, \qquad \vec{A}(1) = \frac{\mu_0}{4\pi} \int \frac{\vec{J}(2)}{r_{12}}\, dV_2 \tag{A.66}$$

If the distributions of charges and currents are **time-dependent**, the potentials of the Lorenz gauge at the point 1 and time t are obtained from the distributions of charge ρ and current $\vec{J}$ at the positions 2 at the retarded times $t' = r_{12}/c$:

$$U(1,t) = \frac{1}{4\pi\epsilon_0} \int \frac{\rho(2, t - r_{12}/c)}{r_{12}}\, dV_2\,, \qquad \vec{A}(1,t) = \frac{\mu_0}{4\pi} \int \frac{\vec{J}(2, t - r_{12}/c)}{r_{12}}\, dV_2\,. \tag{A.67}$$

Again, the scalar potential U only depends on the charge density, the vector potential $\vec{A}$ only depends on the current density $\vec{J}$.

A.3 Electrodynamics in reciprocal space

A.3.1 Fourier transforms of the fields and equations

Spatial Fourier transform

Following § I.B. of [Cohen-Tannoudji et al., 2004], we consider the spatial Fourier Transform of the fields. Accordingly, the vectors $V(\vec{r}, t)$ in real space are connected to the vectors $\vec{\mathcal{V}}(\vec{k}, t)$ in reciprocal space by the relations

$$\vec{V}(\vec{r}, t) = \frac{1}{(2\pi)^{3/2}} \int d^3k\, \vec{\mathcal{V}}(\vec{k}, t)\, e^{i\vec{k}\cdot\vec{r}}\,, \qquad \vec{\mathcal{V}}(\vec{k}, t) = \frac{1}{(2\pi)^{3/2}} \int d^3r\, \vec{V}(\vec{r}, t)\, e^{-i\vec{k}\cdot\vec{r}}\,. \tag{A.68}$$

Note that the units of $V(\vec{r}, t)$ and $\vec{\mathcal{V}}(\vec{k}, t)$ differ by a factor proportional to a volume.
The first equation corresponds to the expansion of a vectorial function $V(\vec{r}, t)$ into plane waves. Since the functions $V(\vec{r}, t)$ here considered are real (electric and magnetic fields, etc.), the complex F.T. functions obey the relations

$$\vec{\mathcal{V}}^*(\vec{k}, t) \;=\; \vec{\mathcal{V}}(-\vec{k}, t)\,, \tag{A.69}$$

so that, when integrating over all the reciprocal space, the imaginary parts cancel out.

Maxwell equations

Taking into account the properties of Fourier transform, the Maxwell equations (A.6)–(A.9) in reciprocal space become

$$i\,\vec{k} \cdot \vec{\mathcal{E}}(\vec{k}, t) \;=\; \frac{1}{\epsilon_0}\, \varrho\,(\vec{k}, t) \tag{A.70}$$

$$i\,\vec{k} \cdot \vec{\mathcal{B}}(\vec{k}, t) \;=\; 0 \tag{A.71}$$

$$i\,\vec{k} \times \vec{\mathcal{E}}\,(\vec{k}, t) \;=\; -\,\frac{\partial}{\partial t}\, \vec{\mathcal{B}}\,(\vec{k}, t) \tag{A.72}$$

$$i\,\vec{k} \times \vec{\mathcal{B}}\,(\vec{k}, t) \;=\; \frac{1}{c^2}\, \frac{\partial}{\partial t} \vec{\mathcal{E}}, (\vec{k}, t) \,+\, \frac{1}{\epsilon_0 c^2}\, \vec{\mathcal{J}}\,(\vec{k}, t) \tag{A.73}$$

- Maxwell equations (A.6)–(A.9) in real space are partial differential equations.
- Maxwell equations (A.70)–(A.73) in reciprocal space are local equations, which introduces a great semplification.

The continuity equation is

$$i\,\vec{k}\cdot\vec{\mathcal{J}}(\vec{k},t) \;+\; \frac{\partial}{\partial t}\,\varrho\,(\vec{k},t)\,. \tag{A.74}$$

Potentials

Local relations hold also between fields and potentials

$$\vec{\mathcal{B}}(\vec{k},t) \;=\; i\,\vec{k}\times\vec{\mathcal{A}}(\vec{k},t)\,, \qquad \vec{\mathcal{E}}(\vec{k},t) \;=\; -i\frac{\partial}{\partial t}\vec{\mathcal{A}}(\vec{k},t) - i\,\vec{k}\mathcal{U}(\vec{k},t)\,, \tag{A.75}$$

and local are the Maxwell equations for potentials

$$k^2\,\mathcal{U} \;=\; \frac{1}{\epsilon_0}\,\varrho \;+\; i\,\vec{k}\cdot\frac{\partial}{\partial t}\vec{\mathcal{A}} \tag{A.76}$$

$$\frac{1}{c^2}\,\frac{\partial^2}{\partial t^2}\vec{\mathcal{A}} + k^2\vec{\mathcal{A}} \;=\; \frac{1}{\epsilon_0 c^2}\,\vec{\mathcal{J}} - i\,\vec{k}\left(i\,\vec{k}\cdot\vec{\mathcal{A}} + \frac{1}{c^2}\frac{\partial}{\partial t}\,\mathcal{U}\right)\,. \tag{A.77}$$

A.3.2 Longitudinal and transverse fields

Definition

Longitudinal and transverse fields (or longitudinal and transverse components of fields) can be defined both in the real and reciprocal space). The definition in reciprocal space is more transparent.

A **longitudinal vector field** is such that

$$\vec{\nabla}\times\vec{V}_{\parallel}(\vec{r}) \;=\; 0\,, \qquad \text{in real space} \tag{A.78}$$

$$i\,\vec{k}\times\vec{\mathcal{V}}_{\parallel}(\vec{k}) \;=\; 0\,, \qquad \text{in reciprocal space} \tag{A.79}$$

for all $\vec{r}$ and all $\vec{k}$.

A **transverse vector field** is such that

$$\vec{\nabla}\cdot\vec{V}_{\perp}(\vec{r}) \;=\; 0\,, \qquad \text{in real space} \tag{A.80}$$

$$i\,\vec{k}\cdot\vec{\mathcal{V}}_{\perp}(\vec{k}) \;=\; 0\,, \qquad \text{in reciprocal space} \tag{A.81}$$

for all $\vec{r}$ and all $\vec{k}$.

Electric and magnetic fields

The first two of Maxwell equations define the longitudinal and transverse character of electric and magnetic fields.

- The magnetic field is purely transverse, since its divergence is always zero..
- The electric field would be purely transverse only if no charge where present anywhere in space.
- The longitudinal component of the electric field is connected to the distribution of charges; for a discrete set of charges one can see that (§ I.B. of [Cohen-Tannoudji et al., 2004])

$$\vec{E}_{\parallel}(\vec{r},t) \;=\; \frac{1}{4\pi\epsilon_0}\,\sum_i q_i\frac{\vec{r}-\vec{r}_i(t)}{|\vec{r}-\vec{r}_i(t)|^3}\,. \tag{A.82}$$

Note: The longitudinal electric field is instantaneous. Actually, one can show that also the transverse electric field $\vec{E}_{\perp}$ has an instantaneous component which cancels that of $\vec{E}_{\parallel}$, so that the total field $\vec{E}=\vec{E}_{\perp}+\vec{E}_{\parallel}$ is actually retarded.

Coulomb gauge and potentials

In the Coulomb gauge,

$$\vec{A}_{\parallel} \;=\; 0\,. \tag{A.83}$$

Energy and momentum

We have seen before that the total energy of a system of particles embedded in an electromagnetic field is

$$H_{\rm tot} \;=\; \sum\nolimits_i \frac{1}{2} m_i v_i^2(t) \;+\; \frac{\epsilon_0}{2} \int d^3r \,\left[E^2(\vec{r},t) + c^2\, B^2(\vec{r},t)\right] \tag{A.84}$$

and the total momentum is

$$\vec{P}_{\rm tot} \;=\; \sum\nolimits_i m_i \vec{v}_i(t) \;+\; \epsilon_0 \int d^3r \,\left[\vec{E}\,(\vec{r},t) \times \vec{B}\,(\vec{r},t)\right] \tag{A.85}$$

The longitudinal part of the field energy corresponds to the Coulomb potential energy

$$H_{\rm long} \;=\; \frac{\epsilon_0}{2} \int d^3r\, E_{\parallel}^2(\vec{r},t) \;=\; U_{\rm coul} \;=\; \frac{1}{8\pi\epsilon_0} \sum_{ij} \frac{q_i q_j}{|\vec{r}_i - \vec{r}_j|} \tag{A.86}$$

(including the divergent self-energy).
The transverse part is

$$H_{\rm trans} \;=\; \frac{\epsilon_0}{2} \int d^3r \,\left[E_{\perp}^2(\vec{r},t) + c^2\, B^2(\vec{r},t)\right] \tag{A.87}$$

The longitudinal part of the field momentum can be transformed to reciprocal space making use of the Parseval relation

$$\vec{P}_{\rm long} \;=\; \epsilon_0 \int d^3r \,\left[\vec{E}_{\parallel}\,(\vec{r},t) \times \vec{B}\,(\vec{r},t)\right] = \;\epsilon_0 \int d^3k \,\left[\vec{\mathcal{E}}_{\parallel}^{*}\,(\vec{r},t) \times \vec{\mathcal{B}}\,(\vec{r},t)\right] \tag{A.88}$$

From the first Maxwell equation in reciprocal space, the relation between $\mathcal{B}$ and $\mathcal{A}$ and the identity $\vec{a} \times (\vec{b} \times \vec{c}) = (\vec{a}\cdot\vec{c})\vec{b} - (\vec{a}\cdot\vec{b})\vec{c}$, one obtains

$$\begin{aligned}
\vec{P}_{\rm long} \;&=\; \epsilon_0 \int d^3k\, \frac{1}{\epsilon_0}\, \varrho^*(\vec{k})\, \frac{\vec{k}}{k^2} \;\times\; \left[i\,\vec{k} \times \vec{\mathcal{A}}\right] \\
&=\; \int d^3k\, \varrho^*(\vec{k}) \,\left[\vec{\mathcal{A}} - \hat{k}(\hat{k}\cdot\vec{\mathcal{A}}\right] \\
&=\; \int d^3k\, \varrho^*(\vec{k}) \,\left[\vec{\mathcal{A}} - \vec{\mathcal{A}}_{\parallel}\right] \;=\; \int d^3k\, \varrho^*(\vec{k})\, \vec{\mathcal{A}}_{\perp}\,.
\end{aligned} \tag{A.89}$$

and finally, coming back to the real space,

$$\vec{P}_{\rm long} \;=\; \int d^3r\, \rho^*(\vec{r})\, \vec{A}_{\perp}(\vec{r}) \;=\; \sum_i q_i \vec{A}_{\perp}\,. \tag{A.90}$$

The transverse part of the field momentum is

$$\vec{P}_{\rm trans} \;=\; \epsilon_0 \int d^3r \,\left[\vec{E}_{\perp}\,(\vec{r},t) \times \vec{B}\,(\vec{r},t)\right] \tag{A.91}$$

The total momentum can thus be expressed as

$$\vec{P}_{\rm tot} \;=\; \sum\nolimits_i m_i \vec{v}_i(t) \;+\; \sum\nolimits_i q_i \vec{A}_{\perp} \;+\; \epsilon_0 \int d^3r \,\left[\vec{E}_{\perp}(\vec{r},t) \times \vec{B}\,(\vec{r},t)\right] \tag{A.92}$$

$$=\; \sum\nolimits_i \vec{P}_i \;+\; \epsilon_0 \int d^3r \,\left[\vec{E}_{\perp}(\vec{r},t) \times \vec{B}\,(\vec{r},t)\right] \tag{A.93}$$

where the quantity

$$\vec{P}_i \;=\; m_i\vec{v}_i + q_i\vec{A}_\perp \tag{A.94}$$

is the conjugate momentum of the position $\vec{r}_i$ in the lagrangian and hamiltonian formalisms (see below).
Substituting

$$\vec{v}_i \;=\; \frac{1}{m_i}(\vec{P}_i - q_i\vec{A}_\perp) \tag{A.95}$$

in (**??**) and assuming the Coulomb gauge, where $\vec{A}_\perp = \vec{A}$, the total energy can be written as

$$H_{\rm tot} \;=\; \sum_i \frac{1}{2m_i}\left[\vec{P}_i - q_i\vec{A}\right]^2 \;+\; U_{\rm coul} \;+\; H_{\rm trans} \tag{A.96}$$

A.4 Normal coordinates

In real space, the last two Maxwell equations in vacuum, (A.13) and (A.14), lead to the wave equations for the fields $\vec{E}$ and $\vec{B}$, (A.15) and (A.16).
Wave equations are obtained for the scalar and vector potentials in the Lorenz gauge and for the vector potential in the Coulomb gauge.
We want now to study the description of waves in the reciprocal space. To that purpose, let us consider the transverse part of the last two Maxwell equations (A.72) and (A.73) in vacuum. The transverse parts are sufficient to describe electromagnetic waves (let us put $\vec{\mathcal{J}} = 0$).
In reciprocal space the equations can be rewritten

$$\frac{\partial}{\partial t}\vec{\mathcal{B}}(\vec{k},t) \;=\; -i\,\vec{k}\times\vec{\mathcal{E}}_\perp(\vec{k},t) \tag{A.97}$$

$$\frac{\partial}{\partial t}\vec{\mathcal{E}}_\perp(\vec{k},t) \;=\; i\,c^2\,\vec{k}\times\vec{\mathcal{B}}(\vec{k},t) \tag{A.98}$$

say, making the cross product of $\vec{k}$ by the first equation,

$$\vec{k}\times\frac{\partial}{\partial t}\vec{\mathcal{B}}(\vec{k},t) \;=\; i\,k^2\,\vec{\mathcal{E}}_\perp(\vec{k},t) \tag{A.99}$$

$$\frac{\partial}{\partial t}\vec{\mathcal{E}}_\perp(\vec{k},t) \;=\; i\,c^2\,\vec{k}\times\vec{\mathcal{B}}(\vec{k},t) \tag{A.100}$$

Multiplying the second equation by c/k and summing the two equations, one obtains

$$\frac{\partial}{\partial t}\left(\vec{\mathcal{E}}_\perp \pm c\hat{k}\times\vec{\mathcal{B}}\right) \;=\; \pm i\omega\,\left(\vec{\mathcal{E}}_\perp \pm c\hat{k}\times\vec{\mathcal{B}}\right) \tag{A.101}$$

where $\omega = ck$ and $\hat{k} = \vec{k}/k$.

Classical normal coordinates

It is convenient to introduce a new complex vector variable

$$\vec{\alpha}(\vec{k},t) \;=\; -\frac{i}{2}\sqrt{\frac{2\epsilon_0}{\hbar\omega}}\;\left[\vec{\mathcal{E}}_\perp(\vec{k},t) + c\,\hat{k}\,\times\vec{\mathcal{B}}(\vec{k},t)\right] \tag{A.102}$$

where the normalisation constant under square root has been written in a form that facilitates the transition to the quantum approach.
The (real) fields are thus expressed as

$$\vec{\mathcal{E}}_\perp(\vec{k},t) \;=\; i\sqrt{\frac{\hbar\omega}{2\epsilon_0}}\;\left[\vec{\alpha}(\vec{k},t) + \vec{\alpha}^{\,*}(-\vec{k},t)\right] \tag{A.103}$$

$$\vec{\mathcal{B}}(\vec{k},t) \;=\; \frac{i}{c}\sqrt{\frac{\hbar\omega}{2\epsilon_0}}\;\left[\hat{k}\times\vec{\alpha}(\vec{k},t) - \hat{k}\times\vec{\alpha}^{\,*}(-\vec{k},t)\right] \tag{A.104}$$

The vector potential is (Coulomb gauge)

$$\vec{\mathcal{A}}(\vec{k},t) \;=\; \vec{\mathcal{A}}_{\perp}(\vec{k},t) \;=\; \sqrt{\frac{\hbar}{2\epsilon_0\omega}}\left[\vec{\alpha}(\vec{k},t)+\vec{\alpha}^{\,*}(-\vec{k},t)\right] \tag{A.105}$$

Normal coordinates and harmonic oscillators

The Maxwell equations in vacuum correspond to the equation for the complex vector variable α (normal coordinate)

$$\frac{d}{dt}\,\vec{\alpha}(\vec{k},t) \;=\; -i\omega\,\vec{\alpha}(\vec{k},t)\,. \tag{A.106}$$

This equation is the equation of the normal coordinates of harmonic oscillators.
Let us consider a classical harmonic oscillator, of coordinate x and momentum p. The Hamilton equations are

$$\frac{dx}{dt}=\frac{\partial H}{\partial p}=\frac{p}{m}\,,\qquad \frac{dp}{dt}=-\frac{\partial H}{\partial x}=-m\omega^2 x \tag{A.107}$$

Introducing the new adimensional dynamical variables

$$\hat{x}=\sqrt{\frac{m\omega}{\hbar}}\,x\,,\qquad \hat{p}=\sqrt{\frac{1}{m\omega\hbar}}\,p \tag{A.108}$$

(where the factor $\hbar$ is introduced to simplify the transition to the quantum case) the Hamitlon equations become very symmetrical

$$\frac{d\hat{x}}{dt}=\omega\,\hat{p}\,,\qquad \frac{d\hat{p}}{dt}=-\omega\,\hat{p} \tag{A.109}$$

Finally, let us introduce the complex variable α (and its complex conjugate α^*)

$$\alpha(t) \;=\; \frac{1}{\sqrt{2}}\,(\hat{x}+i\hat{y})\;,\qquad \alpha^*(t) \;=\; \frac{1}{\sqrt{2}}\,(\hat{x}-i\hat{y}) \tag{A.110}$$

The Hamitlon equations for $\hat{x}$ and $\hat{p}$ can be expressed into a single equation for α

$$\frac{d\alpha(t)}{dt} \;=\; -i\omega\,\alpha(t) \tag{A.111}$$

whose solution is

$$\alpha(t) \;=\; \alpha_0\,e^{-i\omega t} \tag{A.112}$$

The total classical energy is

$$H \;=\; \frac{p^2}{2m}+\frac{1}{2}m\omega^2 x \;=\; \frac{1}{2}\hbar\omega\,(\hat{p}^2+\hat{x}^2) \;=\; \hbar\omega\,|\alpha_0|^2. \tag{A.113}$$

The normal variables $\vec{\alpha}(\vec{k},t)$ behave as harmonic oscillators. They define the normal modes of the classical electromagneti field.
The quantization of the electromagnetic field is achieved by substituting the normal variables α and α^* with annihilation and creation operators.

Classical real-space quantities (continuum case)

Let us now come back to the electromagnetic field in real space and take into account that $\alpha(t) = \alpha_0\,\exp(-i\omega t)$.
The fields and the potential vector are

$$\vec{E}_{\perp}(\vec{r},t) \;=\; i\int d^3k\sum\nolimits_{\epsilon}\mathcal{E}_{\omega}\left[\alpha_{\epsilon 0}(\vec{k})\,\hat{\epsilon}\,e^{i(\vec{k}\cdot\vec{r}-\omega t)} \;+\; \alpha^*_{\epsilon 0}(\vec{k})\,\hat{\epsilon}\,e^{-i(\vec{k}\cdot\vec{r}-\omega t)}\right] \tag{A.114}$$

$$\vec{B}(\vec{r},t) \;=\; i\int d^3k\sum\nolimits_{\epsilon}\mathcal{B}_{\omega}\left[\alpha_{\epsilon 0}(\vec{k})\,\hat{k}\times\hat{\epsilon}\,e^{i(\vec{k}\cdot\vec{r}-\omega t)} \;+\; c.c.\right] \tag{A.115}$$

$$\vec{A}_{\perp}(\vec{r},t) \;=\; \int d^3k\sum\nolimits_{\epsilon}\mathcal{A}_{\omega}\left[\alpha_{\epsilon 0}(\vec{k})\,\hat{\epsilon}\,e^{i(\vec{k}\cdot\vec{r}-\omega t)} \;+\; c.c.\right] \tag{A.116}$$

where

$$\mathcal{E}_\omega \;=\; \sqrt{\frac{\hbar\omega}{2\epsilon_0(2\pi)^3}}\,, \qquad \mathcal{B}_\omega = \frac{\mathcal{E}_\omega}{c}\,, \qquad \mathcal{A}_\omega = \frac{\mathcal{E}_\omega}{\omega} \tag{A.117}$$

and $\hat{\epsilon}$ is the polarisation unit vector (2 directions, normal to $\vec{k}$).
The transverse field energy and momentum are

$$H_{\text{trans}} \;=\; \int d^3k \sum\nolimits_\epsilon \frac{\hbar\omega}{2}\left[\alpha^*_\epsilon(\vec{k})\alpha_\epsilon(\vec{k}) + \alpha_\epsilon(\vec{k})\alpha^*_\epsilon(\vec{k})\right] \tag{A.118}$$

$$\vec{P}_{\text{trans}} \;=\; \int d^3k \sum\nolimits_\epsilon \frac{\hbar\vec{k}}{2}\left[\alpha^*_\epsilon(\vec{k})\alpha_\epsilon(\vec{k}) + \alpha_\epsilon(\vec{k})\alpha^*_\epsilon(\vec{k})\right] \tag{A.119}$$

where $\omega = ck$.

Classical real-space quantities (discrete case)

Let us introduce the expressions of the field quantities in the discrete case, where the Fourier integrals are substituted by the Fourier series.
The fields and the potential vector are now

$$\vec{E}_\perp(\vec{r},t) \;=\; i\sum_{\vec{k}s}\sqrt{\frac{\hbar\omega_{\vec{k}s}}{2\epsilon_0 V}}\left[\alpha_{\vec{k}s}\,e^{i(\vec{k}\cdot\vec{r})} \;+\; \alpha^*_{\vec{k}s}\,e^{-i(\vec{k}\cdot\vec{r})}\right]\hat{\epsilon}_{\vec{k}s} \tag{A.120}$$

$$\vec{B}(\vec{r},t) \;=\; i\sum_{\vec{k}s}\sqrt{\frac{\hbar\omega_{\vec{k}s}}{2\epsilon_0 c^2 V}}\left[\alpha_{\vec{k}s}\,e^{i(\vec{k}\cdot\vec{r})} \;+\; \alpha^*_{\vec{k}s}\,e^{-i(\vec{k}\cdot\vec{r})}\right](\vec{k}\times\hat{\epsilon}_{\vec{k}s}) \tag{A.121}$$

$$\vec{A}_\perp(\vec{r},t) \;=\; \sum_{\vec{k}s}\sqrt{\frac{\hbar}{2\epsilon_0 V\omega_{\vec{k}s}}}\left[\alpha_{\vec{k}s}\,e^{i(\vec{k}\cdot\vec{r})} \;+\; \alpha^*_{\vec{k}s}\,e^{-i(\vec{k}\cdot\vec{r})}\right]\hat{\epsilon}_{\vec{k}s} \tag{A.122}$$

where s is the polarisation index and

$$\alpha \;=\; \alpha_0\,e^{i\omega t}\,. \tag{A.123}$$

The transverse field energy and momentum are

$$H_{\text{trans}} \;=\; \sum_{\vec{k}s}\frac{\hbar\omega_{\vec{k}s}}{2}\left[\alpha^*_{\vec{k}s}\alpha_{\vec{k}s} + \alpha_{\vec{k}s}\alpha^*_{\vec{k}s}\right] \tag{A.124}$$

$$\vec{P}_{\text{trans}} \;=\; \sum_{\vec{k}s}\frac{\hbar\vec{k}}{2}\left[\alpha^*_{\vec{k}s}\alpha_{\vec{k}s} + \alpha_{\vec{k}s}\alpha^*_{\vec{k}s}\right] \tag{A.125}$$

where $\omega_{\vec{k}s} = ck$.

A.5 Quantisation of the field

Quantum operators

The transition to the quantum treatment can be obtained by substituting the normal variables $\alpha(\vec{k})$ and $\alpha^*(\vec{k})$ with the annihilation and creation operators $a(\vec{k})$ and $a^\dagger(\vec{k})$.
The commutation relations for annihilation and creation operators in the continuum case are

$$\begin{aligned}[a_\epsilon(\vec{k}),\, a_{\epsilon'}(\vec{k}')] = 0\,, \qquad [a^\dagger_\epsilon(\vec{k}),\, a^\dagger_{\epsilon'}(\vec{k}')] = 0\\ [a_\epsilon(\vec{k}),\, a^\dagger_{\epsilon'}(\vec{k}')] = \delta_{\epsilon\epsilon'}\delta(\vec{k}-\vec{k}')\end{aligned} \tag{A.126}$$

The fields and the potential operators are

$$\vec{E}_\perp(\vec{r},t) = i\sum_{\vec{k}s}\sqrt{\frac{\hbar\omega_{\vec{k}s}}{2\epsilon_0 V}}\left[a_{\vec{k}s}\,e^{i(\vec{k}\cdot\vec{r})} + a^\dagger_{\vec{k}s}\,e^{-i(\vec{k}\cdot\vec{r})}\right]\hat{\epsilon}_{\vec{k}s} \tag{A.127}$$

$$\vec{B}(\vec{r},t) = i\sum_{\vec{k}s}\sqrt{\frac{\hbar\omega_{\vec{k}s}}{2\epsilon_0 c^2 V}}\left[a_{\vec{k}s}\,e^{i(\vec{k}\cdot\vec{r})} + a^\dagger_{\vec{k}s}\,e^{-i(\vec{k}\cdot\vec{r})}\right](\vec{k}\times\hat{\epsilon}_{\vec{k}s}) \tag{A.128}$$

$$\vec{A}_\perp(\vec{r},t) = \sum_{\vec{k}s}\sqrt{\frac{\hbar}{2\epsilon_0 V\omega_{\vec{k}s}}}\left[a_{\vec{k}s}\,e^{i(\vec{k}\cdot\vec{r})} + a^\dagger_{\vec{k}s}\,e^{-i(\vec{k}\cdot\vec{r})}\right]\hat{\epsilon}_{\vec{k}s} \tag{A.129}$$

From creation and annihilation operators one obtains the number operator

$$N_{\vec{k}s} = a^\dagger_{\vec{k}s}a_{\vec{k}s}\,. \tag{A.130}$$

The Hamiltonian operator is

$$H_{\text{trans}} = \sum_{\vec{k}s}\hbar\omega_{\vec{k}s}\left[a^\dagger_{\vec{k}s}a_{\vec{k}s}+\frac{1}{2}\right] = \sum_{\vec{k}s}\hbar\omega_{\vec{k}s}\left[N_{\vec{k}s}+\frac{1}{2}\right] \tag{A.131}$$

and the momentum operator is

$$\vec{P}_{\text{trans}} = \sum_{\vec{k}s}\hbar\vec{k}\left[a^\dagger_{\vec{k}s}a_{\vec{k}s}+\frac{1}{2}\right] = \sum_{\vec{k}s}\hbar\vec{k}\left[a^\dagger_{\vec{k}s}a_{\vec{k}s}\right]. \tag{A.132}$$

In the last step we used the fact that $\sum_{\vec{k}s}\vec{k}=0$, since for eack $\vec{k}$ there is an equivalent $-\vec{k}$.

Single-mode operators

Let us consider the number operator $N_{\vec{k}s}$ for the mode $\vec{k}s$. The eigenvalue equation is

$$N_{\vec{k}s}\,|n_{\vec{k}s}\langle = n_{\vec{k}s}\,|n_{\vec{k}s}\rangle\,. \tag{A.133}$$

The eigenstatesof $N_{\vec{k}s}$ are orthogonal

$$\langle m_{\vec{k}s}|n_{\vec{k}s}\rangle = \delta_{mn}\,. \tag{A.134}$$

To the mode $\vec{k}s$ a Hilbert subspace is associated, whose vectors are linear combinations of the eigenvectors of $N_{\vec{k}s}$:

$$|\Phi_{\vec{k}s}\rangle = \sum\nolimits_{n_{\vec{k}s}} c_{n_{\vec{k}s}}|n_{\vec{k}s}\rangle\,. \tag{A.135}$$

The creation and annihilation operators act on the eigenstates of $N_{\vec{k}s}$ as

$$a^\dagger_{\vec{k}s}\,|n_{\vec{k}s}\rangle = \sqrt{n_{\vec{k}s}+1}\;|n_{\vec{k}s}+1\rangle \tag{A.136}$$

$$a_{\vec{k}s}\,|n_{\vec{k}s}\rangle = \sqrt{n_{\vec{k}s}}\;|n_{\vec{k}s}-1\rangle \tag{A.137}$$

Eigenvalues and eigenstate of the total Hamiltonian

Let us consider the total Hamiltonian of the free electromagnetic field

$$H_{\text{trans}} = \sum\nolimits_{vecks}\hbar\omega_{\vec{k}s}\,[n_{\vec{k}s}+1/2] \tag{A.138}$$

The eigenvalues of the total Hamiltonian are

$$E_{\text{field}} = \sum_{\vec{k}s}\hbar\omega_{\vec{k}s}\left[n_{\vec{k}s}+\frac{1}{2}\right] \tag{A.139}$$

The stationary eigenstates of the Hamiltonian are

$$|\{n_{\vec{k}s}\}\rangle = |n_{\vec{k}_1 s_1}, n_{\vec{k}_2 s_2}, \ldots n_{\vec{k}_i s_i}, \ldots\rangle . \tag{A.140}$$

A pure state of the electromagnetic field is a linear combination of basis states $|\{n_{\vec{k}s}\}\rangle$.
The effects of the creation, annihilation and number operators on the basis states are:

$$a^\dagger_{\vec{k}_i s_i} |\ldots, n_{\vec{k}_i s_i}, \ldots\rangle = \sqrt{n_{\vec{k}_i s_i} + 1}\, |\ldots, n_{\vec{k}_i s_i} + 1, \ldots\rangle \tag{A.141}$$

$$a_{\vec{k}_i s_i} |\ldots, n_{\vec{k}_i s_i}, \ldots\rangle = \sqrt{n_{\vec{k}_i s_i}}\, |\ldots, n_{\vec{k}_i s_i} - 1, \ldots\rangle \tag{A.142}$$

$$N_{\vec{k}_i s_i} |\ldots, n_{\vec{k}_i s_i}, \ldots\rangle = n_{\vec{k}_i s_i} |\ldots, n_{\vec{k}_i s_i}, \ldots\rangle \tag{A.143}$$

Expectation value of the Electric field

The expectation value of the electric field $\vec{E}$ at a given position $\vec{r}$ and at a given time t is

$$\langle \vec{E}(\vec{r}, t)\rangle = \langle \Phi | \vec{E}(\vec{r}, t) | \Phi \rangle , \tag{A.144}$$

where $|\Phi\rangle$ is a pure state of the electromagnetic field, linear combination of basis states $|\{n_{\vec{k}s}\}\rangle$.
If the pure state Φ corresponds to a basis state, say if the number of photon per mode is well defined, the expectation value is identically zero.
The phase and the number of photons are complementary variables.

A.6 Matter-radiation interaction

In this last section of Appendix A, we introduce some basic elements of the mechanism of interaction of radiation with matter. The main goal is to support and complement the treatment of Section 2.2. To this aim, it is necessary to insert in the Schrödinger equation a suitable Hamiltonia.
The unperturbed Hamiltonian of a material system (electron, atom, ...) immersed in an electromagnetic field is the sum of the hamiltonians of the material system $H_{\rm at}$ and of the electromagnetic field $H_{\rm trans} = H_{\rm rad}$:

$$H_0 = H_{\rm at} + H_{\rm rad} , \tag{A.145}$$

independent of time.
The corresponding stationary eigenstates are

$$|\Psi\rangle = |\Phi_{\rm at}\rangle \otimes |\{n_{\vec{k}s}\}\rangle . \tag{A.146}$$

In the following, in order to derive a suitable expression for the Hamiltonian, we start from the Lagrangian approach including the electromagnetic field, we obtain the expression of the conjugate momentum and we conclude with the Hamiltonian approach. We consider first the classical case and then the quantum case.

A.6.1 Classical treatment

It is convenient to start the classical treatment of the matter-radiation interaction by the Lagrange approach and then quite naturally to introduce the Hamilton approach, which is fundamental for the subsequent quantum treatment.

Lagrangian approach for purely mechanical systems

The most general approach to the laws of motion of mechanical systems is given by the Principle of least action (or, more correctly, of stationary action), otherwise known as Hamilton principle. An axiomatic introduction can be found in Chapter 1 of "Mechanics", by [Landau and Lifschitz, 1976]. We limit ourselves here to a simpler approach, restricting our attention to a system composed by a single particle (typically an electron).

For a *single non relativistic particle* one defines a Lagrange function as the difference between the kinetic and the potential energies (Feynman II, Chapter 19 [Feynman et al., 1977]).

$$L(\vec{r},\vec{v}) \;=\; E_k - E_p \;=\; mv^2/2 - V(\vec{r})\,. \tag{A.147}$$

Let us assume that at times t_1 and t_2 the particle is in positions $\vec{r}_1$ and $\vec{r}_2$, respectively. The principle of least action asserts that the motion of the particle between the times t_1 and t_2 is such that the *action*, say the time integral of the Lagrange function of L, is minimum (or stationary):

$$\delta \int_{t_1}^{t_2} L(\vec{r},\vec{v})\,dt \;=\; 0\,. \tag{A.148}$$

By standard variational methods one finds that the least action principle leads to the Lagrange equation

$$\frac{d}{dt}\frac{\partial L}{\partial \vec{v}} - \frac{\partial L}{\partial \vec{r}} \;=\; 0\,. \tag{A.149}$$

Substituting L from (A.153) into (A.149) one obtains the Newton equation of motion

$$m\vec{a} = \vec{F} = -\vec{\nabla}V \tag{A.150}$$

For *complex mechanical systems* (e.g. constrained systems) the Lagrange function is expressed in terms of a suitable set of independent generalised coordinates $\{q_i\}$ and their derivatives $\{\dot{q}_i\}$: $L(q_i,\dot{q}_i)$. The least action principle leads, for each one of the generalised coordinates, to an eqution of motion

$$\frac{d}{dt}\frac{\partial L}{\partial \dot{q}_i} - \frac{\partial L}{\partial q_i} \;=\; 0\,. \tag{A.151}$$

Lagrangian approach including the electromagnetic field

The extension to relativistic particles and/or to systems embedded in an electromagnetic field is far from trivial, the Lagrange function cannot be simply expressed as the difference between kinetic and potential energies. In that cases, one seeks for a Lagrange function suitably defined so that the least action principle leads to the known classical laws of motion.

Let us consider a particle embedded in an electromagnetic field, characterised by the potentials $\vec{A}$ and U (for simplicity we neglect the potential energy V due to other interactions).
One can show that a good Lagrange function is

$$L \;=\; \frac{1}{2}mv^2 \;+\; q\,\vec{v}\cdot\vec{A} - q\,U \;+\; \frac{\epsilon_0}{2}\int d^3r\,\left[E^2(\vec{r}) - c^2B^2(\vec{r})\right]\,, \tag{A.152}$$

where we can distinguish three contributions: *a)* the kinetic energy of the particle, *b)* the interaction of the particle with the electromagnetic field (expressed in terms of the vector and scalar potentials, $\vec{A}$ and U, respectively) and *c)* the spatial integral of the electric and magnetic fields.

Note: It is evident that one cannot consider the Lagrange function (A.152) simply as the difference between kinetic and potential energy contributions. As matter of fact, in the integral the electric and magnetic field contributions have opposite sign.

In our applications it is reasonable to consider the electromagnetic field sufficiently strong so that the integral in (A.152) is unaffected by the interaction with a single particle. In the following we can thus neglect the electric and magnetic fields integral and consider the Lagrange function limited to the first three terms

$$L \;=\; mv^2/2 \;+\; q\,\vec{v}\cdot\vec{A} \;-\; q\,U\,, \tag{A.153}$$

where $\vec{v}$ depends on time, $\vec{A}$ depends both on time and position, U depends only on position. It is worth remembering that the actual values of the potentials $\vec{A}$ and U are not univocally determined, but depend on the gauge choice.

We will now show that the Coulomb-Lorentz force acting on the charge q, say $m\vec{a} = q\vec{E} + q\vec{v} \times \vec{B}$, can be derived in the Lagrangian formalism if one assumes the non-relativistic Lagrange function (A.153).
Actually, by substituting in (A.149) the Lagrangian L from (A.153)

$$\frac{\partial L}{\partial \vec{v}} \;=\; m\vec{v} \;+\; q\vec{A}\,, \tag{A.154}$$

$$\frac{d}{dt}\,\frac{\partial L}{\partial \vec{v}} \;=\; \frac{d}{dt}\,\left[m\vec{v} + q\vec{A}\right] \;=\; m\vec{a} \;+\; q\,\frac{\partial \vec{A}}{dt} \;+\; q\,(\vec{v}\cdot\vec{\nabla})\vec{A}\,, \tag{A.155}$$

$$\begin{aligned}\frac{\partial L}{\partial \vec{r}} \;&=\; q\,\vec{\nabla}(\vec{A}\cdot\vec{v}) \;-\; q\,\vec{\nabla}U \\ &=\; \underbrace{(\vec{A}\cdot\vec{\nabla})\,\vec{v}}_{0} + (\vec{v}\cdot\vec{\nabla})\vec{A} \;+\; \vec{v}\times(\vec{\nabla}\times\vec{A}) \;+\; \underbrace{\vec{A}\times(\vec{\nabla}\times\vec{v})}_{0} \;-\; q\,\vec{\nabla}U\,,\end{aligned} \tag{A.156}$$

one obtains the expression of the Coulomb-Lorentz force

$$m\vec{a} \;=\; -q\,\left[\vec{\nabla}U + \frac{\partial \vec{A}}{\partial t}\right] \;+\; q\,\vec{v}\times\,(\vec{\nabla}\times\vec{A}) = \;q\,\vec{E} \;+\; q\,\vec{v}\times\vec{B}\,, \tag{A.157}$$

which is independent of the gauge choice.

Hamiltonian approach

The Lagrangian L is a function of position $\vec{r}$ and velocity $\vec{v}$.
An alternative approach to classical mechanics is the Hamiltonian approach, which plays a fundamental role in the transition from classical to quantum mechanics.
To introduce the Hamiltonian approach, let us first define the *generalized momentum* $\vec{P}$ canonically conjugate to the position vector $\vec{r}$ of a single particle: $\vec{P} = \partial L/\partial \vec{r}$.
In the absence of electromagnetic fields,

$$\vec{P} \;=\; \frac{\partial L}{\partial \vec{v}} \;=\; m\vec{v}\,, \tag{A.158}$$

the generalised momentum is equal to the mechanical momentum, $\vec{P} = m\vec{v}$.
In the presence of an electromagnetic field, from (A.153) one finds instead

$$\vec{P} \;=\; \frac{\partial L}{\partial \vec{v}} \;=\; m\vec{v} \;+ q\vec{A}. \tag{A.159}$$

Note that now $\vec{P} \neq m\vec{v}$, the conjugate momentum is different from the mechanical momentum $m\vec{v}$. While the mechanical momentum $m\vec{v}$ is an observable quantity, the conjugate momentum $\vec{P}$ is not, since it depends on the value of $\vec{A}$, which in turns depends on the gauge choice. The coniugate momentum thus depends on the gauge choice.

One can substitute the Lagrange function $L(\vec{r},\vec{v})$ with the new Hamilton function $H(\vec{r},\vec{P})$ without losing any physical information on the system by means of a Legendre transform:

$$\begin{aligned}H(\vec{r},\vec{P}) \;&=\; \vec{v}\cdot\frac{\partial L}{\partial \vec{v}} - L \\ &=\; \vec{v}\cdot(m\vec{v} + q\vec{A}) - mv^2/2 - q\vec{v}\cdot\vec{A} + qU \\ &=\; mv^2/2 + qU \;=\; \frac{1}{2m}\,\left|\vec{P} - q\vec{A}\right|^2 \;+\; qU.\end{aligned} \tag{A.160}$$

The second-order Lagrange equation of motion (A.149) is substituted by two first-order Hamilton equations of motion:

$$\frac{d\vec{r}}{dt} = \frac{\partial H}{\partial \vec{P}}\,, \tag{A.161}$$

$$\frac{d\vec{P}}{dt} = -\frac{\partial H}{\partial \vec{r}}\,. \tag{A.162}$$

From the first Hamilton equation (A.161) one recovers the expression for the mechanical momentum

$$m\vec{v} = \vec{P} - q\vec{A} \tag{A.163}$$

so that one can see that the Hamilton function

$$H \;=\; \frac{1}{2}\,mv^2 \;+\; qU \tag{A.164}$$

corresponds to the total energy (kinetic plus potential).

Note: It has been noted above that the mechanical momentum is gauge invariant, the canonical momentum is not. By converse, the mechanical momentum, in the presence of an electromagnetic field, doesn't have a classical canonical Poisson structure or a quantum commutator structure: the commutator of the mechanical momentum with itself is non-vanishing.

We need now to show that the classical Coulomb-Lorentz force can be obtained from the Hamilton equations. From (A.163) one obtains

$$\frac{d\vec{P}}{dt} \;=\; m\,\frac{d\vec{v}}{dt} \;+\; q\,\frac{d\vec{A}}{dt} \tag{A.165}$$

From the second Hamilton equation (A.162) one obtains

$$\frac{d\vec{P}}{dt} \;=\; \frac{q}{m}\left(\vec{P} - q\vec{A}\right)\,\frac{\partial \vec{A}}{\partial \vec{r}} \;-\; q\vec{\nabla}U\,. \tag{A.166}$$

By equating the right sides of the two last equations, one finds

$$\begin{aligned} m\,\frac{d\vec{v}}{dt} &= \frac{q}{m}\left(\vec{P} - q\vec{A}\right)\,\frac{\partial \vec{A}}{\partial \vec{r}} \;-\; q\,\frac{d\vec{A}}{dt} \;-\; q\vec{\nabla}U \\ &= q\vec{v}\,\frac{\partial \vec{A}}{\partial \vec{r}} - q(\vec{v}\cdot\vec{\nabla})\vec{A} \;- q\frac{\partial \vec{A}}{\partial t} \;-\; q\vec{\nabla}U \\ &= q(\vec{v}\times\vec{B}) \;+\; q\vec{E}\,. \end{aligned} \tag{A.167}$$

Interaction of an atom with the electromagnetic field

Let us now consider the specific problem of interest here, say the interaction of the electromagnetic field of an X-ray beam with an atom. To that purpose:

a) One can consider only the interaction with electrons, and neglect the contribution of the nucleus to the Hamiltonian, because it has a much larger mass than the electrons.
b) The generic charge q is substituted by the electron charge $q = -e$.
c) The electromagnetic field is conveniently treated within the interaction gauge (Coulomb gauge with zero scalar potential), so that the U scalar field reduces to the potential V describing the electrostatic interaction between the electrons and the nucleus and between the electrons.

The non-relativistic classical hamiltonian (A.160) is expressed as the sum over the contributions of all the electrons:

$$H \;=\; \sum_j \frac{1}{2m}\,\left[\vec{P}_j + e\vec{A}(\vec{r}_j, t)\right]^2 \;+\; V(\vec{r}_1 \ldots \vec{r}_N) \tag{A.168}$$

where j labels the N electrons within the atom. The time dependence of the vector potential has been evidenced.
Again, the quantity within square parentheses represents the sum of the mechanical momenta of the electrons.

A.6.2 Quantum treatment

The transition from the classical to the quantum hamiltonian is made by substituting the classical quantities with the corresponding operators. In the following, the notation $\vec{P}$ thus indicates the canonical momentum operator.
For explicit calculations, one generally works in the coordinate representation, where

$$\vec{P}_j \;\rightarrow\; -i\hbar\vec{\nabla}_j, \qquad \vec{A} \;\rightarrow\; \vec{A}, \;\ldots \tag{A.169}$$

Hamiltonian of an atom interacting with an electromagnetic field

In the *radiation gauge* and if the electron spin is neglected, the quantum hamiltonian of an atom in an electromagnetic field has the same expression as the classical hamiltonian, provided we consider $\vec{P}$ as an operator:

$$H = \sum_j \left\{ \frac{1}{2m} \left[\vec{P}_j + e\vec{A}(\vec{r}_j, t) \right]^2 \right\} \;+\; V(\vec{r}_1 \ldots \vec{r}_N) \,. \tag{A.170}$$

If the *electron spin* is also considered, the total Hamiltonian becomes

$$H = \sum_j \left\{ \frac{1}{2m} \left[\vec{P}_j + e\vec{A}(\vec{r}_j, t) \right]^2 + \frac{e}{m} \vec{S}_j \cdot \vec{B}(\vec{r}_j) \right\} \;+\; V(\vec{r}_1 \ldots \vec{r}_N) \,. \tag{A.171}$$

For one electron,

$$H = \left\{ \frac{1}{2m} \left[\vec{P} + e\vec{A}(\vec{r}, t) \right]^2 + \frac{e}{m} \vec{S} \cdot \vec{B}(\vec{r}) \right\} \;+\; V(\vec{r}) \,. \tag{A.172}$$

Let us now calculate the square of the binomial expressions $[\vec{P} + e\vec{A}(\vec{r})]^2$:

$$[\vec{P} + e\vec{A}(\vec{r})]^2 \;=\; P^2 + \; e\left(\vec{P} \cdot \vec{A} + \vec{A} \cdot \vec{P} \right) \;+\; e^2 A^2 \,. \tag{A.173}$$

The *radiation gauge* guarantees that, since $\vec{\nabla}$ commutes with $\vec{A}$, the commutativity of the classical product $\vec{P} \cdot \vec{A}$ is preserved; in radiation gauge, $\vec{\nabla} \cdot \vec{A}\psi = \vec{A} \cdot \vec{\nabla}\psi$.
The (one-electron) Hamiltonian can be written as

$$H = \left\{ \frac{P^2}{2m} \;+\; \frac{e}{m} \vec{A} \cdot \vec{P} \;+\; \frac{e^2}{2m} A^2 \;+ \frac{e}{m} \vec{S} \cdot \vec{B}(\vec{r}) \right\} \;+\; V(\vec{r}) \,. \tag{A.174}$$

The Hamiltonian can be divided into the sum of two terms, the unperturbed hamiltonian and the interaction hamiltonian:

$$H = H_0 + H_{\mathrm{int}}. \tag{A.175}$$

Unperturbed hamiltonian

The first term H_0 of (A.175) is the unperturbed hamiltonian

$$H_0 = \sum_j \frac{P_j^2}{2m} + V(\vec{r}_1 \ldots \vec{r}_N) \,. \tag{A.176}$$

In the absence of the electromagnetic field, the canonical momenta P_j correspond to the mechanical momenta $m\vec{v}_j$.

By solving the time-independent Schrödinger equation $H_0|\phi\rangle = E|\phi\rangle$ one obtains the energies E_i and the corresponding stationary eigenstates $|\phi_i\rangle$.
When the electromagnetic field is switched on,

$$\vec{P}_j = m\vec{v}_j \quad \rightarrow \quad \vec{P}_j + e\vec{A} = m\vec{v}_j \tag{A.177}$$

For one electron

$$H_0 = \frac{P^2}{2m} + V(\vec{r}) \; . \tag{A.178}$$

Interaction hamiltonian

The second term H_{int} of (A.175) represents the (time-dependent) interaction between the electromagnetic field and the electrons. If the electrons spin is neglected

$$H_{\text{int}} \; = \; \frac{e}{m} \sum_j \vec{A}(\vec{r},t) \cdot \vec{P}_j \; + \; \frac{e^2}{2m} \sum_j A^2(\vec{r}_j,t) \tag{A.179}$$

To take into account also the electron spin and its interaction with the magnetic field, the interaction hamiltonian is modified as:

$$H_{\text{int}} \; = \; \frac{e}{m} \sum_j \vec{A}(\vec{r},t) \cdot \vec{P}_j \; + \; \frac{e}{m} \sum_j \vec{S}_j \cdot \vec{B}(\vec{r}_j,t) \; + \; \frac{e^2}{2m} \sum_j A^2(\vec{r}_j,t) \tag{A.180}$$

The three terms have different magnitudes.

Appendix B

Time-dependent perturbation theory

Let us review here the basics of the time-dependent perturbation theory, focusing the attention on its application to the interaction of matter and radiation [Merzbacher, 1970], [Cohen-Tannoudji et al., 1973],[Chen and Kotlarchyk, 1997].

B.1 Introduction: time evolution of quantum systems

B.1.1 The evolution operator

The state vector $|\Psi(t)\rangle$ of a quantum system obeys the time-dependent Schrödinger equation

$$i\hbar\frac{\partial}{\partial t}|\Psi(t)\rangle \;=\; H(t)\,|\Psi(t)\rangle\,, \tag{B.1}$$

where a time-dependent Hamiltonian is considered here for the sake of generality.
In our applications, $|\Psi(t)\rangle$ can represent the quantum state of the system matter+radiation or the quantum state of only the atomic system.
The time evolution of the system from an initial time t_i to a final time t_f is given by the evolution operator $U(t_f, t_i)$,

$$|\Psi(t_f)\rangle \;=\; U(t_f, t_i)\,|\Psi(t_i)\rangle\,. \tag{B.2}$$

Inserting (B.2) into the Schrödinger equation (B.1), one finds the differential equation for the evolution operator:

$$i\hbar\frac{\partial}{\partial t_f}U(t_f, t_i) \;=\; H(t)\,U(t_f, t_i)\,. \tag{B.3}$$

Together with the initial condition $U(t_i, t_i) = 1$, the differential equation (B.3) completely defines the evolution operator $U(t_f, t_i)$.
The differential equation (B.3) and the initial condition $U(t_i, t_i) = 1$ can be summarised into a unique integral equation:

$$U(t_f, t_i) \;=\; 1 \;-\; \frac{1}{i\hbar}\int_{t_i}^{t_f} H(t')\,U(t', t_i)\,dt'\,. \tag{B.4}$$

B.1.2 Transition amplitude

Let us consider a system prepared in a state $|\Psi_i\rangle$ at time t_i.
The basic quantum mechanical problem of interest here is to evaluate the amplitude of probability of finding the system in the state $|\Psi_f\rangle$ at a subsequent time t_f.
The amplitude of probability is the matrix element of the evolution operator
[Cohen-Tannoudji et al., 2001]

$$\langle\Psi_f|\,U(t_f, t_i)\,|\Psi_i\rangle\,. \tag{B.5}$$

Properties of the transition amplitudes

Transition amplitudes are multiplicative quantities.
Let us consider the transition from an initial stationary state $|\Psi_1\rangle$ at time t_1 to a final stationary state $|\Psi_3\rangle$ at time t_3.
Let us assume that at time t_2 the system is in an intermediate stationary state.

1. If the intermediate state $|\Psi_2\rangle$ is observed, the transition amplitudes multiply:

$$\langle\Psi_3|\,U(t_3,t_1)\,|\Psi_1\rangle \;=\; \langle\Psi_3|\,U(t_3,t_2)\,|\Psi_2\rangle\;\langle\Psi_2|\,U(t_2,t_1)\,|\Psi_1\rangle \tag{B.6}$$

2. If the intermediate state is not observed and is thus unknown,

$$\langle\Psi_3|\,U(t_3,t_1)\,|\Psi_1\rangle \;=\; \sum\nolimits_n \langle\Psi_3|\,U(t_3,t_2)\,|\Psi_n\rangle\;\langle\Psi_n|\,U(t_2,t_1)\,|\Psi_1\rangle \tag{B.7}$$

and the sum over the intermediate states gives rise to interference effects.

Perturbative methods

The calculation of transition amplitudes is generally performed by a perturbative approach, which is based on the decomposition of the total Hamiltonian into an unperturbed part H_0 and a perturbation term $H_{\rm int}$.
The perturbation term can describe the coupling between two quantum subsystems of the entire system (e.g. an atom and the electromagnetic field) or the interaction of a quantum system with an external perturbation (e.g. an atom and a classical electromagnetic field).
In the following subsections, we compare the time evolution of un-perturbed systems (§ B.1.3) and of interacting systems (§ B.1.4).

B.1.3 Time evolution of un-perturbed systems

If the Hamiltonian operator is independent of time, $H(t) = H_0$, the integration of the differential equation (B.3) with the initial condition $U(t_i, t_i) = 1$ gives the trivial dependence on time

$$U^{(0)}(t_f,t_i) \;=\; \exp[-iH_0(t_f-t_i)/\hbar]\,. \tag{B.8}$$

One can easily verify that the evolution operator $U^{(0)}(t',t_i) = \exp[-iH_0(t'-t_i)/\hbar$ obeys the integral equation (B.4) with $H(t') = H_0$, independent of time.

Stationary Schrödinger equation

For a time-independent hamiltonian H_0 (un-perturbed system) the stationary Schrödinger equation is

$$H_0\,|\phi_n\rangle \;=\; E_n\,|\phi_n\rangle\,, \tag{B.9}$$

where E_n are the energy eigenvalues and $|\phi_n\rangle$ are the stationary eigenstates of the un-perturberd Hamiltonian H_0. The matrix elements of the unperturbed hamiltonian are

$$\langle\phi_n|\,H_0\,|\phi_k\rangle \;=\; E_n\,\delta_{nk}\,. \tag{B.10}$$

Time-dependent Schrödinger equation

The time-dependent Schrödinger equation for the un-perturbed system with time-independent Hamiltonian is

$$i\hbar\frac{\partial}{\partial t}|\Psi(t)\rangle \;=\; H_0\,|\Psi(t)\rangle\,, \tag{B.11}$$

and, taking into account (B.8) and putting $t_f = t$ and $t_i = 0$, the time dependence of the generic state $|\Psi(t)\rangle$ is given by

$$|\Psi(t)\rangle \;=\; e^{-iH_0t/\hbar}\,|\Psi(0)\rangle\,. \tag{B.12}$$

The state $|\Psi(t)\rangle$ can be projected on the basis of the stationary eigenstates of H_0:

$$|\Psi(t)\rangle \;=\; \sum_n c_n(t)|\phi_n\rangle\,, \qquad c_n(t) \;=\; \langle\phi_n|\Psi(t)\rangle\,, \tag{B.13}$$

where the time dependence of $|\Psi(t)\rangle$ is transferred to the time dependence of the coefficients $c_n(t)$. Applying the evolution operator to each one of the stationary eigenstates $|\phi_n\rangle$ and making again use of (B.8) one finds

$$|\Psi(t)\rangle \;=\; \sum_n b_n\, e^{-iE_nt/\hbar}\,|\phi_n\rangle\,, \qquad c_n(t) \;=\; b_n\, e^{-iE_nt/\hbar}\,, \tag{B.14}$$

where $b_n = c_n(0)$ are constant values.
The probability of finding the system in the eigenstate $|\phi_n\rangle$ is $|c_n(t)|^2 = |b_n|^2$, independent of time.

Note: The un-perturbed system can be the sum of two non-interacting quantum sub-systems, such as an atom and the electromagnetic field or a thermal neutron and an atomic nucleus, as well as a quantum atomic system embedded in a classical electromagnetic field.

B.1.4 Time evolution of interacting systems

Let us now introduce the interaction between the two quantum sub-systems or the interaction between a quantum system and the classical external field.
The total hamiltonian is now

$$H(t) \;=\; H_0 \;+\; H_{\rm int}(t)\,, \tag{B.15}$$

where the time-dependent interaction term $H_{\rm int}(t)$ is here considered as a weak perturbation with respect to the unperturbed hamiltonian H_0.
The state $|\Psi(t)\rangle$ can again be projected on the basis of the eigenstates of H_0, but now the time dependence of the coefficients $c_n(t)$ cannot be reduced to the trivial one (B.14); now

$$|\Psi(t)\rangle \;=\; \sum_n c_n(t)|\phi_n\rangle \;=\; \sum_n b_n(t)\, e^{-iE_nt/\hbar}|\phi_n\rangle \tag{B.16}$$

and a residual weak time dependence affects the coefficients $b_n(t)$.
The probability of finding the system in the eigenstate $|\phi_n\rangle$ is now $|c_n(t)|^2 = |b_n(t)|^2$ and can change in time.

Example 1: A thermal neutron or a photon, spatially localised as wave-packets, are scattered by an atom; the effect of the interaction is limited to a short time interval.

Example 2: Often the interacting systems are described in terms of non-localised states, e.g. the quantum description of the electromagnetic fields in terms of number of photons per normal mode or the classical description of the electromagnetic field as a radiation beam. In these situations, the interaction is adiabatically switched on at time t_i and switched off at time t_f. The interaction is described in terms of a transition rate (transition probability per unit time).

The problem

Our problem is to determine the transition rate (transition probability per unit time) from an initial stationary eigenstate $|\phi_i\rangle$ of H_0 to a final stationary eigenstate $|\phi_f\rangle$ of H_0.
To that purpose, we need to evaluate the transition amplitude

$$\langle\phi_f|\,U(t_f,t_i)\,|\phi_i\rangle\,. \tag{B.17}$$

The problem is solved along the following guidelines:

1. One works within the interaction picture, where the trivial time-dependence of the initial and final stationary states is eliminated; the interaction picture is a mixture of
   a) Heisenberg picture for the un-perturbed system, whose Hamiltonian is H_0;
   b) Schrödinger picture for the interaction described by the Hamiltonian $H_{\rm int}$
2. A perturbative approach is employed.

Adiabatic switching of the interaction

In a number of situations, typically when considering the interaction of a system with a beam, it is convenient to adiabatically switch-on the interaction at a time t_i and switch off it at a time t_f. This can be achieved by multiplying $H_{\rm int}$ by a parameter λ which is zero for $t < t_i$ and for $t > t_f$, and becomes adiabatically 1 in the interaction interval.
If the interaction time becomes infinite ($t_i \to -\infty, t_f \to +\infty$), the matrix element of the evolution operator

$$\langle \phi_f | \, U(t_f, t_i) \, | \phi_i \rangle \, . \tag{B.18}$$

corresponds to the matrix element of the S scattering matrix.

B.2 Time-dependent perturbation approach

Let $|\phi_n\rangle$ be a stationary eigenstate of the system matter+radiation in the Schrödinger picture,

$$|\phi_n(t)\rangle \;=\; |\phi_{\rm at}\rangle \otimes |\phi_{\rm rad}\rangle \;=\; |\phi_{\rm at}\rangle \otimes |\{n_{\vec{k}s}\}\rangle \, , \tag{B.19}$$

or a stationary state of an atom embedded in a classical electromagnetic field.
We will calculate the transition amplitudes and the transition probabilities between two stationary states by an iterative solution of the integral equation for the evolution operator.
To evidence the advantage of the interaction picture, we will first solve the problem in the Schrödinger picture and then in the interaction picture.

B.2.1 Schrödinger picture

Once the Hamiltonian has been separated into an unperturbed term H_0 and an interaction term $H_{\rm int}$, the integral equation for the evolution operator in the Schrödinger picture can be written as ([Cohen-Tannoudji et al., 2001] page 26)

$$\begin{aligned} U(t_f, t_i) \;&=\; e^{-iH_0(t_f - t_i)/\hbar} \;+\; \frac{1}{i\hbar} \int_{t_i}^{t_f} d\tau \, e^{-iH_0(t_f-\tau)/\hbar} \, H_{\rm int}(\tau) \, U(\tau, t_i) \\ &=\; U^{((0)}(t_f, t_i) \;+\; \frac{1}{i\hbar} \int_{t_i}^{t_f} d\tau \, U^{((0)}(t_f, \tau) \, H_{\rm int}(\tau) \, U(\tau, t_i) \end{aligned} \tag{B.20}$$

where

$$e^{-iH_0(t_f - t_i)/\hbar} \;=\; U^{((0)}(t_f, t_i) \, , \quad e^{-iH_0(t_f-\tau)/\hbar} \;=\; U^{((0)}(t_f, \tau) \tag{B.21}$$

are the un-perturbed evolution operators associated to H_0.
One can easily see that the above expression of $U(t_f, t_i)$ verifies the differential equation

$$i\hbar \, \frac{\partial}{\partial t_f} U(t_f, t_i) \;=\; (H_0 + H_{\rm int}) \, U(t_f, t_i) \tag{B.22}$$

and the initial condition $U(t_i, t_i) = 1$.

Iterative solution of the integral equation

The time-dependent perturbation theory is based on the iterative solution of the integral equation for the evolution operator. To obtain an iterative solution, the evolution operator in the Schrödinger picture is expanded as

$$U(t_f, t_i) \;=\; U^{((0)}(t_f, t_i) \;+\; \sum_{n=1}^{\infty} U^{(n)}(t_f, t_i) \, . \tag{B.23}$$

The **zero order** term corresponds to the first term in the right-hand member of (B.20), say to the unperturbed evolution operator

$$U^{((0)}(t_f,t_i) = e^{-iH_0(t_f-t_i)/\hbar} \tag{B.24}$$

The **first order** term in the approximation is obtained by substituting $U(t,t_i) = U^{(0)}(t,t_i)$ within the integral of the integral equation (B.20), so that:

$$\begin{aligned} U^{(1)}(t_f,t_i) &= \frac{1}{i\hbar}\int_{t_i}^{t_f} d\tau\, e^{-iH_0(t_f-\tau)/\hbar}\, H_{\rm int}(\tau)\, e^{-iH_0(\tau-t_i)/\hbar} \\ &= \frac{1}{i\hbar}\int_{t_i}^{t_f} d\tau\; U^{(0)}(t_f,\tau)\, H_{\rm int}(\tau)\, U^{(0)}(\tau,t_i)\,. \end{aligned} \tag{B.25}$$

The integral over the time τ contains 2 unperturbed evolution operators, one from time t_i to time τ, the other from time τ to time t_f, separated by the interaction operator $H_{\rm int}$.

The **second order** term in the approximation is obtained by substituting $U(\tau,t_i) = U^{(0)}(\tau,t_i) + U^{(1)}(\tau,t_i)$ in the integral of the integral equation (B.20), so that:

$$U^{(2)}(t_f,t_i) \;=\; \left(\frac{1}{i\hbar}\right)^2 \int_{t_1}^{t_f} d\tau_2 \int_{t_i}^{t_1} d\tau_1\, e^{-iH_0(t_f-\tau_2)/\hbar}\, H_{\rm int}(\tau_2)\, e^{-iH_0(\tau_2-\tau_1)/\hbar}\, H_{\rm int}(\tau_1)\, e^{-iH_0(\tau_1-t_i)/\hbar}\,. \tag{B.26}$$

Now there are 3 unperturbed evolution operators separated by 2 interaction operators.

And so on with higher order terms. The general expression for the term of order n is

$$U^{(n)}(t_f,t_i) \;=\; \left(\frac{1}{i\hbar}\right)^n \int_{t_{n-1}}^{t_f} d\tau_n \ldots \int_{t_i}^{t_1} d\tau_1\; e^{-iH_0(t_f-\tau_n)/\hbar}\, H_{\rm int}(\tau_n)\ldots H_{\rm int}(\tau_1)\, e^{-iH_0(\tau_1-t_i)/\hbar}\,, \tag{B.27}$$

where $t_f \geq t_{n-1} \geq \ldots \geq t_1 \geq t_i$. There are $n+1$ unperturbed evolution operators separated by n interaction operators.

Expansion of the transition amplitude

By inserting the different orders of approximation of $U(t_f,t_i)$ into the expression of the transition amplitude between the stationary states $|\Phi_i\rangle$ and $|\Phi_f\rangle$

$$c_{fi}(t) \;=\; \langle\Phi_f|\, U(t_f,t_i)\, |\Phi_i\rangle \tag{B.28}$$

and inserting the completeness relation on the eigenstates of H_0 between any two successive $H_{\rm int}$ operators, one obtains the corresponding expansion of the transition amplitude.
The **zero order** term is

$$c_{fi}^{(0)}(t) \;=\; \langle\Phi_f|\, e^{-iH_0(t_f-t_i)/\hbar}\, |\Phi_i\rangle \;=\; e^{-iE(t_f-t_i)/\hbar}\;\delta_{fi} \tag{B.29}$$

The **first order** term is

$$\begin{aligned} c_{fi}^{(1)(t)} &= \frac{1}{i\hbar}\int_{t_i}^{t_f} d\tau\; e^{-iE_f(t_f-\tau)/\hbar}\; \langle\Phi_f|\, H_{\rm int}\, |\Phi_i\rangle\; e^{-iE_i(\tau-t_i)/\hbar}. \\ &= e^{-iE(t_f-t_i)/\hbar}\; \frac{1}{i\hbar}\int_{t_i}^{t_f} d\tau\; e^{iE_f\tau/\hbar}\; \langle\Phi_f|\, H_{\rm int}\, |\Phi_i\rangle\; e^{-iE_i\tau/\hbar} \end{aligned} \tag{B.30}$$

The **second order** term is obtained by inserting the completeness relation $\sum_k |\Phi_k\rangle\langle\Phi_k|$ between

the two interaction operators $H_{\rm int}$:

$$\begin{aligned} c_{fi}^{(2)}(t) &= \left(\frac{1}{i\hbar}\right)^2 \int_{t_1}^{t_f} d\tau_2 \int_{t_i}^{t_1} d\tau_1 \\ &\quad \sum_k e^{-iE_f(t_f-\tau_2)/\hbar} \langle\Phi_f| H_{\rm int} |\Phi_k\rangle e^{-iE_1(\tau_2-\tau_1)/\hbar} \langle\Phi_k| H_{\rm int} |\Phi_i\rangle e^{-iE_i(\tau_1-t_i)/\hbar} \\ &= e^{-iE(t_f-t_i)/\hbar} \left(\frac{1}{i\hbar}\right)^2 \int_{t_1}^{t_f} d\tau_2 \int_{t_i}^{t_1} d\tau_1 \\ &\quad \sum_k e^{iE_f\tau_2/\hbar} \langle\Phi_f| H_{\rm int} |\Phi_k\rangle e^{-iE_1(\tau_2-\tau_1)/\hbar} \langle\Phi_k| H_{\rm int} |\Phi_i\rangle e^{-iE_i\tau_1/\hbar} \end{aligned} \tag{B.31}$$

where the sum is over the intermediate virtual states Φ_k.

The extension to higher-order terms is trivial.
The term of order n contains the product of n interaction factors and $n+1$ free evolution factors and $n-1$ sums over intermediate virtual states.
Notice that all transition amplitude terms contain the factor $e^{-iE(t_f-t_i)/\hbar}$, which represents the free evolution of the initial and final states. When calculating the transition probabilities, the squared modulus of this factor is equal to one.

B.2.2 Interaction picture

In the following, eigenstates and operators in the interaction picture are characterised by a tilde.
The stationary eigenstates of the un-perturbed hamiltonian in the interaction picture $|\tilde{\phi}_n(t)\rangle$ are connected to the eigenstates of the Schrödinger picture $|\phi_n(t)\rangle$ by

$$|\tilde{\phi}_n(t)\rangle = e^{iH_0t/\hbar} |\phi_n(t)\rangle . \tag{B.32}$$

In the interaction picture, the stationary eigenstates have no time dependence at all.
The connection between the evolution operators in the interaction and Schrödinger pictures is

$$\tilde{U}(t_f,t_i) = e^{iH_0t/\hbar} U(t_f,t_i) e^{-iH_0t/\hbar} , \tag{B.33}$$

and the connection between the interaction hamiltonians in the two pictures is

$$\tilde{H}_{\rm int} = e^{iH_0t/\hbar} H_{\rm int} e^{-iH_0t/\hbar} . \tag{B.34}$$

In the interaction picture, the time dependence of the evolution operator is only due to the interaction hamiltonian; the corresponding differential equation is

$$i\hbar\frac{\partial}{\partial t_f}\tilde{U}(t_f,t_i) = \tilde{H}_{\rm int}(t_f)\,\tilde{U}(t_f,t_i) , \tag{B.35}$$

The integral equation for the evolution operator in the interaction picture is

$$\tilde{U}(t_f,t_i) = 1 + \frac{1}{i\hbar}\int_{t_i}^{t_f} d\tau\, \tilde{H}_{\rm int}(\tau)\,\tilde{U}(\tau,t_i) . \tag{B.36}$$

Iterative solution of the integral equation

The integral equation for the evolution operator can be solved by an iterative method.
The evolution operator in the interaction picture is expanded as

$$\tilde{U}(t_f,t_i) = 1 + \sum_{n=1}^{\infty} \tilde{U}^{(n)}(t_f,t_i) \tag{B.37}$$

The **zero order** term is

$$\tilde{U}^{(0)}(t_f,t_i) = 1 . \tag{B.38}$$

The **first order** term in the approximation is obtained by substituting $U(t,t_i) = U^{(0)}(t,t_i) = 1$ in the integral equation:

$$\begin{aligned} \tilde{U}^{(1)}(t_f,t_i) &= \frac{1}{i\hbar}\int_{t_i}^{t_f} d\tau\, \tilde{H}_{\rm int}(\tau) \\ &= \frac{1}{i\hbar}\int_{t_i}^{t_f} d\tau\, e^{iH_0\tau/\hbar} H_{\rm int}(\tau)\, e^{-iH_0\tau/\hbar}\,. \end{aligned} \tag{B.39}$$

The **second order** term in the approximation is

$$\begin{aligned} \tilde{U}^{(2)}(t_f,t_i) &= \left(\frac{1}{i\hbar}\right)^2 \int_{t_1}^{t_f} d\tau_2 \int_{t_i}^{t_1} d\tau_1\, \tilde{H}_{\rm int}(\tau_2)\, \tilde{H}_{\rm int}(\tau_1) \\ &= \left(\frac{1}{i\hbar}\right)^2 \int_{t_1}^{t_f} d\tau_2 \int_{t_i}^{t_1} d\tau_1 e^{iH_0\tau_2}\, H_{\rm int}(\tau_2)\, e^{-iH_0(\tau_2-\tau_1)} H_{\rm int}(\tau_1)\, e^{-iH_0\tau_1} \end{aligned} \tag{B.40}$$

And so on with higher order terms.
As one can see, in the interaction picture the free evolution exponentials

$$e^{-iH_0 t_f/\hbar}\,, \qquad e^{iH_0 t_i/\hbar} \tag{B.41}$$

relative to the initial and final states are missing.

Transition amplitudes

As for the Schrödinger picture, even for the interaction picture the transition amplitude between the stationary states $|\Phi_i\rangle$ and $|\Phi_f\rangle$

$$\tilde{c}_{fi} = \langle\Phi_f|\, \tilde{U}(t_f,t_i)\, |\Phi_i\rangle \tag{B.42}$$

can be expanded as a sum of terms of increasing order
The **zero order** term is

$$\tilde{c}^{(0)}_{fi} = \delta_{fi} \tag{B.43}$$

The **first order** term is

$$\tilde{c}^{(1)}_{fi}(t) = \frac{1}{i\hbar}\int_{t_i}^{t_f} d\tau\; e^{iE_f\tau/\hbar}\, \langle\Phi_f|\, H_{\rm int}(\tau)\, |\Phi_i\rangle\; e^{-iE_i\tau/\hbar} \tag{B.44}$$

The **second order** term is obtained by inserting a completeness relation between the two interaction operators $H_{\rm int}$:

$$\begin{aligned} \tilde{c}^{(2)}_{fi}(t) =& \left(\frac{1}{i\hbar}\right)^2 \int_{t_1}^{t_f} d\tau_2 \int_{t_i}^{t_1} d\tau_1 \\ & \sum\nolimits_{\Phi_1} e^{iE_f\tau_2/\hbar}\, \langle\Phi_f|\, H_{\rm int}(\tau_2)\, |\Phi_1\rangle\, e^{-iE_1(\tau_2-\tau_1)/\hbar}\, \langle\Phi_1|\, H_{\rm int}(\tau_1)\, |\Phi_i\rangle\, e^{-iE_i\tau_1/\hbar} \end{aligned} \tag{B.45}$$

The extension to higher-order terms is trivial.
The term of order n contains the product of n interaction factors and $n+1$ free evolution factors and $n-1$ sums over intermediate virtual states.

Transition probabilities

The transition amplitudes $\tilde{c}^{(n)}_{fi}$ of the interaction picture differ from the transition amplitudes $c^{(n)}_{fi}$ of the Schrödinger picture for the absence of the factor $e^{-iE(t_f-t_i)/\hbar}$, which represents the free evolution of the initial and final states. Since the squared modulus of this factor is equal to one, the transition probabilities between an initial and a final state are the same in the Schrödinger and in the interaction pictures:

$$|\langle\phi_f|U|\phi_i\rangle|^2 = \left|\langle\phi_f|\tilde{U}|\phi_i\rangle\right|^2 \tag{B.46}$$

In what follows, we gain a deeper insight on the first-order approximation and the so-called Golden Rule for the interaction of atoms with the electromagnetic field (§ B.4) as well as on the electric dipole approximation (§ B.5). A short introduction is given to the second-order approximation (§ B.6).
Reference: [Cohen-Tannoudji et al., 1973, Cohen-Tannoudji et al., 2001].

B.3 Interaction Hamiltonian

Let us now restrict our attention to the problem of an atomic system interacting with the electromagnetic field. See Appendix A for the description of the electromagnetic field and an introduction to the interaction Hamiltonian.

B.3.1 Total Hamiltonian of an atom

If the *radiation gauge* is used ($\vec{\nabla}\cdot\vec{A}=0,\ \phi=0$) and if the electron spin is neglected, the hamiltonian of an atom in an electromagnetic field is better expressed in terms of the vector potential $\vec{A}$:

$$\hat{H} = \sum_j \left\{ \frac{1}{2m} \left[\vec{P}_j + e\vec{A}(\vec{r}_j,t)\right]^2 \right\} + V(\vec{r}_1 \ldots \vec{r}_N)\,, \tag{B.47}$$

where $\vec{P}_j$ is the quantum operator of the generalized momentum of the j-th electron and V is the potential energy due to the Coulomb interactions inside the atom.
If the *electron spin* is also considered, the total Hamiltonian becomes

$$\hat{H} = \sum_j \left\{ \frac{1}{2m} \left[\vec{P}_j + e\vec{A}(\vec{r}_j,t)\right]^2 + \frac{e}{m}\,\vec{S}_j\cdot\vec{B}(\vec{r}_j) \right\} + V(\vec{r}_1 \ldots \vec{r}_N)\,, \tag{B.48}$$

where $\vec{S}_j$ is the spin of the j-th electron and $\vec{B}=\nabla\times\vec{A}$ is the magnetic field.

Decomposition of the total Hamiltonian

Let us focus our attention on the squared expressions in (B.47):

$$\left[\vec{P}+e\vec{A}\right]^2 = P^2 + e\left[\vec{P}\cdot\vec{A}+\vec{A}\cdot\vec{P}\right] + e^2A^2\,. \tag{B.49}$$

In principle, $\vec{P}$ and $\vec{A}$ (which is a function of position $\vec{r}$) don't commute.
We can however exploit the gauge properties of the potentials to simplify this expression.
In the position representation, the time-dependent Schrödinger equation of an electron in the electromagnetic field is

$$i\hbar\frac{\partial}{\partial t}\psi(\vec{r},t) = \left[-\frac{\hbar^2}{2m}\nabla^2 - i\hbar\frac{e}{2m}\left(\vec{\nabla}\cdot\vec{A}+\vec{A}\cdot\vec{\nabla}\right) + \frac{e^2}{2m}A^2 - e\phi\right]\psi(\vec{r},t)\,. \tag{B.50}$$

In the radiation gauge, $\nabla\cdot\vec{A}=0$ and $\phi=0$, so that

$$\vec{\nabla}\cdot(\vec{A}\psi) = \vec{A}\cdot(\vec{\nabla}\psi) + (\vec{\nabla}\cdot\vec{A})\psi = \vec{A}\cdot(\vec{\nabla}\psi) \tag{B.51}$$

say

$$\left(\vec{\nabla}\cdot\vec{A}+\vec{A}\cdot\vec{\nabla}\right)\psi = 2\,\vec{A}\cdot\vec{\nabla}\psi \tag{B.52}$$

and the Schrödinger equation becomes

$$i\hbar\frac{\partial}{\partial t}\psi(\vec{r},t) = \left[-\frac{\hbar^2}{2m}\nabla^2 - i\hbar\frac{e}{m}\left(\vec{A}\cdot\vec{\nabla}\right) + \frac{e^2}{2m}A^2\right]\psi(\vec{r},t)\,. \tag{B.53}$$

Once the square of the binomial $[\vec{P}_j + e\vec{A}(\vec{r}_j)]^2$ has been calculated in radiation gauge, the total-Hamiltonian can be decomposed into the sum of two terms, the unperturbed hamiltonian and the interaction hamiltonian:

$$\hat{H} = \hat{H}_0 + \hat{H}_{\rm int}. \tag{B.54}$$

Unperturbed hamiltonian

The first term $\hat{H}_0$ is the unperturbed hamiltonian, say the hamiltonian of the atom in absence of electromagnetic field:

$$\hat{H}_0 = \sum_j \frac{P_j^2}{2m} + V(\vec{r}_1 \ldots \vec{r}_N)\,. \tag{B.55}$$

By solving the time-independent Schrödinger equation $\hat{H}_0|\phi\rangle = E|\phi\rangle$ one obtains the energies E_i and the corresponding stationary eigenstates $|\phi_i\rangle$.

Interaction hamiltonian

The second term $\hat{H}_I$ represents the (time-dependent) interaction between the electromagnetic field and the electrons. If the electrons spin is neglected

$$\hat{H}_{\rm int} \;=\; \frac{e}{m}\sum_j \vec{A}(\vec{r},t)\cdot\vec{P}_j \;+\; \frac{e^2}{2m}\sum_j A^2(\vec{r}_j,t) \tag{B.56}$$

The *radiation gauge* guarantees that, since$\vec{\nabla}$ commutes with $\vec{A}$, the commutativity of the classical product $\vec{P}\cdot\vec{A}$ is preserved; in radiation gauge, $\vec{\nabla}\cdot\vec{A}\psi = \vec{A}\cdot\vec{\nabla}\psi$.

To take into account also the electron spin and its interaction with the magnetic field, the interaction hamiltonian is modified as:

$$\hat{H}_{\rm int} \;=\; \frac{e}{m}\sum_j \vec{A}(\vec{r},t)\cdot\vec{P}_j \;+\; \frac{e}{m}\sum_j \vec{S}_j\cdot\vec{B}(\vec{r}_j,t) \;+\; \frac{e^2}{2m}\sum_j A^2(\vec{r}_j,t) \tag{B.57}$$

The three terms have different magnitudes.

Note: In the full quantum approach, the vector potential is an operator, decomposed into a sum of creation and destruction operators for the different normal modes, which operate on the quantum state of the field, creating and destroying single photons.
In the semiclassical approach, quantum mechanics applies only to the atomic system.

B.3.2 Feynman diagrams

The different levels of approximation can be schematically visualised by means of Feynman diagrams.
Time is represented by the vertical axis. The trajectories of the interacting particles are represented by lines, which can be different depending on the type of particle (electrons, photons...).
First-order processes are characterised by one interaction vertex, where the particles meet and interact (by emitting or absorbing new particles, deflecting one another, or changing type).
Second order processes are characterised by the presence of two interaction vertices, connected by a vertical line which represents virtual states where energy conservation is not respected.

For the interaction of electromagnetic radiation with electrons, it is important to consider at least the following different processes:

a) First-order in the approximation (one interaction vertex) and first-order in the interaction ($\vec{A} \cdot \vec{P}$ term of the interaction Hamiltonian)
These processes correspond to the absorption or emission of one photon by an atom.
b) First-order in the approximation (one interaction vertex) and second-order in the interaction, (terms A^2 term in the interaction Hamiltonian).
These processes can correspond to
- absorption or emission of two photons by an atom
- scattering of one photon by an electron

c) Second-order in the approximation (two interaction vertices connected by a line of virtual states) and first-order in the interaction (terms $\vec{A} \cdot \vec{P}$ term in the interaction Hamiltonian).

B.4 First-order approximation and Golden Rule

The **first-order** transition amplitude in the interaction picture is

$$\begin{aligned} \tilde{c}_{fi}^{(1)}(t) &= \frac{1}{i\hbar} \int_{t_i}^{t_f} dt \, \langle \Phi_f | \, H_{\rm int} \, | \Phi_i \rangle \, e^{i(E_f - E_i)t/\hbar} \\ &= \frac{1}{i\hbar} \int_{t_i}^{t_f} dt \, \langle \Phi_f | \, H_{\rm int} \, | \Phi_i \rangle \, \exp(i\omega_{fi} t) \end{aligned} \tag{B.58}$$

where $\omega_{fi} = E_f - E_i/\hbar$ is the Bohr frequency.
Correspondingly, the first-order transition probability is

$$\mathcal{P}_{fi}^{(1)}(t) \; = \; |c_{fi}^{(1)}(t)|^2 \; = \; \frac{1}{\hbar^2} \left| \int_{t_i}^{t_f} dt \, \langle \Phi_f \, | \, H_{\rm int} \, | \, \Phi_i \rangle \exp(i\omega_{fi} t) \right|^2 \tag{B.59}$$

Let us now separately considering two different situations:

1. Interaction Hamiltonian $H_{\rm int}$ non explicitly depending on time.
2. Interaction Hamiltonian $H_{\rm int}$ explicitly depending on time, for example with a sinusoidal dependence.

B.4.1 Interaction Hamiltonian not depending explicitly on time

Examples of processes where the interaction Hamiltonian doesn't depend explicitly on time:

a) scattering of electrons by a Coulomb potential,
b) scattering of thermal neutrons by an effective Fermi potential,
c) scattering of X-ray photons by electrons, where the time dependence of the vector potential is cancelled for the terms of second-order in the interaction, A^2, which correspond to the annihilation of a photon of given $\vec{k}$ and the creation of a photon of a given $\vec{k}\,'$.

It is convenient to distinguish two cases:

1. Transition between sharply defined initial and final states
2. Transition between initial and/or final states not sharply defined

1. Transition between sharply defined initial and final states

Since the matrix element is independent of time, it can be factorized out of the integral in (B.58). Moreover, it is convenient to choose a time scale such that $t_i = -T/2$ and $t_f = +T/2$, where T is the duration of the interaction, so that the integral is easily peformed and the transition amplitude becomes

$$\begin{aligned} \tilde{c}_{fi}^{(1)}(T) &= -i \, \langle \Phi_f | \, H_{\rm int} \, | \Phi_i \rangle \int_{-T/2}^{+T/2} \frac{dt}{\hbar} \, e^{i\omega_{fi} t} \\ &= -2\pi i \, \langle \Phi_f | \, H_{\rm int} \, | \Phi_i \rangle \, \delta^{(T)}(\omega_{fi}) \end{aligned} \tag{B.60}$$

where the delta function is

$$\delta^{(T)}(\omega_{fi}) \;=\; \frac{1}{2\pi}\int_{-T/2}^{+T/2}\frac{dt}{\hbar}\,e^{i\omega_{fi}t} \;=\; \frac{1}{\pi\hbar}\,\frac{\sin(\omega_{fi}T/2)}{(\omega_{fi})} \tag{B.61}$$

The $\delta^{(T)}$ function is a diffraction function with the following properties

a) the maximum amplitude is $T/2\pi\hbar$ for $\omega_{fi}=0$, say for $E_f=E_i$, where $E_f=E_i$ is here the total energy of the two interacting sub-systems
b) the width of the central peak is of the order of $4\pi\hbar/T$,
c) for $T\to\infty$, $\delta^{(T)}(\omega_{fi})\to\delta(\omega_{if})$,
d) it expresses the energy conservation to within a $\hbar/T$ uncertainty.

The transition probability is the squared modulus of the transition amplitude:

$$\mathcal{P}_{fi}^{(1)}(T) \;=\; |c_{fi}^{(1)}(T)|^2 \;=\; \frac{4}{\hbar^2}\;|\langle\Phi_f\,|\,H_{\rm int}\,|\,\Phi_i\rangle|^2\;\left[\frac{\sin(\omega_{\rm fi}T/2)}{\omega_{\rm fi}}\right]^2 \tag{B.62}$$

The behaviour of the transition probability $\mathcal{P}_{\rm fi}^{(1)}(t)$ is represented in Fig. B.1 for a given duration t of the interaction. Its main properties are:

a) Peak for $\omega_{fi}=0$, say for $E_f=E_i$ (energy conservation).
b) Peak width $\propto T^{-1}$; the violation of the energy conservation is possible for short times, according to the time-energy uncertainty principle, $\Delta E\,\Delta T\geq\hbar$. For $t\to\infty$, energy is conserved.
c) Peak height $\propto T^2$. The transition probability increases indefinitely with the square of the interaction time T, and the transition probability per unit time $w_{fi}=d\mathcal{P}_{fi}/dt$ linearly increase with the interaction time T.
This result is clearly unphysical for long interaction times, and depends on the inadequacy of the first-order approximation when long times are considered for a transition between two sharply defined levels.

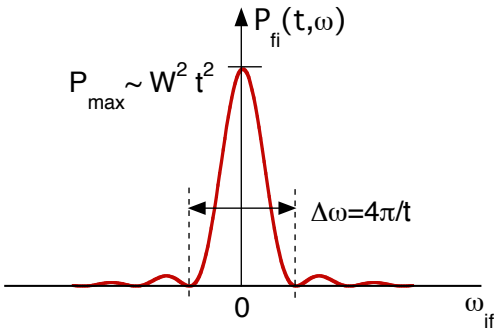

Figure B.1: Plot of the probability $P_{\rm fi}(t,\omega)$ as a function the Bohr frequency for a given time t.

2. Transition between non sharply defined initial and/or final states

In practical applications, the initial and/or the final states are generally not sharply defined. In general, at least one of the two states consists of a range of closely spaced energy eigenstates, which can be treated as a continuum with density of states $g(E)$.
For example: no real incoming and outgoing beams in a scattering experiment are perfectly mono-energetic, and no real photon beams in absorption experiments are perfectly mono-chromatic.
Let us assume, for simplicity, that the energy of the initial state E_i is sharply defined and the energy of the final state spans a continuum of levels with density $g(E_f)$.

The transition probability has to be modified in order to take into account the energy spread of the incoming and/or outgoing beams:

$$\mathcal{P}_{fi}^{(1)}(T) = \left|c_{fi}^{(1)}(T)\right|^2 = \frac{4}{\hbar^2} \int dE_f\, g(E_f)\, |\langle\Phi_f \,|\, H_{\rm int} \,|\, \Phi_i\rangle|^2 \left[\frac{\sin(\omega_{\rm fi}T/2)}{\omega_{\rm fi}}\right]^2$$
$$= \frac{4}{\hbar^2} \int d\omega_{fi}\, g(E_i+\hbar\omega_{fi})\, |\langle\Phi_f \,|\, H_{\rm int} \,|\, \Phi_i\rangle|^2 \left[\frac{\sin(\omega_{\rm fi}T/2)}{\omega_{\rm fi}}\right]^2 \quad \text{(B.63)}$$

For a sufficiently long interaction time T, the only significant transitions are those where the total energy of the two interacting subsystems is conserved, $E_f = E_i$. The function $[\sin(\omega_{fi}t/2)/\omega_{fi}]^2$ is sharply peaked around the value $\omega_{fi} = 0$. The matrix element and the density of states $g(E_f)$ are comparatively much more slowly varying with frequency and can be extracted from the integral, so that

$$\mathcal{P}_{fi}^{(1)}(T) = \left|c_{fi}^{(1)}(T)\right|^2 = \frac{4}{\hbar^2}\, |\langle\Phi_f \,|\, H_{\rm int} \,|\, \Phi_i\rangle|^2\, g(E_f) \int d\omega_{fi} \left[\frac{\sin(\omega_{fi}T/2)}{\omega_{fi}}\right]^2 \quad \text{(B.64)}$$

The integral is of the form

$$\int_{-\infty}^{+\infty} \frac{\sin^2 \alpha x}{x^2} = \pi\alpha\,, \quad \text{(B.65)}$$

where $x = \omega_{fi}$ and $\alpha = T/2$, so that finally

$$\mathcal{P}_{\rm fi}^{(1)}(t) = |c_{fi}^{(1)}(t)|^2 == \frac{2\pi}{\hbar}\, t\, |\langle\Phi_f \,|\, H_{\rm int} \,|\, \Phi_i\rangle|^2\, g(E_f)\,. \quad \text{(B.66)}$$

The transition probability is now linearly dependent on time, and the transition rate

$$w_{fi}^{(1)} = \frac{2\pi}{\hbar}\, |\langle\Phi_f \,|\, H_{\rm int} \,|\, \Phi_i\rangle|^2\, g(E_f)\,. \quad \text{(B.67)}$$

is time-independent.
This expression has been named Golden Rule by Enrico Fermi.

B.4.2 Sinusoidal perturbation and first-order approximation

Let us now consider an interaction Hamiltonian explicitly depending on time. For concreteness, we consider a case of interest here, say the interaction of the electromagnetic field with an atomic electron. We follow a semi-classical approach, where the atom is considered as a quantum system and the electromagnetic field as a classical system. The stationary quantum states $|\phi\rangle$ refer thus only to the atom.

The interaction Hamiltonian

The interaction Hamiltonian is

$$H_{\rm int} = \frac{e}{m}\, \vec{A}\cdot\vec{p}, \quad \text{(B.68)}$$

where $e > 0$ is the elementary charge, $\vec{A}$ is the vector potential of the electromagnetic field and $\vec{p}$ the generalized momentum of the electron (see § A.6).
The time and space dependence of the vector potential of a monochromatic electromagnetic wave is given by

$$\vec{A}(\vec{r},t) = A_0\hat{\epsilon}\, \sin(\omega t - \vec{k}\cdot\vec{r}) = \frac{1}{2i}\, A_0\, \hat{\epsilon}\left[e^{i\omega t}e^{-i\vec{k}\cdot\vec{r}} + e^{-i\omega t}e^{i\vec{k}\cdot\vec{r}}\right], \quad \text{(B.69)}$$

where A_0 is the amplitude and $\hat{\epsilon}$ is the polarisation unit vector.
The matrix element of the interaction hamiltonian between two stationary states of the unperturbed hamiltonian H_0 of the atomic system is

$$[H_{\rm int}(t)]_{fi} = \langle\phi_f|H_{\rm int}(t)|\phi_i\rangle$$
$$= \frac{e}{2im}\, A_0 \left[\langle\phi_f|e^{i\omega t}e^{-i\vec{k}\cdot\vec{r}}\,\hat{\epsilon}\cdot\vec{p}|\phi_i\rangle - \langle\phi_f|e^{-i\omega t}e^{i\vec{k}\cdot\vec{r}}\,\hat{\epsilon}\cdot\vec{p}|\phi_i\rangle\right] \quad \text{(B.70)}$$

Transition amplitude

The first-order transition amplitude in the interaction picture, according to (B.44), is

$$\tilde{c}_{fi}^{(1)}(T) = \frac{1}{i\hbar}\int_0^T d\tau \ \langle\phi_f|\, H_{\rm int}(\tau)\,|\phi_i\rangle \ \exp(i\omega_{fi}\tau) \tag{B.71}$$

where $\omega_{fi} = E_f - E_i/\hbar$ is the Bohr frequency. Here E_f and E_i are the (generally different) energies of two atomic levels and $H_{\rm int}(\tau)$ is explicitly dependent on time.
Substituting the expression (B.70) of the interaction Hamiltonian and extracting from the integral the time-independent part one gets

$$\begin{aligned}\tilde{c}_f^{(1)}(T) &= -\frac{eA_0}{2\hbar m} \\ &\times \left[\langle\phi_f|e^{-i\vec{k}\cdot\vec{r}}\hat{\epsilon}\cdot\vec{p}|\phi_i\rangle\int_0^T e^{i\omega\tau}e^{i\omega_{fi}\tau}d\tau \ - \langle\phi_f|e^{i\vec{k}\cdot\vec{r}}\hat{\epsilon}\cdot\vec{p}|\phi_i\rangle\int_0^T e^{-i\omega\tau}e^{i\omega_{fi}\tau}d\tau\right].\end{aligned} \tag{B.72}$$

The two integrals can be easily calculated, leading to

$$\tilde{c}_f^{(1)}(T) = -\frac{eA_0}{2\hbar m}\left[\langle\phi_f|e^{-i\vec{k}\cdot\vec{r}}\hat{\epsilon}\cdot\vec{p}|\phi_i\rangle\frac{1-e^{i(\omega_{fi}+\omega)T}}{\omega_{fi}+\omega} - \langle\phi_f|e^{i\vec{k}\cdot\vec{r}}\hat{\epsilon}\cdot\vec{p}|\phi_i\rangle\frac{1-e^{i(\omega_{fi}-\omega)T}}{\omega_{fi}-\omega}\right]. \tag{B.73}$$

In (B.70), $\omega > 0$ (external field frequency), and two potentially resonant terms are present:

a) the first term is resonant for $\omega = -\omega_{fi}$, say $\omega_{fi} = (E_f - E_i)/\hbar < 0$ (emission of energy from the atom to the external field);
b) the second term is resonant for $\omega = \omega_{fi}$, say $\omega_{fi} = (E_f - E_i)/\hbar > 0$ (absorption of energy from the external field).

For absorption processes, $\omega_{fi} > 0$: the first term in square parentheses is anti-resonant, the second one is resonant. For ω sufficiently close to ω_{fi}, we can neglect the anti-resonant term.

Transition probability for absorption

Let us consider here the case $\omega_{fi} > 0$ (absorption of radiation); if ω is not too different from ω_{fi}, the first term (emission) in the transition amplitude (B.73) can be neglected. The first-order probability that at time T the atomic system is in the state $|\phi_f\rangle$, say that during the time interval from 0 to T the transition $|\phi_i\rangle \to |\phi_f\rangle$ took place, can be calculated as

$$\mathcal{P}_{fi}(T,\omega) \ = \ \frac{|W_{fi}|^2}{4\hbar^2}\left|\frac{1-e^{i(\omega_{fi}-\omega)T}}{\omega_{fi}-\omega}\right|^2 \ = \ \frac{|W_{fi}|^2}{4\hbar^2}\left\{\frac{\sin[(\omega_{fi}-\omega)T]/2}{(\omega_{fi}-\omega)/2}\right\}^2, \tag{B.74}$$

where

$$W_{fi} = \frac{eA_0}{m}\left\langle\phi_f\left|e^{i\vec{k}\cdot\vec{r}}\hat{\epsilon}\cdot\vec{p}\right|\phi_i\right\rangle,$$

The first-order probability $\mathcal{P}_{fi}(T,\omega)$ depends on two factors:

a) the time-independent matrix element W_{fi} which has no time dependence,
b) a time-dependent factor, which depends on the frequency ω of the perturbation and on the Bohr frequency ω_{fi}.

Resonance condition

The behavior of the transition probability (B.74) is represented in Fig. B.2 as a function of ω for a given value of interaction time T.
The function $P_{fi}(t,\omega)$ has a peak in correspondence of $\omega = \omega_{fi}$ (resonance condition) and progressively weaker oscillations when ω becomes different from ω_{fi}.. The resonance peak becomes higher and narrower when interaction time T increases:

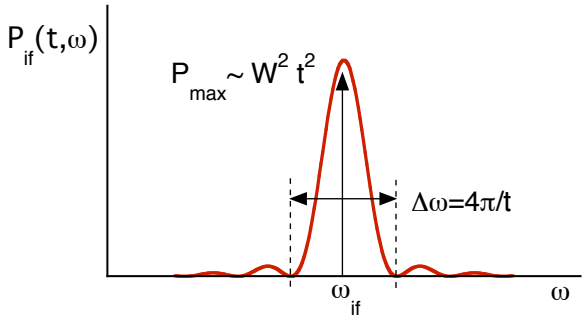

Figure B.2: Plot of the absorption probability $P_{if}(t,\omega)$ as a function the perturbation frequency ω for a given time t.

- the peak height depends on time as $P_{fi}(T,\omega_{fi}) = (|W_{fi}|^2/2\hbar^2)T^2$
- the peak width is inversely proportional to the interaction time, $\Delta\omega = 2\pi/T$

Let us consider now the two relevant cases:

1. the sinusoidal perturbation induces a transition from a discrete state to another discrete state,
2. the sinusoidal perturbation induces a transition from a discrete state to a state belonging to a continuum.

1. Transitions to discrete states

We want to evaluate the transition rate from an initial discrete state $|\phi_i\rangle$ to a final discrete state $|\phi_f\rangle$ of the atomic system, induced by a sinusoidal perturbation of frequency ω. We focus again the attention on the case of absorption, $\omega_{fi} > 0$.
According to Fig. B.2, when the interaction time T increases, the peak of the absorption probability progressively narrows around the value $\omega = \omega_{fi}$, and its value $P_{fi}(T,\omega_{fi}) = (|W_{fi}|^2/2\hbar^2)T^2$ increases with the square of time T.
For a purely monochromatic perturbation, this means that the transition rate $w_{fi} = dP_{fi}/dT$ increases indefinitely with time.
This result is un-physically for long interaction times, since the probability of the final state cannot exceed the value 1.
This problem depends on the inadequacy of the first-order approximation when long times are considered. The first-order perturbation approximation can be considered suitable for interaction times T included between the two limits

$$\frac{1}{\omega} \ll T \ll \frac{\hbar}{|W_{fi}|} \tag{B.75}$$

Taking into account higher order perturbation terms, or using other kinds of approximation (e.g. the secular equation), one can show that the system oscillates in time between the initial and final states.

2. Transitions to continuum states. Golden Rule

Let us now consider the first-order probability per unit time of the transition from an initial atomic discrete state $|\phi_i\rangle$ to a final state belonging to a continuous distribution of energy values, induced by a sinusoidal perturbation of frequency ω. The discrete value ω_{fi} of Fig. B.2 becomes now a continuous distribution of values.
Since the final state of energy $E_f = \hbar\omega_f$ belongs to a continuum, we can only evaluate the probability that after an interaction time T the system is in a final state whose energy belongs to

an interval ΔE_f centered on E_f,

$$\delta\mathcal{P}_{fi}(T, E_f) \;=\; \frac{1}{4\hbar^2} \int_{\Delta E_f} |\tilde{W}_{fi}|^2\, \rho(E) \left\{ \frac{\sin[(\tilde{\omega}-\omega)T]/2}{(\tilde{\omega}-\omega)/2} \right\}^2 dE\,, \tag{B.76}$$

where $\rho(E)$ is the density of final states, $\tilde{\omega} = (E - E_i)/\hbar$ and

$$\tilde{W}_{fi} = \frac{eA_0}{m} \left\langle \phi_f(E) \left| e^{i\vec{k}\cdot\vec{r}} \hat{\epsilon}\cdot\vec{p} \right| \phi_i \right\rangle ,$$

It is now convenient to consider the asymptotic behavior of the factor in curly brackets for $T \to \infty$. Exploiting the properties of the delta function, one finds

$$\left\{ \frac{\sin[(\tilde{\omega}-\omega)T]/2}{(\tilde{\omega}-\omega)/2} \right\}^2 \quad \xrightarrow[T\to\infty]{} \quad 2\pi T\; \delta(\tilde{\omega}-\omega)\,, \tag{B.77}$$

so that the probability of absorption becomes

$$\delta\mathcal{P}_{fi}(T, E_f) \;=\; \frac{\pi}{2\hbar}\, T \int_{\Delta E_f} |\tilde{W}_{fi}|^2\, \rho(E)\, \delta(E - E_i - \hbar\omega)\, dE\,, \tag{B.78}$$

and calculating the integral one finds finally

$$\delta\mathcal{P}_{fi}(T, E_f) \;=\; \frac{\pi}{2\hbar}\, T\, |W_{fi}|^2\, \rho(E_f)\,, \tag{B.79}$$

where $E_f = E_i + \hbar\omega$ and

$$W_{fi} = \frac{eA_0}{m} \left\langle \phi_f \left| e^{i\vec{k}\cdot\vec{r}} \hat{\epsilon}\cdot\vec{p} \right| \phi_i \right\rangle ,$$

The probability (B.79) that the system is in one of the final states whose energy belongs to a small energy interval ΔE around E_f increases proportionally to the time T (when T increases, the width ΔE decreases).
The transition rate is thus

$$\begin{aligned} w_{fi} \;=\; \frac{d}{dT}\delta\mathcal{P}_{fi} \quad &= \quad \frac{\pi}{2\hbar}\, |W_{fi}|^2\, \rho(E_f) \\ &= \quad \frac{\pi e^2 A_0^2}{2\hbar m^2}\; |\langle\phi_f| e^{i\vec{k}\cdot\vec{r}}\hat{\epsilon}\cdot\vec{p}|\phi_i\rangle|^2\; \rho(E_f) \end{aligned} \tag{B.80}$$

where $\rho(E_f$ is the density of final states at the value $E = E_f$.
Equation (B.80) was called *Golden rule* by Enrico Fermi, in view of its widespread applications.

Non-monochromatic radiation No real radiation beam is perfectly monohromatic.
Let us now consider a non-monochromatic perturbation, such that the perturbation frequency ω is distributed over an interval around a central value ω_0, with density $\rho(\omega)$.
The problem is formally similar to that of the transition to a contiuuum of states. One can easily see that (B.80) is modified to

$$w_{if} \;=\; \frac{\pi}{2\hbar}\, |W_{fi}|^2\, \rho(\omega_0) \tag{B.81}$$

where $\hbar\omega_0 = E_f - E_i$.

Note The expression of the transition rate (B.80) for a sinusoidal perturbation is 4 times smaller than the expression for a time-independent perturbation (B.67). See also eq. C-36 and C-37 in Chapter XIII of [Cohen-Tannoudji et al., 1973].

B.5 Electric dipole approximation

Let us consider the interaction Hamiltonian responsible for the processes of one photon absorption or stimulated emission

$$H_{\rm int} \;=\; \frac{e}{m}\,\vec{A}\cdot\vec{p} \tag{B.82}$$

an seek a conveniently approximate expression for the Golden Rule matrix element $|\langle\phi_f|e^{i\vec{k}\cdot\vec{r}}\hat{\epsilon}\cdot\vec{p}|\phi_i\rangle|^2$.
A good starting point is the expansion of the exponential

$$e^{i\vec{k}\cdot\vec{r}} \;=\; 1 \;+\; i\vec{k}\cdot\vec{r} \;-\; \frac{(\vec{k}\cdot\vec{r})^2}{2!}\;... \tag{B.83}$$

If we consider only the first term of the expansion, $e^{i\vec{k}\cdot\vec{r}} = 1$ (electric dipole approximation) the transition rate becomes

$$w_{fi} \;=\; \frac{\pi e^2 A_0^2}{2\hbar m^2}\;|\langle\phi_f|\hat{\epsilon}\cdot\vec{p}|\phi_i\rangle|^2\;\rho(E_f)\,. \tag{B.84}$$

The dipole approximation corresponds to considering the electromagnetic field constant over the dimension of the interacting system.

Alternative expressions of the dipole operator

One can express the dipole operator in an alternative form with that appearing in (B.84). In the alternative form the dipole operator is expressed in terms of the position operator of the electron $\vec{r}$ instead of the momentum operator $\vec{p}$.
Let us first demonstrate the commutation relation

$$[\vec{r}, H_0] \;=\; \frac{i\hbar}{m}\,\vec{p}, \tag{B.85}$$

where H_0 is the unperturbed Hamiltonian of the atom and $\vec{p}$ is the generalised momentum (corresponding to $-i\hbar\vec{\nabla}$ in the coordinate representation).
The demonstration can be based on the following points:

a) In the Hamiltonian H_0 we can retain only the kinetic term $p^2/2m$, since the potential term only depends on the position and thus commutes with $\vec{r}$.
b) Since $[r_i, p_j] = 0$ for $i \neq j$, we can separately consider the commutators of the three components of the position and momentum vectors $[r_k, p_k^2]$.
c) One can easily verify that $[r_k, p_k^2] = 2i\hbar p_k$, so that finally

$$[\vec{r}, H_0] \;=\; \left[\vec{r}, \frac{p^2}{2m}\right] \;=\; \frac{i\hbar}{m}\,\vec{p}\,.$$

Exploiting now the commutation relation (B.85), one can perform the following substitutions:

$$\begin{aligned}
\langle\phi_f|\,\vec{p}\,|\phi_i\rangle \;&=\; \frac{m}{i\hbar}\,\langle\phi_f|\,\vec{r}H_0 - H_0\vec{r}\,|\phi_i\rangle \\
&=\; im\,\frac{E_f - E_i}{\hbar}\,\langle\phi_f|\,\vec{r}\,|\phi_i\rangle \\
&=\; im\,\omega\,\langle\phi_f|\,\vec{r}\,|\phi_i\rangle\,,
\end{aligned} \tag{B.86}$$

where ω is the Bohr angular frequency connecting the initial and final electron states, corresponding to the angular frequency of the absorbed photon.
Substituting the matrix element of (B.86) in (B.84), one obtains the alternative expression of the transition rate

$$w_{fi} \;=\; \frac{\pi e^2 A_0^2\omega}{2\hbar}\;|\,\langle\,\phi_f|\;\hat{\epsilon}\cdot\vec{r}\;|\phi_i\,\rangle\,|^2\;\;S_0^2\;\rho(\epsilon_f)\,. \tag{B.87}$$

Expression as a function of the electric field

Taking into account that in the radiation gauge

$$\vec{E} = -\frac{\partial \vec{A}}{\partial t} \tag{B.88}$$

and that we are considering a sinusoidal dependence on time of the vector potential, the dipole transition rate can be written as

$$w_{fi} = \frac{\pi e^2 E_0^2}{2\hbar} \left|\langle \phi_i | \hat{\epsilon} \cdot \vec{r} | \phi_f \rangle\right|^2 \rho(E_f) \tag{B.89}$$

B.6 Second-order approximation

The second-order transition amplitude is

$$\begin{aligned} \tilde{c}_{fi}^{(2)} = & \left(\frac{1}{i\hbar}\right)^2 \int_{t_1}^{+T/2} d\tau_2 \int_{-T/2}^{t_1} d\tau_1 \\ & \sum\nolimits_k \langle \Phi_f | H_{\text{int}} | \Phi_k \rangle \langle \Phi_k | H_{\text{int}} | \Phi_i \rangle \, e^{i(E_f - E_k)\tau_2/\hbar} \, e^{i(E_k - E_i)\tau_1/\hbar} , \end{aligned} \tag{B.90}$$

with the restriction $-T/2 \leq \tau_1 \leq \tau_2 \leq +T/2$.
The condition $\tau_1 \leq \tau_2$ can be expressed by the Heaviside function

$$\theta(\tau_2 - \tau_1) = \begin{cases} 1 & \text{for } \tau_2 > \tau_1 \\ 0 & \text{for } \tau_2 < \tau_1 \end{cases} \tag{B.91}$$

One can show that

$$e^{-iE_k(\tau_2 - \tau_1)/\hbar} \, \theta(\tau_2 - \tau_1) = \lim_{\epsilon \to 0^+} \frac{i}{2\pi} \int_{-\infty}^{+\infty} \frac{e^{-iE(\tau_2 - \tau_1)}}{E + i\epsilon - E_k} \, dE \tag{B.92}$$

As a consequence, one can re-write

$$\begin{aligned} \tilde{c}_{fi}^{(2)} = & \left(\frac{1}{i\hbar}\right)^2 \frac{i}{2\pi} \int_{t-T/2}^{+T/2} d\tau_2 \int_{-T/2}^{+T/2} d\tau_1 \\ & \int_{-\infty}^{+\infty} dE \, \sum\nolimits_k \lim_{\epsilon \to 0^+} \frac{\langle \Phi_f | H_{\text{int}} | \Phi_k \rangle \langle \Phi_k | H_{\text{int}} | \Phi_i \rangle}{E + i\epsilon - E_k} \, e^{i(E_f - E)\tau_2/\hbar} \, e^{i(E - E_i)\tau_1/\hbar} . \end{aligned} \tag{B.93}$$

The integrals on τ_1 and τ_2 can be performed as for the first-order approximation, giving

$$\begin{aligned} \tilde{c}_{fi}^{(2)} = & \left(\frac{1}{i\hbar}\right)^2 2\pi i \\ & \int_{-\infty}^{+\infty} dE \, \sum\nolimits_k \lim_{\epsilon \to 0^+} \frac{\langle \Phi_f | H_{\text{int}} | \Phi_k \rangle \langle \Phi_k | H_{\text{int}} | \Phi_i \rangle}{E + i\epsilon - E_k} \, \delta^{(T)}(E_f - E) \, \delta^{(T)}(E - E_i) . \end{aligned} \tag{B.94}$$

The two $\delta^{(T)}$ functions are different from zero in a narrow interval of width $\simeq \hbar/T$.
In many cases, the fraction inside the integral varies comparatively slowly with respect to the $\delta^{(T)}$ functions, so that it can be extracted from the integral

$$\tilde{c}_{fi}^{(2)} \propto \lim_{\epsilon \to 0^+} \sum\nolimits_k \frac{\langle \Phi_f | H_{\text{int}} | \Phi_k \rangle \langle \Phi_k | H_{\text{int}} | \Phi_i \rangle}{E + i\epsilon - E_k} \int_{-\infty}^{+\infty} dE \, \delta^{(T)}(E_f - E) \, \delta^{(T)}(E - E_i) . \tag{B.95}$$

One can show that

$$\int_{-\infty}^{+\infty} dE \, \delta^{(T)}(E_f - E) \, \delta^{(T)}(E - E_i) = \delta^{(T)}(E_i - E_f) \tag{B.96}$$

so that

$$\tilde{c}_{fi}^{(2)} = -2\pi i \left[\lim_{\epsilon \to 0^+} \sum\nolimits_k \frac{\langle \Phi_f | H_{\text{int}} | \Phi_k \rangle \langle \Phi_k | H_{\text{int}} | \Phi_i \rangle}{E + i\epsilon - E_k} \right] \delta^{(T)}(E_i - E_f) . \tag{B.97}$$

Transition probabilities

According to the above treatment, the total transition amplitude is, to second-order approximation,

$$\tilde{c}_{fi} \;=\; \delta_{fi} - 2\pi i\, \delta^{(T)}(E_f - E_i) \left[\langle \Phi_f | \, H_{\rm int} \, | \Phi_i \rangle + \lim_{\epsilon \to 0^+} \sum\nolimits_k \frac{\langle \Phi_f | \, H_{\rm int} \, | \Phi_k \rangle \langle \Phi_k | \, H_{\rm int} \, | \Phi_i \rangle}{E + i\epsilon - E_k} \right] \quad \text{(B.98)}$$

We want to calculate the transition probability from an initials eigen-state of the unperturbed Hamiltonian $|\Phi_i\rangle$ to a different final eigen-state $|\Phi_f\rangle$.
Since $\delta_{fi} = 0$, the transition probability is

$$\tilde{\mathcal{P}}_{fi} \;=\; 4\pi^2 \left[\delta^{(T)}(E_f - E_i) \right]^2 \left[\langle \Phi_f | \, H_{\rm int} \, | \Phi_i \rangle + \lim_{\epsilon \to 0^+} \sum\nolimits_k \frac{\langle \Phi_f | \, H_{\rm int} \, | \Phi_k \rangle \langle \Phi_k | \, H_{\rm int} \, | \Phi_i \rangle}{E + i\epsilon - E_k} \right]^2 \quad \text{(B.99)}$$

Appendix C

Theory of scattering

Basic references:

- [Merzbacher, 1970], Chapters 11 and 19.
- [Cohen-Tannoudji et al., 1973], Chapter 8

C.1 Scattering of a wave-packet

Let us consider a scattering potential $V(r)$ centred at the origin of the reference frame, isotropic and decreasing towards infinity faster than $1/r$ (of range a).

Hamiltonian and Schródinger equation

The Hamiltonian is

$$H = H_0 + V(r) \tag{C.1}$$

and the Schrödinger equation is

$$\left[-\frac{\nabla^2}{2\mu} + V(r)\right]\ \Psi(\vec{r}) \ = \ E\,\Psi(\vec{r}) \tag{C.2}$$

It is convenient to substitute

$$E = \frac{\hbar^2 k^2}{2\mu}\,; \qquad V(r) = \frac{\hbar^2}{2\mu}\,U(r) \tag{C.3}$$

so that the Schrödinger equation becomes

$$\left[\nabla^2 + k^2 - U(r)\right]\ \Psi(\vec{r})] \ = \ 0\,. \tag{C.4}$$

Free-particle wave-packet

At time $t = 0$ an incoming wave-packet centred at position $\vec{r}_0$ is described by

$$\Psi(\vec{r},0) = \frac{1}{(2\pi)^{3/2}} \int \phi(\vec{k}) e^{i\vec{k}\cdot(\vec{r}-\vec{r}_0)} d^3k = \frac{1}{(2\pi)^{3/2}} \int \phi(\vec{k}) e^{i\vec{k}\cdot\vec{r}}\, e^{-i\vec{k}\cdot\vec{r}_0} d^3k \tag{C.5}$$

where $\phi(\vec{k})$ is a smooth function of narrow width centred on $\vec{k}_0$.
Equation (C.5) corresponds to an expansion in plane waves $\exp(i\vec{k}\cdot\vec{r})$, eigenfunctions of the unperturbed Hamoltonian $H_0 = p^2/2m$.

Scattered particle wave-packet

One can show that the Schrödinger equation for the full Hamiltonian $H = H_0 + V(r)$

$$H\Psi_{\vec{k}}^{(+)} \;=\; E\Psi_{\vec{k}}^{(+)} \tag{C.6}$$

is asymptotically ($r \to \infty$) satisfied by eigenfunctions

$$\Psi_{\vec{k}}^{(+)}(\vec{r}) \;=\; \frac{1}{(2\pi)^{3/2}}\left[e^{i\vec{k}\cdot\vec{r}} + f_{\vec{k}}(\hat{r})\frac{e^{ikr}}{r}\right] \tag{C.7}$$

and that the wave-packet at time $t = 0$ can be expanded in terms of the wavefunctions (C.7) (in place of plane waves)

$$\Psi(\vec{r},0) = \frac{1}{(2\pi)^{3/2}}\int \phi(\vec{k})\, e^{-i\vec{k}\cdot\vec{r}_0}\, \Psi_{\vec{k}}^{(+)}(\vec{r})\, d^3k \tag{C.8}$$

The wave packet at time t is

$$\Psi(\vec{r},t) = \frac{1}{(2\pi)^{3/2}}\int \phi(\vec{k})\, e^{-i\vec{k}\cdot\vec{r}_0}\, \Psi_{\vec{k}}^{(+)}(\vec{r})\, e^{-iEt/\hbar}\, d^3k \tag{C.9}$$

where $E = \hbar\omega = \hbar^2k^2/2m$.
Substituting (C.7) into (C.9) one gets

$$\begin{aligned}\Psi(\vec{r},t) = {} & \frac{1}{(2\pi)^{3/2}}\int \phi(\vec{k})\, e^{i\vec{k}\cdot(\vec{r}-\vec{r}_0)}\, e^{-iEt/\hbar}\, d^3k \\ & + \frac{1}{(2\pi)^{3/2}}\int \phi(\vec{k})\, e^{-i\vec{k}\cdot\vec{r}_0}\, f_{\vec{k}}(\hat{r})\frac{e^{ikr}}{r}\, e^{-iEt/\hbar}\, d^3k\end{aligned} \tag{C.10}$$

where the first term on the right represents the incoming wave-packet and the the second term represents the scattered wave-packet.
Approximately, (C.10) can be rewritten as for a particle moving with velocity $\vec{v}_0 = \hbar\vec{k}_0/m$

$$\begin{aligned}\Psi(\vec{r},t) = {} & \Psi(\vec{r} - \vec{v}_0 t, 0)\, e^{iE_0t/\hbar} \\ & + \frac{f_{\vec{k}_0}(\hat{r})}{r}\, \Psi(r\hat{k}_0 - \vec{v}_0 t, 0)\, e^{iE_0t/\hbar}\end{aligned} \tag{C.11}$$

The differential scattering cross section is connected to the scattering amplitude by

$$\frac{d\sigma}{d\Omega} \;=\; |f_{\vec{k}_0}(\hat{r})|^2\,. \tag{C.12}$$

C.2 Green's functionc in scattering theory

We need now to prove that

a) the wavefunctions (C.7) are solutions of the stationary Schrödinger equation (C.6)
b) the incoming wave packet (C.5) can be expanded into the basis of wavefunctions (C.7), leading to (C.8)

To that purpose, the formalism of Green's functions is particularly suitable. Let us consider here only the first point (a). For point (b), refer to Merzbacher, Chapter 11.

C.2.1 The integral Schrödinger equation

Let us rewrite the stationary Schrödinger equation

$$\left(-\frac{\hbar^2}{2m}\nabla^2 + V\right)\Psi = E\,\Psi \tag{C.13}$$

as

$$(\nabla^2 + k^2)\,\Psi = U\,\Psi \tag{C.14}$$

where $k^2 = 2mE/\hbar^2$ and $U = 2mV/\hbar^2$.
Let us consider (C.14) as if it were an inhomogeneous differential equation (the inhomogeneity being $U\Psi$)). The solution of (C.14) is thus the sum of an arbitrary solution of the homogeneous equation plus a particular solution of the "inhomogeneous" equation. One can verify, by substitution, that the differential equation (C.14) is equivalent to the integral equation

$$\Psi_{\vec{k}}(\vec{r}) \;=\; \frac{1}{(2\pi)^{3/2}}\,e^{i\vec{k}\cdot\vec{r}} \;-\; \frac{1}{4\pi}\int G(\vec{r},\vec{r}')\,U(\vec{r}')\,\Psi_{\vec{k}}(\vec{r}')\,d^3r' \tag{C.15}$$

where $G(\vec{r},\vec{r}')$ is a Green function, say a function satisfying the equation

$$(\nabla^2 + k^2)\,G(\vec{r},\vec{r}') = -4\pi\,\delta(\vec{r}-\vec{r}')\,. \tag{C.16}$$

C.2.2 Choice of the Green's function

A Green's function fulfilling the boundary conditions of our problem is the outgoing Green's function

$$G_+(|\vec{r}-\vec{r}'|) \;=\; \frac{\exp(ik\,|\vec{r}-\vec{r}'|)}{|\vec{r}-\vec{r}'|} \tag{C.17}$$

One can show that (C.17) is a solution of (C.16) by a procedure based on the Fourier transform

$$\begin{aligned} G_+(\vec{r}) \;&=\; \frac{1}{2\pi^2}\int \frac{e^{i\vec{k}'\cdot\vec{r}}}{k'^2-k^2}\,d^3k' \\ &=\; \lim_{\eta\to 0} G_{+\eta}(\vec{r}) = \frac{1}{2\pi^2}\lim_{\eta\to 0}\int \frac{e^{i\vec{k}'\cdot\vec{r}}}{k'^2-(k^2+i\eta)}\,d^3k'\,. \end{aligned} \tag{C.18}$$

Integrating over the angles,

$$G_+(r) \;=\; \frac{e^{ikr}}{r} \;=\; \lim_{\eta\to 0} G_{+\eta}(r) \;=\; -\frac{1}{\pi r}\,\frac{d}{dr}\int_{-\infty}^{+\infty}\frac{e^{ik'r}}{k'^2-(k^2+i\eta)}\,dk' \tag{C.19}$$

C.2.3 Scattering wavefuntions

Substituting (C.17) into the integral equation (C.15) on finds

$$\Psi^{(+)}_{\vec{k}}(\vec{r}) \;=\; \frac{1}{(2\pi)^{3/2}}\,e^{i\vec{k}\cdot\vec{r}} \;-\; \frac{1}{4\pi}\int \frac{\exp(ik\,|\vec{r}-\vec{r}'|)}{|\vec{r}-\vec{r}'|}\,U(\vec{r}')\,\Psi^{(+)}_{\vec{k}}(\vec{r}')\,d^3r' \tag{C.20}$$

If now the potential energy is short ranged, such that $U(r') \neq 0$ only for $r' < a$, and we consider large distances $r' \gg a$, (C.20) can be rewritten as

$$\Psi^{(+)}_{\vec{k}}(\vec{r}) \;\simeq\; \frac{1}{(2\pi)^{3/2}}\,e^{i\vec{k}\cdot\vec{r}} \;-\; \frac{e^{ikr}}{4\pi r}\int e^{-i\vec{k}'\cdot\vec{r}'}\,U(\vec{r}')\,\Psi^{(+)}_{\vec{k}}(\vec{r}')\,d^3r' \tag{C.21}$$

where $\vec{k}' = k\hat{r}$.
Equation (C.21) corresponds to (C.7)

$$\Psi^{(+)}_{\vec{k}}(\vec{r}) \;\simeq\; \frac{1}{(2\pi)^{3/2}}\left[e^{i\vec{k}\cdot\vec{r}} + f^{(+)}_{\vec{k}}(\hat{r})\frac{e^{ikr}}{r}\right] \tag{C.22}$$

where

$$f^{(+)}_{\vec{k}}(\hat{r}) \;=\; \frac{(2\pi)^{3/2}}{4\pi}\int e^{-i\vec{k}'\cdot\vec{r}'}\,U(\vec{r}')\,\Psi^{(+)}_{\vec{k}}(\vec{r}')\,d^3r' \tag{C.23}$$

C.3 Formal theory of scattering

We look at the scattering process as a transition from an unperturbed state to another unperturbed state, both described as plane waves, eigenstates of the unperturbed Hamiltonian H_0.
Let the total Hamiltonian be

$$H \;=\; H_0 + V \;=\; p^2/2m + V\,. \tag{C.24}$$

The stationary Schrödinger equation for the unperturbed Hamiltonian is

$$H_0\,|\Psi_s\rangle \;=\; E_s\,|\Psi_s\rangle\,, \tag{C.25}$$

where the stationary states $|\Psi_s\rangle$ correspond to plane waves.
The time-dependent Schrödinger equation for the total Hamiltonian

$$i\hbar\,\frac{\partial}{\partial t}\,|\Psi(t)\rangle \;=\; H\,|\Psi(t)\rangle \tag{C.26}$$

has the general solution

$$|\Psi(t)\rangle \;=\; \sum\nolimits_s c_s(t)\,e^{-iE_s t/\hbar}\,|\Psi_s\rangle\,. \tag{C.27}$$

Inserting (C.27) into (C.26) one finds the time derivatives of the coefficients c_r

$$i\hbar\,\frac{dc_r}{dt} \;=\; \sum\nolimits_s c_s(t)\,\langle\Psi_r|V|\Psi_s\rangle\,e^{i\omega_{rs}t}\,, \tag{C.28}$$

where

$$\omega_{rs} \;=\; (E_r - E_s)/\hbar\,. \tag{C.29}$$

Equation (C.28) corresponds to (**??**) of Appendix B.

Perturbation theory versus formal theory of scattering

Within the time dependent perturbation theory, to first order the solution of (C.28) is given by (**??**), which, for a constant potential V in the present notation, becomes

$$c_r(t) \;=\; -\frac{i}{\hbar}\,\langle\Psi_r|V|\Psi_s\rangle\int_o^t e^{i\omega_{rs}t'}\,dt' + \delta_{rs}\,. \tag{C.30}$$

In the formal theory of scattering, the first-order expression (C.30) is substituted by an exact expression

$$c_r(t) \;=\; -\frac{i}{\hbar}\,\langle\Psi_r|T|\Psi_s\rangle\int_o^t e^{i\omega_{rs}t'}\,e^{\alpha t'}\,dt' + \delta_{rs}\,, \tag{C.31}$$

where

- the unknown transition matrix T_{rs} substitutes the known matrix V_{rs}, to avoid the perturbation approximation
- the quantity $1/\alpha$ roughly measures the time duration of the interaction;
  equation (C.31) correctly gives the values $c_r(t)$ only for times $|t| \ll (1/\alpha)$;
  after the limit $t_0 \to -\infty$ has been calculated, also the limit $\alpha \to 0$ has to be taken.

Assuming the existence of the matrix T_{rs}, upon integrating (C.31) one obtains

$$c_r(t) \;=\; \frac{\langle\Psi_r|T|\Psi_s\rangle\,e^{i\omega_{rs}t}e^{\alpha t}}{-(E_r - E_s) + i\hbar\alpha} + \delta_{rs}\,, \tag{C.32}$$

since $\exp(\alpha t_0) = 0$ for $t_0 \to -\infty$ and $\alpha \to 0$

Transition operator

As we have seen in Appendix B, the first-order time-dependent perturbation theory leads, for a constant potential, to the following expression for the transition rate (Golden Rule):

$$\frac{d}{dt}|c_r|^2 \;=\; \frac{2\pi}{\hbar}\,|\langle\Psi_r|V|\Psi_s\rangle|^2\,\delta(E_r-E_s)\,. \tag{C.33}$$

In the formal scattering theory one assumes, by a similar procedure, that the transition rate can be expressed exactly by a similar expression

$$\frac{d}{dt}|c_r|^2 \;=\; \frac{2\pi}{\hbar}\,|\langle\Psi_r|T|\Psi_s\rangle|^2\,\delta(E_r-E_s)\,, \tag{C.34}$$

where the elements of the transition matrix Trs are connected to the elements of the potential energy matrix V_{rs} by the following expression:

$$\langle\Psi_r|T|\Psi_s\rangle \;=\; \langle\Psi_r|V|\Psi_s\rangle \;+\; \sum\nolimits_n \frac{\langle\Psi_r|V|\Psi_n\rangle\langle\Psi_n|T|\Psi_s\rangle}{-(E_n-E_s)+i\hbar\alpha}\,. \tag{C.35}$$

Note: Equation (C.35) is valid only if the unperturbed states form a quasi-continuum. The present treatment would fail for perfectly discrete states.

Lippman-Schwinger equation

To connect the formal theory of scattering with the wave-packet approach of § C.2, is is convenient to introduce a set of states $|\Psi_s^{(+)}\rangle$ such that

$$\langle\Psi_r|T|\Psi_s\rangle \;=\; \langle\Psi_r|V|\Psi_s^{(+)}\rangle \;=\; \sum\nolimits_j\langle\Psi_r|V|\Psi_j\rangle\langle\Psi_j|\Psi_s^{(+)}\rangle\,. \tag{C.36}$$

Substituting in (C.35) one obtains an exact expression containing only V

$$\langle\Psi_r|V|\Psi_s^{(+)}\rangle \;=\; \langle\Psi_r|V|\Psi_s\rangle \;+\; \sum\nolimits_n \frac{\langle\Psi_r|V|\Psi_n\rangle\langle\Psi_n|V|\Psi_s^{(+)}\rangle}{E_s-E_n+i\hbar\alpha}\,. \tag{C.37}$$

Since (C.37) must be true for all r, one gets

$$\begin{aligned} |\Psi_s^{(+)}\rangle \;&=\; |\Psi_s\rangle \;+\; \sum\nolimits_n \frac{|\Psi_n\rangle\langle\Psi_n|V|\Psi_s^{(+)}\rangle}{E_s-E_n+i\hbar\alpha} \\ &=\; |\Psi_s\rangle \;+\; \sum\nolimits_n \frac{|\Psi_n\rangle\langle\Psi_n|V|\Psi_s^{(+)}\rangle}{E_s-H_0+i\hbar\alpha} \end{aligned} \tag{C.38}$$

and, exploiting the completeness, on arrives at the Lippman-Schwinger implicit equation

$$\boxed{|\Psi_s^{(+)}\rangle \;=\; |\Psi_s\rangle \;+\; \frac{1}{E_s-H_0+i\hbar\alpha}\,V\,|\Psi_s^{(+)}\rangle} \tag{C.39}$$

Lippman-Schwinger equation (C.39) and Green function formalism of § C.2

Let's start from (C.38) and project it in the coordinate representation, where

$$\langle\vec{r}|\Psi_s\rangle = \frac{1}{(2\pi)^{3/2}}e^{i\vec{k}\cdot\vec{r}}\,;\quad \langle\vec{r}|\Psi_s^{(+)}\rangle = \Psi_s^{(+)}(\vec{r})\,;\quad \langle\vec{r}'|V|\vec{r}''\rangle = V(\vec{r})\delta\,(\vec{r}'-\vec{r}'')\,. \tag{C.40}$$

If $|\Psi_s\rangle$ are momentum eigenfunctions, we can substitute the sum over the energy values by the integral over the wavevectors k, and get the alternative expression of (C.39)

$$\Psi_s^{(+)}(\vec{r}) \;=\; \frac{1}{(2\pi)^{3/2}}e^{i\vec{k}\cdot\vec{r}} \;-\; \frac{1}{(2\pi)^3}\int\left[\int\frac{e^{i\vec{k}'\cdot(\vec{r}-\vec{r}')}}{k'^2-(k^2+i\eta)}\,d^3k'\right]\frac{2m}{\hbar^2}\,V(\vec{r}')\,\Psi_s^{(+)}(\vec{r}')\,d^3r' \tag{C.41}$$

Comparing with the definition of the Green's function (C.18) and remembering that $2mV/\hbar^2 = U$, one can see that (C.39) corresponds to (C.20).
The Green's function $G_+(\vec{r},\vec{r}')$ introduced in § C.2 corresponds thus, in the coordinate representation to the Green' operator $G_+(E)$ appearing in the Lippman-Schwinger equation (C.39):

$$G_+(\vec{r},\vec{r}') \;=\; -i\frac{4\pi\hbar^2}{2m}\,\langle\vec{r}|G_+(E)|\vec{r}'\rangle\,, \tag{C.42}$$

where

$$G_+(E) \;=\; \frac{1}{E - H_0 + i\hbar\alpha}\,. \tag{C.43}$$

Series expansion

The Lippman-Schwinger equation (C.39) can be rewritten, using the shorthand notation of the Green's operator (C.43), as

$$|\Psi_s^{(+)}\rangle \;=\; |\Psi_s\rangle \;+\; G_+(E)\,V\,|\Psi_s^{(+)}\rangle\,, \tag{C.44}$$

say

$$|\Psi_s^{(+)}\rangle\;[1 - G_+(E)\,V] = \;|\Psi_s\rangle\,, \tag{C.45}$$

so that

$$|\Psi_s^{(+)}\rangle = \;[1 - G_+(E)\,V]^{-1}\;|\Psi_s\rangle\,. \tag{C.46}$$

The power series expansion

$$[1 - G_+(E)\,V]^{-1} \;=\; 1 \;+\; G_+(E)\,V \;+\; [G_+(E)\,V]^2 \;+\; [G_+(E)\,V]^3 \;+\; \cdots \tag{C.47}$$

leads to the series expansion of (C.46)

$$|\Psi_s^{(+)}\rangle = \;|\Psi_s\rangle \;+\; G_+(E)\,V\,|\Psi_s\rangle \;+\; G_+(E)\,V\,G_+(E)\,V\,|\Psi_s\rangle \;+\; \cdots \tag{C.48}$$

The n-th Born approximation corresponds to truncating the series (C.48) after n terms.

Incoming and outgoing waves

The states $|\Psi_s^{(+)}\rangle$ form a complete set of orthonormal eigenstates of the total Hamitonian H, corresponding to outgoing waves.
An alternative set of orthonormal eigenstates of the total Hamiltonian H is formed by the outgoing wave states $|\Psi_s^{(-)}\rangle$, which obey the equation

$$|\Psi_s^{(-)}\rangle \;=\; |\Psi_s\rangle \;+\; G_-(E)\,V\,|\Psi_s^{(-)}\rangle\,, \tag{C.49}$$

where $G_-(E)$ is the Green operator

$$G_-(E) \;=\; \frac{1}{E - H_0 - i\hbar\alpha}\,. \tag{C.50}$$

Scattering matrix

Appendix D

Statistics

In this Appendix, we recall some basic concepts of statistical thermodynamics that are relevant for the treatment of thermal disorder in EXAFS. Besides, we consider the most commonly used procedures for calculating partition functions and average values.
The basic problem is to calculate average values of physical observables over a set of possible configurations, due to thermal and structural disorder. Examples of observables are the EXAFS function or the quantities which allow to parametrize its analytical expression, such as the cumulants. Since low-temperature quantum effects are non negligible in accurate EXAFS analyses, we will rely on a quantum approach.

D.1 The density operator

Linear superposition and statistical mixing

To evaluate the statistical properties of a quantum system, it is convenient to introduce the *statistical density operator*, which operates on mixed quantum states [Messiah, 1970, Cohen-Tannoudji et al., 1973].
Let us first recall the difference between a pure state, a linear superposition of pure states and a statistical mixing of pure states.

A **pure state** is a linear superposition

$$|\psi(t)\rangle = \sum_n c_n(t)|u_n\rangle \tag{D.1}$$

where the $|u_n\rangle$ form an orthonormal basis (here considered discrete for simplicity) and c_n are complex numbers representing probability amplitudes and satisfying the relation $\sum |c_n(t)|^2 = 1$.
The knowledge of $|\psi(t)\rangle$ implies the full knowledge of the dynamical state of the system. The time evolution is given by the Schrödinger equation; one can exactly predict the statistical distribution of the results of measurements at any time.

A **mixed state** is a statistical mixing of pure states $|\psi_k(t)\rangle$, each one having a probability p_k, where $p_k \leq 1$ are real numbers such that $\sum p_k = 1$.
Mixed states describe statistical mixtures of pure states, when the dynamical state of a system is known incompletely.

Density operator for a pure state

Let us consider again a *pure state*. Two alternative and equivalent approaches are possible to evaluate the expectation value of an observable, one based on the vector state, one on the density operator.

In the first approach, the state of the system is described by the vector $|\psi\rangle$ of Eq. (D.1), with the normalization condition

$$\sum\nolimits_n |c_n|^2 = 1. \tag{D.2}$$

The expectation value of an observable A is

$$\langle A\rangle \;=\; \langle\psi|A|\psi\rangle \;=\; \sum_{mn} c_n^* c_m \langle u_n|A|u_m\rangle \;=\; \sum_{mn} c_n^* c_m\, A_{nm}\,. \tag{D.3}$$

Let us now introduce the alternative description, by observing that

$$c_n^* c_m = \langle u_n|\psi\rangle\langle\psi|u_m\rangle \tag{D.4}$$

are the matrix elements in the base $\{|u_m\rangle\}$ of the operator $w = |\psi\rangle\langle\psi|$, which is called *density operator*. The *density matrix* w, whose elements are

$$w_{nm} = \langle u_n|w|u_m\rangle = c_n^* c_m\,, \tag{D.5}$$

characterizes the quantum state in an equivalent way as the vector $|\psi\rangle$.
The normalization condition (conservation of probability) is expressed in terms of the trace of the density matrix:

$$\sum\nolimits_n |c_n|^2 = \sum\nolimits_n w_{nn} = \mathrm{Tr}(w) = 1\,. \tag{D.6}$$

The expectation value of the observable A is

$$\begin{aligned}\langle A\rangle \;&=\; \sum_{mn} c_m c_n^* A_{nm} = \sum_{mn}\langle u_m|w|u_n\rangle\langle u_n|A|u_m\rangle \\ &=\; \sum_{m}\langle u_m|wA|u_m\rangle = \mathrm{Tr}(wA)\,,\end{aligned} \tag{D.7}$$

say it is given by the trace of the product of the two matrices wA.

Statistical density operator

Let us now consider a statistical mixture of pure states $|\psi_k\rangle$, each one characterised by a probability p_k.
The expectation value of an observable A is now

$$\begin{aligned}\langle A\rangle \;&=\; \sum_k p_k \sum_{mn} (c_k)_m (c_k)_n^* A_{nm} = \sum_k p_k \sum_{mn}\langle u_m|w_k|u_n\rangle\langle u_n|A|u_m\rangle \\ &=\; \sum_m \langle u_m|\tilde{w}A|u_m\rangle = \mathrm{Tr}(\tilde{w}A)\,,\end{aligned} \tag{D.8}$$

where $\tilde{w}$ is the statistical density operator

$$\tilde{w} \;=\; \sum_k p_k\, w_k \;=\; \sum_k p_k\, |\psi_k\rangle\langle\psi_k|\,. \tag{D.9}$$

The density operator is hermitian and time-dependent. On can show that $\mathrm{Tr}(\tilde{w}A) = \mathrm{Tr}(A\tilde{w})$ and that $\mathrm{Tr}(\tilde{w}) = 1$.

D.2 Systems in thermodynamic equilibrium

Let us consider a system in thermodynamic equilibrium with a reservoir at temperature $T = 1/k_B\beta$. If the Hamiltonian H is independent of time, there are stationary states of energy E_n, eigenstate $|\phi_n\rangle$ and eigenfunction $\phi_n(x)$ (for simplicity, we consider here only non-degenerate states).

D.2.1 Density operator and partition function

We follow here the approach by [Chen and Kotlarchyk, 1997], § 7.2.
The classical expression for entropy

$$S \;=\; -k_B \sum p_i \,\ln p_i \tag{D.10}$$

is substituted by the quantum expression in terms of the density operator

$$S \;=\; -k_B \,\mathrm{Tr}(\tilde{w}\,\ln \tilde{w}) \tag{D.11}$$

If a basis is chosen where $\tilde{w}$ is diagonal, the entropy can be expressed as

$$S \;=\; -k_B \sum_n \tilde{w}_{nn}\,\ln \tilde{w}_{nn} \tag{D.12}$$

In order to find an explicit expression of the density operator, one maximises the entropy with the constraints that the total probability is constant and equal to 1 and the total average energy $\langle E\rangle$ is constant (conditions for the canonical distribution).
By introducing the two Lagrange multipliers λ and β, the extremum condition for entropy becomes

$$\delta S \;=\; \mathrm{Tr}\left[(1+\lambda) + \ln\tilde{w} + \beta H\right]\,\delta\tilde{w} \;=\; 0 \tag{D.13}$$

The quantity within square parentheses is zero, due to the arbitrariness of $\delta\tilde{w}$, so that the statistical density operator is

$$\tilde{w} \;=\; e^{-(1+\lambda)}\,e^{-\beta H} \;=\; \frac{1}{Z}\,e^{-\beta H} \tag{D.14}$$

where the quantity Z is determined by the condition that

$$\mathrm{Tr}\,(\tilde{w}) \;=\; 1 \;=\; \frac{1}{Z}\,\mathrm{Tr}\,\left(e^{-\beta H}\right) \tag{D.15}$$

so that

$$Z \;=\; \mathrm{Tr}\,\left(e^{-\beta H}\right) \;=\; e^{-\beta F}\,. \tag{D.16}$$

Z is the *Partition Function* and $F = U - TS$ is the Helmholtz free energy.

Energy representation

The partition function Z in the energy representation is given by

$$Z \;=\; \mathrm{Tr}\,\left(e^{-\beta H}\right) \;=\; \sum_n \langle\phi_n|\,e^{-\beta\ H}\,|\phi_n\rangle \;=\; \sum_n \langle\phi_n|\phi_n\rangle\,e^{-\beta E_n} \;=\; \sum_n e^{-\beta E_n}. \tag{D.17}$$

The elements of the statistical density matrix are

$$\tilde{w}_{mn} \;=\; \frac{1}{Z}\,\langle\phi_m|\,e^{-\beta H}\,|\phi_n\rangle \;=\; \frac{1}{Z}\,e^{-\beta E_n}\,\delta_{mn}. \tag{D.18}$$

The average value of an operator A is

$$\langle A\rangle \;=\; \mathrm{Tr}(\tilde{w}A) \;=\; \frac{1}{Z}\sum_n \langle\phi_n|\,Ae^{-\beta H}\,|\phi_n\rangle \;=\; \frac{1}{Z}\sum_n e^{-\beta E_n}\,\langle\phi_n|A|\phi_n\rangle \;=\; \frac{1}{Z}\sum_n A_{nn}\,e^{-\beta E_n}. \tag{D.19}$$

The probability density that a continuous observable X (e.g. a position coordinate) assumes a value x in the pure state $|\Psi_k\rangle$ is $\rho_k(x) = |\langle x|\Psi_k\rangle|^2 = \langle\Psi_k|x\rangle\langle x|\Psi_k\rangle$; otherwise stated, it is the average value of the projector $P_x = |x\rangle\langle x|$. For a statistical mixture of pure states, the probability density $\rho(x)$ is the average value of the $\rho_k(x)$, say the average value of the projector P_x:

$$\rho(x) \;=\; \mathrm{Tr}(\tilde{w}P_x) \;=\; \frac{1}{Z}\sum_n \langle\phi_n|\,x\rangle\langle x\,|e^{-\beta H}\,|\phi_n\rangle \;=\; \frac{1}{Z}\sum_n |\phi_n(x)|^2\,e^{-\beta E_n}. \tag{D.20}$$

Coordinate representation

Let us now consider the coordinate representation, for a system with one degree of freedom. The partition function Z is given by

$$Z \;=\; \mathrm{Tr}\left(e^{-\beta H}\right) \;=\; \int dx\, \langle x|\, e^{-\beta H}\, |x\rangle \;=\; \int dx \sum_n \langle x|\phi_n\rangle\langle\phi_n|\, e^{-\beta E_n}\, |x\rangle \;=\; \sum_n e^{-\beta E_n}. \quad \text{(D.21)}$$

The elements of the statistical density matrix are

$$\tilde{w}(x,x') \;=\; \frac{1}{Z}\,\langle x|\, e^{-\beta H}\, |x'\rangle \;=\; \frac{1}{Z}\sum_n e^{-\beta E_n}\,\phi_n^*(x)\,\phi_n(x'). \quad \text{(D.22)}$$

The average value of an operator A is

$$\langle A\rangle \;=\; \mathrm{Tr}(\tilde{w}A) \;=\; \frac{1}{Z}\int dx\,\langle x|\, Ae^{-\beta H}\, |x\rangle \;=\; \frac{1}{Z}\sum_n e^{-\beta E_n}\int dx\,\phi_n^*(x)\,A\,\phi_n(x). \quad \text{(D.23)}$$

By comparing Eq. (D.20) with Eq. (D.22) one can see that the probability density in coordinate representation is

$$\rho(x) \;=\; \tilde{w}(x,x). \quad \text{(D.24)}$$

Differential equation for the density operator

A *non-normalised statistical density operator* is sometimes introduced ([Feynman, 1972])

$$\tilde{w}^* \;=\; e^{-\beta H}. \quad \text{(D.25)}$$

The density operator depends on temperature. One can demonstrate that the non-normalised operator $\tilde{w}^*$ obeys the differential equation

$$\partial\tilde{w}^*/\partial\beta \;=\; -\,H\,\tilde{w}^* \quad \text{(D.26)}$$

with the initial condition

$$\tilde{w}^*(0) \;=\; 1, \quad \text{(D.27)}$$

corresponding to a uniform distribution over all the available energy states for $\beta = 0$, say $T = \infty$. It is worth noting that Eq. (D.26) is formally similar to the time-dependent Schrödinger equation

$$i\hbar\partial|\Psi\rangle/\partial t \;=\; \hat{H}\,|\Psi\rangle, \quad \text{(D.28)}$$

provided the substitution $\beta \to it/\hbar$ is made.
The integration of Eq. (D.26) with initial condition (D.27) allows one, in principle, to determine the density matrix in coordinate representation $\tilde{w}^*(x,x';\beta)$, once the Hamiltonian is known. This procedure is feasible in exact way only for particularly simple hamiltonians.
The normalised density matrix $\tilde{w}(x,x';\beta) = \tilde{w}^*(x,x';\beta)/Z$ can then be recovered, since $Z = \mathrm{Tr}(e^{-\beta H}) = \mathrm{Tr}(\tilde{w}^*)$.

D.3 Classical approximation

In the classical approximation (say for high enough temperature), the instantaneous state of a one-dimensional system is defined by its position x and momentum p. For a system in thermal equilibrium with a reservoir at temperature $T = 1/k_B\beta$, the probability density of the point (x,p) in phase space is given by

$$\rho(x,p) \;=\; \frac{e^{-\beta E(x,p)}}{Z} \;=\; \frac{e^{-\beta E(x,p)}}{\int dx \int dp\, e^{-\beta E(x,p)}}, \quad \text{(D.29)}$$

and the average value of a quantity $A(x,p)$ is given by

$$\langle A(x,p)\rangle \;=\; \frac{1}{Z}\int dx\,dp\,A(x,p)\,\rho(x,p). \tag{D.30}$$

If the potential energy is independent of p, the total energy is $E(x,p) = p^2/2m + V(x)$, so that the partition function Z can be calculated as

$$Z \;=\; \int dp\,e^{-\beta p^2/2m}\int dx\,e^{-\beta V(x)} \;=\; \sqrt{2m\pi/\beta}\int dx\,e^{-\beta V(x)}. \tag{D.31}$$

The probability density for a given value of position x is then

$$\rho(x) \;=\; \frac{\int dp\,e^{-\beta p^2/2m}\,e^{-\beta V(x)}}{Z} \;=\frac{e^{-\beta V(x)}}{\int dx\,e^{-\beta V(x)}}, \tag{D.32}$$

and the average value of a quantity $A(x,p)$ is

$$\langle A\rangle \;=\; \frac{\int\,dx\,A(x)\,e^{-\beta V(x)}}{\int\,dx\,e^{-\beta V(x)}}. \tag{D.33}$$

D.4 Calculation techniques

The basic problem of quantum statistical thermodynamics is the calculation of partition function (Eqs. D.16 or D.17 or D.21), average values (Eqs. D.19 or D.23) and probability distributions (Eqs. D.20 or D.24) within a suitable representation.
The knowledge of the partition function as a function of temperature is sufficient to calculate the thermodynamic functions; for example:

$$\begin{aligned}
\text{internal energy}: \quad U &= k_B T^2[\partial(\ln Z)/\partial T]_V \\
\text{entropy}: \quad S &= (U/T) + k_B \ln Z \\
\text{Helmoltz free energy}: \quad F &= -k_B T \ln Z \\
\text{pressure}: \quad P &= k_B T[\partial(\ln Z)/\partial V]_T
\end{aligned}$$

In the case of EXAFS in SS approximation, we want to calculate the distribution of distances $\rho(r)$ and its cumulants, which are the average values of suitable operators. This typically requires the knowledge of the density matrix in coordinate representation and the calculation of integrals like that in Eq. (D.23).
Different approaches are possible, depending on the complexity of the system under study and the sought accuracy.

Exact analytical calculations

Exact analytical calculations of the density matrix are possible only for particularly simple systems. In § D.5 we show the treatment for the harmonic oscillator, made in the energy representation: the use of creation and annihilation operators allows one to calculate moments and cumulants from the knowledge of energy eigenvalues and eigenvectors (Ref. [Cohen-Tannoudji et al., 1973] and Ch. 6 of Ref. [Feynman, 1972]).
An alternative treatment in the coordinate representation can be found in Ref. [Feynman, 1972], Ch.2. It is based on the solution of Eq. (D.26) to determine the density matrix $w(x,x';\beta)$.

Perturbative approaches

Approximate calculations of the density matrix can be done through a perturbative expansion (general reference [Feynman, 1972], Ch. 2; for EXAFS [Frenkel and Rehr, 1993, Yokoyama, 1999]).

Suppose that the hamiltonian can be expressed as

$$H \;=\; H_0 + H_1, \tag{D.34}$$

where H_1 can be considered as a small perturbation to the hamiltonian H_0. Suppose further that the differential equation (D.26) is exactly solvable for H_0, so that the un-normalised statistical density operator $\tilde{w}_0^* = \exp(-\beta H_0)$ can be calculated. In our case, H_0 is the Hamiltonian of the harmonic oscillator, whose eigenvalues E_n and eigenfunctions $|n\rangle$ can be exactly calculated (§ D.5). One can demonstrate that the un-normalised statistical density operator $\tilde{w}^* = \exp(-\beta H)$ obeys the integral equation

$$\tilde{w}^*(\beta) \;=\; \tilde{w}_0^*(\beta) \;-\; \int_0^\beta \tilde{w}_0^*(\beta-\beta')\, H_1\, \tilde{w}^*(\beta')\, d\beta'. \tag{D.35}$$

To *first order* approximation, Eq. (D.35) can be solved, by substituting $\tilde{w}^*(\beta') \simeq \tilde{w}_0^*(\beta')$ inside the integral, so that

$$\tilde{w}^*(\beta) \;\simeq\; \tilde{w}_0^*(\beta) \;-\; \int_0^\beta \tilde{w}_0^*(\beta-\beta')\, H_1\, \tilde{w}_0^*(\beta')\, d\beta', \tag{D.36}$$

or equivalently [Frenkel and Rehr, 1993, Yokoyama, 1999]

$$\begin{aligned} \tilde{w}^*(\beta) \;=\; e^{-\beta H} \quad &\simeq \quad e^{-\beta H_0}\left[1 - \int_0^\beta e^{\beta' H_0}\, H_1\, e^{-\beta' H_0}\, d\beta'\right] \\ &\simeq \quad e^{-\beta H_0}\left[1 - \int_0^\beta \tilde{H}_1\, d\beta'\right], \end{aligned} \tag{D.37}$$

where $\tilde{H}_1 = e^{\beta' H_0} H_1 e^{-\beta' H_0}$.
The approximated density operator $\tilde{w}^*$ obtained through Eq. (D.36) can further be substituted inside the integral of Eq. (D.35), to obtain a *second order* approximate equation. And so on.
The thermal average of a quantity A is given exactly by

$$\langle A\rangle \;=\; \mathrm{Tr}(\tilde{w}A) \;=\; \frac{1}{Z}\,\mathrm{Tr}\left[A\, e^{-\beta H}\right], \qquad (H = H_0 + H_1) \tag{D.38}$$

The first-order approximation gives [Yokoyama, 1999]

$$\mathrm{Tr}\left[A\, e^{-\beta H}\right] \;\simeq\; \mathrm{Tr}\left[A\, e^{-\beta H_0}\, \left(1 - \int_0^\beta e^{\beta' H_0}\, H_1\, e^{-\beta' H_0}\, d\beta'\right)\right] \tag{D.39}$$

and

$$\frac{1}{Z} \;\simeq\; \frac{1}{Z_0}\left[1 + \frac{1}{Z_0}\,\mathrm{Tr}\left(e^{-\beta H_0}\int_0^\beta e^{\beta' H_0}\, H_1\, e^{-\beta' H_0}\, d\beta'\right)\right] \tag{D.40}$$

By calculating the integrals using E_n and $|n\rangle$ from H_0, one obtains

$$\begin{aligned} \langle A\rangle \;\simeq\; & \frac{1}{Z_0}\sum_n e^{-\beta E_n}\,\langle n|A|n\rangle \\ & + \frac{1}{Z_0}\sum_{n,n'} \frac{e^{-\beta E_n} - e^{-\beta E_{n'}}}{E_n - E_{n'}}\,\langle n|A|n'\rangle\langle n'|H_1|n\rangle \\ & + \frac{\beta}{Z_0^2}\sum_n e^{-\beta E_n}\,\langle n|A|n\rangle \sum_{n'} e^{-\beta E_{n'}}\,\langle n'|H_1|n'\rangle \end{aligned} \tag{D.41}$$

where for $n = n'$ the 0/0 factor in the second term should be replaced by

$$\frac{e^{-\beta E_n} - e^{-\beta E_{n'}}}{E_n - E_{n'}} \;=\; -\beta\, e^{-\beta E_n}. \tag{D.42}$$

Path-integral approach

An alternative approach for the calculation of the statistical density matrix can be made within the framework of the path-integral techniques, first introduced by Feymnan. Here, to simplify notation, we will consider only the one-dimensional case.
The un-normalised statistical density matrix in coordinate representation (Eq. D.22 multiplied by Z)

$$\tilde{w}^*(x_1, x_2; \beta) \;=\; \sum_n e^{-\beta E_n}\, \phi_n^*(x_2)\, \phi_n(x_1). \tag{D.43}$$

is formally similar to the expression for the propagator or kernel, say the probability amplitude that a particle is in position x_1 at time t_1 and position x_2 at time t_2:

$$k(x_1, t_1; x_2, t_2) \;=\; \sum_n e^{-(i/\hbar)(t_2-t_1)E_n}\, \phi_n^*(x_2)\, \phi_n(x_1). \tag{D.44}$$

The two equations can be exchanged by the substitution $\beta \;\leftrightarrow\; (i/\hbar)\,(t_2 - t_1)$ (already introduced when discussing Eq. D.26), or equivalently

$$U \;=\; \hbar\beta \;\leftrightarrow\; i\,(t_2 - t_1), \tag{D.45}$$

where U is an *imaginary time*.
The kernel (D.44) can be calculated by a path-integral:

$$k(x_1, t_1; x_2, t_2) \;=\; \int_{x_1}^{x_2} \exp\left[\frac{i}{\hbar}\int_{t_1}^{t_2} \mathcal{L}(x, \dot{x}, t)\, dt\right] \mathcal{D}x(t). \tag{D.46}$$

In a formally analogous way, the un-normalised statistical density matrix (D.43) can be calculated by the path-integral:

$$\tilde{w}^*(x_1, x_2; U) \;=\; \int_{x_1}^{x_2} \exp\left[-\frac{1}{\hbar}\int_0^U \left\{(m/2)[\dot{x}(u)]^2 + V[x(u)]\right\}\, du\right] \mathcal{D}x(u). \tag{D.47}$$

The exact evaluation of the path-integral is again possible only in a few cases for simple potentials. However, the path-integral approach allows the development of new interesting approximations, like the the one based on the Effective Potential.

Numerical techniques

Molecular Dynamics and Monte Carlo method.

D.5 The harmonic oscillator

The one-dimensional harmonic oscillator is an example of systems for which an exact analytical calculation of the density matrix is possible [Cohen-Tannoudji et al., 1973]. The Hamiltonian operator is

$$H_0 \;=\; \frac{P^2}{2m} + \frac{1}{2} m\omega_0^2\, X^2\,. \tag{D.48}$$

Energy eigenvalues and eigenstates

The Hamiltonian operator is then

$$H_0 \;=\; \frac{P^2}{2m} + \frac{1}{2} m\omega_0^2\, X^2\,. \tag{D.49}$$

It is convenient to introduce the a-dimensional reduced observables

$$\hat{X} = \sqrt{\frac{m\omega_0}{\hbar}}\, X\,, \qquad \hat{P} = \frac{1}{\sqrt{m\hbar\omega_0}}\, P\,, \tag{D.50}$$

so that the commutator is $[\hat{X}, \hat{P}] = i$ and the reduced Hamiltonian is

$$\hat{H}_0 = \frac{H_0}{\hbar\omega_0} \;=\; \frac{1}{2}\,(\hat{X}^2 + \hat{P}^2)\,. \tag{D.51}$$

It is further convenient to substitute $\hat{X}$ and $\hat{P}$ by their linear combinations, the (non hermitian) operators of creation and destruction

$$a^\dagger = \frac{1}{\sqrt{2}}\,(\hat{X} - i\hat{P})\,, \qquad a = \frac{1}{\sqrt{2}}\,(\hat{X} + i\hat{P})\,, \tag{D.52}$$

whose commutator is $[a, a^\dagger] = 1$.
It is easy to see that

$$a^\dagger a \;=\; \frac{1}{2}\,(\hat{X}^2 + \hat{P}^2 - 1)\,, \tag{D.53}$$

so that

$$\hat{H}_0 = a^\dagger a + \frac{1}{2} \;=\; aa^\dagger - \frac{1}{2}\,. \tag{D.54}$$

By defining the (hermitian) number operator

$$N = a^\dagger a, \tag{D.55}$$

one finds

$$\hat{H}_0 = N + 1/2\;: \tag{D.56}$$

the eigenvectors of $\hat{H}_0$ are eigenvectors of N and viceversa. One can then first solve the eigenvalues equation for N

$$N\,|\phi_\nu\rangle \;=\; \nu\,|\phi_\nu\rangle \tag{D.57}$$

One finds that the spectre of N is represented by non negative integer numbers

$$\nu = 0, 1, 2, \ldots n, \ldots \qquad |\phi_\nu\rangle = |n\rangle\,, \tag{D.58}$$

the energy levels are non degenerate and the eigenvalues of the Hamiltonian H_0 are

$$E_n \;=\; (1/2 + n)\,\hbar\omega \qquad (n = 0 \ldots \infty) \tag{D.59}$$

The action of the creation and destruction operators on the eigenstates are the following

$$a^\dagger\,|n\rangle \;=\; \sqrt{n+1}\,|n+1\rangle, \qquad a\,|n\rangle \;=\; \sqrt{n}\,|n-1\rangle. \tag{D.60}$$

As a consequence, the average displacement is zero:

$$\langle X\rangle = \sqrt{\frac{\hbar}{2m\omega_0}}\,\langle n|\,a^\dagger + a\,|n\rangle \;=\; 0\,. \tag{D.61}$$

One can easily see that

$$\langle x^2\rangle \;=\; \frac{\hbar}{m\omega_0}\left(\frac{1}{2} + n\right) = \frac{E_n}{m\omega_0^2}\,. \tag{D.62}$$

Thermal equilibrium

If the oscillator is in equilibrium with a reservoir at temperature T, its state is a statistical mixture of eigenstates $|n\rangle$, weighted by $\exp(-\beta E_n)$, where $\beta = 1/k_B T$.
The thermodynamical properties can be calculated from the density operator

$$\hat{w} \;=\; (1/Z_0)\;e^{-\beta\hat{H}_0}, \qquad Z_0 \;=\; \mathrm{Tr}\,(e^{-\beta\hat{H}_0}). \tag{D.63}$$

In the energy representation, where $\hat{H}_0$ is diagonal, the harmonic partition function Z_0 is

$$Z_0 \;=\; \sum_{n=0}^{\infty}\langle n|e^{-\beta\hat{H}_0}|n\rangle \;=\; \sum_{n=0}^{\infty} e^{-(n+1/2)\beta\hbar\omega} \;=\; \frac{e^{-\beta\hbar\omega/2}}{1 - e^{-\beta\hbar\omega}}. \tag{D.64}$$

Average energy

The average energy is given by

$$\langle \hat{H}_0 \rangle \;=\; \mathrm{Tr}(\hat{H}_0 \hat{w}) \;=\; \frac{1}{Z_0}\,\mathrm{Tr}(\hat{H}_0\, e^{-\beta \hat{H}_0}) \;=\; \frac{1}{Z_0}\,\sum_{n=0}^{\infty}(n{+}1/2)\hbar\omega e^{-\beta(n+1/2)\hbar\omega} \;=\; \hbar\omega\,\left[\frac{1}{2}+\frac{1}{e^{\beta\hbar\omega}-1}\right]. \tag{D.65}$$

Let us study the temperature dependence of the average energy.

- For $T \to 0$ ($\beta \to \infty$), it easy to see that $\langle H \rangle \to \hbar\omega/2$ (zero point energy). The zero point energy is proportional to the angular frequency ω.
- For $T \to \infty$ ($\beta \to 0$), one can show that $\langle H \rangle \to k_B T$ (classical approximation). The demonstration is based on the expansion $1/(e^x - 1) \simeq [x + x^2/2 + \ldots]^{-1} \simeq (1/x)[1 - x/2 + \ldots]$, where $x = \beta\hbar\omega$. The behaviour for $T \to \infty$ is independent of ω.

A characteristic temperature θ can be associated to the angular frequency: $\theta = \hbar\omega/k_B = h\nu/k_B$. Numerically, θ [K] = 48 ν [THz].

Distribution of positions and its moments

The probability density for the displacement x can be calculated, according to Eq. (D.20), as

$$\rho(x) \;=\; \frac{1}{Z_0}\sum\nolimits_{n=0}^{\infty}\rho_n(x)\, e^{-\beta E_n}, \qquad \text{where} \quad \rho_n(x) \;=\; |\phi_n(x)|^2. \tag{D.66}$$

One can demonstrate [Cohen-Tannoudji et al., 1973] that the distribution has a gaussian shape:

$$\rho(x) \;=\; (1/\sigma\sqrt{2\pi})\, e^{-x^2/2\sigma^2} \tag{D.67}$$

where $\langle x \rangle = 0$.
The moments of the distribution can be calculated by using the creation and destruction operators. The position operator can be expressed as

$$x \;=\; \sqrt{\hbar/m\omega}\,\hat{x} \;=\; \sqrt{\hbar/2m\omega}\,(a^\dagger + a) \;=\; \sigma_0\,(a^\dagger + a), \tag{D.68}$$

where the notation $\sigma_0 = \sqrt{\hbar/2m\omega}$ has been introduced for convenience.
The momentum of order k can be calculated as

$$\langle x^k \rangle \;=\; \frac{1}{Z_0}\,\mathrm{Tr}\,(x^k e^{-\beta H_0}) \;=\; \frac{1}{Z_0}\,\sum_{n=0}^{\infty}\langle n|x^k|n\rangle\, e^{-\beta E_n}. \tag{D.69}$$

It is easy to verify that $\langle n|x|n\rangle = 0$ for every n, so that the *1st moment* is always zero,

$$\langle x \rangle \;=\; 0. \tag{D.70}$$

One can also verify that $\langle n|x^2|n\rangle = \sigma_0^2\,(2n+1)$ for every n; since $\langle x\rangle$=0, the *2nd central moment* (variance σ^2) is in this case equal to the second initial moment $\langle x^2 \rangle$:

$$\sigma^2 \;=\; \langle x^2 \rangle \;=\; \frac{\sigma_0^2}{Z_0}\,\sum_{n=0}^{\infty}(2n+1)\, e^{-(n+1/2)\beta\hbar\omega}. \tag{D.71}$$

Defining $z = \exp(-\beta\hbar\omega)$ and remembering that $\sigma_0^2 = \hbar/2m\omega$, it easy to calculate σ^2, which can be expressed in different equivalent ways:

$$\sigma^2 \;=\; \sigma_0^2\,\frac{1+z}{1-z} \;=\; \sigma_0^2 \coth\left(\frac{\beta\hbar\omega}{2}\right) \;=\; \frac{\hbar}{m\omega}\,\left[\frac{1}{2}+\frac{1}{e^{\beta\hbar\omega}-1}\right]. \tag{D.72}$$

Comparing Eqs. (F.220) and (D.72) one can see that $\sigma^2 = \langle H \rangle/k_0 = \langle H \rangle/m\omega^2$.
Let us study the temperature dependence of σ^2.

- For $T \to 0$, $\sigma^2 \to \sigma_0^2 = \hbar/2m\omega = \hbar\omega/2k_0$.
- For $T \to \infty$, $\sigma^2 \to \sigma_\infty = k_B T/m\omega^2 = k_B T/k_0$. The behaviour of σ^2 for $T \to \infty$ depends on ω; the slope of $\sigma^2(T)$ is inversely proportional to the force constant k_0.

One can at last verify that $\langle n|x^3|n\rangle = 0$ for every n; the *3rd central moment* is in this case equal to $\langle x^3\rangle = 0$.

Appendix E

Probability and Cumulants

E.1 Moments of a random variable distribution

References: Chapter 7 of [Gnedenko, 1976], Chapter 15 of [Cramér, 1966].
Let us consider the probability density function $\Phi(r)$ of the random variable r.

Initial moments

The *initial moments* α_n of the distribution $\Phi(r)$ are defined as

$$\alpha_n = \langle r^n \rangle = \frac{1}{\alpha_0} \int_{-\infty}^{\infty} r^n \ \Phi(r) \ dr, \qquad (n = 1, 2, ...) \tag{E.1}$$

where

a) $\alpha_0 = \int \Phi(r)\, dr$ is the normalisation integral. For a probability distribution, $\alpha_0 = 1$.
With reference to EXAFS,
   i) for the real distribution $\rho(r)$, $\alpha_0 = 1$;
   ii) for the effective distribution $P(r, \lambda)$ in general $\alpha_0 \neq 1$.

b) $\alpha_1 = m$ is the mean value, or expectation value, of the random variable r.

The initial moment α_n only exists if the integral $\int |r^n| \ \Phi(r)\, dr$ exists; if the moment α of order n exists, all moments of order $k < n$ exist too.
It is often important to know whether a distribution is uniquely determined by its moments. The problem is far from trivial. A useful criterion is the following. Let $\alpha_0, \alpha_1 \ldots$ be the moments of a distribution $Phi(r)$, all of which are assumed to be finite. If the series $\sum \alpha_\nu r^\nu / \nu!$ is absolutely convergent for some $r > 0$, then $\Phi(r)$ is the only distribution whose moments are $\alpha_0, \alpha_1 \ldots$.

Central moments

The *central moments* μ_n of the distribution $\Phi(r)$ are defined as

$$\mu_n = \langle (r - \langle r \rangle)^n \rangle = \frac{1}{\alpha_0} \int_{-\infty}^{\infty} (r - \langle r \rangle)^n \ \Phi(r) \ dr, \qquad (n = 1, 2, ...) \tag{E.2}$$

whence

$$\begin{aligned}
\mu_0 &= 1 && \text{(E.3)} \\
\mu_1 &= 0 && \text{(E.4)} \\
\mu_2 &= \alpha_2 - \alpha_1^2 && \text{(E.5)} \\
\mu_3 &= \alpha_3 - 3\alpha_1\alpha_2 + 2\alpha_1^3 && \text{(E.6)} \\
\mu_4 &= \alpha_4 - 4\alpha_3\alpha_1 + 6\alpha_1^2\alpha_2 - 3\alpha_1^4 && \text{(E.7)} \\
&... &&
\end{aligned}$$

Meaning of leading central moments:

$\mu_2 = \sigma^2 = \langle (r - \langle r \rangle)^2 \rangle$ is the variance of the distribution, the most common measure of dispersion. Its square root σ is the standard deviation.

$\mu_3 = \langle (r - \langle r \rangle)^3 \rangle$ is the simplest measure of skewness or asymmetry.
The a-dimensional coefficient of skewness is $\gamma_1 = \mu_3/\sigma^3$: for $\gamma_1 > 0$ the long tail is on the positive side with respect to mean.
An alternative measure of skewness, introduced by Pearson, is the difference between mean and mode, divided by the standard deviation: $(m - r_0)/\sigma$.

$\mu_4 = \langle (r - \langle r \rangle)^4 \rangle$ measures the flatness (or kurtosis or excess).
The a-dimensional coefficient of kurtosis is $\gamma_2 = \mu_4/\sigma^4 - 3$. For a gaussian distribution $\gamma_2 = 0$. Positive values of γ_2 indicate that the distribution is more tall and slim than a gaussian distribution with the same mean and variance.

E.2 Characteristic function

The *characteristic function* of a distribution $\Phi(r)$ is its Fourier transform $\Psi(t)$:

$$\Psi(t) \;=\; \int_{-\infty}^{\infty} \Phi(r)\; e^{itr}\; dr \;=\; \langle e^{itr} \rangle. \tag{E.8}$$

Considering the application to EXAFS, let $2k$ be the conjugate variable and let us consider the possibility of non-normalised distributions (such as the effective distribution), so that:

$$\Psi(2k) \;=\; \int_{-\infty}^{\infty} \Phi(r)\; e^{2ikr}\; dr \;=\; \alpha_0\, \langle e^{2ikr} \rangle. \tag{E.9}$$

Properties of the characteristic function

1. Since $|e^{itr}| = 1$, the integrals in (E.8) and (E.9) always exists.
   General case: $|\Psi(t)| \le 1$, $\Psi(0) = 1$ and $\Psi(-t) = \Psi^*(t)$.
   EXAFS case: $|\Psi(2k)| \le \alpha_0$, $\Psi(0) = \alpha_0$ and $\Psi(-2k) = \Psi^*(2k)$ ($\alpha_0 = 1$ for real distribution).
2. The characteristic function $\Psi(t)$ is a complex function of a real variable:
   $\Psi(t) = |\Psi(t)| \exp[i\theta(t)]$.
3. There is a one-to-one correspondence between a distribution $\Phi(r)$ and its characteristic function $\Psi(t)$. If two distributions are equal, so are their characteristic functions, and conversely.

E.2.1 Moments and characteristic function: normalised distribution

If all moments α_n exist, the characteristic function $\langle e^{itx} \rangle$ can be expanded in Mac Laurin series around the origin $t = 0$:

$$\Psi(t) \;=\; \langle e^{itx} \rangle \;=\; \sum_{n=0}^{\infty} \frac{(it)^n}{n!} \alpha_n \;=\; 1 + \sum_{n=1}^{\infty} \frac{(it)^n}{n!} \alpha_n \,. \tag{E.10}$$

One can easily verify that α_n is connected to the n-th derivative of $\Psi(t)$ at the origin $t = 0$:

$$\left[\frac{d^n \Psi(t)}{dt^n} \right]_{t=0} \;=\; i^n\, \alpha_n \,. \tag{E.11}$$

E.2.2 Moments and characteristic function: EXAFS case

In the EXAFS case (E.10) becomes

$$\Psi(2k) \;=\; \alpha_0\, \langle e^{2ikx} \rangle \;=\; \alpha_0 \left[\; 1 + \sum_{n=1}^{\infty} \frac{(2ik)^n}{n!} \alpha_n \;\right]. \tag{E.12}$$

and (E.11) becomes

$$\left[\frac{d^n\Psi(2k)}{d(2k)^n}\right]_{k=0} \;=\; i^n\;\alpha_0\;\alpha_n\,, \tag{E.13}$$

where $\alpha_0 = 1$ for the real distribution, $\alpha_0 \neq 1$ for the effective distribution.

E.3 Cumulants of a distribution

References: Chapter 7 of [Gnedenko, 1976], Chapter 15 of [Cramér, 1966].

E.3.1 Cumulants for a normalised distribution

The *second characteristic function* is the logarithm of $\Psi(t)$:

$$\ln\Psi(t) \;=\; \ln|\Psi(t)| \;+\; i\theta(t). \tag{E.14}$$

The *cumulants* or *semi-invariants* C_n of $\Psi(t)$ are the n-th derivatives of $\ln\Psi(t)$ calculated at the origin $k = 0$ and divided by i^n:

$$\left[\frac{d^n \ln\Psi(t)}{dt^n}\right]_{t=0} \;=\; i^n\,C_n\,. \tag{E.15}$$

The second characteristic function can be expanded in Mac Laurin series around $k = 0$ as

$$\ln\Psi(t) \;=\sum_{n=1}^{\infty}\frac{(it)^n}{n!}\;C_n\,. \tag{E.16}$$

The convergence interval of (E.16) depends on the properties of the distribution $\Phi(r)$.

Relations between cumulants and moments

The cumulants can be expressed as a function of the initial moments by comparing (E.16) with the logarithm of (E.12), expanded according to

$$\ln(1+x) \;=\; \sum_{n=1}^{\infty}\frac{(-1)^{n+1}}{n}\,x^2\,; \tag{E.17}$$

by equating the coefficients of the terms with the same power of k, one obtains

$$\begin{aligned}
C_1 &= \alpha_1\\
C_2 &= \alpha_2 - \alpha_1^2\\
C_3 &= \alpha_3 - 3\alpha_2\alpha_1 + 2\alpha_1^3\\
C_4 &= \alpha_4 - 4\alpha_3\alpha_3 - 1\alpha_2^2 + 12\alpha_2\alpha_1^2 - 6\alpha_1^4\\
C_5 &= \alpha_5 - 5\alpha_4\alpha_1 - 10\alpha_3\alpha_2 + 20\alpha_3\alpha_1^2 + 30\alpha_2^2\alpha_1 - 60\alpha_2\alpha_1^3 + 24\alpha_1^5
\end{aligned} \tag{E.18}$$

The connection between cumulants and central moments is [Cramér, 1966]

$$\begin{aligned}
C_2 &= \mu_2\\
C_3 &= \mu_3\\
C_4 &= \mu_4 - 3\mu_2^2\\
C_5 &= \mu_5 - 10\mu_2\mu_3\\
C_6 &= \mu_6 - 15\mu_2\mu_4 - 10\mu_3^2 + 30\mu_2^3
\end{aligned} \tag{E.19}$$

E.3.2 Cumulants for the EXAFS case

In the EXAFS case it is convenient to explicitly consider a conjugate variable $t = 2k$ and to account for the fact that the effective distribution is not normalised to one.
The *second characteristic function* is now the logarithm of $\Psi(2k)$; from (E.9)

$$\ln\Psi(2k) \;=\; \ln\left[\alpha_0 \left\langle e^{2ikr}\right\rangle\right] \;=\; C_0 \;+\; \ln\langle e^{2ikr}\rangle\,, \tag{E.20}$$

where

$$C_0 \;=\; \ln\alpha_0 \;\begin{cases} = 0 & \text{for the a distribution normalised to one (e.g. the real distribution)} \\ \neq 0 & \text{for a not normalised distribution (e.g. the effective distribution)} \end{cases}$$

The expansion (E.16) becomes

$$\ln\Psi(2k) \;=\; C_0 + \sum_{n=1}^{\infty} \frac{(2ik)^n}{n!}\, C_n \;=\; \sum_{n=0}^{\infty} \frac{(2ik)^n}{n!}\, C_n. \tag{E.21}$$

The convergence interval of (E.21) depends on the properties of the distribution $\Phi(r)$.

The connection between the cumulants and the initial and central moments is again given by (E.18) and (E.19), with the addition of C_0 [Vaccari, 2006]

$$\begin{array}{lll} C_0 = \ln\alpha_0 & & \\ C_1 = \alpha_1 & & \\ C_2 = \alpha_2 - \alpha_1^2 & & = \mu_2 \\ C_3 = \alpha_3 - 3\alpha_2\alpha_1 + 2\alpha_1^3 & & = \mu_3 \\ C_4 = \alpha_4 - 4\alpha_3\alpha_3 - 1\alpha_2^2 + 12\alpha_2\alpha_1^2 - 6\alpha_1^4 & & = \mu_4 - 3\mu_2^2 \\ C_5 = \alpha_5 - 5\alpha_4\alpha_1 - 10\alpha_3\alpha_2 + 20\alpha_3\alpha_1^2 + 30\alpha_2^2\alpha_1 - 60\alpha_2\alpha_1^3 + 24\alpha_1^5 & & \end{array} \tag{E.22}$$

The connections between cumulants and moments can be inverted [Vaccari, 2006]:

$$\begin{aligned} \alpha_1 &= C_1 \\ \alpha_2 &= C_2 + C_1^2 \\ \alpha_3 &= C_3 + 3C_2C_1 + C_1^3 \\ \alpha_4 &= C_4 + 4C_3C_1 + 6C_2C_1^2 + 3C_2^2 + C_1^4 \\ \alpha_5 &= C_5 + 5C_4C_1 + 10C_3C_2 + 10C_3C_1^2 + 15C_2^2C_1 + 10C_2C_1^3 + C_1^5 \end{aligned} \tag{E.23}$$

E.3.3 Cumulant expansion of EXAFS

An EXAFS signal is proportional to the configurational average

$$\chi(k) \;\propto\; \left\langle \frac{\exp[-2r/\lambda(k)]}{r^2}\, \exp(2ikr) \right\rangle \;=\; \int_0^{\infty} P(r,\lambda)\, \exp(2ikr)\, dr\,, \tag{E.24}$$

where $P(r,\lambda) = \rho(r)\, \exp(-2r/\lambda)/r^2$ is an effective distribution and $\rho(r)$ is the real distribution. The effective distribution is defined only for $r > 0$. The integral to the left of (E.24) can be extended to $-\infty$ and corresponds to the characteristic function of the effective distribution.
The expansion (E.21) in cumulant series gives

$$\begin{aligned} \Psi(2k) \;&=\; \int_{-\infty}^{\infty} P(r,\lambda)\, \exp(2ikr)\, dr \;=\; \exp\left[\sum_{n=0}^{\infty} \frac{(2ik)^n}{n!} C_n\right] \\ &=\; \exp\left[C_0 - 2k^2C_2 + \frac{2}{3}k^4C_4 - \frac{4}{45}k^6C_6 ...\right]\; \exp\left[2ikC_1 - \frac{4}{3}ik^3C_3 + \frac{4}{45}ik^5C_5 ...\right] \end{aligned} \tag{E.25}$$

The C_n are the cumulants of the effective distribution.

The EXAFS function for a coordination shell (or more generally for a scattering path) is thus

$$\chi_s(k) \;=\; \frac{S_0^2}{k}\; N_s\; \mathrm{Im}\Big\{ f_s(k,\pi)\; e^{2i\delta_1}\; \Psi(2k) \Big\} \tag{E.26}$$

By inserting the cumulant expansion (E.26) and substituting $f_s(k,\pi)\; e^{2i\delta_1} = |f_s(k,\pi)|\; e^{i\phi}$, (E.26) becomes

$$\chi_s(k) \;=\; \frac{S_0^2}{k}\; N_s\; |f_s(k,\pi)|\; \exp\left(C_0 - 2k^2 C_2 + \frac{2}{3}k^4 C_4 ... \right)\; \sin\left(2kC_1 - \frac{4}{3}k^3 C_3 ... + \phi \right) \tag{E.27}$$

Even and odd cumulants determine the amplitude and the phase of the EXAFS function, respectively.

Meaning of EXAFS cumulants

Fro EXAFS analysis one obtains directly the cumulants of the effective distribution $P(r,\lambda)$.

a) C_0 depends on the normalisation of the distribution $P(r,\lambda)$.
$P(r,\lambda)$ is not normalised to one due to the factor $e^{-2r/\lambda}/r^2$. For not too large distributions,

$$e^{C_0} \;\simeq\; \frac{e^{-2C_1/\lambda}}{C_1^2} \tag{E.28}$$

b) C_1 is the average value of the distribution $P(r,\lambda)$.

c) C_2 is the variance of the distribution $P(r,\lambda)$.

d) C_3 measures the asymmetry (skewness) of $P(r,\lambda)$: positive and negative values of C_3 correspond to distributions with the tail at high or low values of r, respectively.
The a-dimensional asymmetry coefficient is $\gamma_1 = C_3/C_2^{3/2}$.

e) C_4 measures the degree of flatness (kurtosis) of $P(r,\lambda)$: positive and negative values of C_4 correspond to distributions more peaked of more flattened than a gaussian distribution, respectively;
The a-dimensional flatness coefficient is $\gamma_2 = C_4/C_2^2$.

If $P(r,\lambda)$ is gaussian, the cumulants C_n with $n > 2$ are zero. The extent of C_3, C_4 ... thus measures the deviation of $P(r,\lambda)$ with respect to the normal behaviour. In particular, C_3 is zero for distributions symmetrical with respect to the average value C_1.

Cumulants of the real distribution

The cumulants C_n^* of the real distribution $\rho(r)$ are different from the cumulants C_n of the effective distribution.
Different procedures for connecting the cumulants of the real and of the effective distributions (C_n^* and C_n, respectively) have been proposed, limited to the first cumulant [Freund et al., 1989, Bunker, 1983] or extended to higher order cumulants [Fornasini et al., 2001]. A relatively good approximation for $n \geq 1$ is obtained by the recursion formula [Vaccari, 2006, Vaccari et al., 2007]

$$C_n^* \;\sim\; C_n + 2C_{n+1}\big(1/C_1 + 1/\lambda\big) \quad \text{for} \quad n = 1, 2, 3, \ldots \tag{E.29}$$

The difference between the first cumulants ($n = 1$) of the real and effective distributions is significant and Eq. (4.11) is included in most data analysis packages. For higher order cumulants ($n \geq 2$), the difference is smaller and is frequently neglected.
The lowest-order EXAFS cumulants C_n^* are related to the initial and central moments of the real distribution by

$$C_1^* \;=\; \langle r \rangle \tag{E.30}$$

$$C_2^* \;=\; \mu_2 \;=\; \big\langle (r - \langle r \rangle)^2 \big\rangle \tag{E.31}$$

$$C_3^* \;=\; \mu_3 \;=\; \big\langle (r - \langle r \rangle)^3 \big\rangle \tag{E.32}$$

$$C_4^* \;=\; \mu_4 - 3\mu_2^2 \;=\; \big\langle (r - \langle r \rangle)^4 \big\rangle - 3\mu_2^2 \tag{E.33}$$

can thus be evaluated as averages over a canonical ensemble.
The meanings of the leading cumulants of the real distribution are:

a) $C_0^* = 0$ for the real distribution, which is normalised to one.
b) $C_1^* = \langle r \rangle$ is the average value of the distribution $\rho(r)$.
c) $C_2^* = \mu_2^* = \left\langle (r - \langle r \rangle)^2 \right\rangle$ is the variance of the distribution $\rho(r)$.
d) $C_3^* = \mu_3^* = \left\langle (r - \langle r \rangle)^3 \right\rangle$ measures the asymmetry (skewness) of $\rho(r)$: positive and negative values of C_3^* correspond to distributions with the tail at high or low values of r, respectively. The a-dimensional asymmetry coefficient is $\gamma_1 = C_3^*/(C_2^*)^{3/2}$.
e) $C_4^* = \mu_4^* - 3(\mu_2^*)^2$ measures the degree of flatness (kurtosis) of the distribution: positive and negative values of C_4^* correspond to distributions more peaked of more flattened than a gaussian distribution, respectively.
The a-dimensional flatness coefficient is $\gamma_2 = C_4^*/(C_2^*)^2$.

If $\rho(r)$ is gaussian, the cumulants C_n^* with $n > 2$ are zero. The extent of C_3^*, C_4^* ... thus measures the deviation of the distribution with respect to the normal behaviour. In particular, C_3^* is zero for distributions symmetrical with respect to the average value C_1^*.

An experimental EXAFS spectrum, which is included between two values k_{min} and k_{max}, samples only part of the full characteristic function. This limitation prevents from reconstructing the effective distribution by direct Fourier transform of the EXAFS signal. In some cases, the cumulant method allows one to extrapolate the EXAFS signal to $k = 0$ with enough accuracy to reconstruct the distance distribution.
If the cumulant series is fast convergent, a limited number of cumulants C_n^* is sufficient to reconstruct the characteristic function $\Psi(2k)$ and hence the distribution $\rho(r)$ with good accuracy.

E.3.4 Alternative definitions

A - Real distribution of distances

$$\langle \exp(2ikr) \rangle = \exp\left[\sum_{n=0}^{\infty} \frac{(2ik)^n}{n!} C_n^* \right] \tag{E.34}$$

Taking into account the relation between cumulants and central and initial moments and If only longitudinal displacements are considered ($\Delta u_\perp = 0$):

$$\begin{array}{lllll} C_1^* & = \langle r \rangle & & & = R \\ C_2^* & = \langle (r - \langle r \rangle)^2 \rangle & = \langle r^2 \rangle - \langle r \rangle^2 & & = \langle \Delta u_\parallel^2 \rangle \\ C_3^* & = \langle (r - \langle r \rangle)^3 \rangle & = \langle r^3 \rangle - 3\langle r^2 \rangle \langle r \rangle + 2\langle r \rangle^3 & & = \langle \Delta u_\parallel^3 \rangle \end{array} \tag{E.35}$$

B - Effective distribution of distances

$$\left\langle \frac{\exp[-2r/\lambda(k)]}{r^2} \exp(2ikr) \right\rangle = \exp\left[\sum_{n=0}^{\infty} \frac{(2ik)^n}{n!} C_n \right] \tag{E.36}$$

$$\begin{array}{ll} C_1 & \simeq C_1^* - (2C_2^*/C_1^*)\,(1 + C_1^*/\lambda) \\ C_2 & \simeq C_2^* \\ C_3 & \simeq C_3^* \end{array} \tag{E.37}$$

C - Distribution of deviations from average distance $R = \langle r \rangle$

$$\left\langle \exp(2ik\Delta u_\parallel) \right\rangle = \exp\left[\sum_{n=0}^{\infty} \frac{(2ik)^n}{n!} \sigma^{(n)} \right] \tag{E.38}$$

If only longitudinal displacements are considered ($\Delta u_\perp = 0$),

$$\begin{aligned}
\sigma^{(1)} &= \langle \Delta u_\parallel \rangle && = 0 && = C_1^* - R \\
\sigma^{(2)} &= \langle \Delta u_\parallel^2 \rangle - \langle \Delta u_\parallel \rangle^2 && = \langle \Delta u_\parallel^2 \rangle && = C_2^* \\
\sigma^{(3)} &= \langle \Delta u_\parallel^3 \rangle - 3\langle \Delta u_\parallel^2 \rangle \langle \Delta u_\parallel \rangle + 2\langle \Delta u_\parallel \rangle^3 && = \langle \Delta u_\parallel^3 \rangle && = C_3^*
\end{aligned} \tag{E.39}$$

D - Distribution of deviations from rest distance R^0

$$\langle \exp(2ik\Delta_\alpha) \rangle = \exp\left[\sum_{n=0}^{\infty} \frac{(2ik)^n}{n!} M_n \right] \tag{E.40}$$

where $\Delta_\alpha = \Delta u_\parallel^0$ [Fujikawa and Miyanaga, 1993].
If only longitudinal displacements are considered ($\Delta u_\perp = 0$), one can verify that

$$\begin{aligned}
M_1 &= \langle \Delta_\alpha \rangle && = C_1^* - R_0 \\
M_2 &= \langle \Delta_\alpha^2 \rangle - \langle \Delta_\alpha \rangle^2 && = C_2^* \\
M_3 &= \langle \Delta_\alpha^3 \rangle - 3\langle \Delta_\alpha^2 \rangle \langle \Delta_\alpha \rangle + 2\langle \Delta_\alpha \rangle^3 && = C_3^*
\end{aligned} \tag{E.41}$$

E.4 Distributions of two variables

References: [Ventsel, 1973, Gnedenko, 1976]

E.4.1 Theorems on moments of one-dimensional distributions

Let us consider any two continuous random variables X and Y with multivariate distribution $f(x, y$ of any form. One can demonstrate ([Ventsel, 1973], § 10.2):

1. The expectation value of the sum $X + Y$ is always the sum of the expectation values:

$$\begin{aligned}
\mathbf{m}[X+Y] &= \iint_{-\infty}^{+\infty} (x+y)\, f(x,y)\, dx\, dy \\
&= \iint_{-\infty}^{+\infty} x\, f(x,y)\, dx\, dy + \iint_{-\infty}^{+\infty} y\, f(x,y)\, dx\, dy \\
&= \mathbf{m}[X] + \mathbf{m}[Y] = m_x + m_y\,.
\end{aligned} \tag{E.42}$$

2. The expectation value of the difference $Y - X$ is always the difference of the expectation values:

$$\mathbf{m}[Y-X] = \mathbf{m}[Y] - \mathbf{m}[X] = m_y - m_x\,. \tag{E.43}$$

3. The variance D of the distribution of the sum $X + Y$ is

$$\begin{aligned}
&\mathbf{D}[X+Y] \\
&= \iint_{-\infty}^{+\infty} \left[(x+y) - (m_x+m_y)\right]^2 f(x,y)\, dx\, dy \\
&= \iint_{-\infty}^{+\infty} \left[(x-m_x) + (y-m_y)\right]^2 f(x,y)\, dx\, dy \\
&= \iint_{-\infty}^{+\infty} \left[(x-m_x)^2 + 2(x-m_x)(y-m_y) + (y-m_y)^2\right] f(x,y)\, dx\, dy \\
&= \mathbf{D}[X] + 2\sigma[XY] + \mathbf{D}[Y] = D_x + 2\sigma_{xy} + D_y\,,
\end{aligned} \tag{E.44}$$

where

$$\sigma_{xy} \;=\; \langle (x - m_x)\,(y - m_y) \rangle \tag{E.45}$$

is the covariance of X and Y. If X and Y are statistically independent, $\sigma_{xy} = 0$.

4. The variance D of the distribution of the difference $Y - X$ is

$$\mathbf{D}[Y - X] = \mathbf{D}[Y] - 2\sigma[XY] + \mathbf{D}[X] = D_y - 2\sigma_{xy} + D_x\,, \tag{E.46}$$

where again

$$\sigma_{xy} \;=\; \langle (x - m_x)\,(y - m_y) \rangle \tag{E.47}$$

is the covariance of X and Y, and if X and Y are statistically independent, $\sigma_{xy} = 0$.

5. The third moment (equal to the third cumulant) of the difference $Y - X$ is

$$\begin{aligned} & \mu_{\mathbf{3}}[Y - X] \\ = \;& \iint_{-\infty}^{+\infty} \left[(y - x) - (m_y - m_x) \right]^3 \, f(x,y)\, dx\, dy \\ = \;& \iint_{-\infty}^{+\infty} \left[(y - m_y) - (x - m_x) \right]^3 \, f(x,y)\, dx\, dy \\ = \;& \mu_3[Y] - 3\mathbf{m}[(y - m_y)^2 (x - m_x)] + 3\mathbf{m}[(y - m_y)(x - m_x)^2] + \mu_3[X] \end{aligned} \tag{E.48}$$

If X and Y are statistically independent, the expectation values of the products are equal to the products of the expectation values so that the second and third terms are zero and

$$\mu_3[Y - X] \;=\; \mu_3[Y] - \mu_3[X]\,. \tag{E.49}$$

The rendom variables of EXAFS (x_a and x_b or u_a and u_b) are *not* independent.

E.4.2 Composition of normal distributions

The normal distribution is stable: the composition of two normal distributions is again a normal distribution.

Let us consider two normally distributed vriables X and Y:

$$f_x(x) = \frac{1}{\sigma_x \sqrt{2\pi}} \exp\left[-\frac{(x - m_x)^2}{2\sigma_x^2} \right]; \qquad f_y(y) = \frac{1}{\sigma_y \sqrt{2\pi}} \exp\left[-\frac{(y - m_y)^2}{2\sigma_y^2} \right]. \tag{E.50}$$

Distribution of the sum $X + Y$

Let $Z = X + Y$. One can show ([Ventsel, 1973], § 12.6) that Z is distributed according to a normal distribution $f_z(z)$. The mean of the distribution $f_z(z)$ always is

$$m_z \;=\; m_x + m_y\,. \tag{E.51}$$

For X and Y independent, the variance of the distribution $f_z(z)$ is

$$\sigma_z^2 \;=\; \sigma_x^2 + \sigma_y^2\,. \tag{E.52}$$

If X and Y are not independent, the variance of the distribution $f_z(z)$ is

$$\sigma_z^2 \;=\; \sigma_x^2 + \sigma_y^2 + 2\,\sigma_{xy}\,, \tag{E.53}$$

where

$$\sigma_{xy} \;=\; \langle (x - m_x)\,(y - m_y) \rangle \tag{E.54}$$

is the covariance of X and Y.

Appendix F

Vibrational dynamics

This Appendix contains a basic approach to vibrational dynamics.
A short review of the adiabatic approximation is given in Section F.1.
In Section F.2, the potential energy of a two-atomic system is expanded in powers of the atomic displacements: the harmonic approximation is introduced and the effects of anharmonicity are discussed.
In Section F.3, the power expansion is generalised to a many-atomic system (Born-von Karman expansion). Attention is focused on the harmonic approximation. The dynamical matrix and its solution in terms of eigenfrequency and eigenvectors are introduced.
The vibrational dynamics of crystals in the harmonic approximation is considered in Section F.4, where the translational symmetry is exploited to introduce the Fourier transformed dynamical matrix.
In Section F.5 the quantisation of normal modes is introduced.
In Section F.6 the mean square displacements and the mean square relative displacements are expressed as a function of eigenfrequencies and eigenvectors of the dynamical matrix.
Section F.7 [not finished...] is dedicated to the anharmonic crystal.

F.1 Born-Oppenheimer adiabatic approximation

The stationary Schrödinger equation for a many-atomic system, such as a molecule or a crystal, is

$$H\,\Psi_{\rm tot} \;=\; E\,\Psi_{\rm tot}\,, \tag{F.1}$$

where the total wavefunction $\Psi_{\rm tot}$ depends on the coordinates of the n electrons and of the N nuclei:

$$\Psi_{\rm tot} \;=\; \Psi_{\rm tot}(\vec{r}_1,\ldots,\vec{r}_n\,;\vec{R}_1\,\ldots,\vec{R}_N) \;=\; \Psi_{\rm tot}(r,R)\,. \tag{F.2}$$

In the last term of (F.2), r and R are short-hand notations for the full sets of electrons and nuclei coordinates, respectively.

Ions and valence electrons

In many cases, instead of considering separately all the electrons, it is convenient to distinguish the ions from the valence electrons:

a) ions = nuclei + core electrons (say electrons which don't contribute to the inter-atomic interaction),
b) valence electrons = external electrons, which contribute to the inter-atomic interaction.

In such cases, R and N refer to ions, and r and n refer to valence electrons in (F.2).

Note: The distribution of valence electrons is peculiar of the different crystal types. It can be experimentally detected by refined analyses of high-accuracy X-ray diffraction spectra.

F.1.1 Total Hamiltonian

The total Hamiltonian (neglecting relativistic terms) is

$$H \;=\; T_n + V_{nn} + T_e + V_{ne} + V_{ee}\,. \tag{F.3}$$

The total kinetic energy operator for nuclei (or for ions) is

$$T_n \;=\; -\sum_A \frac{\hbar^2}{2M_A}\,\nabla_A^2\,. \tag{F.4}$$

The total kinetic energy operator for electrons (or for valence electrons) is

$$T_e \;=\; -\sum_i \frac{\hbar^2}{2m}\,\nabla_i^2\,. \tag{F.5}$$

The total potential energy of the interaction between nuclei (or between ions) is

$$V_{nn} \;=\; \frac{1}{2}\sum_A \sum_{B\neq A} \frac{Z_A Z_B}{|\vec{R}_A - \vec{R}_B|}\,, \tag{F.6}$$

where Z_A and Z_B are the nuclear (or ionic) charges.
The total potential energy for the interaction between electrons (or between valence electrons) is

$$V_{ee} \;=\; \frac{1}{2}\sum_i \sum_{j\neq i} \frac{e^2}{|\vec{r}_i - \vec{r}_j|}\,. \tag{F.7}$$

The total potential energy of electrostatic interaction between electrons and nuclei (or between valence electrons and ions) is

$$V_{ne} \;=\; -\sum_{iA} \frac{e\,Z_A}{|\vec{r}_i - \vec{R}_A|}\,. \tag{F.8}$$

F.1.2 Separation of nuclear and electronic motion

In principle, the time-independent Schrödinger equation for the full system contains all the information on its stationary states. Its solution is however a prohibitive task.
The Born-Oppenheimer approximation consists in de-coupling the Schrödinger equation for electrons from the Schrödinger equation for nuclei.
The physical basis of such an approximation is the fact that the mass of nuclei is from about 2×10^3 to about 10^5 times larger than the electron mass. As a consequence, if the linear momenta of electrons and nuclei are of the same order of magnitude, the motion of electrons is much faster than the motion of nuclei, so that electrons can be considered as instantaneously following the nuclei.

Factorisation of the total wave-function

The Born-Oppenheimer approximation assumes that the total wave-function can be factorised:

$$\Psi_{\rm tot} \;=\; \Psi_e(r\,;R)\;\;\Phi_n(R)\,, \tag{F.9}$$

where

a) the nuclear wave-function $\Phi_n(R)$ only depends on the nuclear coordinates R,
b) the electron wave-function $\Psi_e(r\,;R)$ depends directly on the electron coordinates r and parametrically on the nuclear coordinates R.

The electron wave-function can be a Slater determinant of spin-orbitals and is normalised within the electrons configuration space,

$$\int \Psi_e^*\,\Psi_e\,d\tau \;=\; 1\,. \tag{F.10}$$

F.1.3 Electronic Schrödinger equation

Let us consider the nuclei at fixed positions R. The Schrödinger equation for the electrons is

$$H_e\,\Psi_e(r\,;R) \;=\; [T_e + V_{ne} + V_{ee} + V_{nn}]\;\Psi_e(r\,;R) \;=\; E_e\,\Psi_e(r\,;R)\,. \tag{F.11}$$

Note that the Hamiltonian H_e in (F.11) includes the $V_{nn}(R)$ potential energy term of the nuclei. The eigenvalues of the Hamiltonian H_e

$$E_e \;=\; \int \Psi_e^*\,H_e\,\Psi_e\,d\tau \;=\; E_e(R) \tag{F.12}$$

parametrically depend on the set R of nuclear coordinates.

Adiabatic approximation

The meaning of the adiabatic approximation can be better grasped by considering a dynamical situation, where the positive ions are in motion with respect to their equilibrium positions. Let us suppose that, for a given set R of ion coordinates, the electrons system is in a given eigenstate $\Psi_e(r\,;R)$ of the Hamiltonian $H_e(R)$. When the values of the ion coordinates are modified, the Hamiltonian $H_e(R)$ and the wave-function $\Psi_e(r\,;R)$ are in turn modified. Within the adiabatic approximation, the electron wavefunction $\Psi_e(r\,;R)$ evolves remaining at any time an eigenstate of $H_e(R)$.
The adiabatic approximation is valid if the nuclear motion is sufficiently slow with respect to the relaxation time of the electron cloud.
When the adiabatic approximation is not valid, the electron wave-function is a linear combination of eigenstates of the evolving Hamiltonian $H_e(R)$.

Note: The term "adiabatic" is generally used in Thermodynamics to describe processes without exchange of heat between system and environment. The quantum mechanical adiabaticity considered here is closer to the thermodynamical concept of a quasi-static process, and has no relation with heat exchange.

F.1.4 Schrödinger equation for ions

Let us consider again the total Schrödinger equation

$$H\,\Psi_{\rm tot} \;=\; E\,\Psi_{\rm tot}\,, \tag{F.13}$$

where now the Hamiltonian includes also the nuclear kinetic term, $H = H_e + T_n$, and the total wave-function is $\Psi_{\rm tot} = \Psi_e(r\,;R)\Phi_n(R)$.
The Schrödinger equation can thus be rewritten as

$$H_e\,(\Psi_e\Phi_n) + T_n\,(\Psi_e\Phi_n) \;=\; E\,(\Psi_e\Phi_n)\,, \tag{F.14}$$

say, taking into account the results obtained for the electronic Schrödinger equation,

$$E_e(R)\,\Psi_e\,\Phi_n + T_n\,(\Psi_e\Phi_n) \;=\; E\,\Psi_e\,\Phi_n\,. \tag{F.15}$$

In the first term, the electron wave-function Ψ_e can already be integrated over the electron configuration space.
Let us consider in more detail the T_n term:

$$\begin{aligned} T_n\,(\Psi_e\Phi_n) \;&=\; -\sum\nolimits_A \frac{\hbar^2}{2M_A}\,\left(\vec{\nabla}_A\cdot\vec{\nabla}_A\right)\,(\Psi_e\Phi_n) \\ &=\; -\sum_A \frac{\hbar^2}{2M_A}\,\left[\left(\nabla_A^2\Psi_e\right)\Phi_n + 2\left(\vec{\nabla}_A\Psi_e\right)\left(\vec{\nabla}_A\Phi_n\right) + \Psi_e\left(\nabla_A^2\Phi_n\right)\right]\,. \end{aligned} \tag{F.16}$$

A further approximation consists in considering negligible the first and second terms within the square parentheses, where the nuclear kinetic operators act on the electron wavefunctions. In other terms, the interaction between electrons and atomic vibrations (electron-phonon interaction) is neglected. Within this approximation, we only consider the third term, where the electronic function Ψ_e is factorised.
When integrating the Schrödinger equation over the electrons configuration space, the electron wave-function gives rise to the normalization value 1, while the nuclear wavefunction is unaffected. We finally obtain the Schrödinger equation for the nuclei

$$[T_n + E_e(R)]\ \Phi_n \ = \ E\,\Phi_n \tag{F.17}$$

or

$$[T_n + V(R)]\ \Phi_n \ = \ E\,\Phi_n\,, \tag{F.18}$$

where $V(R) = E_e(R)$.

F.1.5 The potential energy surface (PES)

The function $V(R) = E_e(R)$ appearing in (F.17) and (F.18) is the ground-state energy of a system of interacting electrons moving in the field of fixed ("clamped") nuclei.
It is referred to as clamped ions energy or potential energy surface (PES) or Born-Oppenheimer energy surface. It represents the potential energy for the nuclear dynamics.

a) The equilibrium ground-state of the system (at $T = 0$) corresponds to the absolute minimum of the Born-Oppenheimer energy surface with respect to the set of nuclear coordinates. Partial minima correspond to metastable equilibrium ground states.

b) The finite temperature dynamical properties of ions (atomic vibrations) depend on the behaviour of the Born-Oppenheimer energy surface in the vicinity of the equilibrium configuration, say on its derivatives of second and higher order evaluated at the equilibrium configuration.

PES calculation

The PES can in principle be obtained by solving the electronic Schrödinger equation (F.11) for a convenient number of ionic configurations R. An exact solution of the Schrödinger equation is out of question but for the simplest systems (harmonic oscillator, single particle in a central field, squared-walled box). Numerical solutions are unmanageable even for relatively small molecules, in view of the large number of variables involved to get a sufficiently accurate picture of the wave-function in the configuration space.
The problem is generally solved according to the following guidelines.

1. The problem is simplified by taking into account the symmetry of the system. Symmetry considerations don't introduce approximations.
2. The approximation is made of treating each electron as moving independently in an average field from the others. The ground state energy of the system is obtained self-consistently by variational methods. Typical examples are based on the Hartree-Foch-Slater method or the more recent Density Functional Theory (DFT).

F.1.6 Harmonic approximation and anharmonicity

Within the adiabatic approximation, the Schrödinger equation for nuclei is written as

$$[T_n + V(R)]\ \Phi_n \ = \ E\,\Phi_n\,, \tag{F.19}$$

where $V(R) = E_e(R)$ is the potential energy surface (PES) defined in the configuration space of the nuclear coordinates $R = \{R_1, R_2, \ldots, R_N\}$.

As we have seen, the static equilibrium properties of the system correspond to the minimum of the PES. The vibrational properties depend on the local curvature of the PES near the equilibirum position.
The study of the local curvature of the PES can be made at different levels of approximation. The harmonic approximation is sufficient to account for the low-temperature behaviour of the vibrational specific heat or for the temperature effect on diffraction patterns. The inclusion of anharmonicity is necessary to account for thermal expansion and for the finite value of thermal conductivity; anharmonicity gives also a contribution the the high-temperature specific heat.

F.2 Two-atomic system (one degree of freedom)

Two-atomic molecules are the simplest cases of vibrational dynamics which can be encountered in physical systems. They are characterised by one degree of freedom, corresponding to the interatomic distance r. As usual, the dynamics of the relative motion is described in terms of the reduced mass $\mu = m_1 m_2/(m_1 + m_2)$.
The treatment of the one-dimensional oscillator presented in this § F.2, besides being directly applicable to two-atomic molecules, allows us to introduce in a relatively simple case some concepts which are further developed in subsequent sections dedicated to the vibrational dynamics of crystals (e.g. classical and quantum approaches, harmonic approximation and anarmonicity).

F.2.1 Power expansion of the potential energy

Let $V(r)$ be the potential energy of a system of two atoms or of two ions, r being their instantaneous distance. If only small variations of distance r with respect to the position r_0 of the potential energy minimum are considered, the potential energy is convenient expanded in a Taylor series:

$$V(r) = V(r_0) + \left(\frac{dV}{dr}\right)_0 (r - r_0) + \frac{1}{2!}\left(\frac{d^2V}{dr^2}\right)_0 (r - r_0)^2 + \frac{1}{3!}\left(\frac{d^3V}{dr^3}\right)_0 (r - r_0)^3 + \cdots \qquad \text{(F.20)}$$

- The first term $V(r_0)$ is the static binding energy.
- The second term is zero, because the first derivative of the potential energy is zero at the minimum position.
- The harmonic approximation consists in considering the expansion only up to the second-order term.
- Higher order terms are called anharmonic terms.

For our purposes, it is further convenient to set $V(r_0) = 0$ and rewrite (F.20) in terms of the ionic displacements $u = r - r_0$, introducing the force constants k_i:

$$V(u) = \frac{1}{2} k_0 u^2 + k_3 u^3 + k_4 u^4 + \cdots \qquad \text{(F.21)}$$

Here k_0 is the harmonic (second order) force constant, $k_i (i > 2)$ are the anharmonic force constants. In general, the third-order force constant is negative, $k_3 < 0$, corresponding to a repulsive branch of the potential energy steeper than the attractive branch.

F.2.2 The harmonic approximation

Although no realistic potential energy is truly harmonic, the harmonic approximation $V(u) = k_0 u^2/2$ is very important, for a number of reasons.

- The Schrödinger equation of the harmonic oscillator can be exactly solved, leading to the quantisation of energy levels $E_n = (n + 1/2)\hbar\omega_0$, where $\omega_0 = \sqrt{k_0/\mu}$.
- The harmonic approximation allows a good reproduction of the main features of several important thermal properties of matter, such as specific heats.

- The harmonic approximation is a good starting point for treating anharmonic effects (quasi-harmonic approximation, perturbative approaches).

In the following, we consider the classical and quantum description of a single harmonic oscillator and then of a statistical ensemble of harmonic oscillators.

Classical harmonic oscillator

The dynamical state of a classical harmonic oscillator corresponding to a two-atomic system is characterised by the time dependence of the displacement u

$$u(t) = A\cos(\omega_0 t) + \phi\,, \quad \text{where} \;\; \omega_0 = \sqrt{k_0/\mu}\,. \tag{F.22}$$

The frequency ω_0 is independent of the amplitude A and the total energy is

$$E = \frac{1}{2}\,\mu\dot{u}^2 + \frac{1}{2}\mu\omega_0^2 x^2 = \frac{1}{2}\mu\omega_0^2 A^2\,. \tag{F.23}$$

One can easily derive the two average values

$$\langle u\rangle = 0\,, \qquad \langle u^2\rangle = E/\mu\omega_0^2\,. \tag{F.24}$$

Since $\langle u\rangle = 0$, the average distance is equal to the rest distance:

$$\langle r\rangle = r_0 + \langle u\rangle = r_0\,. \tag{F.25}$$

Quantum harmonic oscillator

The dynamical state of a quantum harmonic oscillator is characterised by the eigenvector of the Hamiltonian H_0, which is contemporarily eigenvector of the number operator $N = a^\dagger a$

$$|n\rangle \tag{F.26}$$

where n is the number of energy quanta $\hbar\omega_0$. The total energy of the state $|n\rangle$ is

$$E_n = (1/2 + n)\,\hbar\omega_0\,. \tag{F.27}$$

One can show (see § F.8.1) that, as for the classical approximation,

$$\langle u\rangle = 0\,, \qquad \langle u^2\rangle = E_n/\mu\omega_0^2\,. \tag{F.28}$$

Note: It is worth remembering that the true dissociation energy D of a two-atomic molecule is determined by the joint effect of the static binding energy and of the zero-point energy:

$$D = -V(r_0) - \hbar\omega_0/2 = |V(r_0)| - \hbar\omega_0/2\,. \tag{F.29}$$

Classical statistics of the harmonic oscillator

In the *classical approximation*, the average energy of an harmonic oscillator is connected to the temperature by the equipartition theorem:

$$\langle E\rangle \;=\; k_B T \;=\; 1/\beta\,. \tag{F.30}$$

The average displacement from the equilibrium position is

$$\langle u\rangle \;=\; \frac{\int u\exp[-\beta V(u)]\;du}{\int \exp[-\beta V(u)]\;du} \;=\; 0\,, \tag{F.31}$$

where $V(u) = k_0 u^2/2$. The integral is zero because u is an odd function and $V(u)$ is an even function. Since $\langle u\rangle = 0$, independent of temperature, the harmonic oscillator doesn't exhibit thermal expansion.
The mean square displacement is

$$\langle u^2\rangle \;=\; \frac{\int u^2\exp[-\beta V(u)]\;du}{\int \exp[-\beta V(u)]\;du} \;= \frac{k_B T}{k_0} \;=\; \frac{E}{k_0}\,, \tag{F.32}$$

proportional to the temperature (and to the energy) and inversely proportional to the force constant k_0.

Quantum statistics of the harmonic oscillator

The hamiltonian operator is

$$H_0 \;=\; T + V(u) \;=\; p^2/2\mu + k_0 u^2/2 \tag{F.33}$$

and its eigenvalues are

$$E_n \;=\; (1/2 + n)\,\hbar\omega_0 \qquad (n = 0 \ldots \infty) \tag{F.34}$$

The average energy is

$$\langle H_0 \rangle \;=\; \frac{1}{Z_0}\,\mathrm{Tr}(H_0\, e^{-\beta H_0}) \;=\; \hbar\omega_0 \left[\frac{1}{2} + \frac{1}{e^{\beta\hbar\omega_0} - 1}\right], \tag{F.35}$$

where $\beta = 1/k_B T$ and Z_0 is the partition function

$$Z_0 \;=\; \mathrm{Tr}\,(e^{-\beta H_0}) \;=\; \frac{e^{-\beta\hbar\omega_0/2}}{1 - e^{-\beta\hbar\omega_0}}. \tag{F.36}$$

The probability density for the displacement u has a gaussian shape centred on $\langle u \rangle = 0$:

$$\rho(u) \;=\; (1/\sigma\sqrt{2\pi})\, e^{-u^2/2\sigma^2}\,. \tag{F.37}$$

The moments of the distribution can be calculated as

$$\langle u^k \rangle \;=\; \frac{1}{Z_0}\,\mathrm{Tr}\,(u^k e^{-\beta H_0}) \;=\; \frac{1}{Z_0}\sum_{n=0}^{\infty} \langle n|u^k|n\rangle\, e^{-\beta E_n}. \tag{F.38}$$

Making use of (F.38) one finds that there is no thermal expansion,

$$\langle u \rangle \;=\; 0\,, \tag{F.39}$$

and that the mean square displacement is

$$\sigma^2 \;=\; \langle u^2 \rangle \;=\; \frac{\hbar}{\mu\omega_0}\left[\frac{1}{2} + \frac{1}{e^{\beta\hbar\omega_0} - 1}\right] \;=\; \frac{\langle E \rangle}{k_0}\,. \tag{F.40}$$

For $T \to \infty$, σ^2 tends to the classical limit $k_B T/k_0$. For $T \to 0$, instead, the quantum behaviour is at variance with the classical behaviour:

$$\sigma^2 \to \sigma_0^2 = \hbar/2\sqrt{k_0\mu} = \hbar/2\mu\omega_0 \tag{F.41}$$

F.2.3 Anharmonicity effects

Approximate classical approach

An introductory idea of the main effects of anharmonicity can be gained by considering a single oscillator with a weak third-order term in the potential energy

$$V(u) = \frac{1}{2}\,k_0\,u^2 + k_3\,u^3\,, \tag{F.42}$$

where $k_3 < 0$, and looking for an approximate classical solution of the equation of motion.

Note: A purely cubic potential (F.42) would lead to system instability for large enough oscillations; a suitable fourth-order term is necessary to guarantee stability. We consider here only the cubic term for simplicity, with the basic assumption that oscillations are sufficiently weak to allow stability.

The classical acceleration is

$$\ddot{u} \;=\; \frac{F}{\mu} \;=\; -\frac{k_0}{\mu}\,u - \frac{3k_3}{\mu}\,u^2 \;=\; -\omega_0^2\,u - s\,\omega_0^2\,u^2 \tag{F.43}$$

where $s = 3k_3/k_0$. The relevance of the cubic term of the potential energy increases when the amplitude A of the vibrations increases. The assumed weakness of the cubic term corresponds to the condition $sA \ll 1$.
The simplest correction to the harmonic oscillator solution is of the form

$$u(t) = u_0 + A\left[\cos(\omega t) + \eta\cos(2\omega t)\right] , \tag{F.44}$$

where the oscillation centre u_0 and the frequency ω are a-priori unknown and the anharmonicity is supposed to introduce a weak oscillating perturbation ($\eta \ll 1$) with frequency 2ω. By inserting (F.44) into (F.43), taking into account that $\eta \ll 1$ and $sA \ll 1$ and considering only the leading terms terms, one gets two important results:

1. The centre of oscillation u_0 depends on the amplitude A according to

$$u_0 = -\frac{3k_3}{2k_0}A^2 > 0 \tag{F.45}$$

When the amplitude A increases, the average distance increases (k_3 is negative), say there is thermal expansion:

$$\langle r\rangle = r_0 + \langle u\rangle = r_0 + u_0 = r_0 - \frac{3k_3}{2k_0}A^2 \tag{F.46}$$

2. The frequency of oscillations decreases when the amplitude A increases, according to

$$\omega^2 = \omega_0^2(1 - s^2A^2) \tag{F.47}$$

By substituting A^2 from (F.45) in (F.47) one finds

$$\omega^2 = \omega_0^2\left(1 + \frac{6k_3}{k_0}\,u_0\right) \tag{F.48}$$

To first approximation, thus, the decrease of frequency is proportional to the thermal expansion u_0. In general, the relation between thermal expansion and frequency is not linear. For some applications, one can consider the oscillator as if it where harmonic, the only effect of anharmonicity being the variation of frequency (quasi-harmonic approximation).

Approximate quantum approach

The quantum approach is based on considering the anharmonic terms of the potential energy as a perturbation with respect to the harmonic oscillator. Let us consider only the cubic term in the potential energy ([Cohen-Tannoudji et al., 1973], Complement A_{xi}).
The harmonic hamiltonian H_0 is modified by adding the cubic perturbation $W = \sigma\hbar\omega_0\hat{X}^3$.

$$H \;=\; H_0 + W \;=\; \frac{1}{2}\,\hbar\omega_0\,(\hat{X}^2 + \hat{P}^2) + \sigma\hbar\omega_0^2\hat{X}^3\,. \tag{F.49}$$

The energy values E_n^0 of the harmonic oscillator are modified according to the perturbation theory as

$$E_n \;=\; E_n^0 + \langle n|W|n\rangle \;+\; \sum_{n\neq n'}\frac{|\langle n'|W|n\rangle|^2}{E_n - E_{n'}} \;+\; \ldots \tag{F.50}$$

Taking into account that $\hat{X} = (a^\dagger + a)/\sqrt{2}$ and that $na^\dagger = a^\dagger(N+1)$, one finds

$$\hat{X}^3 = \frac{1}{2^{3/2}}\,\left[(a^\dagger)^3 + a^3 + 3(N-1)a^\dagger + 3Na\right] , \tag{F.51}$$

corresponding to the creation or destruction of three or of one quantum of energy.
The only non-zero matrix elements of $\hat{W}$ are thus those connecting states that differ for one or three quanta:

$$n' = n+1, \quad n' = n-1, \quad n' = n+3, \quad n' = n-3\,. \tag{F.52}$$

The first-order term in the perturbation expansion is zero.
From the second-order term one finds

$$E_n \;=\; \left(n+\frac{1}{2}\right)\hbar\omega_0 \;-\; \frac{15}{4}\sigma^2(n+1/2)^2\hbar\omega_0 \;-\; \frac{7}{16}\sigma^2\hbar\omega_0 \;+\; \ldots \tag{F.53}$$

The energy levels are reduced with respect to the unperturbed harmonic case.
The difference between the energies of adjacent levels is no more constant

$$E_n - E_{n-1} \;=\; \hbar\omega_0\left[1-\frac{15}{2}\,\sigma^2\,n\right] \tag{F.54}$$

but depends on the value n.
At last, one can show that the eigenstates of the anharmonic oscillator are different from the eigenstates $|n\rangle$ of the harmonic oscillator, being contaminated by the states $|n+1\rangle, |n-1\rangle, |n+3\rangle, |n-3\rangle$.
Basic results:

1. The energy levels are down-shifted with respect to the harmonic levels, the extent of the shift increasing with the quantum number n. This fact corresponds to a reduction of the frequency of the fundamental absorption or emission line, and to the appearance of less intense satellite lines.
2. The eigenfunctions of the level E_n are now a linear combination of the harmonic oscillator eigenfunctions $|n\rangle, |n+1\rangle, |n-1\rangle, |n+3\rangle, |n-3\rangle$.
   As a consequence, the u and p operators can have non-zero matrix elements for eigenstates of the Hamiltonian, which are superpositions of harmonic eigenstates with different quantum numbers.
   In particular, one can show that $\langle u\rangle \neq 0$.

Classical statistics of the anharmonic oscillator

For a canonical ensemble of classical anharmonic oscillators, the average values of $\langle u\rangle$ and $\langle u^2\rangle$ are calculated trhough (F.31) and (F.32), respectively, where now the potential energy $V(u)$ is given by (F.21). One finds that tthe average displacement is

$$\langle u\rangle \;=\; -\,\frac{3k_3}{k_0^2}\,k_BT \;-\; \frac{3k_3}{k_0^4}\left(\frac{45k_3^2}{k_0}-32k_4\right)(k_BT)^2 \;+\; ... \tag{F.55}$$

To first order, $\langle u\rangle$ is positive ($k_3<0$): there is a positive thermal expansion which linearly depends on temperature. The second-order correction is proportional to T^2, and is generally quite small.
The mean square displacement is

$$\langle u^2\rangle \;=\; \frac{k_BT}{k_0}\;\left[1+\;\frac{3}{k_0^2}\left(\frac{12k_3^2}{k_0}-4k_4\right)(k_BT)\;+...\right] \tag{F.56}$$

To first order, one recovers the same expression as for the harmonic oscillator,

$$\langle u^2\rangle \;=\; \langle A^2\rangle/2 \;=\; k_BT/k_0\,. \tag{F.57}$$

The frequency is again $\omega_0=(k_0/\mu)^{1/2}$.
The second order correction is proportional to T^2. Neglecting the contribution of k_4, the second order correction gives a softening of the force constant with respect to the harmonic value k_0, corresponding to a progressive reduction of the frequency when T increases:

$$\omega_0^2 \;\rightarrow\; \omega^2=\omega_0^2\left[1-\left(\frac{36k_3^2}{k_0^3}\right)k_BT\right] \tag{F.58}$$

Two important consequences of the third-order term in the potential energy expansion are thus the following:

1. There is thermal expansion, positive if $k_3<0$. Within the classical approximation, to first order the thermal expansion is proportional to T.
2. The frequency of oscillations decreases when the temperature increases.

Quantum statistics of the anharmonic oscillator

The hamiltonian operator for the anharmonic oscillator can be expressed as the sum

$$H \;=\; H_0 + H_1\,, \tag{F.59}$$

where

$H_0 = p^2/2\mu + k_0u^2/2$ is the (unperturbed) harmonic Hamiltonian
$H_1 = k_3u^3 + k_4u^4 + \ldots$ is the contribution of anharmonicity.

The statistical quantum approach to anharmonicity is based on considering the anharmonic part H_1 as a perturbation with respect to the unperturbed harmonic Hamiltonian H_0.
The factor $\exp(-\beta H)$, which substitutes $\exp(-\beta H_0)$ in (F.38), obeys the integral equation

$$e^{-\beta H} \;\simeq\; e^{-\beta H_0}\left[1 - \int_0^\beta e^{-(\beta'-\beta)H_0}\, H_1\, e^{-\beta' H}\, d\beta'\right]. \tag{F.60}$$

To first order, imposing $H = H_0$ in the last factor within the integral,

$$e^{-\beta H} \;\simeq\; e^{-\beta H_0}\left[1 - \int_0^\beta e^{-(\beta'-\beta)H_0}\, H_1\, e^{-\beta' H_0}\, d\beta'\right]. \tag{F.61}$$

To first order, one finds that the thermal expansion expansion is

$$\langle u\rangle \;\simeq\; -\frac{3k_3}{k_0}\,\frac{\hbar}{\mu\omega_0}\left[\frac{1}{2} + \frac{1}{\exp(\hbar\omega_0/k_BT) - 1}\right] \;=\; -\frac{3k_3}{k_0}\,\sigma^2\,. \tag{F.62}$$

where σ^2 is the variance of the harmonic oscillator.
As for the variance $\langle u^2\rangle$, to first order one finds again the variance of the harmonic oscillator.

Important remark

In both the classical approximation and the quantum treatment one finds that the inclusion of anharmonic terms

a) produces only slight variations of the energy and of the variance of the distribution; as a consequence, the harmonic approximation is very effective in predicting the specific heats and the mean square atomic displacements;
b) is necessary to account for thermal expansion.

A note on nomenclature

It is convenient, in view of the applications to many-atomic systems, to distinguish the three different inter-atomic distances introduced above.

1. The rest distance r_0 corresponds to the minimum of the static potential energy $V(r)$;it is a constant, independent of temperature.
   The expression "rest distance" is conventional; it refers to a classical distance for $T = 0$.
2. The instantaneous distance $r(t)$ is variable with time.
3. The average distance is $\langle r(t)\rangle = r_0 + \langle u(t)\rangle$.
   - In the harmonic approximation, $\langle u\rangle = 0$ and $\langle r(t)\rangle = r_0$, the average distance coincides with the rest distance.
   - As an effect of anharmonicity, the average distance is different from the rest distance and depends on temperature.

F.3 Many-atomic systems

Let us now consider a system composed of $\mathcal{N}$ atoms (a molecule, a nano-cluster, a crystal, a non-crystalline solid). The potential energy surface $V[\{\vec{r}(m)\}]$ is defined for the $3\mathcal{N}$-dimensional configuration space ($m = 1, 2, \ldots, \mathcal{N}$ labels the single atoms).
Atoms oscillate around the average positions $\{\vec{R}(m)\}$, and the instantaneous positions are

$$\vec{r}(m) \;=\; \vec{R}(m) + \vec{u}(m)\,. \tag{F.63}$$

F.3.1 Expansion of the potential energy

If the atomic displacements $\vec{u}(m)$ are small, the potential energy $V[\{\vec{r}(m)\}]$ can be expanded as a Taylor series about the *average* configuration (Born-von Karman expansion):

$$V\;[\{\vec{r}(m)\}] \;=\; V_0 + V_1 + V_2 + V_3 + \cdots \tag{F.64}$$

The **zero-order term**

$$V_0 \;=\; V\left[\{\vec{R}(m)\}\right] \tag{F.65}$$

is the potential energy corresponding to the average configuration $\{\vec{R}(m)\}$.
The **first-order term** is

$$V_1 \;=\; \sum_{\alpha m} \Phi(\alpha m)\, u_\alpha(m)\,, \tag{F.66}$$

where $\alpha = x, y, z$ labels the cartesian coordinates and the quantities

$$\Phi(\alpha m) \;=\; \left[\frac{\partial V}{\partial u_\alpha(m)}\right]_{\{\vec{R}\}} \tag{F.67}$$

are the first-order coupling parameters. Here and below, the derivatives are calculated for the average configuration $\{\vec{R}(m)\}$.
The **second-order term** is

$$V_2 \;=\; \frac{1}{2} \sum_{\substack{\alpha m \\ \alpha' m'}} \Phi\begin{pmatrix} \alpha\, m \\ \alpha' m' \end{pmatrix}\; u_\alpha(m)\, u_{\alpha'}(m') \tag{F.68}$$

where the quantities

$$\Phi\begin{pmatrix} \alpha\, m \\ \alpha' m' \end{pmatrix} = \left(\frac{\partial^2 V}{\partial u_\alpha(m)\, \partial u_{\alpha'}(m')}\right)_{\{\vec{R}\}} \tag{F.69}$$

are the second-order coupling parameters or force constants.
As a consequence of the invariance of second partial derivatives with respect to the order of derivation, the force constants are invariant with respect to the exchange of the indices:

$$\Phi\begin{pmatrix} \alpha\, m \\ \alpha' m' \end{pmatrix} = \Phi\begin{pmatrix} \alpha' m' \\ \alpha\, m \end{pmatrix} \tag{F.70}$$

The **third-order term** is

$$V_3 \;=\; \frac{1}{3!} \sum_{\substack{\alpha m \\ \alpha' m' \\ \alpha'' m''}} \Phi\begin{pmatrix} \alpha\; m \\ \alpha'\, m' \\ \alpha'' m'' \end{pmatrix}\, u_\alpha(m)\, u_{\alpha'}(m')\, u_{\alpha''}(m'')\,, \tag{F.71}$$

where

$$\Phi\begin{pmatrix} \alpha\; m \\ \alpha'\, m' \\ \alpha'' m'' \end{pmatrix} \;=\; \left(\frac{\partial^3 V}{\partial u_\alpha(m)\, \partial u_{\alpha'}(m')\, \partial u_{\alpha''}(m'')}\right)_{\{\vec{R}\}} \tag{F.72}$$

are the third-order coupling parameters.
And so on with higher order terms.

F.3.2 Harmonic approximation

The harmonic approximation consists in truncating the Taylor expansion (F.64) at the 2nd-order term V_2 (quadratic in the atomic displacements).
In the harmonic approximation, the average atomic positions $\{\vec{R}(m)\}$, around which atoms vibrate, are equal to rest positions $\{\vec{R}^0(m)\}$, which correspond to the minimum of the potential energy surface. As a consequence, the first order term (F.66) is zero, $V_1 = 0$.
For an anharmonic system, the average positions $\vec{R}(m)$ are different from the rest positions $\{\vec{R}^0(m)\}$ and are *a priori* unknown.

F.3.3 Dynamical equations and force constants

The vibrational contribution to the potential energy is V_2 given by (F.68) for a generic many-atomic system.

Hamiltonian function

The kinetic energy is

$$T \;=\; \frac{1}{2}\sum_{\alpha m} M_m\, \dot{u}^2_\alpha(m)\,, \tag{F.73}$$

where M_m is the mass of atom m, so that the Hamiltonian is

$$\mathcal{H} \;=\; V_0 \;+\; \frac{1}{2}\sum_{\alpha m} M_m\, \dot{u}^2_\alpha(m) \;+\; \frac{1}{2}\sum_{\substack{\alpha m\\ \alpha' m'}} \Phi\begin{pmatrix}\alpha\, m\\ \alpha' m'\end{pmatrix}\, u_\alpha(m)\, u_{\alpha'}(m')\,. \tag{F.74}$$

Forces

The force acting on atom m in direction α is

$$F_\alpha(m) = -\,\frac{\partial V_2}{\partial u_\alpha(m)} = -\sum_{\alpha'\;\, m'} \Phi\begin{pmatrix}\alpha\, m\\ \alpha' m'\end{pmatrix}\, u_{\alpha'}(m')\,. \tag{F.75}$$

Equation (F.75) expresses the force acting on atom m as the sum of the contributions from the interactions with all the other atoms.

Note: The expression (F.68) contains both quadratic terms , such as

$$\frac{1}{2}\sum_{\substack{\alpha m\\ \alpha m}} \Phi\begin{pmatrix}\alpha m\\ \alpha m\end{pmatrix}\, u^2_\alpha(m)\,, \qquad \frac{1}{2}\sum_{\substack{\alpha' m'\\ \alpha' m'}} \Phi\begin{pmatrix}\alpha' m'\\ \alpha' m'\end{pmatrix}\, u^2_{\alpha'}(m')$$

and cross-product terms, such as

$$\frac{1}{2}\sum_{\substack{\alpha m\\ \alpha' m'}} \Phi\begin{pmatrix}\alpha\, m\\ \alpha' m'\end{pmatrix}\, u_\alpha(m)\, u_{\alpha'}(m')\,, \qquad \frac{1}{2}\sum_{\substack{\alpha' m'\\ \alpha m}} \Phi\begin{pmatrix}\alpha' m'\\ \alpha\, m\end{pmatrix}\, u_{\alpha'}(m')\, u_\alpha(m)\,.$$

Because of the invariance (F.70) with respect to the exchange of indices, the cross terms are two by two equal, so that the factors 1/2 disappear in (F.75).

Meaning of force constants

To grasp the physical meaning of the force constants, let us choose a central atom m at rest and assume that all other atoms are at rest, with the exception of only one atom (m'), which is displaced by $u_{\alpha'}(m')$ along the α' direction. From (F.75),

$$F_\alpha(m) = -\Phi\begin{pmatrix}\alpha\, m\\ \alpha' m'\end{pmatrix}\, u_{\alpha'}(m')\,. \tag{F.76}$$

Each force constant $\Phi\left(\begin{smallmatrix}\alpha\, m\\ \alpha' m'\end{smallmatrix}\right)$ is thus the opposite of the force exerted on atom m in direction α when the atom m' is displaced a unit distance in direction α', all other atoms remaining fixed.
According to (F.75), the force acting on a given atom depends on the contributions of all the atomic displacements, including the displacement of the atom m itself.
If only atom m is displaced along the direction α',

$$F_\alpha(m) = -\Phi\begin{pmatrix}\alpha\, m\\ \alpha' m\end{pmatrix} u_{\alpha'}(m)\,. \tag{F.77}$$

Note: In principle, force constants connect each atom m with all other atoms m' of the crystal.
Actyally, in real crystals only the force constants connecting neighbouring atoms are relevant.

Constraint of force constants

Let us consider a rigid movement of the system, where all atoms undergo the same displacement $\vec{u}$ of components $u_{\alpha'}$. The force on the generic atom m induced by the equal displacements of all the atoms has to be zero:

$$0 \;=\; F_\alpha(m) = -\sum_{\alpha' m'} \Phi\begin{pmatrix}\alpha\, m\\ \alpha' m'\end{pmatrix} u_{\alpha'}(m') = -\sum_{\alpha'} u_{\alpha'} \sum_{m'} \Phi\begin{pmatrix}\alpha\, m\\ \alpha' m'\end{pmatrix} \tag{F.78}$$

Since the displacement $u_{\alpha'}$ is arbitrary, (F.78) gives

$$\sum_{m'} \Phi\begin{pmatrix}\alpha\, m\\ \alpha' m'\end{pmatrix} = 0\,. \tag{F.79}$$

From this equality, we can obtain, for the force constants where $m' = m$:

$$\Phi\begin{pmatrix}\alpha\, m\\ \alpha' m\end{pmatrix} = -\sum_{m' \neq m} \Phi\begin{pmatrix}\alpha\, m\\ \alpha' m'\end{pmatrix}\,. \tag{F.80}$$

Physically, (F.80) means that displacing the atom m by a unit distance in a given direction, all other atoms staying at rest, has the same effect as displacing all the other atoms by an opposite unit distance, the atom m staying at rest.

Dynamical equations

Solving the Hamilton equations one obtains that the classical dynamical equation for the α-th component of the displacement of atom m is

$$\boxed{M_m\, \ddot{u}_\alpha(m) = -\sum_{\alpha' m'} \Phi\begin{pmatrix}\alpha\, m\\ \alpha' m'\end{pmatrix} u_{\alpha'}(m')} \tag{F.81}$$

There are $3\mathcal{N}$ such dynamical equations, three for each atom m. Globally, they form a system of $3n\mathcal{N}$ coupled equations corresponding to $3\mathcal{N}$ coupled harmonic oscillators.

Solutions of the dynamical equations

The system of equations (F.81) describes the behaviour of $3\mathcal{N}$ coupled harmonic oscillators. It is thus reasonable to seek solutions of the oscillatory type

$$\boxed{u_\alpha(m,t) \;=\; \frac{1}{\sqrt{M_m}}\, \mathbf{Re}\left[\, w_\alpha(m)\, e^{-i\omega t}\right]} \tag{F.82}$$

The amplitudes $w_\alpha(m)$ are complex quantities, to account for the phase relationships between the displacements of different atoms, and depend both on the dynamical equation and on the initial conditions.
In (F.82), the mass M_m appears explicitly, for symmetry reasons that will be made clear below.
By substituting the values $u_\alpha(m,t)$ of (F.82) into the dynamical equation (F.81) one gets

$$-\sqrt{M_m}\,\omega^2\, w_\alpha(m)\, e^{-i\omega t} = -\sum_{\alpha' m'} \Phi\begin{pmatrix}\alpha\; m\\ \alpha'\; m'\end{pmatrix} \frac{1}{\sqrt{M_{m'}}}\, w_{\alpha'}(m')\, e^{-i\omega t}. \tag{F.83}$$

F.3.4 Dynamical matrix and normal modes

By introducing the mass-adjusted force constants

$$D^0 \begin{pmatrix} \alpha\ m \\ \alpha'\ m' \end{pmatrix} \;=\; \frac{\Phi \left(\begin{smallmatrix} \alpha\ m \\ \alpha'\ m' \end{smallmatrix} \right)}{\sqrt{M_m\, M_{m'}}}\,, \tag{F.84}$$

equations (F.83) can be rewritten as

$$\omega^2\, w_\alpha(m) \;-\; \sum_{\alpha' m'} D^0 \begin{pmatrix} \alpha\ m \\ \alpha'\ m' \end{pmatrix} w_{\alpha'}(m') \;=\; 0 \tag{F.85}$$

Equation (F.85) is representative of a system of $3\mathcal{N}$ coupled equations.
By considering

- the terms $w_\alpha(m)$ as elements of a $3\mathcal{N}$-size column vector U,
- the terms $D^0 \left(\begin{smallmatrix} \alpha\ m \\ \alpha'\ m' \end{smallmatrix} \right)$ as elements of a $3\mathcal{N} \times 3\mathcal{N}$ matrix, the (mass-adjusted) *real-space dynamical matrix* $\mathbf{D^0}$,

the system of dynamical equations (F.85) can be synthesised as a matrix equation:

$$\boxed{\omega^2\, U \;=\; \mathbf{D^0}\, U} \tag{F.86}$$

or more explicitly

$$\omega^2 \begin{pmatrix} \cdots \\ w_\alpha(m) \\ \cdots \\ \cdots \end{pmatrix} = \begin{pmatrix} \cdots & \cdots & \cdots & \cdots \\ \cdots & \cdots & D^0 \left(\begin{smallmatrix} \alpha\ m \\ \alpha' m' \end{smallmatrix} \right) & \cdots \\ \cdots & \cdots & \cdots & \cdots \\ \cdots & \cdots & \cdots & \cdots \end{pmatrix} \begin{pmatrix} \cdots \\ \cdots \\ w_{\alpha'}(m') \\ \cdots \end{pmatrix} \tag{F.87}$$

Eigenfrequencies and eigenvectors

The solution of (F.87) is a typical eigenvalue problem. By imposing that the secular determinant is zero, $\det[\mathbf{D^0} - \omega^2 \mathbf{I}] = 0$, one obtains an algebraic equation, whose solution gives in principle

→ $3\mathcal{N}$ eigenfrequencies ω_j ($j = 1, 2, \ldots, 3\mathcal{N}$), corresponding to $3\mathcal{N}$ independent normal modes. The number of normal modes is three times the number of atoms in the system.

The invariance of the force constants with respect to the exchange of indices (F.70) ensures that the real-space dynamical matrix $\mathbf{D}^0$ is symmetric, and the eigenvalues are real. The physical meaning requires that the eigenvalues ω^2 are positive quantities too.

For each eigenfrequency ω_j, say for each normal mode, (F.87) gives an eigenvector U_j with $3\mathcal{N}$ components describing the relative amplitudes and the phase relationships of the atomic motions corresponding to the normal mode.
In total there are thus

→ $3\mathcal{N}$ eigenvectors U_j, each one with $3\mathcal{N}$ components.

By this treatment, the coupled motions of $\mathcal{N}$ atoms are described in terms of $3\mathcal{N}$ independent harmonic oscillators.
The practical solution of (F.87) is difficult for a large number $\mathcal{N}$ of atoms, e.g. for large molecules or nanoclusters. It represents an impossible task for a crystal: a dramatic improvement is however obtained if one takes into account the translational symmetry of the crystal, as we see in the next section F.4.

F.4 Harmonic dynamics in crystals

References: [Leibfried and Ludwig, 1961, Maradudin et al., 1971, Willis and Pryor, 1975, Brüesch, 1982].

For crystals, in order to exploit the translational symmetry, it is convenient to factorize the total number $\mathcal{N}$ of atoms as $\mathcal{N} = Nn$, where N is the number of primitive cells, n is the number of atoms per primitive cell.

The positions of atoms are labelled by two indices, ℓ for the primitive cells and κ for the positions inside the cell:

$$\vec{R}(m) \;=\; \vec{R}(\ell\kappa) \;=\; \vec{R}((\ell) + \vec{R}(\kappa) \tag{F.88}$$

1. The positions of the primitive cells are given by the Bravais lattice vectors

$$\vec{R}(\ell) = \ell_1\vec{a}_1 + \ell_2\vec{a}_2 + \ell_3\vec{a}_3 \tag{F.89}$$

   where ℓ_1, ℓ_2, ℓ_3 are integer numbers. The index ℓ labels the primitive cells: $\ell = 1, \ldots, N$.
2. The positions of the atoms inside a primitive cell are given by

$$\vec{R}(\kappa) = x_1\vec{a}_1 + x_2\vec{a}_2 + x_3\vec{a}_3 \tag{F.90}$$

   where x_1, x_2, x_3 are fractional coordinates. The index κ (the Greek letter kappa) is unnecessary for Bravais crystals, say for crystals with one atom per primitive cell (such as Cu, Ag, Au or the noble gas solids).

Note: When studying the effects of atomic vibrations ("lattice dynamics"), one considers only primitive cells, not conventional cells.

Crystal potential energy

The potential energy of the crystal $V[\{\vec{r}(\ell\kappa)\}]$ is defined in a $3nN$-dimensional configuration space. Atoms oscillate around the average positions $\{\vec{R}(\ell\kappa)\}$, and the instantaneous positions are

$$\vec{r}(\ell\kappa) \;=\; \vec{R}(\ell\kappa) + \vec{u}(\ell\kappa)\,. \tag{F.91}$$

We again rely on the potential energy expansion (F.64).

The **second-order term** (the only one relevant in the harmonic approximation) is expressed as

$$V_2 \;=\; \frac{1}{2}\sum_{\substack{\alpha\ell\kappa\\ \alpha'\ell'\kappa'}} \Phi\begin{pmatrix}\alpha\,\ell\,\kappa\\ \alpha'\ell'\kappa'\end{pmatrix}\, u_\alpha(\ell\kappa)\, u_{\alpha'}(\ell'\kappa') \tag{F.92}$$

where the second-order coupling parameters are

$$\Phi\begin{pmatrix}\alpha\,\ell\,\kappa\\ \alpha'\ell'\kappa'\end{pmatrix} = \left(\frac{\partial^2 V}{\partial u_\alpha(\ell\kappa)\,\partial u_{\alpha'}(\ell'\kappa')}\right)_{\{\vec{R}\}}\,. \tag{F.93}$$

F.4.1 Constraints on force constants

As for any system, the force constants are invariant with respect to the exchange of the indices:

$$\Phi\begin{pmatrix}\alpha\,\ell\,\kappa\\ \alpha'\ell'\kappa'\end{pmatrix} = \Phi\begin{pmatrix}\alpha'\ell'\kappa'\\ \alpha\,\ell\,\kappa\end{pmatrix}\,. \tag{F.94}$$

The constraint due to the invariance of the potential energy with respect to translations of the whole system (F.79) becomes

$$\sum_{\ell'\kappa'} \Phi\begin{pmatrix}\alpha\,\ell\,\kappa\\ \alpha'\ell'\kappa'\end{pmatrix} = 0\,. \tag{F.95}$$

For the consequences of the invariance with respect to rotations see [Maradudin et al., 1971].

In crystals, further constraints are present, depending

a) on general lattice invariance properties, such as invariance under lattice translation;
b) on the symmetry properties of a given crystal.

We introduce here the constraint due to translational invariance.
For an infinite crystal, lattice translations shift primitive cells: $\ell \to \ell + T$, $\ell' = \ell' + T$ and atomic positions are modified accordingly

$$(\ell, \kappa) \longrightarrow (\ell + T, \kappa) \qquad (\ell', \kappa') \longrightarrow (\ell' + T, \kappa') \tag{F.96}$$

The force constants must be invariant with respect to lattice translations:

$$\Phi \begin{pmatrix} \alpha,\ \ell + T,\ \kappa \\ \alpha',\ \ell' + T,\ \kappa' \end{pmatrix} = \Phi \begin{pmatrix} \alpha\ \ell\ \kappa \\ \alpha'\ \ell'\ \kappa' \end{pmatrix} \tag{F.97}$$

In particular, for $T = -\ell$ and for $T = -\ell'$, respectively, (F.97) becomes

$$\Phi \begin{pmatrix} \alpha\ \ell\ \kappa \\ \alpha'\ \ell'\ \kappa' \end{pmatrix} = \Phi \begin{pmatrix} \alpha,\ \ 0,\ \ \kappa \\ \alpha',\ \ell' - \ell,\ \kappa' \end{pmatrix} = \Phi \begin{pmatrix} \alpha,\ \ell - \ell',\ \kappa \\ \alpha',\ \ \ 0,\ \ \kappa' \end{pmatrix} \tag{F.98}$$

The force constants only depend on the differences $\ell - \ell'$, say on the relative positions of primitive cells, not on their absolute positions.
For finite crystals, the same conclusions hold, provided suitable boundary conditions are imposed (see below).
By substituting $L = \ell - \ell'$, (F.79) is more conveniently written as:

$$\Phi \begin{pmatrix} \alpha\ \ell\ \kappa \\ \alpha'\ \ell'\ \kappa' \end{pmatrix} = \Phi \begin{pmatrix} \alpha,\ \ \ 0,\ \ \kappa \\ \alpha',\ -L,\ \kappa' \end{pmatrix} = \Phi \begin{pmatrix} \alpha,\ L,\ \kappa \\ \alpha',\ 0,\ \kappa' \end{pmatrix} . \tag{F.99}$$

F.4.2 Periodic boundary conditions

To take advantage of the translational symmetry properties for a finite crystal, it is convenient to introduce the periodic boundary conditions.
Let us consider a crystal of parallelepiped shape. The lengths of the three edges of the parallelepiped are $N_1 a_1, N_2 a_2, N_3 a_3$, respectively. There are $N = N_1 N_2 N_3$ primitive cells.
The periodic boundary conditions on the atomic displacements impose that

$$\vec{u}(\vec{r} + N_\alpha \vec{a}_\alpha) \ = \ \vec{u}(\vec{r}) \qquad (\alpha = 1, 2, 3) . \tag{F.100}$$

According to (F.100), the displacement of an atom sitting on one face of the parallelepiped is equal to the displacement of the corresponding atom on the opposite face.

Irreducible representations and boundary conditions

In group theory one cans show that for a one-dimensional linear chain there are N one-dimensional irreducible representation of the group of translations, whose simplest basis functions are

$$e^{iqx} , \qquad q = \frac{2\pi}{a} \frac{m}{N} \quad (-N/2 < m \leq N/2) , \tag{F.101}$$

where the values q are confined within the first Brillouin Zone.
A translation $T = sa$ is represented, in the basis e^{iqx} (say for a given q) by the complex number

$$\left(e^{isa}\right)^q \ = \ e^{iqsa} \ = \ e^{iqT} . \tag{F.102}$$

For a *three-dimensional* crystal with periodic boundary conditions, one can build up $N = N_1 N_2 N_3$ one-dimensional irreducible representations whose basis functions are

$$e^{i\vec{q}\cdot\vec{r}} , \qquad q_i = b_i \frac{m_i}{N_i} \quad (-N_i/2 < m_i \leq N_i/2) , \tag{F.103}$$

where b_i is the magnitude of the $\vec{b}_i$ primitive vector of reciprocal space. A translation $\vec{T}$ is represented, in the basis $e^{i\vec{q}\cdot\vec{r}}$ (say for a given $\vec{q}$) by the complex number

$$e^{i\vec{q}\cdot\vec{T}}\,. \tag{F.104}$$

The vectors $\vec{q}$ form a grid of equally spaced points within the first Brillouin Zone of the reciprocal space. They label the N irreducible representations of the translation group. When the crystal size increases, the number $N = N_1N_2N_3$ of primitive cells in the real space increases, and the density of $\vec{q}$ points in reciprocal space increases accordingly.
The basis functions (F.103) are plane waves, of wavelength $\lambda = 2\pi/q$.

F.4.3 Spatial periodicity of eigenvectors

For an irreducible representation characterised by the wavevector $\vec{q}$, the effect of a translation $\vec{T}$ on an eigenvector $w_\alpha(\ell\kappa)$ is the multiplication by (F.104).
By identifying $\vec{T} = \vec{R}(\ell)$, one can thus express each eigenvector, in the $\vec{q}$ representation, as a product

$$\boxed{w_\alpha(\ell\kappa) \;=\; w_\alpha(\kappa)\; e^{i\vec{q}\cdot\vec{R}(\ell)}.} \tag{F.105}$$

Note: For the monatomic one-dimensional linear chain, (F.105) reduces to $w(\ell) = \; w\, \exp[iqR(\ell)]$.

The atomic displacement (F.82) becomes

$$u_\alpha(\ell k,t) \;=\; \frac{1}{\sqrt{M_\kappa}}\,\mathbf{Re}\left[\, w_\alpha(\kappa)\, e^{i\vec{q}\cdot\vec{R}(\ell)}\, e^{-i\omega t}\right]\,. \tag{F.106}$$

F.4.4 The Fourier-transformed dynamical matrix

By substituting (F.105) into (F.85) for a given value of $\vec{q}$, one gets

$$\omega^2\, w_\alpha(\kappa)\; e^{i\vec{q}\cdot\vec{R}(\ell)} \;-\; \sum_{\alpha'\ell'\kappa'} D^0\begin{pmatrix}\alpha\;\ell\;\kappa\\ \alpha'\;\ell'\;\kappa'\end{pmatrix}\; e^{i\vec{q}\cdot\vec{R}(\ell')}\, w_{\alpha'}(\kappa') \;=\; 0\,. \tag{F.107}$$

Moving $e^{i\vec{q}\cdot\vec{R}(\ell)}$ to the right of (F.107), substituting $L = \ell - \ell'$ as in (F.99) and summing over L one obtains

$$\omega^2\, w_\alpha(\kappa) \;-\; \sum_{\alpha'\kappa'}\left\{\sum_L\; D^0\begin{pmatrix}\alpha\;L\;\kappa\\ \alpha'\;0\;\kappa'\end{pmatrix}\, e^{-i\vec{q}\cdot\vec{R}(L)}\right\}\; w_{\alpha'}(\kappa') \;=\; 0\,. \tag{F.108}$$

For each one of the N wavevectors $\vec{q}$, one can define a quantity

$$D_{\vec{q}}\begin{pmatrix}\alpha\kappa\\ \alpha'\kappa'\end{pmatrix} \;=\; \sum_L D^0\begin{pmatrix}\alpha\;L\;\kappa\\ \alpha'\;0\;\kappa'\end{pmatrix}\, e^{-i\vec{q}\cdot\vec{R}(L)} \tag{F.109}$$

corresponding to the term included in curly brackets in (F.108).
For each one of the N wavevectors $\vec{q}$ there is thus a system of $3n \times 3n$ coupled equations

$$\omega^2\, w_\alpha(\kappa) \;=\; \sum_{\kappa'\alpha'} D_{\vec{q}}\begin{pmatrix}\alpha\kappa\\ \alpha'\kappa'\end{pmatrix}\, w_{\alpha'}(\kappa'). \tag{F.110}$$

By considering

- the terms $w_\alpha(\kappa)$ as elements of a $3n$-sized column vector $U_{\vec{q}}$,
- the terms $D_{\vec{q}}\left(\begin{smallmatrix}\alpha\kappa\\ \alpha'\kappa'\end{smallmatrix}\right)$ as elements of a $3n \times 3n$ matrix, the *Fourier transformed dynamical matrix* $\mathbf{D}_{\vec{q}}$ (frequently simply referred to as dynamical matrix),

the system of equations (F.110) can be synthesised as a matrix equation:

$$\boxed{\omega^2\, U_{\vec{q}} \;=\; \mathbf{D}_{\vec{q}}\, U_{\vec{q}}} \tag{F.111}$$

or more explicitly

$$\omega^2 \begin{pmatrix} \cdots \\ w_\alpha(\kappa) \\ \cdots \\ \cdots \end{pmatrix} = \begin{pmatrix} \cdots & \cdots & \cdots & \cdots \\ \cdots & \cdots & D_{\vec{q}}\left(\begin{smallmatrix} \alpha & \kappa \\ \alpha' & \kappa' \end{smallmatrix}\right) & \cdots \\ \cdots & \cdots & \cdots & \cdots \\ \cdots & \cdots & \cdots & \cdots \end{pmatrix} \begin{pmatrix} \cdots \\ \cdots \\ w_{\alpha'}(\kappa') \\ \cdots \end{pmatrix} \tag{F.112}$$

Note: In principle, to evaluate the Fourier transformed dynamical matrix for a given $\vec{q}$ one should evaluate the sum (F.109) over all values of L. Actually, due to the short range of most interactions, in general only a few terms of the sum are significant.

Eigenfrequencies and eigenvectors of the FT dynamical matrix

The solution of (F.112) is again an eigenvalue problem.

A) By imposing that the secular determinant be zero, one obtains an algebraic equation, whose solution gives

   $3n$ eigenvalues or eigenfrequencies $\omega(\vec{q}, s)$ which are labeled by the wavevector $\vec{q}$ and by the branch index $s = 1, 2, \ldots, 3n$, which correspond to $3n$ independent normal modes of wavevector $\vec{q}$.

   The Fourier-transformed dynamical matrix $\mathbf{D}_{\vec{q}}$ has complex elements. One can show that it is Hermitian

$$D_{\vec{q}}\begin{pmatrix} \alpha'\kappa' \\ \alpha\kappa \end{pmatrix} \;=\; D^*_{\vec{q}}\begin{pmatrix} \alpha\kappa \\ \alpha'\kappa' \end{pmatrix}, \tag{F.113}$$

   so that its eigenvalues are real. The stability of the lattice further requires that the eigenvalues ω^2 are positive quantities too.
   The functions $\omega_s(\vec{q})$ can be considered as the $3n$ *branches* of a multivalued function $\omega(\vec{q})$. The relation $\omega_s(\vec{q})$ is the dispersion relation of branch s.

B) For each one of the $3n$ eigenfrequency $\omega(\vec{q}s)$, say for each normal mode, (F.112) gives an eigenvector $U_{\vec{q}s}$ with $3n$ components that describe the relative amplitudes and the phase relationships of the atomic motions corresponding to the normal mode.
   In total, for a given wavevector $\vec{q}$, there are thus

   $3n$ eigenvectors $U_{\vec{q}s}$, each one with $3n$ components $u_\alpha(\kappa|\vec{q}s)$.

F.4.5 Atomic displacements and normal coordinates

The displacement of each atom $(\ell\kappa)$ is the sum of the contributions of all the $3nN$ independent normal modes. The contribution of a normal mode $(\vec{q}s)$ to the displacement of atom $(\ell\kappa)$ is

$$u_\alpha(\ell\kappa, t\,|\,\vec{q}s) = \frac{1}{\sqrt{M_\kappa}}\mathbf{Re}\left[\, w_\alpha(\kappa|\vec{q}s)\, e^{i\vec{q}\cdot\vec{R}(\ell)}\, e^{-i\omega(\vec{q}s)t}\,\right]. \tag{F.114}$$

This contribution is determined from the knowledge of the dynamical matrix only to within a factor; actually, the eigenvector components $w_\alpha(\kappa|\vec{q}s)$ depend on the energy stored in the normal mode.
It is convenient to factorize the quantities $w_\alpha(\kappa|\vec{q}s)$, separating the information on the magnitude of the relative motion of atoms inside the primitive cell from the contributions due to the total energy (which depends on temperature).
To this effect, (F.114) is rewritten as

$$u_\alpha(\ell\kappa, t\,|\,\vec{q}s) = \frac{1}{\sqrt{m_\kappa}}\,\mathbf{Re}\left[\mathrm{e}_\alpha(\kappa|\vec{q}s)\,\frac{Q(\vec{q}s, t)}{\sqrt{N}}\quad e^{i\vec{q}\cdot\vec{R}(\ell)}\right] \tag{F.115}$$

where:

a) The factor $\mathrm{e}_\alpha(\kappa|\vec{q},s)$ is a component of the *normalized eigenvector* $\mathrm{e}(\vec{q},s)$, which describes the displacement patterns of the n atoms inside each primitive cell.

b) The quantity
$$Q(\vec{q}s,t) = Q_0(\vec{q}s)\exp[-i\omega(\vec{q}s)t] \tag{F.116}$$
is the normal coordinate of mode $(\vec{q}s)$; the amplitude Q_0 is a complex quantity, which depends on the initial conditions and on the energy stored in the normal mode $(\vec{q}s)$. One can show that $Q(-\vec{q}s,t) = Q^*(\vec{q}s,t)$.

c) The factor $1/\sqrt{N}$ can be justified as follows. The number of primitive cells N is proportional to the number of normal modes $3nN$. The energy stored in each normal mode, proportional to the square of the normal coordinate (see below) is independent of N. The energy of the normal mode is distributed over all the atoms, whose number is proportional to N.

The total displacement of atom $(\ell\kappa)$ can be calculated by summing up the contributions of all normal modes within the first B.Z.:
$$u_\alpha(\ell\kappa,t) = \frac{1}{\sqrt{N\,m_\kappa}}\sum_{\vec{q}s}\left[\mathrm{e}_\alpha(\kappa|\vec{q}s)\,e^{i\vec{q}\cdot\vec{R}(\ell)}\,Q(\vec{q}s,t)\right] \tag{F.117}$$

Any pair of values $\vec{q}$ and $-\vec{q}$ in the first B.Z. correspond to two plane waves traveling in opposite direction and sharing the same frequency.
The displacement $u_\alpha(\ell\kappa,t)$ is a real quantity, since $Q(-\vec{q}s,t) = Q^*(\vec{q}s,t)$.

Properties of eigenvectors and eigenfrequencies

One can demonstrate [Maradudin et al., 1971] that the eigenvectors satisfy the orthonormality and closure relations
$$\sum_{\kappa\alpha}\mathrm{e}^*_\alpha(\kappa|\vec{q}s)\,\mathrm{e}_\alpha(\kappa|\vec{q}s') \;=\; \delta_{ss'}\,, \tag{F.118}$$

$$\sum_{s}\mathrm{e}^*_\alpha(\kappa'|\vec{q}s)\,\mathrm{e}_{\alpha'}(\kappa|\vec{q}s) \;=\; \delta_{\alpha\alpha'}\,\delta_{\kappa\kappa'}\,. \tag{F.119}$$

The Fourier transformed dynamical matrix satisfy
$$D_{-\vec{q}}\begin{pmatrix}\alpha\kappa\\ \alpha'\kappa'\end{pmatrix} \;=\; D^*_{\vec{q}}\begin{pmatrix}\alpha\kappa\\ \alpha'\kappa'\end{pmatrix}\,, \tag{F.120}$$

and as a consequence
$$\omega^2_j(-\vec{q}) \;=\; \omega^2(\vec{q})\,. \tag{F.121}$$

Alternative eigenvectors

For the solution of particular dynamical problems (e.g. long wavelength modes) it is convenient to introduce an alternative dynamical matrix
$$C_{\vec{q}}\begin{pmatrix}\alpha\kappa\\ \alpha'\kappa'\end{pmatrix} \;=\; e^{i\vec{q}\cdot\vec{R}(\kappa)}\,D_{\vec{q}}\begin{pmatrix}\alpha\kappa\\ \alpha'\kappa'\end{pmatrix}\,e^{-i\vec{q}\cdot\vec{R}(\kappa)}\,. \tag{F.122}$$

The two matrices share the same eigenfrequencies.
The eigenvectors of the new matrix $\mathbf{C}$ are connected to the eigenvectors of the matrix $\mathbf{D}$ by
$$\tilde{w}_\alpha(\kappa|\vec{q}s) \;=\; \mathrm{e}_\alpha(\kappa|\vec{q}s)\,e^{-i\vec{q}\cdot\vec{R}(\kappa)}\,. \tag{F.123}$$

F.4.6 Acoustic and optic branches

One can show that, for $\vec{q} = 0$, three of the $3n$ dispersion relations $\omega_s(\vec{q})$ go to zero, $\omega(0) = 0$ (acoustic branches); the frequencies of the remaining $3n-3$ branches don't vanish (optic branches).

Actually, for $\vec{q} = 0$, the Fourier transformed dynamical matrix (F.109) becomes

$$D_{\vec{q}=0}\begin{pmatrix}\alpha\kappa\\ \alpha'\kappa'\end{pmatrix} = \sum_L D^0\begin{pmatrix}\alpha\ L\ \kappa\\ \alpha'\ 0\ \kappa'\end{pmatrix} = \sum_L \frac{\Phi\begin{pmatrix}\alpha\ L\ \kappa\\ \alpha'\ 0\ \kappa'\end{pmatrix}}{\sqrt{m_\kappa m_{\kappa'}}}\,. \tag{F.124}$$

The coupled equations (F.110) can thus be rewritten, for the normalised eigenvectors $\mathrm{e}_\alpha(\kappa|0s)$ and for $\vec{q} = 0$, as

$$\omega^2(0s)\ \frac{\mathrm{e}_\alpha(\kappa|0s)}{\sqrt{m_\kappa}} = \sum_{\alpha' L\kappa'} \Phi\begin{pmatrix}\alpha L\kappa\\ \alpha' 0\kappa'\end{pmatrix}\ \frac{1}{m_\kappa}\ \frac{\mathrm{e}_{\alpha'}(\kappa'|0s)}{\sqrt{m_{\kappa'}}}. \tag{F.125}$$

Let us consider two cases:

1. The ratio $\mathrm{e}_{\alpha'}(\kappa'|0s)/\sqrt{m_{\kappa'}}$ is independent of κ'.
   The ratio can be factorized with respect to the sum, so that the constraint (F.95) imposes $\omega = 0$. This condition leads to three acoustic branches, one for each value of $\alpha = x, y, z$.
2. The ratio $\mathrm{e}_{\alpha'}(\kappa'|0s)/\sqrt{m_{\kappa'}}$ depends on κ'.
   In this case it cannot be factorized and (F.95) cannot be applied.

We can thus distinguish:

a) In primitive crystals there is $n = 1$ atom per cell and $3n = 3$ branches. The three branches are acoustic.
b) In non-primitive crystals there are $n > 1$ atoms per cell and a total of $3n > 3$ branches.
   The condition that the ratio $\mathrm{e}_{\alpha'}(\kappa'|0s)/\sqrt{m_{\kappa'}}$ is independent of κ' is fulfilled only if all atoms in the cell move in phase, say for three acoustic branches $\alpha = x, y, z$.
   For the remaining $3n - 3$ branches (acoustic branches) $\omega^2(0s) \neq 0$.

F.4.7 On the 1st Brillouin Zone

Periodic boundary conditions

The periodic boundary conditions on the atomic displacements impose that

$$\vec{u}(\vec{r} + N_\alpha \vec{a}_\alpha) = \vec{u}(\vec{r}) \qquad (\alpha = 1, 2, 3)\,. \tag{F.126}$$

We want now to show that (F.126) is automatically fulfilled by the choice of wavevectors $\vec{q}$ of (F.103), say $q_\alpha = b_\alpha\, m_\alpha/N_\alpha$. To this purpose let us express the contributions to the two displacements of (F.126) due to a given normal mode of wavevector $\vec{q}$ according to (F.114):

$$u_\alpha(\vec{R}, t) = \frac{1}{\sqrt{M}}\ \mathbf{Re}\left\{ w_\alpha(\kappa|\vec{q})\ \exp\left[i\vec{q}\cdot\vec{R}\right]\ \exp(-i\omega t)\ \right\} \tag{F.127}$$

$$u_\alpha(\vec{R} + N_\alpha\vec{a}_\alpha, t) = \frac{1}{\sqrt{M}}\ \mathbf{Re}\left\{ w_\alpha(\kappa|\vec{q})\ \exp\left[i\vec{q}\cdot(\vec{R} + N_\alpha\vec{a}_\alpha)\right]\ \exp(-i\omega t)\ \right\} \tag{F.128}$$

Since $\vec{q}$ is a vector of the reciprocal space, such that

$$\vec{q} = (m_1/N_1)\vec{b}_1 + (m_2/N_2)\vec{b}_2 + (m_3/N_3)\vec{b}_3\,, \tag{F.129}$$

and recalling the relation between primitive vectors of real and reciprocal space:

$$\vec{a}_i \cdot \vec{b}_j = 2\pi\,\delta_{ij} \tag{F.130}$$

one can easily show that (F.128) is equal, to (F.127).

Eigenfrequencies and eigenvectors

One can demonstrate that the frequencies and eigenvectors corresponding to any wavevector $\vec{q}$ are unmodified if a reciprocal lattice vector $\vec{G}$ is added to $\vec{q}$. Actually, the Fourier transformed dynamical matrices corresponding to $\vec{q}+\vec{G}$ and to $\vec{q}$ are identical

$$D_{\vec{q}+\vec{G}}\begin{pmatrix}\alpha\ \kappa\\ \alpha'\kappa'\end{pmatrix} = \sum_L D^0\begin{pmatrix}\alpha\ L\ \kappa\\ \alpha'\ 0\ \kappa'\end{pmatrix}\exp\left\{i\left[\vec{q}+\vec{G}\right]\cdot\vec{R}(L)\right\} = D_{\vec{q}}\begin{pmatrix}\alpha\ \kappa\\ \alpha'\kappa'\end{pmatrix} \tag{F.131}$$

because $\exp(i\vec{G}\cdot\vec{R})=1$.

1st Brillouin Zone and crystal symmetry

The 1st B.Z. is invariant with respect to all the symmetry operations of the point group of the crystal.
If we apply all the point symmetry operations different from identity to a vector $\vec{q}$ belonging to the 1st B.Z., we obtain distinct vectors still belonging to the 1st B.Z. (This wouldn't be the case for other choices of primitive cells of the reciprocal space).
If h is the number of symmetry elements of the point group of the crystal, the 1st B.Z. can be divided into h irreducible elements of volume V_b/h.
The application of any symmetry operation (different from the identity) to any vector $\vec{q}$ belonging to a given irreducible element leads to a vector outside the given irreducible element.
The frequencies of normal modes have the point symmetry of the crystal. As a consequence, an irreducible element of teh 1st B.Z. contains all the information on the dispersion relations.

F.5 Energy of normal modes. Phonons

As is evident in (F.117), from the classical point of view each normal mode $(\vec{q}s)$ is a travelling wave of wavevector $\vec{q}$, whose frequency is obtained by diagonalising the Fourier transformed dynamical matrix $\mathbf{D}_{\vec{q}}$.

F.5.1 Energy and normal coordinates

The kinetic energy is

$$T = \frac{1}{2}\sum_{\alpha\ell\kappa} m_\kappa\,\dot{u}^2_\alpha(\ell\kappa) \tag{F.132}$$

The harmonic part of the potential vibrational energy is

$$V_2 = \frac{1}{2}\sum_{\substack{\alpha\ell\kappa\\ \alpha'\ell'\kappa'}}\Phi_2\begin{pmatrix}\alpha\,\ell\,\kappa\\ \alpha'\ell'\kappa'\end{pmatrix}\,u_\alpha(\ell\kappa)\,u_{\alpha'}(\ell'\kappa') \tag{F.133}$$

We want now to express the kinetic and potential energies in terms of the normal coordinates, substituting the expression (F.117) of atomic displacement in (F.132) and (F.133).

Useful relation

As a preliminary step, it is convenient to introduce the relation

$$\sum_\ell e^{i\vec{q}\cdot\vec{R}(\ell)} = \begin{cases} N & \text{for } \vec{q}=0 \text{ or } \vec{q}=\vec{G}\,,\\ 0 & \text{otherwise}\,.\end{cases} \tag{F.134}$$

Relation (F.223) is a consequence of the lattice periodicity; actually, the sum on the left is unchanged if an arbitrary $\vec{R}(\ell')$ is added to $\vec{R}(\ell)$ in the sum, so that:

$$\sum_\ell e^{i\vec{q}\cdot\vec{R}(\ell)} = \sum_\ell e^{i\vec{q}\cdot[\vec{R}(\ell)+\vec{R}(\ell')]} = \left[\sum_\ell e^{i\vec{q}\cdot\vec{R}(\ell)}\right] e^{i\vec{q}\cdot\vec{R}(\ell')}\,. \tag{F.135}$$

Eq. (F.224) requires that $e^{i\vec{q}\cdot\vec{R}(\ell')} = 1$, which is possible only if condition (F.223) is fulfilled. As a consequence of (F.223),

$$\sum_{\ell} e^{i(\vec{q}+\vec{q}')\cdot\vec{R}(\ell)} \;=\; \begin{cases} N & \text{for } \vec{q}+\vec{q}' = 0 \text{ or } \vec{q}+\vec{q}' = \vec{G}\,, \\ 0 & \text{otherwise}\,. \end{cases} \tag{F.136}$$

It can be convenient to rewrite (F.223) as [Maradudin, 1974]

$$\Delta(\vec{q}) \;=\; \frac{1}{N}\sum_{\ell} e^{i\vec{q}\cdot\vec{R}(\ell)} \;=\; \begin{cases} 1 & \text{for } \vec{q} = 0 \text{ or } \vec{q} = \vec{G} \\ 0 & \text{otherwise}\,. \end{cases} \tag{F.137}$$

and (F.225) as

$$\Delta(\vec{q}+\vec{q}') \;=\; \frac{1}{N}\sum_{\ell} e^{i(\vec{q}+\vec{q}')\cdot\vec{R}(\ell)} \;=\; \begin{cases} 1 & \text{for } \vec{q}+\vec{q}' = 0 \text{ or } \vec{q}+\vec{q}' = \vec{G} \\ 0 & \text{otherwise}\,. \end{cases} \tag{F.138}$$

Kinetic energy

Substituting the atomic displacements (F.117), since only the normal coordinates depend on time, the kinetic energy becomes

$$T \;=\; \frac{1}{2}\,\frac{1}{N}\sum_{\alpha\kappa}\sum_{\vec{q}s}\sum_{\vec{q}'s} \mathrm{e}_\alpha(\kappa|\vec{q}s)\,\mathrm{e}_\alpha(\kappa|\vec{q}'s')\,\dot{Q}(\vec{q}s)\,\dot{Q}(\vec{q}'s')\sum_{\ell} e^{i(\vec{q}+\vec{q}')\cdot\vec{R}(\ell)}\,. \tag{F.139}$$

Taking into account that according to (F.225) the last sum is N if $\vec{q} = -\vec{q}'$, otherwise it is zero, and considering the orthonormality relation of eigenvectors, one gets

$$T \;=\; \frac{1}{2}\sum_{\vec{q}s}\dot{Q}(\vec{q}s)\,\dot{Q}(-\vec{q}s) \;=\; \frac{1}{2}\sum_{\vec{q}s}\dot{Q}(\vec{q}s)\,\dot{Q}^*(\vec{q}s)\,. \tag{F.140}$$

Potential energy

Let's start from the harmonic potential energy (F.92) expressed as a function of atomic displacements

$$V_2 \;=\; \frac{1}{2}\sum_{\substack{\alpha\ell\kappa \\ \alpha'\ell'\kappa'}} \Phi_2\begin{pmatrix}\alpha\,\ell\,\kappa \\ \alpha'\ell'\kappa'\end{pmatrix}\,u_\alpha(\ell\kappa)\,u_{\alpha'}(\ell'\kappa') \tag{F.141}$$

Substituting the atomic displacements with their expressions (F.117) in terms of the normal coordinates, the potential energy becomes

$$V_2 \;=\; \frac{1}{2N}\sum_{\substack{\vec{q}s \\ \vec{q}'s'}} Q(\vec{q}s)\;Q(\vec{q}'s')\sum_{\substack{\alpha\ell\kappa \\ \alpha'\ell'\kappa'}} \frac{\Phi_2\left(\begin{smallmatrix}\alpha\,\ell\,\kappa \\ \alpha'\ell'\kappa'\end{smallmatrix}\right)}{\sqrt{m_\kappa\,m_{\kappa'}}}\,e^{i\vec{q}\cdot\vec{R}(\ell)}\,e^{i\vec{q}'\cdot\vec{R}(\ell')}\,\mathrm{e}_\alpha(\kappa|\vec{q}s)\,\mathrm{e}_{\alpha'}(\kappa'|\vec{q},'s') \tag{F.142}$$

Lets first eliminate the sums over ℓ and ℓ'. To that purpose, multipliying (F.228) by

$$1 \;=\; e^{i\vec{q}'\cdot[\vec{R}(\ell)-\vec{R}(\ell)]}$$

and recalling the definition of Fourier transformed dynamical matrix,

$$\sum_{\ell} e^{i(\vec{q}+\vec{q}')\cdot\vec{R}(\ell)}\sum_{\ell'} e^{i\vec{q}'\cdot[\vec{R}(\ell')-\vec{R}(\ell)]}\,\frac{\Phi_2\left(\begin{smallmatrix}\alpha\,\ell\,\kappa \\ \alpha'\ell'\kappa'\end{smallmatrix}\right)}{\sqrt{m_\kappa\,m_{\kappa'}}} \;=\; N\,\Delta(\vec{q}+\vec{q}')\,D_{\vec{q}'}\begin{pmatrix}\alpha\kappa \\ \alpha'\kappa'\end{pmatrix}$$

so that (F.228) becomes

$$V_2 \;=\; \frac{1}{2}\sum_{\substack{\vec{q}s \\ \vec{q}'s'}} Q(\vec{q}s)\;Q(\vec{q}'s')\sum_{\substack{\alpha\kappa \\ \alpha'\kappa'}} D_{\vec{q}'}\begin{pmatrix}\alpha\kappa \\ \alpha'\kappa'\end{pmatrix}\,\Delta(\vec{q}+\vec{q}')\,\mathrm{e}_\alpha(\kappa|\vec{q}s)\,\mathrm{e}_{\alpha'}(\kappa'|\vec{q}'s') \tag{F.143}$$

The values $\vec{q}$ and $\vec{q}'$ are not independent; they are confined within the first Brillouion zone and must fulfill (F.138), so that necessarily $\vec{q}' = -\vec{q}$, so the sum over $\vec{q}'$ can be eliminated.
One can further eliminate the sum over α' and κ' by making use of (F.110) and introducing the mode frequency $\omega(\vec{q}s)$:

$$V_2 \;=\; \frac{1}{2} \sum_{\substack{\vec{q}s \\ \vec{s}'}} Q(\vec{q}s)\; Q(-\vec{q}s')\; \sum_{\alpha\kappa} \omega^2(\vec{q}s)\; \mathrm{e}_\alpha(\kappa|\vec{q}s)\, \mathrm{e}_\alpha(\kappa|-\vec{q}s') \tag{F.144}$$

At last, by substituting

$$\mathrm{e}_\alpha(\kappa|-\vec{q}s) = \mathrm{e}^*_\alpha(\kappa|\vec{q}s)\,, \qquad Q(-\vec{q}s) = Q^*(\vec{q}s)$$

and considering the orthonormality relation of eigenvectors (F.118)

$$\sum_{\kappa\alpha} e^*_\alpha(\kappa|\vec{q}s)\, e_\alpha(\kappa|\vec{q}s') \;=\; \delta_{ss'}$$

one obtains the final expression

$$V_2 \;=\; \frac{1}{2} \sum_{\vec{q}s} \omega^2(\vec{q}s)\, Q(\vec{q}s)\, Q^*(\vec{q}s)\,. \tag{F.145}$$

A classical normal mode $(\vec{q}s)$ can be considered as an independent harmonic oscillator of frequency $\omega(\vec{q}s)$, whose amplitude and time dependence are described by the normal coordinate $Q(\vec{q}s,t) = Q_0(\vec{q}s)\, e^{i\omega(\vec{q}s)t}$. The dimensions of the normal coordinate are $[Q] = [M^{1/2}L]$.

F.5.2 Classical Lagrangian and Hamiltonian

The Lagrange function of the system of vibrating atoms is thus

$$\mathcal{L} \;=\; \frac{1}{2} \sum_{\vec{q}s} \left[\dot{Q}(\vec{q}s)\dot{Q}^*(\vec{q}s) - \omega^2(\vec{q}s) Q(\vec{q}s) Q^*(\vec{q}s) \right]\,, \tag{F.146}$$

It is interesting to compare each term of the Lagrange function (F.146) with the Lagrange function of a harmonic oscillator: $\mathcal{L} = mv^2/2 - m\omega^2 x^2/2$.
Each classical normal mode $(\vec{q}s)$ can be considered as an independent harmonic oscillator of frequency $\omega(\vec{q}s)$, whose amplitude and time dependence are described by the normal coordinate $Q(\vec{q}s,t) = Q_0(\vec{q}s)\, e^{i\omega(\vec{q}s)t}$.
The normal coordinates correspond to generalised coordinates of the Lagrangian formalism.
Introducing the conjugate momenta $P(\vec{q}s) = \partial\mathcal{L}/\partial\dot{Q}(\vec{q}s) = \dot{Q}^*(\vec{q}s)$, one obtains the Hamiltonian

$$\mathcal{H} \;=\; \frac{1}{2} \sum_{\vec{q}s} \left[P(\vec{q}s)P^*(\vec{q}s) + \omega^2(\vec{q}s) Q(\vec{q}s) Q^*(\vec{q}s) \right]\,. \tag{F.147}$$

The classical energy stored in the normal mode $(\vec{q}s)$ is

$$E(\vec{q}s) \;=\; \frac{1}{2}\, \omega^2(\vec{q}s)\, Q_0^2(\vec{q}s)\,. \tag{F.148}$$

F.5.3 Quantization of normal modes

To quantise the normal modes, the classical normal coordinates and momenta are replaced by operators, and the same procedure is followed as for the one-dimensional harmonic oscillator.
By introducing the operators (annihilation and creation)

$$a(\vec{q}s) \;=\; \frac{1}{\sqrt{2\hbar\omega(\vec{q}s)}} \left[\omega(\vec{q}s)\, Q(\vec{q}s) + iP^*(\vec{q}s)\right] \tag{F.149}$$

$$a^\dagger(\vec{q}s) \;=\; \frac{1}{\sqrt{2\hbar\omega(\vec{q}s)}} \left[\omega(\vec{q}s)\, Q^*(\vec{q}s) - iP(\vec{q}s)\right] \tag{F.150}$$

the Hamiltonian can be rewritten as

$$\mathcal{H} \;=\; \sum_{\vec{q}s} \left[a^{\dagger}(\vec{q}s)\, a(\vec{q}s) + \frac{1}{2} \right] \hbar\omega(\vec{q}s) \;=\; \left[n(\vec{q}s) + \frac{1}{2} \right] \hbar\omega(\vec{q}s)\,. \tag{F.151}$$

This leads to the quantization of the energy of normal modes:

$$E(\vec{q}s) \;=\; \left[n(\vec{q}s) + \frac{1}{2} \right] \hbar\omega(\vec{q}s)\,. \tag{F.152}$$

F.5.4 Statistical thermodynamics of normal modes

A crystal can exchange heat with its surroundings. Let us consider here a non-metallic crystal, where thermal energy is only stored by lattice vibrations (in metals, electrons can store energy too). In principle, within the harmonic approximation, normal modes are distinguishable independent oscillators. To account for the possibility of exchanging energy, we have to consider normal modes as not completely independent, but weakly interacting objects.
A total energy level of the crystal can be expressed as

$$\mathcal{E}_j \;=\; V_0 + \sum_{\vec{q}s} \left[n(\vec{q}s) + \frac{1}{2} \right] \hbar\omega(\vec{q}s) \tag{F.153}$$

The partition function of the whole crystal is the sum over all total energy levels

$$Z \;=\; \sum_{j=1}^{\infty} \exp\left[-\beta \mathcal{E}_j\right]\,, \tag{F.154}$$

where $\beta = 1/k_B T$. By substituting (F.153) into (F.154), after some simple calculations, one finds

$$Z \;=\; \exp\left[-\beta V_0\right] \prod_{\vec{q}s} \frac{\exp\left[-\beta\hbar\omega(\vec{q}s)/2\right]}{1-\exp\left[-\beta\hbar\omega(\vec{q}s)\right]}\,. \tag{F.155}$$

The internal energy of the crystal is

$$\begin{aligned} U \;&=\; \langle \mathcal{E} \rangle = k_B T^2 \left(\frac{\partial}{\partial T} \ln Z \right) \\ &=\; V_0 \;+\; \sum_{\vec{q}s} \frac{1}{2}\, \hbar\omega(\vec{q}s) \;+\; \sum_{\vec{q}s} \frac{\hbar\omega(\vec{q}s)}{\exp[\hbar\omega(\vec{q}s)/k_B T]-1}\,. \end{aligned} \tag{F.156}$$

Three contributions are singled out in (F.156):

1. the static cohesive energy V_0
2. the vibrational zero-point energy
3. the vibrational thermal energy (dependent on temperature)

The average vibrational energy stored in normal mode $(\vec{q}s)$ at temperature T is thus

$$\langle E(\vec{q}s|T) \rangle \;=\; \left\{ \frac{1}{2} + \frac{1}{\exp[\hbar\omega(\vec{q}s)/k_B T]-1} \right\} \hbar\omega(\vec{q}s) \tag{F.157}$$

Equivalent alternative expressions are:

$$\langle E(\vec{q}s|T) \rangle \;=\; \frac{\hbar\omega(\vec{q}s)}{2} \coth \frac{\hbar\omega(\vec{q}s)}{2k_B T} \;=\; \frac{\hbar\omega(\vec{q}s)}{2}\, \frac{1+z}{1-z}\,, \tag{F.158}$$

where $z = \exp[-\hbar\omega(\vec{q}s)/k_B T]$.
At high temperatures, the average energy tends to the classical value $\langle E \rangle \to k_B T$, independent of frequency. At low temperatures, the larger is the frequency, the larger is the average energy.

F.5.5 Phonons

The quanta of energy of the normal modes are called *phonons*, by analogy with photons, the quanta of the electromagnetic field. The number $n(\vec{q}s)$ appearing in (F.152) is the number of phonons of mode $(\vec{q}s)$.
The quantum state of a normal mode is characterised by the number $n(\vec{q}s)$ of phonons, say by its energy content. The vibrational quantum state of a crystal is characterised by the numbers of phonons for each normal mode. A phonon is characterized by a frequency ω, a wavevector $\vec{q}$ and an eigenvector $w(\vec{q}s)$.
The number of phonons is not constant. The weak exchange of energy between normal modes and with the surrounding environment, which guarantees the thermodynamic equilibrium, corresponds to the creation and annihilation of phonons. Phonons are created or annihilated when the temperature of a crystal increases or decreases, respectively.
The average energy of a normal mode can be expressed as

$$\langle E(\vec{q}s)\rangle \;=\; \left[\langle n(\vec{q}s)\rangle + \frac{1}{2}\right]\,\hbar\omega(\vec{q}s)\,. \tag{F.159}$$

By comparing with (F.157), the average value of $n(\vec{q}s)$ is given by

$$\langle n(\vec{q}s)\rangle \;=\; \frac{1}{\exp[\hbar\omega(\vec{q}s)/k_BT]-1}\,. \tag{F.160}$$

This expression corresponds to the Bose-Einstein distribution of a set of indistinguishable objects whose total number is variable. Actually phonons of the same frequency are indistinguishable and can be created and destroyed.
A number of phenomena, such as thermal conductivity, can be interpreted by considering phonons as quasi-particles. One often speaks of "phonon gas".

Temperature dependence of normal coordinates

As a consequence of (F.148) and (F.157), the amplitude of the normal coordinate of mode $(\vec{q}s)$ depends on temperature according to

$$\langle Q_0^2(\vec{q}s|T)\rangle \;=\; \left\{\frac{1}{2}+\frac{1}{\exp[\hbar\omega(\vec{q}s)/k_BT]-1}\right\}\,\frac{2\hbar}{\omega(\vec{q}s)}\,. \tag{F.161}$$

Equivalent expression:

$$\langle Q_0^2(\vec{q}s|T)\rangle \;=\; \frac{\hbar}{\omega(\vec{q},s)}\coth\frac{\hbar\omega(\vec{q},s)}{2k_BT}\,. \tag{F.162}$$

F.6 Mean square displacements

F.6.1 Atomic displacement factors

Let us now consider the mean square displacement (MSD) of atom κ along a given direction α induced by mode $(\vec{q}s)$:

$$MSD_\alpha \;=\; \langle u_\alpha^2(\kappa|\vec{q}s)\rangle\,. \tag{F.163}$$

By taking into account the expression (F.115) of the atomic instantaneous displacement and the time average of the normal coordinates (F.158), one gets

$$\begin{aligned}\langle u_\alpha^2(\kappa|\vec{q}s)\rangle \;&=\; \frac{1}{NM_\kappa}\,[\mathrm{e}_\alpha(\kappa|\vec{q}s)]^2\;\langle Q_0^2(\vec{q}s|T)\rangle\\ &=\; \frac{2}{NM_\kappa}\,[\mathrm{e}_\alpha(\kappa|\vec{q}s)]^2\;\frac{\langle E(\vec{q}s|T)\rangle}{\omega^2(\vec{q}s)}\,.\end{aligned} \tag{F.164}$$

The MSD along the direction α depends on the orientation of the normalized eigenvector e and on temperature. The dependence on temperature of the MSD induced by two sets of N normal modes of different frequencies is shown in Fig. F.1 (right).

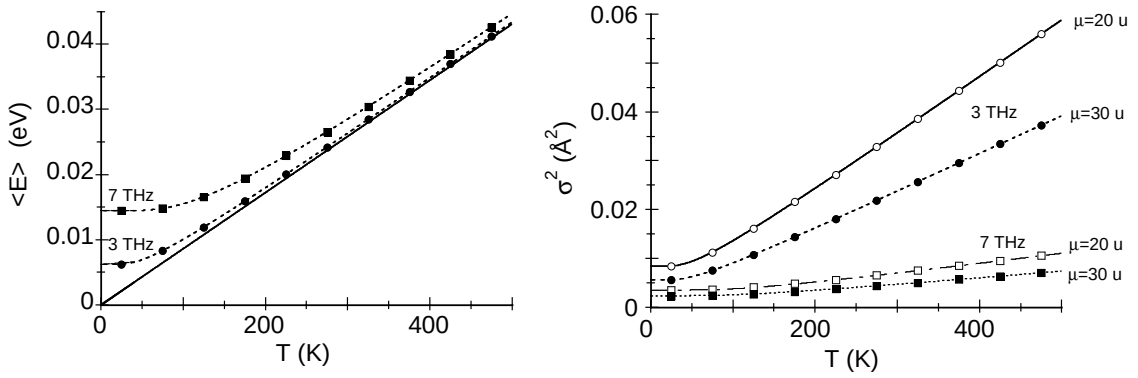

Figure F.1: Left: average energy as a function of temperature for two normal modes of 3 and 7 THz frequencies, respectively; the straight dotted line is the classical approximation. Right: MSD induced on an ion of mass 70 μ along a given direction by N modes of 3 and 7 THz frequencies, respectively.

Debye-Waller factor of diffraction

The MSD along a given direction $\hat{s}$ is responsible for the Debye-Waller factor reducing the intensity of the Bragg peaks due to the family of planes perpendicular to $\hat{s}$. The Debye-Waller factor can be expressed in different forms:

$$\exp\left[-k^2\langle u_s^2(\kappa)\rangle/2\right] \;=\; \exp[-M_s(\kappa)] \;=\; \exp\left[-B_s(\kappa)\sin^2\theta/\lambda^2\right] , \tag{F.165}$$

where $k = 4\pi\sin\theta/\lambda$ is the magnitude of scattering vector.

F.6.2 Mean square relative displacements

At last, let us consider the mean square relative displacement (MSRD) of atom κ' relative to atom κ along a given direction α induced by a normal mode $(\vec{q}s)$. One can easily see that

$$\langle[u_\alpha(\kappa'|\vec{q}s) - u_\alpha(\kappa|\vec{q}s)]^2\rangle \;=\; \frac{1}{N}\,\langle Q_0^2(\vec{q}s|T)\rangle \left|\frac{\mathrm{e}_\alpha(\kappa'|\vec{q}s)e^{i\vec{q}\cdot\vec{R}}}{\sqrt{m(\kappa')}} - \frac{\mathrm{e}_\alpha(\kappa|\vec{q}s)}{\sqrt{m(\kappa)}}\right|^2 \tag{F.166}$$

The total MSRD of an atomic pair is the sum of the contribution of all normal modes. The MSRD gives rise to the damping of the EXAFS signal.

F.7 The anharmonic crystal

Our goal is to find an expression of the total Hamiltonian in terms of normal coordinates, in order to make possible the transition to the quantum treatment.
We take advantage of the work already done for the harmonic case.

F.7.1 The potential energy

Let's again consider the expansion of the potential energy $V[\{\vec{r}(\ell\kappa)\}]$ about the *average* configuration:

$$V\;[\{\vec{r}(\ell\kappa)\}] \;=\; V_0 + V_1 + V_2 + V_3 + \cdots \tag{F.167}$$

If anharmonicity is not negligible, we need to consider also the terms of order different from the second one. We follow here the treatment of [Leibfried and Ludwig, 1961], who inserts the harmonic atomic displacements (F.117) in the expressions of the anharmonic coupling constants (force constants), and of [Barron and Klein, 1974]. We use the eigenvectors e of [Maradudin et al., 1971] instead of the eigenvectors w of [Leibfried and Ludwig, 1961].

First-order term

The first-order term is

$$V_1 \;=\; \sum_{\alpha\ell\kappa} \Phi_1(\alpha\ell\kappa)\, u_\alpha(\ell\kappa)\,, \tag{F.168}$$

with

$$\Phi_1(\alpha\ell\kappa) \;=\; \left[\frac{\partial V}{\partial u_\alpha(\ell\kappa)}\right]_{\{\vec{R}\}} \tag{F.169}$$

The derivatives are always calculated for the average configuration $\{\vec{R}(\ell\kappa)\}$.

By substituting the harmonic atomic displacements (F.117) in (F.168), taking into account that the invariance with respect to lattice translations imposes that

$$\Phi_1(\alpha\ell\kappa) \;=\; \Phi_1(\alpha 0\kappa) \tag{F.170}$$

and making use of the sum rule (F.223), one obtains the first-order term as a function of normal coordinates:

$$V_1 \;=\; \sqrt{N}\sum_s Q(0s) \sum_{\alpha\kappa} \frac{\Phi_1(\alpha 0\kappa)}{\sqrt{m_\kappa}}\, \mathrm{e}_\alpha(\kappa|0s)\,. \tag{F.171}$$

Note that in the harmonic approximation $\Phi_1 = 0$.

Second-order term

The second-order term

$$V_2 \;=\; \frac{1}{2} \sum_{\substack{\alpha\ell\kappa \\ \alpha'\ell'\kappa'}} \Phi_2 \begin{pmatrix} \alpha\,\ell\,\kappa \\ \alpha'\ell'\kappa' \end{pmatrix}\; u_\alpha(\ell\kappa)\, u_{\alpha'}(\ell'\kappa')$$

has already been treated in § F.5 in the harmonic approximation, and was shown to be expressed as a function of normal coordinates as

$$V_2 \;=\; \frac{1}{2} \sum_{\vec{q}s} \omega^2(\vec{q}s)\, Q(\vec{q}s)\, Q^*(\vec{q}s)\,.$$

Third-order term

The third-order term is

$$V_3 \;=\; \frac{1}{3!} \sum_{\substack{\alpha\ell\kappa \\ \alpha'\ell'\kappa' \\ \alpha''\ell''\kappa''}} \Phi_3 \begin{pmatrix} \alpha\;\ell\;\kappa \\ \alpha'\,\ell'\kappa' \\ \alpha''\ell''\kappa'' \end{pmatrix}\; u_\alpha(\ell\kappa)\, u_{\alpha'}(\ell'\kappa')\, u_{\alpha''}(\ell'\kappa'')\,, \tag{F.172}$$

where

$$\Phi_3 \begin{pmatrix} \alpha\;\ell\;\kappa \\ \alpha'\,\ell'\kappa' \\ \alpha''\ell''\kappa'' \end{pmatrix} \;=\; \left(\frac{\partial^3 V}{\partial u_\alpha(\ell\kappa)\, \partial u_{\alpha'}(\ell'\kappa')\, \partial u_{\alpha''}(\ell''\kappa'')}\right)_{\{\vec{R}\}} \tag{F.173}$$

are the third-order coupling parameters.

By substituting the harmonic atomic displacements (F.117) in (F.172) one finds an expression in terms of the normal coordinates:

$$\begin{aligned} V_3 \;&=\; \frac{1}{3!N^{3/2}} \sum_{\substack{\vec{q}\vec{q}'\vec{q}'' \\ ss's''}} Q(\vec{q}s)\, Q(\vec{q}'s')\, Q(\vec{q}''s'') \\ &\times \sum_{\substack{\alpha\ell\kappa \\ \alpha'\ell'\kappa' \\ \alpha''\ell''\kappa''}} \frac{\Phi_3}{\sqrt{m_\kappa m_{\kappa'} m_{\kappa''}}}\, e^{i\left[\vec{q}\cdot\vec{R}(\ell)+\vec{q}'\cdot\vec{R}(\ell')+\vec{q}''\cdot\vec{R}(\ell'')\right]}\; \mathrm{e}_\alpha(\kappa|\vec{q}s)\mathrm{e}_{\alpha'}(\kappa'|\vec{q}'s')\mathrm{e}_{\alpha''}(\kappa''|\vec{q}''s'')\,. \end{aligned} \tag{F.174}$$

To eliminate the sums over atomic coordinates we proceed in a similar way as we did for the second-order term in § F.5. See § 39 of [Born and Huang, 1998].
We exploit the identities

$$\vec{R}(\ell') = \vec{R}(\ell') - \vec{R}(\ell) + \vec{R}(\ell) = \vec{R}(\ell' - \ell) + \vec{R}(\ell)\,, \tag{F.175}$$

$$\vec{R}(\ell'') = \vec{R}(\ell'') - \vec{R}(\ell) + \vec{R}(\ell) = \vec{R}(\ell'' - \ell) + \vec{R}(\ell) \tag{F.176}$$

and the invariance of the coupling parameters with respect to lattice translations

$$\Phi_3 \begin{pmatrix} \alpha & \ell & \kappa \\ \alpha' & \ell' & \kappa' \\ \alpha'' & \ell'' & \kappa'' \end{pmatrix} = \Phi_3 \begin{pmatrix} \alpha & 0 & \kappa \\ \alpha' & \ell' - \ell & \kappa' \\ \alpha'' & \ell'' - \ell & \kappa'' \end{pmatrix} \tag{F.177}$$

We further simplify the summation indices $\ell' - \ell \to \ell'$ and $\ell'' - \ell \to \ell''$, so that (F.174) can be rewritten as

$$V_3 = \frac{1}{3!N^{1/2}} \sum_{\substack{\vec{q}\vec{q}'\vec{q}'' \\ ss's''}} Q(\vec{q}s)\, Q(\vec{q}'s')\, Q(\vec{q}''s'')\ \ \Delta(\vec{q} + \vec{q}' + \vec{q}'') \tag{F.178}$$

$$\times \left\{ \sum_{\substack{\alpha\kappa \\ \alpha'\ell'\kappa' \\ \alpha''\ell''\kappa''}} \frac{\Phi_3}{\sqrt{m_\kappa m_{\kappa'} m_{\kappa''}}}\, e^{i\left[\vec{q}'\cdot\vec{R}(\ell') + \vec{q}''\cdot\vec{R}(\ell'')\right]}\ \mathrm{e}_\alpha(\kappa|\vec{q}s)\mathrm{e}_{\alpha'}(\kappa'|\vec{q}'s')\mathrm{e}_{\alpha''}(\kappa''|\vec{q}''s'') \right\},$$

where, similarly to (F.138),

$$\Delta(\vec{q} + \vec{q}' + \vec{q}'') = \frac{1}{N} \sum_{\ell} e^{i(\vec{q}+\vec{q}'+\vec{q}'')\cdot\vec{R}(\ell)} = \begin{cases} 1 & \text{for } \vec{q} + \vec{q}' + \vec{q}'' = 0 \text{ or } \vec{G} \\ 0 & \text{otherwise}\,. \end{cases} \tag{F.179}$$

One can show [Born and Huang, 1998] that the sum in curly brackets in (F.178) is symmetric with respect to the indices $(\vec{q}s, \vec{q}'s', \vec{q}''s'')$; it is generally expressed in condensed form

$$\Psi \begin{pmatrix} \vec{q}\,\vec{q}'\,\vec{q}'' \\ s\ s'\ s'' \end{pmatrix} = \sum_{\substack{\alpha\kappa \\ \alpha'\ell'\kappa' \\ \alpha''\ell''\kappa''}} \frac{\Phi_3}{\sqrt{m_\kappa m_{\kappa'} m_{\kappa''}}}\, e^{i\left[\vec{q}'\cdot\vec{R}(\ell'-\ell) + \vec{q}''\cdot\vec{R}(\ell''-\ell)\right]}\ \mathrm{e}_\alpha(\kappa|\vec{q}s)\mathrm{e}_{\alpha'}(\kappa'|\vec{q}'s')\mathrm{e}_{\alpha''}(\kappa''|\vec{q}''s'')\,, \tag{F.180}$$

so that (F.178) becomes

$$V_3 = \frac{1}{3!N^{1/2}} \sum_{\substack{\vec{q}\vec{q}'\vec{q}'' \\ ss's''}} \Psi \begin{pmatrix} \vec{q}\,\vec{q}'\,\vec{q}'' \\ s\ s'\ s'' \end{pmatrix}\ Q(\vec{q}s)\, Q(\vec{q}'s')\, Q(\vec{q}''s'')\ \ \Delta(\vec{q} + \vec{q}' + \vec{q}'') \tag{F.181}$$

Generalisation

Eq. (F.181) can be generalised to higher-order terms, so that the anharmonic contribution to the total Hamiltonian can be expressed as a sum of terms [Barron and Klein, 1974]

$$H_{\mathrm{anh}} = \sum_{n=3}^{\infty} \frac{1}{n!N^{(n/2-1)}} \sum_{\substack{\vec{q}_1 \dots \vec{q}_n \\ s_1 \dots s_n}} \Psi \begin{pmatrix} \vec{q}_1 & \dots & \vec{q}_n \\ s_1 & \dots & s_n \end{pmatrix}\ [Q(\vec{q}_1 s_1)\ \dots\ Q(\vec{q}_n s_n)]\ \ \Delta(\vec{q}_1 + \dots + \vec{q}_n) \tag{F.182}$$

The term of order n is the product of n normal coordinates corresponding to normal modes whose n wavevectors are constrained by the Δ function.

F.8 Complements and demonstrations

F.8.1 The one-dimensional quantum harmonic oscillator

The Hamiltonian operator for the quantum harmonic oscillator is

$$H_0 = \frac{P^2}{2m} + \frac{1}{2} m\omega_0^2\, X^2\,, \tag{F.183}$$

where X and P are the position and momentum operators, whose commutator is $[X, P] = i\hbar$. It is convenient to introduce the a-dimensional reduced observables

$$\hat{X} = \sqrt{\frac{m\omega_0}{\hbar}}\, X\,, \qquad \hat{P} = \frac{1}{\sqrt{m\hbar\omega_0}}\, P\,, \tag{F.184}$$

whose commutator is $[\hat{X}, \hat{P}] = i$; the reduced Hamiltonian is

$$\hat{H}_0 = \frac{H_0}{\hbar\omega_0} \;=\; \frac{1}{2}\,(\hat{X}^2 + \hat{P}^2)\,. \tag{F.185}$$

It is further convenient to substitute $\hat{X}$ and $\hat{P}$ by the (non hermitian) operators defined by the linear combinations

$$a^\dagger = \frac{1}{\sqrt{2}}\,(\hat{X} - i\hat{P})\,, \qquad a = \frac{1}{\sqrt{2}}\,(\hat{X} + i\hat{P})\,. \tag{F.186}$$

so that

$$\hat{X} = \frac{1}{\sqrt{2}}\,(a^\dagger + a)\,, \qquad \hat{P} = \frac{i}{\sqrt{2}}\,(a^\dagger - a) \tag{F.187}$$

From $[\hat{X}, \hat{P}] = i$ one can easily verify that the commutator is $[a, a^\dagger] = 1$ and that

$$a^\dagger a \;=\; \frac{1}{2}\,(\hat{X}^2 + i\hat{X}\hat{P} - i\hat{P}\hat{X} + \hat{Y}^2) \;=\; \frac{1}{2}\,(\hat{X}^2 + \hat{P}^2 - 1)\,. \tag{F.188}$$

The reduced Hamiltonian can then be expressed as

$$\hat{H}_0 = a^\dagger a + \frac{1}{2} \;=\; aa^\dagger - \frac{1}{2}\,. \tag{F.189}$$

By defining the (hermitian) number operator

$$N = a^\dagger a, \tag{F.190}$$

the reduced Hamiltonian becomes

$$\hat{H}_0 = N + 1/2\ : \tag{F.191}$$

the eigenvectors of $\hat{H}_0$ are eigenvectors of N and viceversa.
One can then solve the eigenvalues equation for N

$$N\,|\phi_\nu\rangle \;=\; \nu\,|\phi_\nu\rangle \tag{F.192}$$

One finds (see Quantum Mechanics textbooks) that the spectrum of N is represented by non negative integer numbers

$$\nu = 0, 1, 2, \ldots n, \ldots \qquad |\phi_n\rangle = |n\rangle\,, \tag{F.193}$$

the energy levels are non degenerate and the eigenvalues of the Hamiltonian H_0 are

$$E_n^0 \;=\; (1/2 + n)\,\hbar\omega_0 \qquad (n = 0 \ldots \infty) \tag{F.194}$$

The energy difference between any two levels is

$$E_n - E_{n-1} = \hbar\omega_0\,. \tag{F.195}$$

The action of the $a^\dagger$ and a operators on the eigenstates is as follows:

$$a^\dagger\,|n\rangle \;=\; \sqrt{n+1}\,|n+1\rangle, \qquad a\,|n\rangle \;=\; \sqrt{n}\,|n-1\rangle. \tag{F.196}$$

They are called creation and destruction operators, respectively, since they create or destroy a quantum of energy.

From (F.196) and from

$$\hat{X} = \frac{1}{\sqrt{2}} (a^\dagger + a) \tag{F.197}$$

one can easily see that the average displacement $\langle X \rangle$ is zero in the eigenstates $|n\rangle$:

$$\langle X \rangle = \sqrt{\frac{\hbar}{2m\omega_0}} \langle n| a^\dagger + a |n\rangle = \sqrt{\frac{\hbar}{2m\omega_0}} \left[\langle n| a^\dagger |n\rangle + \langle n| a |n\rangle \right] = 0 . \tag{F.198}$$

One can further see that

$$\langle X^2 \rangle = \frac{\hbar}{2m\omega_0} \langle n|(a^\dagger + a)^2|n\rangle = \frac{\hbar}{2m\omega_0} \langle n|a^\dagger a + aa^{dag}|n\rangle \tag{F.199}$$

$$= \frac{\hbar}{m\omega_0} \left(\frac{1}{2} + n \right) = \frac{E_n}{m\omega_0^2} . \tag{F.200}$$

F.8.2 The one-dimensional quantum anharmonic oscillator

Let us consider here for simplicity only the cubic term in the potential energy.
The harmonic hamiltonian H_0 is modified by adding a weak cubic term $W = k^3 X^3$.

$$H = H_0 + W = \frac{1}{2} m\omega_0^2 X^2 + \frac{1}{2m} P^2 + k^3 X^3 . \tag{F.201}$$

Introducing again the a-dimensional reduced observables $\hat{X}$ and $\hat{P}$ and expressing the third order term as $W = \sigma \hbar \omega_0 \hat{X}^3$, where $\sigma = k^3 \hbar^{1/2} / m^{3/2} \omega_0^{5/2}$ (a-dimensional), the Hamiltonian becomes

$$H = H_0 + W = \frac{1}{2} \hbar\omega_0 (\hat{X}^2 + \hat{P}^2) + \sigma \hbar \omega_0 \hat{X}^3 . \tag{F.202}$$

If the third order term is sufficiently weak, one can consider it as a perturbation to the harmonic Hamiltonian.

Energy levels

According to the stationary perturbation theory, the energy eigenvalues E_n of the anharmonic oscillator are obtained from the energy eigenvalues E_n^0 of the harmonic oscillator as

$$E_n = E_n^0 + \langle n|W|n\rangle + \sum_{n \neq n'} \frac{|\langle n'|W|n\rangle|^2}{E_n^0 - E_{n'}^0} + \ldots \tag{F.203}$$

Taking into account that $\hat{X} = (a^\dagger + a)/\sqrt{2}$, one finds

$$\hat{X}^3 = \frac{1}{2^{3/2}} \left[(a^\dagger)^3 + a^\dagger a a^\dagger + a a^\dagger a^\dagger + a a a^\dagger + a^\dagger a^\dagger a + a^\dagger a a + a a^\dagger a + a^3 \right] , \tag{F.204}$$

and exploiting the commutation relations of $a^\dagger$, a and $N = a^\dagger a$

$$\hat{X}^3 = \frac{1}{2^{3/2}} \left[(a^\dagger)^3 + 3N a^\dagger + 3(N+1) a + a^3 \right] , \tag{F.205}$$

where each term corresponds to the creation or destruction of three quanta or of one quantum of energy.
The first-order term in the perturbation expansion, where the final state is equal to the initial state, is thus zero.

The only non-zero matrix elements of W are those connecting states that differ for one or three quanta:

$$\frac{|\langle n+3|W|n\rangle|^2}{E_n^0 - E_{n+3}^0} = \frac{(\sigma\hbar\omega_0)^2}{8}\frac{(n+1)(n+2)(n+3)}{-3\hbar\omega_0} = -\sigma^2\hbar\omega_0\frac{n^3+6n^2+11n+6}{24} \quad \text{(F.206)}$$

$$\frac{|\langle n-3|W|n\rangle|^2}{E_n^0 - E_{n-3}^0} = \frac{(\sigma\hbar\omega_0)^2}{8}\frac{n(n-1)(n-2)}{+3\hbar\omega_0} = +\sigma^2\hbar\omega_0\frac{n^3-3n^2+2n}{24} \quad \text{(F.207)}$$

$$\frac{|\langle n+1|W|n\rangle|^2}{E_n^0 - E_{n+1}^0} = \frac{(\sigma\hbar\omega_0)^2}{8}\frac{9(n+1)^3}{-\hbar\omega_0} = -\sigma^2\hbar\omega_0\frac{9n^3+27n^2+27n+9}{8} \quad \text{(F.208)}$$

$$\frac{|\langle n-1|W|n\rangle|^2}{E_n^0 - E_{n-1}^0} = \frac{(\sigma\hbar\omega_0)^2}{8}\frac{9n^3}{+\hbar\omega_0} = +\sigma^2\hbar\omega_0\frac{9n^3}{8} \quad \text{(F.209)}$$

By adding to the harmonic energy the sum of the four perturbation terms (mind the signs) one finds

$$E_n = \left(n+\frac{1}{2}\right)\hbar\omega_0 - \sigma^2\,\hbar\omega_0\,\frac{30n^2+30n+11}{8} \quad \text{(F.210)}$$

or equivalently

$$E_n = \left(n+\frac{1}{2}\right)\hbar\omega_0 - \frac{15}{4}\sigma^2\left(n+\frac{1}{2}\right)^2\hbar\omega_0 - \frac{7}{16}\sigma^2\hbar\omega_0 + \ldots \quad \text{(F.211)}$$

The energy levels are lowered with respect to the unperturbed harmonic case.
The difference between the energies of adjacent levels is not constant (as for the harmonic oscillator), but depends on the value n:

$$E_n - E_{n-1} = \hbar\omega_0\left[1 - \frac{15}{2}\,\sigma^2\,n\right]. \quad \text{(F.212)}$$

Eigenstates

At last, one can show that the eigenstates of the anharmonic oscillator are different from the eigenstates $|n\rangle$ of the harmonic oscillator, being contaminated by the states $|n+1\rangle, |n-1\rangle, |n+3\rangle, |n-3\rangle$.

F.8.3 Statistics of the one-dimensional harmonic oscillator

Let us consider an harmonic oscillator in equilibrium with a reservoir at temperature $T = 1/k_B\beta$.

Classical statistics

In the classical approximation, the instantaneous state of a one-dimensional system is defined by its position x and momentum p. For a system in thermal equilibrium with a reservoir at temperature $T = 1/k_B\beta$, the probability density of the point (x,p) in phase space is given by

$$\rho(x,p) = \frac{e^{-\beta E(x,p)}}{Z} = \frac{e^{-\beta E(x,p)}}{\int dx \int dp\, e^{-\beta E(x,p)}}, \quad \text{(F.213)}$$

and the average value of a quantity $A(x,p)$ is given by

$$\langle A(x,p)\rangle = \frac{1}{Z}\int dx\,dp\,A(x,p)\,\rho(x,p). \quad \text{(F.214)}$$

If the potential energy is independent of p, the total energy is $E(x,p) = p^2/2m + V(x)$, so that the partition function Z can be calculated as

$$Z = \int dp\, e^{-\beta p^2/2m}\int dx\, e^{-\beta V(x)} = \sqrt{2m\pi/\beta}\int dx\, e^{-\beta V(x)}. \quad \text{(F.215)}$$

The probability density for a given value of position x is then

$$\rho(x) \;=\; \frac{\int dp\, e^{-\beta p^2/2m}\, e^{-\beta V(x)}}{Z} \;= \frac{e^{-\beta V(x)}}{\int dx\, e^{-\beta V(x)}}, \tag{F.216}$$

and the average value of a quantity $A(x,p)$ is

$$\langle A(x)\rangle \;=\; \frac{\int\, dx\, A(x)\, e^{-\beta V(x)}}{\int\, dx\, e^{-\beta V(x)}}. \tag{F.217}$$

For the harmonic oscillator, $V(x) = k_0 x^2/2$.

Quantum statistics

If the oscillator is in equilibrium with a reservoir at temperature T, its state is a statistical mixture of eigenstates $|n\rangle$, weighted by $\exp(-\beta E_n)$, where $\beta = 1/k_B T$.
The thermodynamical properties can be calculated from the statistical density operator

$$\hat{w} \;=\; (1/Z_0)\; e^{-\beta \hat{H}_0}, \qquad Z_0 \;=\; \mathrm{Tr}\,(e^{-\beta \hat{H}_0}). \tag{F.218}$$

In the energy representation, where $\hat{H}_0$ is diagonal, the harmonic partition function Z_0 is

$$Z_0 \;=\; \sum_{n=0}^{\infty} \langle n|e^{-\beta \hat{H}_0}|n\rangle \;=\; \sum_{n=0}^{\infty} e^{-(n+1/2)\beta\hbar\omega} \;=\; \frac{e^{-\beta\hbar\omega/2}}{1-e^{-\beta\hbar\omega}}. \tag{F.219}$$

The average energy is given by

$$\langle \hat{H}_0\rangle \;=\; \mathrm{Tr}(\hat{H}_0\hat{w}) \;=\; \frac{1}{Z_0}\,\mathrm{Tr}(\hat{H}_0\, e^{-\beta \hat{H}_0}) \;=\; \frac{1}{Z_0}\sum_{n=0}^{\infty}(n{+}1/2)\hbar\omega e^{-\beta(n+1/2)\hbar\omega} \;=\; \hbar\omega\left[\frac{1}{2}+\frac{1}{e^{\beta\hbar\omega}-1}\right]. \tag{F.220}$$

a) For $T \to 0$ ($\beta \to \infty$), it easy to see that $\langle H\rangle \to \hbar\omega/2$ (zero point energy). The zero point energy is proportional to the angular frequency ω.

b) For $T \to \infty$ ($\beta \to 0$), one can show that $\langle H\rangle \to k_B T$ (classical approximation). The demonstration is based on the expansion $1/(e^x{-}1) \simeq [x{+}x^2/2{+}\ldots]^{-1} \simeq (1/x)[1{-}x/2{+}\ldots]$, where $x = \beta\hbar\omega$. The behaviour for $T \to \infty$ is independent of ω.

The probability density for the displacement x has a gaussian shape centred on $\langle x\rangle = 0$:

$$\rho(x) \;=\; (1/\sigma\sqrt{2\pi})\, e^{-x^2/2\sigma^2}\,. \tag{F.221}$$

The moments of the distribution can be calculated as

$$\langle x^k\rangle \;=\; \frac{1}{Z_0}\,\mathrm{Tr}\,(x^k e^{-\beta H_0}) \;=\; \frac{1}{Z_0}\sum_{n=0}^{\infty}\langle n|x^k|n\rangle\, e^{-\beta E_n}. \tag{F.222}$$

F.8.4 Normal coordinates and energy

We want to express the kinetic and potential energies in terms of the normal coordinates.

Useful relation

As a preliminary step, it is convenient to introduce the relation

$$\sum_{\ell} e^{i\vec{q}\cdot\vec{R}(\ell)} \;=\; \begin{cases} N & \text{for } \vec{q}=0 \text{ or } \vec{q}=\vec{G}\,, \\ 0 & \text{otherwise}\,. \end{cases} \tag{F.223}$$

Relation (F.223) is a consequence of the lattice periodicity; the sum is unchanged if an arbitrary $\vec{R}(\ell')$ is added to $\vec{R}(\ell)$ in the sum:

$$\sum_{\ell} e^{i\vec{q}\cdot\vec{R}(\ell)} \;=\; \sum_{\ell} e^{i\vec{q}\cdot[\vec{R}(\ell)+\vec{R}(\ell')]} \;=\; \left(\sum_{\ell} e^{i\vec{q}\cdot\vec{R}(\ell)}\right) e^{i\vec{q}\cdot\vec{R}(\ell')}\,. \tag{F.224}$$

This is possible only if conditions (F.223) are fulfilled.
As a consequence of (F.223),

$$\sum_{\ell} e^{i(\vec{q}+\vec{q}')\cdot\vec{R}(\ell)} \;=\; \begin{cases} N & \text{for } \vec{q}+\vec{q}'=0 \text{ or } \vec{q}+\vec{q}'=\vec{G}\,, \\ 0 & \text{otherwise}\,. \end{cases} \tag{F.225}$$

Kinetic energy

Substituting the atomic displacements (F.117) in the expression of the kinetic energy, since only the normal coordinates depend on time, the kinetic energy becomes

$$T \;=\; \frac{1}{2}\frac{1}{N}\sum_{\alpha\kappa}\sum_{\vec{q}s}\sum_{\vec{q}'s} \mathrm{e}_\alpha(\kappa|\vec{q}s)\,\mathrm{e}_\alpha(\kappa|\vec{q}'s')\,\dot{Q}(\vec{q}s)\,\dot{Q}(\vec{q}'s') \sum_{\ell} e^{i(\vec{q}+\vec{q}')\cdot\vec{R}(\ell)}\,. \tag{F.226}$$

Taking into account that according to (F.225) the last sum is N if $\vec{q}=-\vec{q}'$, otherwise it is zero, and considering the orthonormality relation of eigenvectors, one gets

$$T \;=\; \frac{1}{2}\sum_{\vec{q}s}\dot{Q}(\vec{q}s)\,\dot{Q}(-\vec{q}s) \;=\; \frac{1}{2}\sum_{\vec{q}s}\dot{Q}(\vec{q}s)\,\dot{Q}^*(\vec{q}s)\,. \tag{F.227}$$

Potential energy

Substituting the atomic displacements (F.117) in the expression for the potential energy, the potential energy becomes

$$V_2 \;=\; \frac{1}{2N}\sum_{\substack{\vec{q}s\\ \vec{q}'s'}}\sum_{\substack{\alpha\ell\kappa\\ \alpha'\ell'\kappa'}} \frac{\Phi\left(\begin{smallmatrix}\alpha & m\\ \alpha' & m'\end{smallmatrix}\right)}{\sqrt{m_\kappa\, m_{\kappa'}}}\, e^{i\vec{q}\cdot\vec{R}(\ell)}\, e^{i\vec{q}'\cdot\vec{R}(\ell')}\; \mathrm{e}_\alpha(\kappa|\vec{q}s)\,\mathrm{e}_{\alpha'}(\kappa'|\vec{q},'s')\; Q(\vec{q}s)\; Q(\vec{q}'s') \tag{F.228}$$

Multipliying by

$$1 \;=\; e^{i\vec{q}'\cdot[\vec{R}(\ell)-\vec{R}(\ell)]}$$

and recalling the definition of Fourier transformed dynamical matrix, (F.228) becomes

$$V_2 \;=\; \frac{1}{2N}\sum_{\substack{\vec{q}s\\ \vec{q}'s'}}\sum_{\substack{\alpha\kappa\\ \alpha'\kappa'}} D_{\vec{q}'}\begin{pmatrix}\alpha\kappa\\ \alpha'\kappa'\end{pmatrix}\left[\sum_{\ell} e^{i(\vec{q}+\vec{q}')\cdot\vec{R}(\ell)}\right]\; \mathrm{e}_\alpha(\kappa|\vec{q}s)\,\mathrm{e}_{\alpha'}(\kappa'|\vec{q}'s')\; Q(\vec{q}s)\; Q(\vec{q}'s') \tag{F.229}$$

Taking again into account that according to (F.225) the sum in square parentheses is N if $\vec{q}=-\vec{q}'$, otherwise it is zero and making use of the eigenvalue equation of $\mathrm{e}^*_\alpha(\kappa|-\vec{q}s)=\mathrm{e}_\alpha(\kappa|\vec{q}s)$, one obtains

$$V_2 \;=\; \frac{1}{2}\sum_{\substack{\vec{q}s\\ s'}}\sum_{\alpha\kappa}\omega^2(\vec{q}s)\; \mathrm{e}_\alpha(\kappa|\vec{q}s)\,\mathrm{e}^*_\alpha(\kappa|\vec{q}s')\; Q(\vec{q}s)\; Q(-\vec{q}s') \tag{F.230}$$

At last, considering the orthonormality relation of eigenvectors, one finds taht the potential vibrational energy can be expressed as

$$V_2 \;=\; \frac{1}{2}\sum_{\vec{q}s}\omega^2(\vec{q}s)\,Q(\vec{q}s)\,Q(-\vec{q}s) \;=\; \frac{1}{2}\sum_{\vec{q}s}\omega^2(\vec{q}s)\,Q(\vec{q}s)\,Q^*(\vec{q}s)\,. \qquad \text{(F.231)}$$

A classical normal mode $(\vec{q}s)$ can be considered as an independent harmonic oscillator of frequency $\omega(\vec{q}s)$, whose amplitude and time dependence are described by the normal coordinate $Q(\vec{q}s,t) = Q_0(\vec{q}s)\,e^{i\omega(\vec{q}s)t}$. The dimensions of the normal coordinate are $[Q] = [M^{1/2}L]$.

Appendix G

Historical milestones

G.1 X-rays

1895 The evening of eighth of November, W. K. Röntgen, while studying the electric discharges in rarefied gases in his laboratory in Würtzburg, discovers a new radiation, which he designates as "X-rays".

1896 First medical applications of x-ray radiography.

1909–1912 C. G. Barkla, in England, systematically studies absorption and emission spectra of x-rays, discovering absorption edges and characteristic emission lines, and classifying them within different series, K, L, M ...

1912 Friedrich and Knipping, under the suggestion of Max von Laue, experimentally demonstrate that x-rays can be diffracted by crystals, thus showing that x-rays are waves and that crystals are composed by regular arrays of atoms.

1913 First diffraction spectrum from crystals (W.H. Bragg & W.L. Bragg).

Maurice de Broglie (big brother of Louis de Broglie) performs systematic spectroscopy experiments with a rotating crystal monochromator.

Bohr develops its atomic theory.

H.G.J. Moseley expresses the frequencies of x-rays according to the Bohr theory; the Mendeleev table is interpreted as a unique sequence of atoms based on the atomic number Z.

1922 Quantum interpretation of the Compton effect.

G.2 Synchrotron radiation

1944 Ivanenko e Pomeranchuk understand the importance of radiative losses in the performance of electron accelerators.

1947 R.F. Elder for the first time sees the electromagnetic radiation emitted by a synchrotron, at the 70 MeV synchrotron of General Electric in Schenectady (USA).

19446-1953 A number of theorists (among them J. Schwinger, D. Ivanenko, A.A. Solokov, I.M. Ternoc) contribute to the development of the classical theory of synchrotron radiation.

1952 Firs synchrotron beamline, Cornell

1956 Tamboulian e Hartman perform the first experiments with synchtron radiation from the 320 MeV synchrotron of Cornell (angular and spectral distribution, transmission measurements on Be and Al).

1961... Construction of parasitic Synchrotron Radiation beamlines from accelerators dedicated to high energy physics. Some examples:

1961 SURF at the National Bureau of Standards (180 MeV, λ_c=335 Å);

1962 First S.R. beamline at the Frascati synchrotron (1.15 GeV);

1962 750 MeV synchrotron INS-SOR in Tokyo;

1964 S.R. at DESY, Hamburg;

1966 S.R. at the Glasgow synchrotron, 0.33 GeV;

1971 S.R. from the ACO storage ring in Orsay;

1979 S.R. from the Adone storage ring in Frascati (PULS).

1966 The 240 MeV storage ring TANTALUS I of the University of Wisconsin-Madison is the first *dedicated* source of Synchrotron Radiation (2nd generation source).

1981 SRS in the UK is the first dedicated X-ray storage ring

1994 The 6 GeV storage ring of ESRF, Grenoble (France) is the first 3rd generation source of Synchrotron Radiation, followed by

1995 APS in Chicago (7 GeV),

1997 SPRING-8 in Kobe (8 GeV).

G.3 XAFS

A detailed history of XAFS has been written by R. Sturm von Bordwehr [Stumm von Bordwehr, 1989]. A shorter account hs been given by Stern [Stern, 1988]. We will here remember only the most relevant facts.

1918–1919 W. Stenström and H. Fricke independently observe the fine structure at the absorption edges (M edges of Cd and Th, K edge of Cl and P, respectively) while working in the Siegbahn laboratory in Lund [Fricke, 1920].

1920 W. Kossel gives an interpretation of XAFS as due to transitions of the photoelectron from core to shallow levels. This interpretation was actually sound only for near-edge structures, which for a long time have been called "Kossel structures". [W. Kossel, Z. Phys. 1, 119 (1920), Z. Phys. 2, 470 (1920)]

1930 Kievit and Lindsay measure the fine structure in the X-ray absorption spectra of the K series of the elements calcium to gallium [Kievit and Lindsay, 1930]

1931 Ralph Kronig attributes the EXAFS in *solids* to the alternation of allowed and forbidden bands in the density of electronic states, beginning the quantitative development of LRO (long range order) theories. [R. de Laer Kronig, Z. Phys. 70, 317 (1931)]

1931 J.D. Hanawalt observes the temperature dependence of the XAFS. [Z. Phys. 70, 20 (1931) and Phys. Rev. 37, 715 (1931)]

1932 Again Kronig attributes the EXAFS in *molecules* to the scattering of photoelectrons by neighbouring atoms, introducing the SRO (short range order) theories. [R. de Laer Kronig, Z. Phys. 75, 468 (1932)]

1932-36 Kronig's student Petersen calculates the EXAFS of the molecules Cl_2 and $GeCl_4$ and adds the idea of phaseshifts. [H. Petersen, Z. Phys. 76, 768 (1932); 80, 258 (1933); 98, 569 (1936)]

1957 M. Sawada et al. calculate the lifetime of the excited photoelectron and core hole through a mean free path. [T. Shiraiva, T. Ishimura, M. Sawada, J. Phys. Soc. Jpn. 12, 788 (1957)]

1961-1963 V. V. Shmidt introduces the Debye-Waller factor to describe the effects of thermal and structural disorder. [Bull. Acad. Sci. USSR, Phys. Ser. 25, 998 (1961); 27, 392 (1963)]

1971 The EXAFS spectra of Cu, Fe and Ge, measured at 77 K with a laboratory apparatus, are reproduced by a theory where the photo-electron spherical wave is scattered by neighbors of the absorber, treated as point scatterers; photoelectron mean free path and thermal effects are taken into account [Sayers et al., 1971a].

In another paper by the same Authors, it is shown that the Fourier transform of EXAFS with respect to photoelectron wavevector directly gives structural information [Sayers et al., 1971b].

Appendix H

Useful tables

H.1 Physical constants and conversions

Table H.1: Values of some fundamental constants, taken from the 2014 compilation of CODATA (*CODATA Recommended Values of the Fundamental Physical Constants: 2014*, by P. J. Mohr, D. B. Newell and B. N. Taylor, Rev. Mod. Phys. 88, 035009 (2016)).

Constant	*Symbol*	*Value*	*Unit*
Speed of light in vacuum	c	299 792 458	m s^{-1}
Planck constant	h	$6.626\,070\,040(81)\times10^{-34}$	J s
		$4.135\,667\,662(25)\times10^{-15}$	eV s
Planck constant reduced	$\hbar = h/2\pi$	$1.054\,571\,800(13)\times10^{-34}$	J s
		$6.582\,119\,514(40)\times10^{-16}$	eV s
Elementary charge	e	$1.602\,176\,6208(98)\times10^{-19}$	C
Electron mass	m_e	$9.109\,383\,56(11)\times10^{-31}$	kg
		$0.510\,998/,9461(13)$	MeV/c^2
Atomic mass unit	u	$1.660\,539\,040(20)\times10^{-27}$	kg
Avogadro number	N_A	$6.022\,140\,857(74)\times10^{23}$	mol^{-1}
Boltzmann constant	k_B	$1.380\,648\,52(79)\times10^{-23}$	J K^{-1}
		$8.617\,3303(50)\times10^{-5}$	eV K^{-1}

Table H.2: Conversions.

Energy	1 eV	=	$1.602\,176\,6208(98)\times10^{-19}$ J
	θ [K]	=	47.992 447 ν [THz]
	ν [THz]	=	0.241 798 926 E [meV]
	E [meV]	=	4.135 667 662 ν [THz]
	E [meV]	=	0.086 173 303 θ [K]
Phoho-elctron wavenumber	k [$Å^{-1}$]	=	$0.512\,316\,25\,\sqrt{\epsilon\,[\mathrm{eV}]}$, $\epsilon = \hbar\omega - E_b$
Einstein model	θ_E [K]	=	47.992 447 ν_E [THz]
	k_0 [eV/$Å^2$]	=	$4.091\,649\,625\times10^{-3}\nu_E^2$ [THz^2] μ[amu]
Force constant k_0	1 eV/$Å^2$	=	16.021 766 208 N/m
Force constant k_3	1 eV/$Å^3$	=	$16.021\,766\,208\times10^{10}$ N/m^2

H.2 Interatomic distances in crystals

H.2.1 From coordinates to distances

Let

- a, b, c be the cell edges
- α, β, γ be the cell angles

Let the fractional coordinates of two atoms within the cell be (x_1, y_1, z_1) and (x_2, y_2, z_2), respectively.
The distance between the two atoms is given by

$$\begin{aligned} d^2 \;=\; & (x_2 - x_1)^2\, a^2 \;+\; (y_2 - y_1)^2\, b^2 \;+\; (z_2 - z_1)^2\, c^2 \\ & +\; 2\,(x_2 - x_1)\,(y_2 - y_1)\, ab\, \cos\gamma \\ & +\; 2\,(y_2 - y_1)\,(z_2 - z_1)\, ab\, \cos\alpha \\ & +\; 2\,(z_2 - z_1)\,(x_2 - x_1)\, ab\, \cos\beta \end{aligned} \tag{H.1}$$

H.2.2 Distances and coordination numbers

Table H.3: Simple cubic structure (sc).

i	N_i	R_i	
1	6	a	R_1
2	12	$a\sqrt{2}$	$R_1\sqrt{2}$
3	8	$a\sqrt{3}$	$R_1\sqrt{3}$
4	6	$a\sqrt{4}$	$R_1\sqrt{4}$
5	24	$a\sqrt{5}$	$R_1\sqrt{5}$
6	24	$a\sqrt{6}$	$R_1\sqrt{6}$
7	12		
8	30		

Table H.4: Face centred cubic structure (fcc).

i	N_i	R_i	
1	12	$a/\sqrt{2}$	R_1
2	6	a	$R_1\sqrt{2}$
3	24	$a\sqrt{1.5}$	$R_1\sqrt{3}$
4	12	$a\sqrt{2}$	$R_1\sqrt{4}$
5	24		$R_1\sqrt{5}$
6	8		$R_1\sqrt{6}$
7	48		$R_1\sqrt{7}$
8	6		$R_1\sqrt{8}$

Table H.5: Body centred cubic structure (bcc).

i	N_i	R_i	
1	8	$a\sqrt{3}/2$	R_1
2	6	a	$R_1\sqrt{4/3}$
3	12	$a\sqrt{2}$	$R_1\sqrt{8/3}$
4	24	$a\sqrt{11}/2$	$R_1\sqrt{11/3}$
5	24	$a\sqrt{3}$	$2\,R_1$
6	6	$2\,a$	$R_1\sqrt{16/3}$
7	24		$R_1\sqrt{19/3}$
8	24		$R_1\sqrt{20/3}$

Table H.6: Diamond and zincblende structures.

i	N_i	R_i	
1	4	$a\sqrt{3}/4$	R_1
2	12	$a/\sqrt{2}$	$R_1\sqrt{8/3}$
3	12	$a\sqrt{11}/4$	$R_1\sqrt{11/3}$
4	6	a	$R_1\sqrt{16/3}$
5	12	$a\sqrt{19}/4$	$R_1\sqrt{19/3}$
6	24	$a\sqrt{6}/2$	$R_1\sqrt{8}$
7	16		$3\,R_1$
8	12		$R_1\sqrt{32/3}$

Table H.7: NaCl structure.

i	N_i	R_i	
1	6	$a/2$	R_1
2	12	$(a/2)\sqrt{2}$	$R_1\sqrt{2}$
3	8	$(a/2)\sqrt{3}$	$R_1\sqrt{3}$
4	6	a	$2\,R_1$
5	24	$(a/2)\sqrt{5}$	$R_1\sqrt{5}$
6	24	$(a/2)\sqrt{6}$	$R_1\sqrt{6}$

H.3 Nomenclature of core-level (and related) spectroscopies

H.3.1 Excitation spectroscopies

Table H.8: Excitation spectroscopies

XAS	X-ray Absorption Spectroscopy	
EELS	Electron Energy Loss Spectroscopy	(inelastic electron scattering)
XRS	X-ray Raman Scattering	(inelastic X-ray scattering)
XPS	X-ray Photoemission Spectroscopy	(core-electrons excitation)
PES	(Valence) Photoemission Spectroscopy	(valence-electrons excitation)
IPES	Inverse PES	
or BIS	or Bremsstrahlung Isochromat Spectroscopy	

H.3.2 Core decay spectroscopies

Table H.9: Core-hole decay spectroscopies

XES	X-ray Emission Spectroscopy	shallow-core to deep-core transitions
		valence to deep-core transitions
AES	Auger Electron Energy Spectroscopy	final state: 2 shallow core holes
		final state: 1 shallow core and 1 valence hole
		final state: 2 valence holes

H.3.3 Resonant spectroscopies

Atomic excitation is always accompanied by decay processes.
Close to an XAS absorption edge, the decay processes are different from off-resonance excitations.
A major effect is the coherence between excitation and decay.

Table H.10: Resonance spectroscopies

RPES	Resonant Photoemission Spectroscopy
RXPS	Resonant X-ray Photoemission Spectroscopy
RAES	
RIPES	

Appendix I

Basic references

I.1 Fundamental and historical papers

- D. E. Sayers, E. A. Stern and F. W. Lytle: "New technique for investigating noncrystalline structures: Fourier analysis of the extended x-ray-absorption fine- structure", Phys. Rev. Lett., 27, 12041207 (1971).
- E. A. Stern: "Theory of extended x-ray fine structure", Phys. Rev. B 10, 3027 (1974).
- F. W. Lytle, D. E. Sayers and E. A. Stern: "Extended x-ray-absorption fine-structure technique. II. Experimental practice and selected results", Phys. Rev. B 11, 4825 (1975).
- E. A. Stern, D. E. Sayers and F.W. Lytle: "Extended x-ray-absorption fine-structure technique. III. Determination of physical parameters", Phys. Rev. B 11, 4836 (1975).
- C. A. Ashley and S. Doniach: "Theory of extended x-ray absorption edge fine structure (EXAFS) in crystalline solids", Phys. Rev. B 11, 1279 (1975).
- P. A. Lee and J. B. Pendry: "Theory of extended x-ray absorption edge fine structure", Phys. Rev. B 11, 2795 (1975).
- R. Stumm von Bordwehr: "A history of x-ray absorption fine structure", Ann. Phys. Fr., 14, 377-466 (1989).

I.2 Introductory and review papers

- G.S. Brown and S. Doniach: *The Principles of X-Ray Absorption Spectroscopy*, in *Synchrotron Radiation Research*, ed. by Winick and S. Doniach, Plenum 1980, pagg.353–385
- P.A. Lee, P.H. Citrin and B.M. Kincaid: "Extended x-ray absorption fine structure – its strengths and limitations", Rev. Mod. Phys. 53, 769–806 (1981).
- T.M. Hayes and J.B. Boyce: " Extended X-Ray Absorption Fine Structure Spectroscopy", Solid State Physics 27, 173-351 (1982).
- E.A. Stern and S.M. Heald: *Basic principles and applications of EXAFS*, in *Handbook on Synchrotron Radiation*, vol. 1b, ed. by E.E. Koch, North-Holland (1983).
- I.B. Borovskii, R.V. Vedrinskii, V.L. Kraizman and V.P. Sachenko: *EXAFS spectroscopy: a new method for structural investigation*, Sov. Phys. Usp. 29, 539-569 (1986).
- S.J. Gurman: *Interpretation of EXAFS data*, J. Synchrotron Rad., 2, 56–63 (1995)
- E.D. Crozier: *A review of the current status of XAFS spectroscopy*, Nucl. Instr. and Meth. in Phys. Res. B 133, 134-144 (1997).
- G. Dalba and P. Fornasini: *EXAFS Debye-Waller factor and thermal vibrations in crystals*, J. Synchrotron Rad. 4, 243–255 (1995).
- J.J. Rehr and R.C. Albers: *Theoretical approaches to x-ray absorption fine structure*, Rev. Mod. Phys. 72, 621–654 (2000).
- A. Filipponi: *EXAFS for liquids*, J. Phys.: Condens. Matter 13, R23 (2001)

- F. Boscherini: *X-ray absorption fine structure in the study of semiconductor heterostructures and nanostructures*, in *Characterization of semiconductor heterostructures and nanostructures*, ed. by C. Lamberti, Elsevier (2008), pagg. 289–330

I.3 Books and monographs

- B.K. Teo and D.C. Joy, eds.: *EXAFS Spectroscopy: techniques and applications*, Plenum Press (1981).
- B.K. Teo: *EXAFS: basic principles and data analysis*, Springer Verlag (1986).
- D.C. Konigsberger and R. Prins eds.: *X-Ray absorption: principles and application techniques of EXAFS, SEXAFS and XANES*, J. Wiley (1988).
- B. K. Agarwal: *X-Ray spectroscopy. An introduction*, Springer Verlag (1991)
- J. Stöhr: *NEXAFS Spectroscopy*, Springer Series in Surface Sciences 25, Springer Verlag (1996).
- F. de Groot and A. Kotani: *Core level spectroscopy of solids*, CRC Press, Taylor and Francis (2008).
- G. Bunker: *Introduction to XAFS: a practical guide to X-ray absorption fine structure spectroscopy*, Cambridge University Press (2010).
- J. Als-Nielsen and D. McMorrow: *Elements of modern X-ray Physics*, Wiley (2011), Chapter 7: Photoelectric absorption.
- S. Calvin: *XAFS for everyone*, CRC Press, Taylor & Francis Group (2013).
- J. A. von Bookhoven and C. Lamberti eds: *X-ray Absorption and X-ray Emission Spectroscopy. Theory and Applications*, Wiley (2016).

I.4 Proceedings of the XAFS International Conferences

Since the Daresbury Study Weekend of 1981, an International Conference on XAFS has been held every two or three years. The proceedings of the XAFS Conferences are an invaluable source of information on the theoretical progress and on different applications of EXAFS and XANES spectroscopies.

1. Study Weekend *EXAFS for inorganic systems*, Daresbury (UK), March 1981. C.D. Garner and S.S. Hasnain eds., Daresbury Report DL/SCI/R17 (March 1981).
2. *EXAFS and Near Edge Structure*, Frascati (Italy), September 13-17, 1982. A. Bianconi, L. Incoccia and S. Stipcich eds., Springer Series in Chem. Phys. 27 (1983).
3. *EXAFS and Near Edge Structure III*, Stanford (USA), July 16-20, 1984. K.O. Hodgson, B. Hedman and J.E. Penner-Hahn eds:, Springer Proc. in Physics 2 (1984).
4. *EXAFS and Near Edge Structure IV*, Fontevraud (France), July 7-11, 1986. P. Lagarde, D. Raoux and J. Petiau eds., J. Phys. (Paris), Colloque C8 (1986).
5. *XAFS V*, Seattle (USA), August 21-26, 1988. J. Munstre de Leon, E.A. Stern, D.E. Sayers, Y. Ma and J.J. Rehr eds., North-Holland (1989).
6. *XAFS VI: X-ray absorption fine structure*, York (UK), August 5-11, 1990. S. Samar Hasnain ed., Ellis Horwood (1991).
7. *XAFS VII*, Kobe (Japan), August 23-29, 1992. H. Kuroda, Y.T. Ohta, T. Murata, Y. Udagawa and M. Nomura eds., Jpn. J. Appl. Phys., 32 (1993)
8. *XAFS VIII*, Berlin (Germany), August 28 - September 2, 1994. K. Baberschke and D. Arvanitis eds., Physica B, 208 & 209 (1995).
9. *XAFS IX*, Grenoble (France), August 26-30, 1996. J. Goulon, C. Goulon-Ginet and N.B. Brookes eds., J. Phys. IV (Paris), Colloque C2 (1997).
10. *XAFS X*, Chicago (USA), August 10-14, 1998. S.S. Hasnain, J.R. Helliwell, and H. Kamitsubo eds., J. Synchrotron Rad., vol. 6, part 3 (1999).

11. *XAFS XI*, Ako (Japan), 2000. T. Ohta and M. Nomura eds., J. Synchrotron Rad., vol. 8 part 2 (2001).
12. *XAFS XII*, Malmö (Sweden), 2003. N. Mårtensson, D. Arvanitis, and O. Karis eds., Physica Scripta, vol. T115 (2005).
13. *XAFS XIII*, Stanford (USA), July 9-14, 2006. B. Hedman and P. Pianetta eds., AIP Conference Proceedings 882 (2007).
14. *XAFS XIV*, Camerino (Italy), July 26-31, 2009. A Di Cicco and A. Filipponi eds., Journal of Physics: Conference Series, vol. 190 (2009).
15. *XAFS XV*, Beijing (China), July 22-28, 2012. Ziyu Wu ed., Journal of Physics: Conference Series, vol. 430 (2013).
16 *XAFS XVI*, Karlsruhe (Germany), August 23-28, 2015. J-D. Grunwaldt, M. Hagelstein and J. Rothe eds., Journal of Physics: Conference Series, vol. 712 (2017).
17 *XAFS XVII*, Krakow (Poland), August 22-27, 2018. Radiation Physics and Chemistry, vol. 175 (2020).
18 *XAFS XVIII*, Sydney (Australia), July 10-15, 2022.

I.5 Internet sites

- International X-ray Absorption Society: `http://www.ixasportal.net/ixas/`
- GNXAS home page: `http://gnxas.unicam.it/XASLABwww/pag$_$gnxas.html`
- FEFF project home page: `http://leonardo.phys.washington.edu/feff/`

Bibliography

[Abd el All et al., 2012] Abd el All, N., Dalba, G., Diop, D., Fornasini, P., Grisenti, R., Mathon, O., Rocca, F., Thiodjio Sendja, B., and Vaccari, M. (2012). Negative thermal expansion in crystals with the zincblende structure: an exafs study of cdte. *J. Phys.: Condens. Matter*, 24:115403.

[Abd el All et al., 2013] Abd el All, N., Thiodjio Sendja, B., Grisenti, R., Rocca, F., Diop, D., Mathon, O., Pascarelli, S., and Fornasini, P. (2013). Accuracy evaluation in temperature-dependent exafs measurements of CdTe. *J. Synchrotron Rad.*, 20:603–613.

[Ahmed et al., 2013] Ahmed, S. I., Aquilanti, G., Novello, N., Olivi, L., Grisenti, R., and Fornasini, P. (2013). Local vibrational properties of gaas studied by extended x-ray absorption fine structure. *J. Chem. Phys.*, 139:164512.

[Alonso and Finn, 1969] Alonso, M. and Finn, R. J. (1969). *Fundamental University Physics, vol. III, Quantum and Statistical Physics.* Addison-Wesley, Reading, MA.

[Als-Nielsen and McMorrow, 2011] Als-Nielsen, J. and McMorrow, D. (2011). *Elements of Modern X-ray Physics.* John Wiley & Sons, Chichester, UK.

[Artioli, 2002] Artioli, G. (2002). Atomic displacement parameters from diffraction studies: the experimental evidence. In Gramaccioli, C. M., editor, *EMU Notes in Mineralogy, vol. 4: Energy modelling in minerals*, pages 389–405. Eötvös University Press, Budapest.

[Bambynek et al., 1972] Bambynek, W., Crasemann, B., Fink, R. W., Freund, H. U., Mark, H., Swift, C. D., Price, R. E., and Rao, P. V. (1972). X-ray fluorescence yields, auger and coster-kronig transition probabilities. *Rev. Mod. Phys.*, 44:716.

[Barron, 1957] Barron, T. H. K. (1957). Grüneisen parameters for the equation of state of solids. *Annals of Physics*, 1:77–90.

[Barron and Klein, 1974] Barron, T. H. K. and Klein, M. L. (1974). Perturbation theory of anharmonic crystals. In Horton, G. K. and Maradudin, A. A., editors, *Dynamical Properties of Solids: Volume 1, Crystalline solids, fundamentals.*, chapter 7, pages 391–450. Nort-Holland, Amsterdam.

[Beeman and Alben, 1977] Beeman, D. and Alben, R. (1977). Vibrational properties of elemental semiconductors. *Adv. Phys.*, 26:339–361.

[Benfatto et al., 1989] Benfatto, M., Natoli, C. R., and Filipponi, A. (1989). Thermal and structural damping of the multiple- scattering contributions to the x-ray absorption coefficient. *Phys. Rev. B*, 40:9626–9635.

[Beni and Platzman, 1976] Beni, G. and Platzman, P. M. (1976). Temperature and polarisation dependence of extended x-ray absorption fine-structure spectra. *Phys. Rev. B*, 14:1514–1518.

[Bertin, 1975] Bertin, E. P. (1975). *Principles and practice of x-ray spectrometric analysis.* Plenum.

[Böhmer and Rabe, 1979] Böhmer, W. and Rabe, P. (1979). Temperature dependence of the mean square relative displacement of nearest-neighbour atoms derived from exafs spectra. *J. Phys. C: Solid State Phys.*, 12:2465–2474.

[Bohr, 1913] Bohr, N. (1913). On the constitution of atoms and molecules. *Phil. Mag.*, 26:1–25.

[Born and Huang, 1998] Born, M. and Huang, K. (1998). *Dynamical Theory of Crystal Lattices*. Oxford University Press.

[Borovskii et al., 1986] Borovskii, I. B., Vedrinskii, R. V., Kraizman, V. L., and Sachenko, V. P. (1986). Exafs spectroscopy: a new method for structural investigation. *Sov. Phys. Usp.*, 29:539–569.

[Boscherini, 2008] Boscherini, F. (2008). X-ray absorption fine structure in the study of semiconductor heterostructures and nanostructures. In Lamberti, C., editor, *Characterization of semiconductor heterostructures and nanonstructures*, pages 289–330. Elsevier.

[Bragg and Bragg, 1913] Bragg, W. H. and Bragg, W. L. (1913). The reflection of x-rays by crystals. *Proc. R. Soc.*, A88:428–438.

[Bransden and Joachain, 2003] Bransden, B. H. and Joachain, C. J. (2003). *Physics of Atoms and Molecules*. Pearson.

[Brown and Doniach, 1980] Brown, G. S. and Doniach, S. (1980). The principles of x-ray absorption spectroscopy. In Winick, H. and Doniach, S., editors, *Synchrotron Radiation Research*, pages 353–385. Plenum.

[Brüesch, 1982] Brüesch, P. (1982). *Phonons: theory and experiment. I. Lattice Dynamics and Models of Interatomic Forces*, volume 34 of *Springer Series in Solid State Sciences*. Springer, Berlin.

[Bunker, 1983] Bunker, G. (1983). Application of the ratio method of exafs analysis to disordered systems. *Nucl. Instrum. Methods Phys. Res.*, 207:437–444.

[Bunker, 2010] Bunker, G. (2010). *Introduction to XAFS*. Cambridge University Press, Cambridge.

[Chantler et al., 2012] Chantler, C. T., Islam, M. T., Rae, N. A., Tran, C. Q., Glover, J. L., and Barnea, Z. (2012). New consistency tests for high-accuracy measurements of x-ray mass attenuation coefficients by the x-ray extended-range technique. *Acta Cryst. A*, 68:188–195.

[Chantler et al., 2001] Chantler, C. T., Tran, C. Q., Barnea, Z., Paterson, D., Cookson, D. J., and Balaic, D. X. (2001). Measurement of the x-ray mass attenuation coefcient of copper using 8.85 20 kev synchrotron radiation. *Phys. Rev. A*, 64:062506.

[Chen et al., 1989] Chen, C. T., Ma, Y., and Sette, F. (1989). K-shell photoabsorption of the N_2 molecule. *Phys. Rev. A*, 40:6737–6740.

[Chen and Kotlarchyk, 1997] Chen, S. and Kotlarchyk, M. (1997). *Interaction of photons and neutrons with matter*. World Scientific.

[Chen and Kotlarchyk, 2007] Chen, S. and Kotlarchyk, M. (2007). *Interactions of Photons and Neutrons With Matter*. World Scientific.

[Cohen-Tannoudji et al., 1973] Cohen-Tannoudji, C., Diu, B., and Laloë, F. (1973). *Mécanique quantique*. Hermann, Paris.

[Cohen-Tannoudji et al., 2001] Cohen-Tannoudji, C., Dupont-Roc, J., and Grynberg, G. (2001). *Processus d'interaction entre photons ate atomes*. EDP Sciences, CNRS Editions, Paris.

[Cohen-Tannoudji et al., 2004] Cohen-Tannoudji, C., Dupont-Roc, J., and Grynberg, G. (2004). *Photons & atoms*. Wiley-VCH, Weinheim.

[Cramér, 1966] Cramér, H. (1966). *Mathematical Methods of Statistics*. Princeton University Press.

[Crozier et al., 1988] Crozier, E. D., Rehr, J. J., and Ingalls, R. (1988). Amorphous and liquid systems. In Koningsberger, D. C. and Prins, R., editors, *X-ray Absorption*, chapter 9, pages 373–442. J. Wyley & Sons, New York.

[David et al., 1992] David, W. I. F., Ibberson, R. M., Jeffrey, G. A., and Ruble, J. R. (1992). The crystal structure analysis of deuterated benzene and deuterated nitromethane by pulsed neutron powder diffraction: a comparison with single crystal neutron diffraction analysis. *Physica B*, 180-181:597–600.

[de Groot and Kotani, 2008] de Groot, F. and Kotani, A. (2008). *Core level spectroscopy of solids*. CRC Press, Taylor and Francis.

[Dusek et al., 2001] Dusek, M., Petrcek, V., Wunschel, M., Dinnebier, R. E., and van Smaalen, S. (2001). Refinement of modulated structures against x-ray powder diffraction data with jana2000. *J. Appl. Cryst.*, 34:398–404.

[FEFF, 2012] FEFF (2012). Project home page. `http://feffproject.org`.

[Feynman, 1972] Feynman, R. P. (1972). *Statistical Mechanics*. Benjamin, Reading, MA.

[Feynman et al., 1977] Feynman, R. P., Leighton, R. B., and Sands, M. (1977). *The Feynman Lectures on Physics*, volume 2. Addison-Wesley.

[Filipponi, 2001] Filipponi, A. (2001). Exafs for liquids. *J. Phys.: Condens. Matter*, 13:R23–R60.

[Fornasini et al., 2004] Fornasini, P., a Beccara, S., Dalba, G., Grisenti, R., Sanson, A., Vaccari, M., and Rocca, F. (2004). Extended x-ray-absorption fine-structure measurements of copper: local dynamics, anharmonicity, and thermal expansion. *Phys. Rev. B*, 70:174301.

[Fornasini and Grisenti, 2015] Fornasini, P. and Grisenti, R. (2015). On exafs debye-waller factor and recent advances. *J. Synchrotron Rad.*, 22:1242–1257.

[Fornasini et al., 2001] Fornasini, P., Monti, F., and Sanson, A. (2001). On the cumulant analysis of exafs in crystalline solids. *J. Synchrotron Radiat.*, 8:1214–1220.

[Frenkel and Rehr, 1993] Frenkel, A. I. and Rehr, J. J. (1993). Thermal expansion and x-ray absorption fine structure cumulants. *Phys. Rev. B*, 48:585–588.

[Freund et al., 1989] Freund, J., Ingalls, R., and Crozier, E. D. (1989). Extended x-ray absorption fine structure study of copper under high pressure. *Phys. Rev. B*, 39:12537–12547.

[Fricke, 1920] Fricke, H. (1920). The k-characteristic absorption frequencies for the chemical elements magnesium to chromium. *Phys. Rev.*, 16:202–215.

[Friedrich et al., 1912] Friedrich, W., Knipping, P., and Laue, M. (1912). Interferenz-Erscheinungen bei Röntgenstrahlen. *Bayerische Akad. d. Wiss. zu München, Sitzungsber. math.-phys. Kl.*, pages 303–322.

[Fujikawa and Miyanaga, 1993] Fujikawa, T. and Miyanaga, T. (1993). Quantum statistical approach to debye-waller factors in exafs, eels and arxps. i. anharmonic contribution in plane-wave approximation. *J. Phys. Soc. Jpn.*, 62:4108–4122.

[Gnedenko, 1976] Gnedenko, B. V. (1976). *The Theory of Probability*. MIR, Moskow.

[GNXAS, 2015] GNXAS (2015). Home page. `http://gnxas.unicam.it/`.

[Haug et al., 2008] Haug, J., Chassé, A., Schneider, R., Kruth, H., and Dubiel, M. (2008). Thermal expansion and interatomic potentials of silver revealed by extended x-ray absorption fine structure spectroscopy using high-order perturbation theory. *Phys. Rev. B*, 77:184115.

[Hayes and Boyce, 1982] Hayes, T. M. and Boyce, J. B. (1982). Extended x-ray-absorption fine structure spectroscopy. *Solid State Physics*, 37:173–350.

[Heald, 2015] Heald, S. M. (2015). Strategies and limitations for fluorescence detection of xafs at high flux beamlines. *J. Synchrotron Rad.*, 22:436445.

[Hubbell and Seltzer, 1996] Hubbell, J. H. and Seltzer, S. M. (1996). Tables of x-ray mass attenuation coefficients and mass energy-absorption coefficients. NIST website. http://www.nist.gov/pml/data/xraycoef/index.cfm.

[Huber and Herzberg, 1979] Huber, K. P. and Herzberg, G. (1979). *Molecular spectra and molecular structure IV: constants of diatomic molecules*. Van Nostrand Reinhold, New York.

[Joachain, 1975] Joachain, G. J. (1975). *Quantum Collision Theory*. North Holland.

[Kennedy, 1995] Kennedy, B. J. (1995). Structure refinement of $y_2ru_2o_7$ by neutron powder diffraction. *Acta Cryst. C*, 51:790–792.

[Kievit and Lindsay, 1930] Kievit, B. and Lindsay, G. A. (1930). Fine structure in the x-ray absorption spectra of the k series of the elements calcium to gallium. *Phys. Rev.*, 36:648–664.

[Koningsberger and Prins, 1988] Koningsberger, D. C. and Prins, R. (1988). *X-Ray absorption: principles and application techniques of EXAFS, SEXAFS and XANES*. Wyley, New York.

[Landau and Lifschitz, 1976] Landau, L. D. and Lifschitz, E. M. (1976). *Mechanics*. Elsevier.

[Lee et al., 1981] Lee, P. A., Citrin, P. H., Eisenberger, P., and Kincaid, B. M. (1981). Extended x-ray absorption fine structure, its strengths and limitations. *Rev. Mod. Phys.*, 53:769–806.

[Leibfried and Ludwig, 1961] Leibfried, G. and Ludwig, W. (1961). Theory of anharmonic effects in crystals. *Solid State Physics*, 12:275–444.

[Leighton, 1959] Leighton, R. B. (1959). *Principles of Modern Physics*. McGraw Hill Bokk Company, New York.

[Maradudin, 1974] Maradudin, A. A. (1974). Elements of theory of lattice dynamics. In Horton, G. K. and Maradudin, A. A., editors, *Dynamical Properties of Solids: Volume 1, Crystalline solids, fundamentals.*, chapter 1, pages 3–82. Nort-Holland, Amsterdam.

[Maradudin et al., 1971] Maradudin, A. A., Montroll, E. W., Weiss, G. H., and Ipatova, I. P. (1971). *Theory of Lattice Dynamics in the Harmonic Approximation*, volume 3 of *Solid State Physics*. Academic Press.

[Merzbacher, 1970] Merzbacher, E. (1970). *Quantum Mechanics*. John Wiley & Sons.

[Messiah, 1970] Messiah, A. (1970). *Quantum Mechanics*. North-Holland Publishing Company.

[Miyanaga and Fujikawa, 1994] Miyanaga, T. and Fujikawa, T. (1994). Quantum statistical approach to debye-waller factors in exafs, eels and arxps. ii. application to one-dimensional models. *J. Phys. Soc. Jpn.*, 63:1036–1052.

[Moseley, 1913] Moseley, H. G. J. (1913). The high-frequency spectra of the elements. *Philos. Mag.*, 26:1024–1034.

[Müller and Schaich, 1983] Müller, J. E. and Schaich, W. L. (1983). Single-scattering theory of x-ray absorption. *Phys. Rev. B*, 27:6489–6492.

[NIST, 2004] NIST (2004). X-ray mass attenuation coefficients. `http://www.nist.gov/pml/data/xraycoef/`.

[Padežnik Gomilšek et al., 2011] Padežnik Gomilšek, J., Kodre, A., Arčon, I., and Bratina, G. (2011). X-ray absorption of cadmium in the l-edge region. *Phys. Rev. A*, 84:052508.

[Parrat, 1939] Parrat, L. G. (1939). X-ray resonance absorption lines in the argon K spectrum. *Phys. Rev.*, 56:295–297.

[Poiarkova and Rehr, 1999] Poiarkova, A. V. and Rehr, J. J. (1999). Multiple scattering x-ray-absorption fine-structure debye-waller factor calculations. *Phys. Rev. B*, 59:948–957.

[Purans et al., 2008] Purans, J., Afify, N. D., Dalba, G., Grisenti, R., De Panfilis, S., Kuzmin, A., Ozhogin, V. I., Rocca, F., Sanson, A., Tiutiunnikov, S. I., and Fornasini, P. (2008). Isotopic effect in extended x-ray absorption fine structure of germanium. *Phys. Rev. Lett.*, 100:055901.

[Purans et al., 2009] Purans, J., Timoshenko, J., Kuzmin, A., Dalba, G., Fornasini, P., Grisenti, R., Afify, N. D., Rocca, F., Panfilis, S. D., Ozhogin, I., and Tiutiunnikov, S. I. (2009). Femtometer accuracy exafs measurements: isotopic effect in first, second and third coordination shells of germanium. *J. Phys.: Conference Series*, 190:012063.

[Rehr and Alben, 1977] Rehr, J. J. and Alben, R. (1977). Vibrations and electronic states in a model amorphous metal. *Phys. Rev. B*, 16:2400–2407.

[Rehr and Albers, 2000] Rehr, J. J. and Albers, R. C. (2000). Theoretical approaches to x-ray absorption fine structure. *Rev. Mod. Phys.*, 72:621–654.

[Röntgen, 1896] Röntgen, W. K. (1896). On a new kind of rays. *Nature*, 53:274–276.

[Sayers et al., 1971a] Sayers, D. E., Lytle, F. W., and Stern, E. A. (1971a). Point scattering theory of x-ray k-absorption fine structure. In Henke, B. L., Newkirk, J. B., and Mallett, G. R., editors, *Advances in X-ray analysis*, volume 13, pages 248–271. Plenum Press, N.Y.

[Sayers et al., 1971b] Sayers, D. E., Stern, E. A., and Lytle, F. W. (1971b). New technique for investigating noncrystalline structures: fourier analysis of the extended x-ray absorption fine structure. *Phys. Rev. Lett.*, 27:1204–1207.

[Sevillano et al., 1979] Sevillano, E., Meuth, H., and Rehr, J. J. (1979). Extended x-ray absorption fine structure debye-waller factors. i. monatomic crystals. *Phys. Rev. B*, 20:4908–4911.

[Stern, 1974] Stern, E. A. (1974). Theory of extended x-ray fine structure. *Phys. Rev. B*, 10:3027–3037.

[Stern, 1988] Stern, E. A. (1988). Theory of exafs. In Koningsberger, D. C. and Prins, R., editors, *X-Ray absorption: principles and application techniques of EXAFS, SEXAFS and XANES*, pages 3–51. Wyley.

[Stern, 1997] Stern, E. A. (1997). Xafs and thermal averaging. *J. Phys. IV France*, 7:137–140.

[Stern et al., 1991] Stern, E. A., Livins, P., and Zhang, Z. (1991). Thermal vibration and melting from a local perspective. *Phys. Rev. B*, 43:8850–8860.

[Stern et al., 1992] Stern, E. A., Ma, Y., Hanske-Petitpierre, O., and Bouldin, C. E. (1992). Radial distribution function in x-ray-absorption fine structure. *Phys. Rev. B*, 46:687–694.

[Stern et al., 1975] Stern, E. A., Sayers, D. E., and Lytle, F. W. (1975). Extended x-ray-absorption fine-structure technique. iii. determination of physical parameters. *Phys. Rev. B*, 11:4836–4846.

[Stöhr, 1996] Stöhr, J. (1996). *NEXAFS Spectroscopy.* Springer.

[Stumm von Bordwehr, 1989] Stumm von Bordwehr, R. (1989). A history of x-ray absorption fine structure. *Ann. Phys. Fr.*, 14:377–466.

[Teo, 1986] Teo, B. K. (1986). *EXAFS: Basic principles and data analysis.* Springer.

[Thomson et al., 2009] Thomson et al., A. (2009). *X-ray data booklet.* Lawrence Berkeley National Laboratory, Berkeley, CA.

[Touloukian et al., 1977] Touloukian, Y. S., Kirby, R. K., Taylor, R. E., and Desai, P. D. (1977). *Thermophysical Properties of Matter*, volume 13. Plenum, New York.

[Tranquada, 1983] Tranquada, J. M. (1983). *X-ray absorption studies of solids at high pressure.* PhD thesis, University of Washington.

[Tranquada and Ingalls, 1983] Tranquada, J. M. and Ingalls, R. (1983). Extended x-ray-absorption fine-structure study of anharmonicity in cubr. *Phys. Rev. B*, 28:3520–3528.

[Tranquada and Ingalls, 1986] Tranquada, J. M. and Ingalls, R. (1986). X-ray absorption study of cubr at high pressure. *Phys. Rev. B*, 34:4267–4277.

[Tröger et al., 1994] Tröger, L., Yokoyama, T., Arvanitis, D., Lederer, T., Tischer, M., and Baberschke, K. (1994). Determination of bond lengths, atomic mean-square relative displacements, and local thermal expansion by means of soft-x-ray photoabsorption. *Phys. Rev. B*, 49:888–903.

[Vaccari, 2006] Vaccari, M. (2006). *Local Dynamics and Negative Thermal Expansion: an EXAFS Study of CuCl.* PhD thesis, University of Trento, Italy.

[Vaccari and Fornasini, 2005] Vaccari, M. and Fornasini, P. (2005). Thermal effects on exafs: Ensemble averages and real-space approach. *Phys. Rev. B*, 72:092301.

[Vaccari and Fornasini, 2006] Vaccari, M. and Fornasini, P. (2006). Einstein and debye models for exafs parallel and perpendicular mean square relative displacements. *J. Synchrotron Rad.*, 13:321–325.

[Vaccari et al., 2007] Vaccari, M., Grisenti, R., Fornasini, P., Rocca, F., and Sanson, A. (2007). Negative thermal expansion in cucl: an extended x-ray absorption fine structure study. *Phys. Rev. B*, 75:184307.

[Ventsel, 1973] Ventsel, H. (1973). *Théorie des probabilités.* Editions MIR, Moskou.

[Willis and Pryor, 1975] Willis, B. T. M. and Pryor, A. W. (1975). *Thermal Vibrations in Crystallography.* Cambridge University Press.

[XAFS software,] XAFS software. Catalog home page. `http://www.esrf.eu/Instrumentation/software/data-analysis/Links/xafs`.

[Yeh, 1993] Yeh, J. (1993). *Atomic Calculation of Photoionization Cross-sections and Asymmetry Parameters.* Gordon and Breach.

[Yokoyama, 1999] Yokoyama, T. (1999). Path-integral effective-potential theory for exafs cumulants compared with the second-order perturbation. *J. Synchrotron Rad.*, 6:323–325.

[Yokoyama et al., 1996] Yokoyama, T., Kobayashi, K., Ohta, T., and Ugawa, A. (1996). Anharmonic interatomic potentials of diatomic and linear triatomic molecules studied by extended x-ray-absorption fine structure. *Phys. Rev. B*, 53:6111–6122.

[Zangwill, 2012] Zangwill, A. (2012). *Modern Electrodynamics.* Cambridge University Press.